

UNITED STATES DEPARTMENT OF THE INTERIOR

GEOLOGICAL SURVEY

Geologic interrelations relative to gas hydrates within the North Slope of Alaska

Timothy S. Collett¹, Kenneth J. Bird¹, Keith A. Kvenvolden¹ and Leslie B. Magoon¹

This work was funded by the Morgantown Energy Technology Center under U.S. Geological Survey-Department of Energy Agreement No. DE-AI21-83MC20422.

Open-File Report 88-389

This report is preliminary and has not been reviewed for conformity with U.S. Geological Survey editorial standards and stratigraphic nomenclature. Any use of trade names is for descriptive purposes only and does not imply endorsement by the USGS.

¹ U.S. Geological Survey, Menlo Park, California

TABLE OF CONTENTS

Summary	3
Chapter I. Introduction	4
I.A. Project Description	4
I.B. Previous Work	4
I.B.1. Recovered Gas Hydrate	4
I.B.2. Gas-Hydrate Stability	7
I.B.3. Inferred Gas-Hydrate Occurrences	11
Chapter II. Gas-Hydrate Stability	14
II.A. Stability Controls	14
II.A.1. Distribution of Ice-Bearing Permafrost	17
II.A.2. Geothermal Gradient	30
II.A.3. Gas Chemistry	46
II.A.4. Pore-Water Salinity	48
II.A.5. Pore-Pressure	48
II.A.6. Particle Grain-Size	54
II.B. Distribution of the Gas-Hydrate Stability Field	61
Chapter III. Geologic Setting	68
III.A. Regional Geology	68
III.B. Geology of the Prudhoe Bay and Kuparuk River area	77
III.B.1. Stratigraphic Framework	77
III.B.2. Potential Gas-Hydrate Reservoirs	88
III.B.3. Potential Gas-Hydrate Traps	92
Chapter IV. Gas-Hydrate Occurrences	96
IV.A. Well-Log Evaluation	96
IV.B. Gas-Hydrate Distribution	108
IV.C. Gas-Hydrate Reservoir Properties	117
Chapter V. Gas-Hydrate Formation Models	127
V.A. Theoretical Models	127
V.B. North Slope Model	127
Chapter VI. Estimated Resource Volume	132
Chapter VII. Recommended Core Sites	138
VII.A. Cooperative Industry--Government Core-Hole	138
VII.B. Dedicated Core-Hole	138
References Cited	146

SUMMARY

The five primary objectives of the U.S. Geological Survey North Slope Gas Hydrate Project were to: (1) Determine possible geologic controls on the occurrence of gas hydrate; (2) locate and evaluate possible gas-hydrate-bearing reservoirs; (3) estimate the volume of gas within the hydrates; (4) develop a model for gas-hydrate formation; and (5) select a coring site for gas-hydrate sampling and analysis.

Our studies of the North Slope of Alaska suggest that the zone in which gas hydrates are stable is controlled primarily by subsurface temperatures and gas chemistry. Other factors, such as pore-pressure variations, pore-fluid salinity, and reservoir-rock grain size, appear to have little effect on gas hydrate stability on the North Slope. Data necessary to determine the limits of the gas hydrate stability field are difficult to obtain. On the basis of mud-log gas chromatography, core data, and cuttings data, methane is the dominant species of gas in the near-surface (0-1,500 m) sediment. Subsurface temperature information, obtained from 46 high-resolution equilibrated well-bore surveys and from estimates based on well-log identification of the base of ice-bearing permafrost in 98 other wells, indicate that the depth of the 0°C isotherm increases in an irregular way from 220 m in the south to as much as 660 m near the coastline at Prudhoe Bay in the north. Formation-water samples and well-log calculations indicate low pore-fluid salinities (fresh to brackish), ranging from 0.5 to 19.0 ppt. The maximum recorded salinity would only suppress methane hydrate stability temperatures by approximately 1.0°C. Pressure data, obtained from drill-stem testing and well log calculations, indicate a hydrostatic pore-pressure gradient within the near-surface sedimentary rocks, thus having minimal effect on gas hydrate stability. In the near-surface coarse sandstone and conglomerate of the Prudhoe Bay area, grain size has little effect on gas hydrate stability; however, in the more clay-rich sedimentary rocks near Harrison Bay the freezing point of water may be depressed by several degrees Celsius, resulting in a shallower gas hydrate stability field. Our analyses indicate that the region in which methane hydrate is stable is areally extensive beneath the coastal plain province, with thicknesses greater than 1,000 m in the Prudhoe Bay area. Thermal conditions, however, preclude the occurrence of gas hydrates in the north-central part of the National Petroleum Reserve in Alaska and in the foothills east of Umiat.

Gas hydrates were identified in 34 wells utilizing well-log responses calibrated to the response of an interval in one well where gas hydrates were actually recovered in a core by an oil company. Most of the well-log identified gas hydrates occur in six laterally continuous Upper Cretaceous and lower Tertiary sandstone and conglomerate units, and are geographically restricted to the eastern part of the Kuparuk River Unit and the western part of the Prudhoe Bay Unit. All of the mapped occurrences are stratigraphically below a regionally extensive siltstone sequence, deposited during a regional marine transgression in Eocene time. The total mapped area of these six occurrences is about 380 km². The thicknesses of the identified individual gas-hydrate-bearing sequences range from 2 to 28 m, and reservoir porosities average approximately 40 percent. Well-log analyses suggest that the identified reservoirs are about 85 percent saturated with gas hydrate. If theoretical minimum and maximum hydrate numbers are assumed, then the volume of gas within the identified gas hydrates of the North Slope is approximately 2.4×10^{11} to 2.9×10^{11} m³ (STP) [approximately 8 to 10 tcf of gas], or about one-third of the volume of conventional gas in the Prudhoe Bay field. Because of the low drilling density outside of the Prudhoe Bay-Kuparuk River area, many more gas hydrate occurrences may exist.

A possible scenario describing the origin of the inferred gas hydrates on the North Slope involves the migration of thermogenic solution- and free-gas from deeper reservoirs upward along faults into the overlying sedimentary rocks. As the gas migrated into the upper horizons it was either directly converted to gas hydrate or first concentrated in existing structural/stratigraphic traps and later converted to gas hydrate. Major climatic changes may have influenced the depth limits of the gas hydrate occurrences.

We have identified two (dedicated) core-hole sites, the Eileen and the South-End core-holes, at which there is a high probability of recovering a sample of gas hydrate. At the Eileen core-hole site, at least three stratigraphic units may contain gas hydrate. The South-End core-hole site provides an opportunity to study one specific rock unit that appears to contain both gas hydrate and oil.

CHAPTER I. INTRODUCTION

I.A. PROJECT DESCRIPTION

The main goal of the U.S. Geological Survey North Slope Alaska Gas-Hydrate Project is to examine all data from northern Alaska pertaining to gas hydrates in order to achieve the following objectives:

1. Evaluate geologic controls on gas-hydrate occurrences.
2. Define and evaluate possible gas-hydrate-bearing reservoirs.
3. Estimate the volume of gas within the gas-hydrate occurrences.
4. Develop a model for onshore gas-hydrate formation.
5. Select core-hole sites for gas-hydrate study.

The approach to the North Slope gas-hydrate evaluation problem is outlined in table I-1; our program was systematically constructed to develop a data-base which enabled us to produce deliverable items over the duration of the project. The project was subdivided into 4 sections (table I-1). Section 1 was concerned primarily with the parameters that control in-situ gas hydrate formation. Section 2 examined the geologic framework in which gas hydrates could exist. Sections 3 and 4 included the identification and evaluation of in-situ gas hydrates.

The structure of this report is similar to the project outline discussed above; however, the report is further subdivided into 7 chapters. Chapter I describes the project and discusses previous work. Chapter II deals with the evaluation of the physical parameters that control gas hydrate stability on the North Slope. Chapter III describes the near-surface structural/stratigraphic framework. Chapter IV describes the gas hydrate occurrences, and Chapter V presents models explaining the origin of the occurrences. Chapter VI estimates the volume of gas in these occurrences. The report concludes (Chapter VII) with a description of the recommended sites for recovering gas-hydrate cores.

I.B. PREVIOUS WORK

Gas hydrates are crystalline substances composed of water and gas in which a solid-water lattice accommodates gas molecules in a cage-like structure, or clathrate. Gas hydrates have been known as laboratory curiosities since about 1810. Detailed studies of hydrates and their physical properties were not undertaken until Hammerschmidt (1934) published data pertaining to the plugging of natural-gas pipelines due to gas-hydrate formation. The geological occurrence of gas hydrates has been known since the mid 1960's, when gas-hydrate fields were discovered in the U.S.S.R. (see Makogon, 1981 for a review).

The pressure and temperature conditions suitable for the formation of gas hydrates are found in high latitude regions of permafrost and beneath the sea in outer continental margins and ocean basins (Kvenvolden and McMenamin, 1980). The fact that temperatures and pressures associated with permafrost may fall within the stability field of gas hydrates (fig. I-1) was first recognized by Katz (1971). Gas hydrates can occur not only in permafrost but also below the base of permafrost at temperatures above the freezing point of water.

Significant quantities of gas hydrates have been detected in several permafrost regions of the world, including western Siberia (Makogon, 1981), the Mackenzie Delta of Canada (Bily and Dick, 1974), and the North Slope of Alaska (Galate and Goodman, 1982; Collett, 1983a). Estimates of worldwide gas hydrate resources in permafrost regions are as high as 10^{16} m³ of methane (Potential Gas Agency, 1981), an estimate large enough to stimulate interest in gas hydrates as a possible energy source. Gas hydrates also may be a potential drilling hazard because they can cause sediment instability and high pressures in a bore-hole.

I.B.1. RECOVERED GAS HYDRATE

Direct evidence for gas hydrates on the North Slope comes from core-tests, and indirect evidence comes from drilling and open-hole geophysical well logs which suggest the presence of

Table I-1. North Slope Gas Hydrate Project outline.

Section 1. Factors affecting gas-hydrate stability	
	Ice-bearing permafrost
	Geothermal gradient
	Gas chemistry
	Pore-water salinity
	Pore-pressure
	Particle grain-size
Section 2. Geologic framework	
	Stratigraphy
	Depositional environments
	Structure
Section 3. Gas-hydrate identification and distribution	
	Well-log evaluation
	Map in-situ gas hydrates
	Geologic controls
Section 4. Gas-hydrate evaluation	
	Resource estimation
	Core-hole location

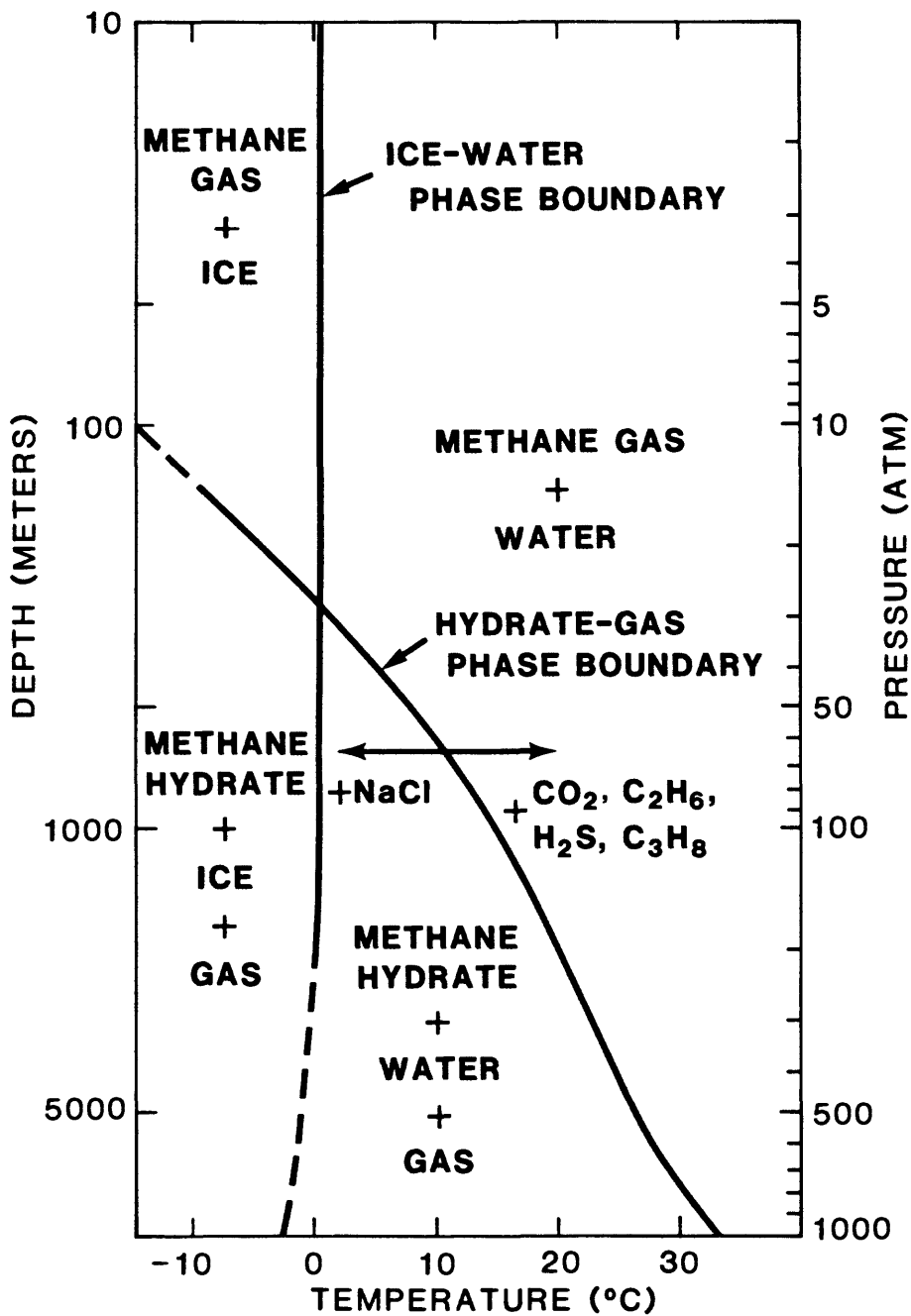


Figure I-1. Phase boundary diagram showing free methane gas and methane hydrate (below the HYDRATE-GAS PHASE BOUNDARY) for a fresh-water, pure methane system. Addition of sodium chloride lowers the temperature of hydrate formation, shifting the stability curve to the left. Addition of carbon dioxide, hydrogen sulfide, propane, or ethane raises the temperature of hydrate formation, shifting the stability curve to the right (from Kvenvolden and McMenamin, 1980).

numerous gas-hydrate layers in the area of the Kuparuk River oil field (Collett and Kvenvolden, 1987). The identified gas hydrates appear to be laterally continuous and extensive; this widespread distribution of in-situ gas hydrates on the North Slope suggests that they may be an unconventional source of natural gas.

The only confirmed natural gas hydrate on the North Slope was obtained in 1972, when ARCO and EXXON successfully recovered a core containing this substance (Collett and Kvenvolden, 1987). The sample was from a depth of 666 m in the Northwest Eileen State-2 well (fig. I-2), located near Prudhoe Bay. The presence of gas in a hydrated state was confirmed by a pressure test while the core was maintained in the core barrel at a temperature of about 1.0 °C. As gas was withdrawn from the core barrel, the pressure dropped, but it subsequently rose to the gas-hydrate equilibrium pressure when the system was closed. This pressure response has been discussed by Hunt (1979, p. 167). If the core had contained only free-gas, the pressure in the barrel would have decreased as gas was withdrawn and the pressure would not have increased when the system was closed.

Data from driller's and open-hole geophysical well logs (fig. I-2) also strongly suggested the presence of naturally occurring in-situ gas hydrates. The mud log indicates that a significant amount of free gas was liberated from the hydrate-containing interval during drilling. Logs, such as resistivity and acoustic transit-time, indicate the presence of gas hydrates by anomalously high resistivities and short transit-times within the suspected gas-hydrate occurrence. The recovered gas-hydrate sample had a gas composition of 92.79% methane, 7.19% nitrogen, and also had minor traces of carbon dioxide, ethane, and propane (personal communication, P. Barker, ARCO Alaska Inc., Anchorage, Alaska).

I.B.2. GAS HYDRATE STABILITY

As discussed earlier, gas hydrates exist under a limited range of temperatures and pressures (fig. I-1). The depth and thickness of the zone of potential gas hydrate stability in permafrost regions can be calculated if the geothermal gradient, pressure gradient, and gas density are known (Bily and Dick, 1974). The geothermal gradients needed to predict the thickness of the gas hydrate stability zone are not easily obtained, especially if permafrost is present. Lachenbruch and others, (1982) published a series of geothermal gradients recorded on the North Slope. Their reported gradients show great lateral variation in the Prudhoe Bay region; this variance indicates that an average regional gradient can not be used to calculate the thickness of the gas-hydrate stability field. A method was developed to evaluate local geothermal gradients on a well-by-well basis (Collett, 1983a). In this procedure, individual geothermal gradients for each well were projected from the base of the ice-bearing permafrost to the surface. Because of a change in thermal conductivity, the geothermal gradient changes abruptly at the base of the ice-bearing permafrost, and this change in the gradient must be accounted for in any gas-hydrate stability calculation. In Collett (1983a), a factor, developed by Lachenbruch and others (1982), was used to correct for this change in the geothermal gradient.

The methane hydrate-stability curve and the depth to the base of the ice-bearing permafrost was used to determine the depth and thickness of the potential methane-hydrate zone at the Northwest Eileen State-2 well (fig. I-3); no effort was made here to correct for the effect of the nitrogen in the methane. The following information was obtained using Collett's (1983a) method: In this example, the depth to the base of the ice-bearing permafrost is approximately 530 m. Temperature surveys from surrounding wells suggest that the mean-annual surface temperature at the Eileen well is -11.0 °C and the base of ice-bearing permafrost is at -1.0 °C. These temperature data have been used to project a geothermal gradient that intersects the methane-hydrate stability curve at 180 m and 960 m, delineating a 780 m zone in which methane hydrate would be stable (fig. I-3). This procedure will be discussed in more detail in Chapter II of this report.

After evaluating logs from 125 wells on the North Slope, Collett (1983a) determined that in order to have an intersection between the methane-hydrate stability curve and a geothermal gradient, the projected gradient within the ice-bearing permafrost must be equal to or less than 4.3°C/100 m (Collett, 1983a). If the geothermal gradient and the methane-hydrate stability curve do not intersect, in-situ gas hydrates will not be stable and will not be present. Given this geothermal gradient, a maximum ice-bearing permafrost depth would be 274 m. In other words, methane hydrate should not be present in North Slope sediment when temperatures are such that ice-bearing permafrost is less than 274 m thick. The shaded area in figure I-4 indicates the region in which methane hydrates would be potentially stable, and the dashed line represents the southern limit of the 274 m ice-bearing

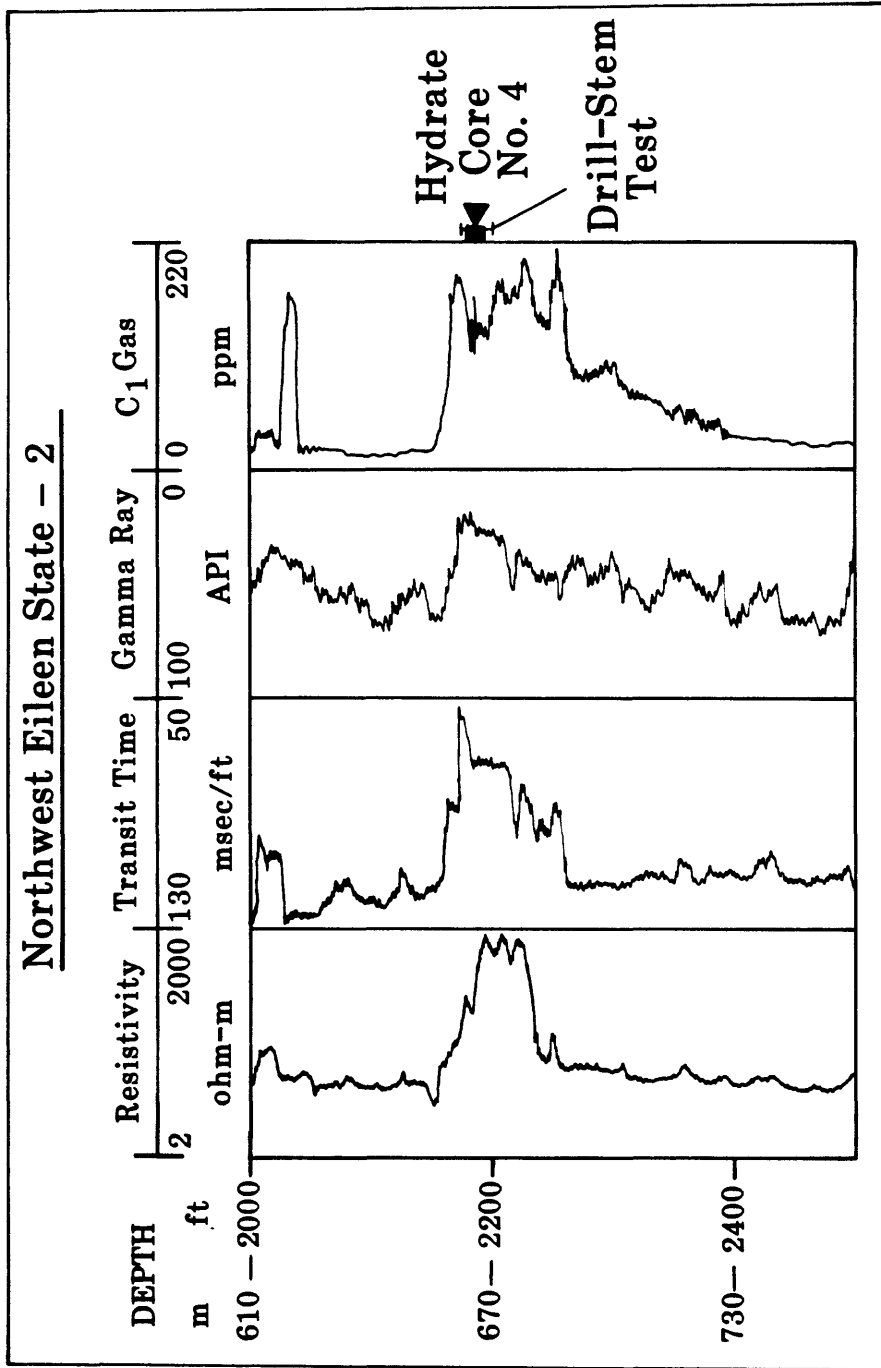


Figure I-2. Selected well logs from an interval in the Northwest Eileen State-2 well and the location of a two-meter core (665 to 667 m) that was shown to contain gas hydrate. A drill-stem test of the interval from 663 to 671 m flowed gas at a rate of 112 m³ (3,960 ft³) per day.

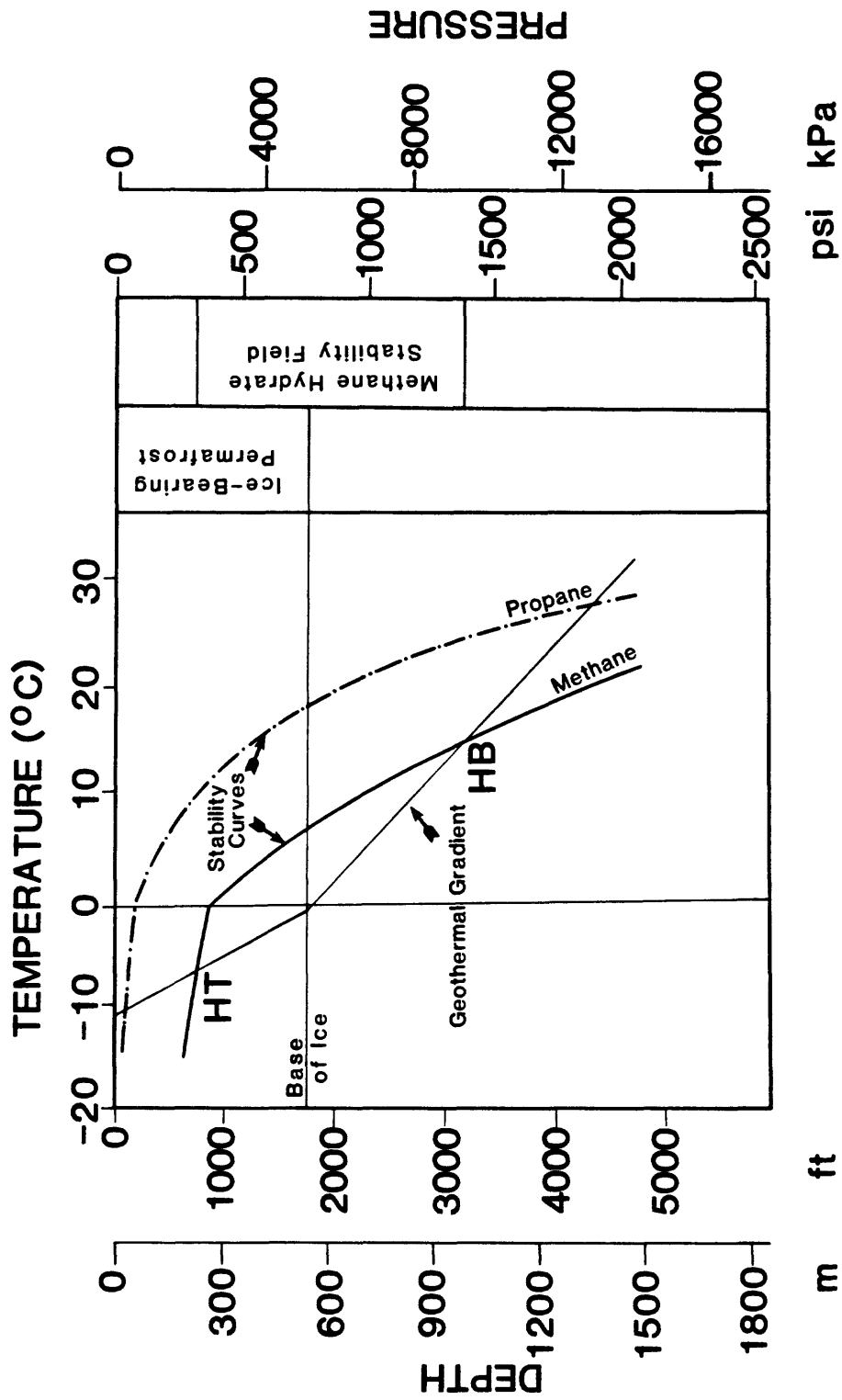


Figure I-3. Gas hydrate phase diagram applied at Northwest Eileen State-2.

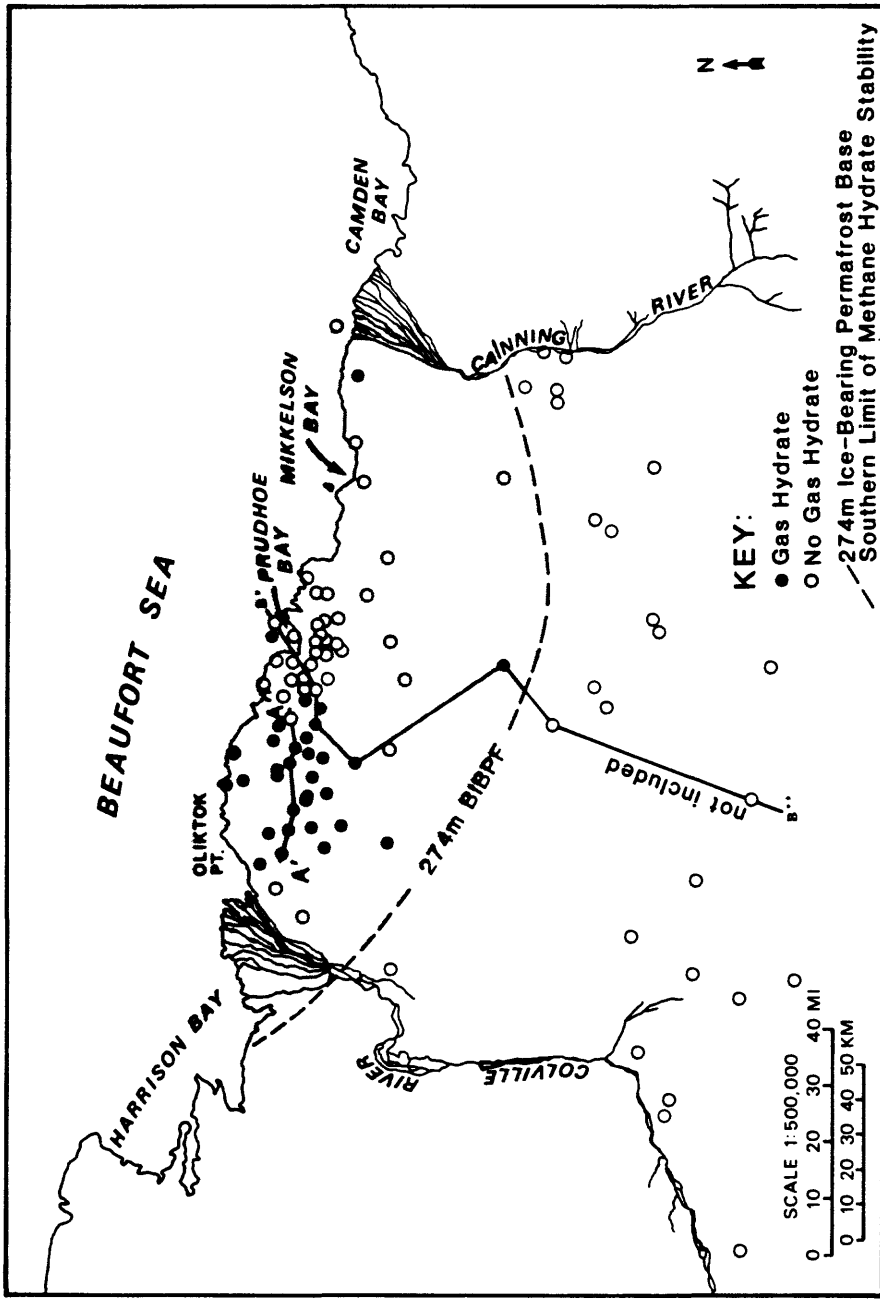


Figure I-4. Locations of North Slope wells having evidence for in-situ gas hydrates. The inferred southern limit of the methane hydrate stability field is shown by a dashed line (Collett, 1983a).

permafrost depth contour. The northern boundary of the methane-hydrate stability field lies offshore beneath the shelf, but its exact position is uncertain.

LB.3. INFERRED GAS-HYDRATE OCCURRENCES

Galate and Goodman (1982) examined 17 wells from the National Petroleum Reserve in Alaska (NPRA) for evidence of in-situ gas hydrates. For this study, they used all available records such as drilling plans, well histories, daily drilling reports, mud reports, geologic data for the area, coring information, and geophysical well logs. Of the 17 wells investigated, they reported that 3 (fig. I-5) showed significant evidence of gas hydrates, and 5 showed some evidence of gas hydrates.

Detailed analysis of a series of open-hole geophysical well logs from 125 wells in the area of the Prudhoe Bay and Kuparuk River oil fields suggests the presence of 102 gas-hydrate occurrences in 32 different wells (Collett, 1983a). Gas hydrates are present in relatively porous, discrete sedimentary units and in many wells in multiple zones; the individual zones range from 2 to 28 m in thickness. Most of the gas-hydrate occurrences appear to be geographically restricted to the Kuparuk Field, west of Prudhoe Bay (fig. I-4).

In the Kuparuk River oil field area, gas hydrates are present in about four to six laterally continuous units that can be delineated in cross section (fig. I-6). The gas hydrates are restricted to a series of sandstone and conglomerate units which are interbedded with multiple, thick siltstone units. The gas-hydrate bearing sandstone and conglomerate represent a marine to non-marine delta front to delta plain depositional package (Collett, 1983a).

The presence of thick coal units in this sequence is consistent with a deltaic environment of deposition. The coal may also serve as a source of the methane necessary for the formation of gas hydrate. Heavy oil, present within this shallow sequence, may also have been a source of methane and heavier gases, such as propane, because dissolved gases are commonly associated with oil accumulations.

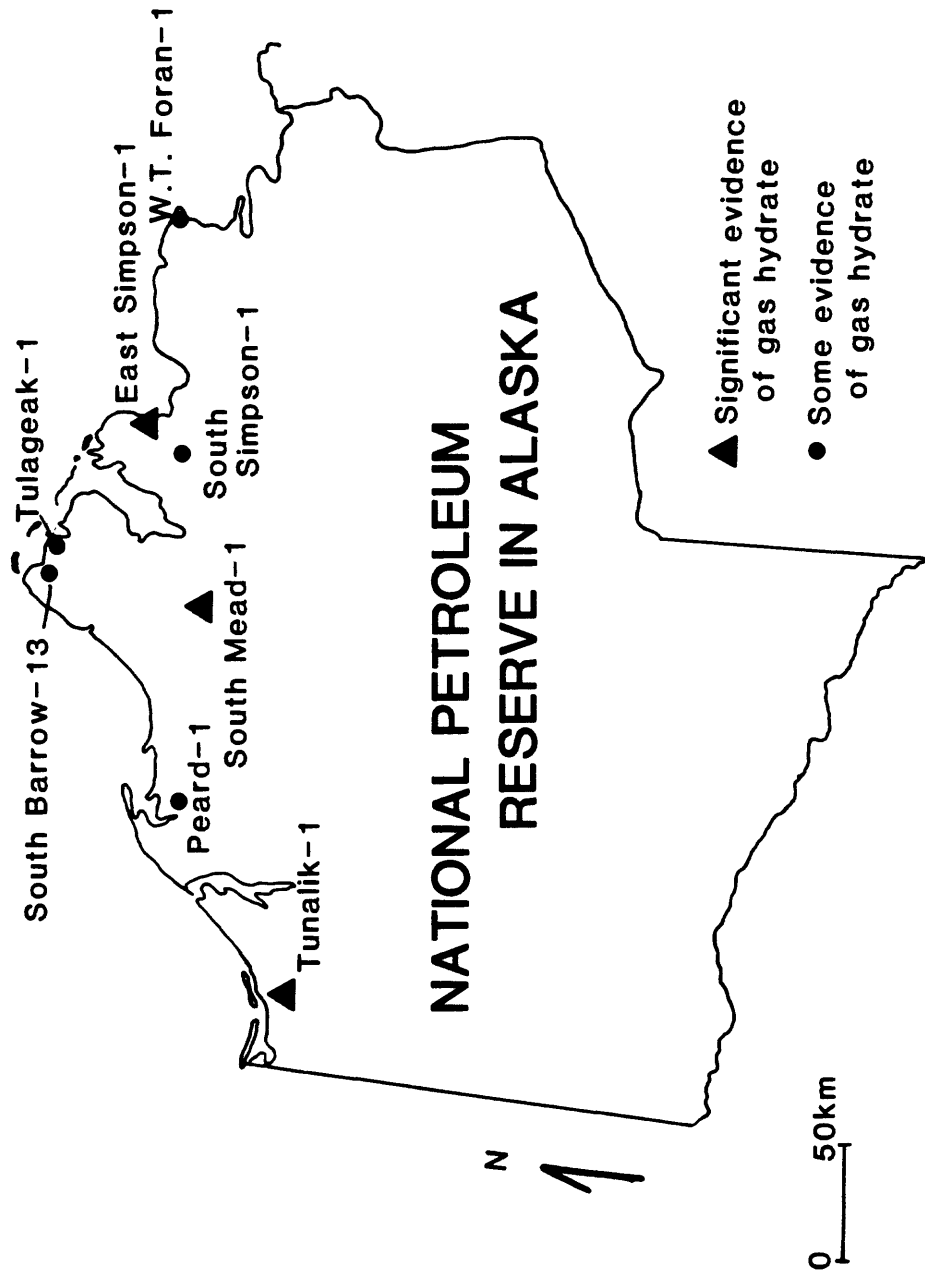


Figure I-5. Map showing the eight wells from the National Petroleum Reserve in Alaska in which Galate and Goodman (1982) indicated gas hydrates may occur.

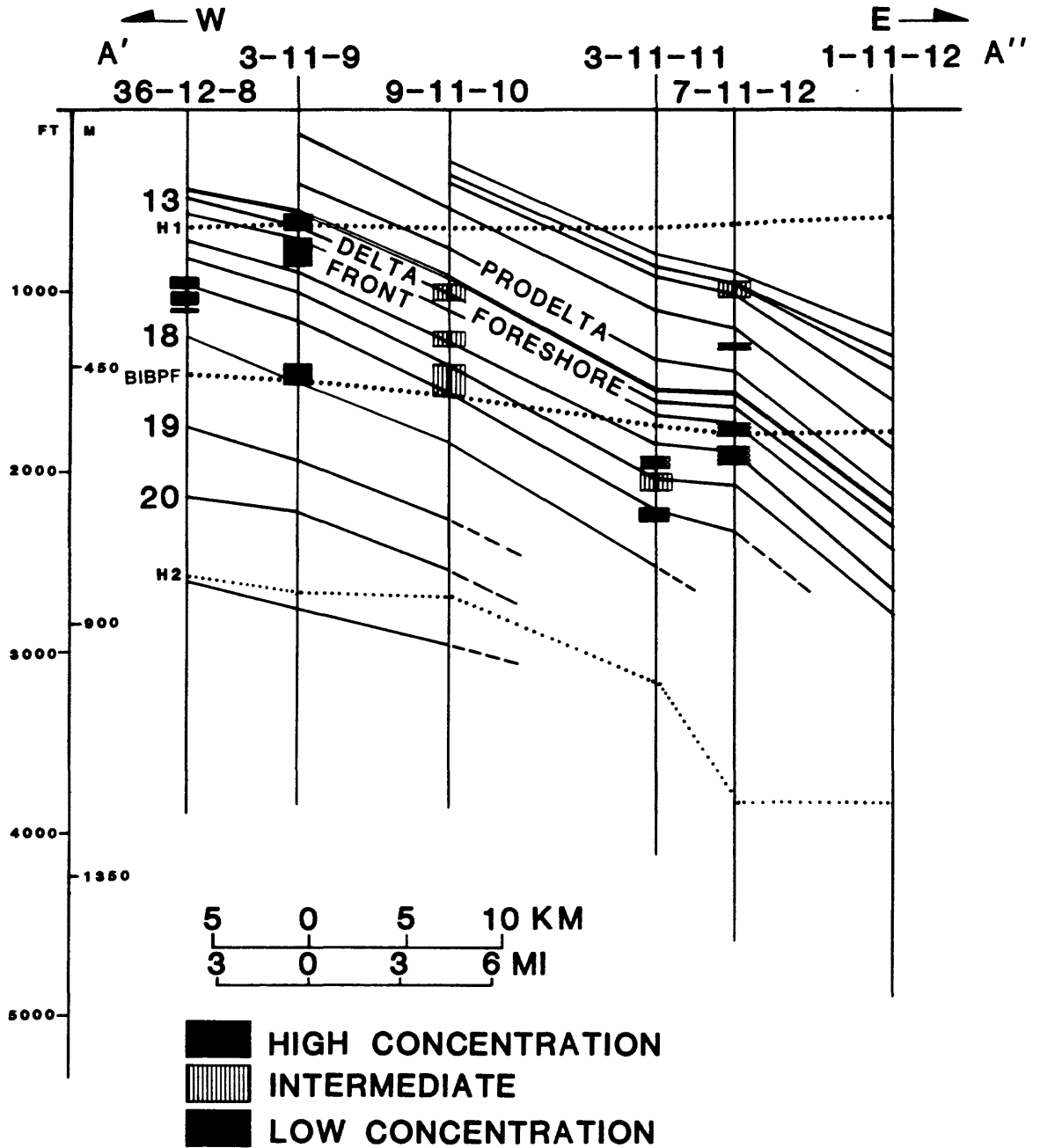


Figure I-6. East to west geologic cross-section through six wells of the Kuparuk River oil field area; well locations are noted by Section, Township, and Range (Collett, 1983a). The stratigraphic framework as depicted is defined by a series of geologic markers (shown as correlation lines). Also shown are the individual gas hydrate occurrences and relative concentrations, the base of ice-bearing permafrost (BIBPF), top (H1) and bottom (H2) of the methane-hydrate stability zone, and the inferred depositional environments for the reservoir rocks. (Location of section shown in figure I-4).

CHAPTER II. GAS-HYDRATE STABILITY

II.A. STABILITY CONTROLS

Chapter II is divided into two sections: Section "A" deals with the evaluation of the physical parameters that control gas-hydrate stability, and in Section "B" the theoretical distribution of the methane-hydrate stability field is mapped.

There are five reservoir and fluid properties that affect the stability of in-situ gas hydrates--geothermal gradients, gas chemistries, pore-fluid salinities, pore-pressures, and reservoir-rock grain sizes (table II-1). The two primary factors are geothermal gradients and gas chemistries. The other three variables are difficult to quantify and often have little effect. In figure II-1 methane-hydrate and propane-hydrate stability curves have been shown along with geothermal gradients assumed for the Northwest Eileen State-2 well on the North Slope. The plot of the two stability curves dramatically illustrates how different gas chemistries can influence the thickness of the gas-hydrate stability field. In this display, the geothermal gradient intersects the methane-hydrate stability curve at 210 and 950 m, delineating a methane-hydrate stability field that is 740 m thick. However, the constructed geothermal gradients intersect the propane stability curve at 60 and 1,330 m, thus delineating a gas-hydrate stability field that is 1,270 m thick. This difference in the thicknesses of the gas hydrate stability fields is a result of the difference in stability of the cage-structure formed by propane or methane. Large gas molecules, such as propane, form a different gas-hydrate cage structure (Structure II) than do smaller methane gas molecules (Structure I). The larger cage structure is stable at higher temperatures and pressures (Makogon, 1981), resulting in a thicker gas-hydrate stability zone.

Subsurface temperature data required to calculate regional geothermal gradients are difficult to obtain. These data can be theoretically derived, but this derivation requires a complete understanding of subsurface regional heat-flow, existing thermal conductivity characteristics of the basin-filling sediments, and mean-annual surface temperatures (Lachenbruch and others, 1982). Geothermal gradients can also be calculated from temperature data (bottom-hole temperature measurements) obtained during normal well-logging operations (Edwardson and others, 1962). Unfortunately, drilling activity can significantly disrupt subsurface equilibrium temperatures, and it may not be possible to correct the recorded temperature because of insufficient information. The most accurate method of determining local and regional geothermal gradients is by conducting high-resolution temperature surveys in wells that have been left undisturbed for a sufficient period of time to allow thermal equilibration in the wellbore. These surveys, however, are not often available; therefore, an alternate method of using known ice-bearing permafrost depths to project local geothermal gradients has been developed; this method will be discussed later.

Salt, such as NaCl, when added to a gas hydrate system, lowers the temperature at which gas hydrates form (Evrenos and others, 1971). The salinity of the water in contact with the gas during the formation of gas hydrate can reduce the freezing point about 3^o to 5^o C per 100 ppt dissolved salt, shifting the stability curves in figure II-1 to the left, and thus reducing the thickness of the gas hydrate stability field.

The effect of grain-size variations and abnormal pore-pressure conditions on gas hydrate equilibrium is unclear. It is known from studies of permafrost, however, that variations in grain sizes and pore pressures affect the freezing point of ice (Anderson and others, 1973; Osterkamp, 1975; Osterkamp and Payne, 1981). Particles with large surface area relative to grain size, such as clay, can reduce the freezing point of water by several degrees Celsius, apparently because of molecular bonding of the water to the particle (Anderson and others, 1973). A similar relation is thought to exist between grains of high surface area and gas-hydrate equilibrium temperatures (oral communication, D. Sloan, Colorado School of Mines, Golden, Colorado). Abnormal formation pressures will affect gas hydrate stability conditions in a manner unlike that of ice. High pore-pressure conditions increase the stability of gas hydrate, but depress the freezing point of ice (Holder and others, 1985). In general, the higher the pressure gradient the thicker the stability zone of gas hydrate.

Table II-1. Variables influencing the limits of the in-situ gas-hydrate stability field and sources of data necessary for evaluating variables.

Variables	Data Sources
Geothermal Gradient	Theoretical derivation; well logging operations; high resolution equilibrated temperature surveys; projection from base ice-bearing permafrost.
Gas Chemistry	Mud log; drill-cuttings; core samples, drill-stem-test; production samples.
Pore-Fluid Salinity	Well logs; drill-stem-test; production samples; core samples.
Pore-Pressure	Drill-stem-test; well logs.
Grain-Size	Drill-cuttings; core; well logs.

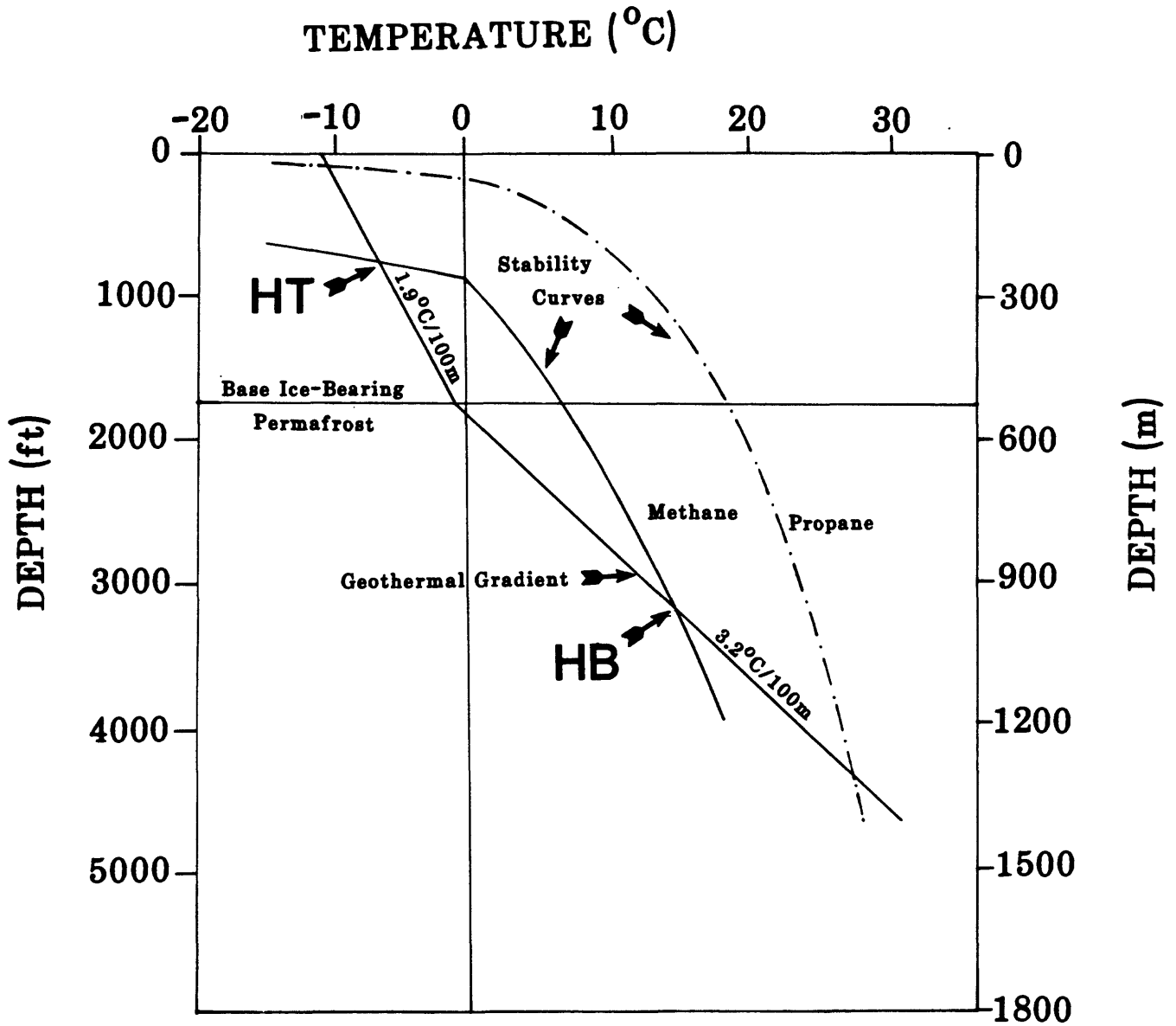


Figure II-1. Phase diagram illustrating the influence of gas chemistry (methane vs. propane) on the zone of gas hydrate stability. Geothermal gradients are those predicted for the Northwest Eileen State-2 well.

II.A.1. DISTRIBUTION OF ICE-BEARING PERMAFROST

Because gas hydrates form within a limited temperature range, subsurface equilibrium temperature data are necessary to calculate the depth and thickness of the gas-hydrate stability field. Acquiring these data is difficult because drilling activity often disrupts equilibrium temperatures in the subsurface, and a well must lie undisturbed until thermal equilibrium is re-established (Lachenbruch and Brewer, 1959). On the North Slope of Alaska, a series of 46 oil and gas exploratory wells, which were considered to be near thermal equilibrium (Lachenbruch and others, 1982; Lachenbruch and others, 1987), were surveyed with high-resolution temperature devices (table II-2). However, several thousand other exploratory and production wells have been drilled on the North Slope and, although they do not have temperature profiles, their geophysical logs often allow discrimination between ice-bearing and non-ice-bearing strata. At the outset of this study, the coincidence of the base of ice-bearing strata and the depth of the 0° C isotherm at Prudhoe Bay (Lachenbruch and others, 1982) appeared to offer an opportunity to expand quickly and inexpensively the size of our subsurface temperature data base merely by using well logs to identify the base of the ice-bearing strata.

Accordingly, the log suites of more than 440 publicly available, North Slope exploratory and production wells were examined. Of these, 156 wells have log responses allowing discrimination of ice-bearing strata, and these log responses were used to map the depth to base of the deepest ice-bearing strata. In wells outside the Prudhoe Bay area, a considerable difference exists between the depth of the 0° C isotherm and the base of ice-bearing strata. This discordance is great enough to diminish the reliability of using well logs alone for estimating the depth of the 0° C isotherm. Nevertheless, understanding the distribution of ice in the subsurface, as determined by well logs, is important for predicting the presence of natural gas hydrates.

In arctic environments, where subsurface temperatures below 0° C persist, a specific terminology is used to describe temperatures and the physical state of pore-filling water in the subsurface. This terminology, however, is often inconsistent (Desai and Moore, 1968; Hoyer and others, 1975; Walker and Stuart, 1976; Osterkamp and Payne, 1981); therefore, permafrost, ice-bearing permafrost, and ice-rich permafrost are defined below.

Permafrost is the thermal condition in soil or rock having temperatures below 0° C which persists over at least two consecutive winters and the intervening summer (Brown and Kupsch, 1974). The presence or absence of water or ice is not included in the definition of permafrost, and the depth to the base of permafrost is the depth to 0° C.

Ice-bearing permafrost refers to soil or rock that contains or is interpreted to contain ice that can be detected by subsurface well logs. Contours on the map in figure II-2 illustrate the depth to the base of the deepest ice-bearing permafrost as determined from subsurface geophysical well logs (exclusive of temperature logs) for 156 exploratory and development wells on the North Slope of Alaska.

Ice-rich permafrost can be identified when high-resolution subsurface temperature surveys are available. Using equilibrated well-bore temperature surveys, Lachenbruch and others (1982) were able to differentiate thawed, water-bearing sedimentary rocks from ice-rich horizons by identifying a "kink" in their temperature profiles in the Prudhoe Bay area. The geothermal gradient of sediments with ice-filled pores is generally different from the geothermal gradient in sediments with water-filled pores. This difference in geothermal gradients is a conspicuous indicator of the base of ice-rich permafrost. In the near-surface, high-porosity sandstone and conglomerate units of the Prudhoe Bay area, the discontinuity in the geothermal gradient represents the ice/water phase boundary at the base of the ice-rich permafrost (Lachenbruch and others, 1982). However, changes in the geothermal gradient in the finer grained sediments west of Prudhoe Bay in the NPRA are not as pronounced and commonly are not present (Lachenbruch and others, 1987).

In the section below are terms and methods used to study ice-bearing permafrost and to interpret the well-log responses. The relations of permafrost, ice-rich permafrost, and ice-bearing permafrost, on the North Slope of Alaska are also discussed.

PERMAFROST

Permafrost, or perennially frozen ground, is widespread in arctic regions and underlies approximately 20 percent of the land area of the world (Ferrians and others, 1969). Information about permafrost thickness and variability in composition is necessary to solve engineering and scientific

Table II-2. North Slope wells for which temperature profiles were made after the well-bore had reached near thermal-equilibrium conditions. [See table II-5 for comparison of depths of ice-bearing permafrost (IBPF) from well logs with depths to base of permafrost (0 °C) and ice-rich layer (IRL) listed here.]

Well Index	Well name	API No. ^{1]}	Depth to 0°C ^{2]} (m)	IRL ^{3]} (m)	Source ^{4]}	Logged ^{5]}
A*	Simpson Core Test-13	5027910013	320		Brewer, 1958	Yes
B	Simpson Core Test-21	5002310001	250		do.	Yes
C	Simpson Core Test-28	5027910026	279		do.	Yes
D	Simpson Core Test-29	5027910027	290		do.	Yes
E	South Barrow Test Well-1	5002310009	204		MacCarthy, 1952	Yes
F*	South Barrow Test Well-3	5002310011	(proj)396		do.	Yes
G	Umiat-11	5028710011	322		Ferrians, 1965	Yes
H*	East Umiat-1	5028710016	235		do.	Yes
I	Topagonuk-1	5027910033	335		do.	Yes
J	Kaolak-1	5029710001	299		do.	Yes
K	BP 33-12-13	5002920047	660	620	Lachenbruch and others, 1982	No
L	BP 04-11-13	5002920025	640	620	do.	No
M	BP 19-10-15	5002920035	595	570	do.	No
N	BP 23-11-13	5002920054	(proj)629	605	do.	No
O*	ARCO N Prudhoe Bay St-1	5002920049	605	560	do.	Yes
P*	BP 08-11-13 (P.B.U. N-1)	5002920079	620	600	do.	Yes
Q	BP 31-11-14	5002920059	650	620	do.	No
R	BP 11-11-13	5002920084	640	620	do.	No
S*	BP 12-11-13 (P.B.U. F-3)	5002920085	640	620	do.	Yes
T	BP 27-11-14	5002920006	625	580	do.	No
U	ARCO E Bay St-1	5002920133	625	580	do.	No
V*	Tulageak-1	5002320018	305		Lachenbruch and others, 1987	Yes
W	West Dease-1	5002320014	280	260	do.	Yes
X*	J.W. Dalton-1	5027920006	410	310	do.	Yes
Y	Tunalik-1	5030120001	290		do.	Yes
Z	Peard Bay-1	5030120002	310	270	do.	Yes
AA	Kugrua-1	5016320002	282	250	do.	Yes
BB	South Meade-1	5016320001	200	160	do.	Yes
CC	Kuyanuk-1	5016320003	330		do.	Yes
DD	East Simpson-1	5027920005	370	280	do.	Yes
EE	Ikpikpuk-1	5027920004	340	280	do.	Yes
FF	Drew Point-1	5027920002	325	250	do.	Yes
GG	East Teshekpuk-1	5010320006	265		do.	No
HH*	North Kalikpik-1	5010320011	215		do.	Yes
II*	Fish Creek-1	5010310001	260	140	do.	Yes
JJ*	South Harrison Bay-1	5010320007	(proj)375		do.	Yes
KK*	Atigaru Point-1	5010320008	405	330	do.	Yes
LL	Awuna-1	5015520001	295		do.	Yes
MM	Lisburne-1	5013720003	290		do.	Yes
NN	Koluktak-1	5011920001	(proj)290		do.	Yes
OO	Seabee Test Well-1	5028720007	310		do.	Yes
PP*	Sinclair/BP Kuparuk-1	5028710018	300		do.	Yes
QQ	Forest Oil Lupine-1	5022320011	240		do.	Yes
RR*	Mobil Echooka-1	5022320008	280	260	do.	Yes
SS	Exxon Canning River A-1	5017920005	282		do.	Yes
TT	Umiat-9	5028710009	(proj)356		do.	Yes

1] American Petroleum Institute well identification number (Alaska Oil and Gas Conservation Commission, 3001 Porcupine Drive, Anchorage, Alaska, 99501).

2] Depths measured from ground level.

3] Depth to base of an ice-rich layer from recorded temperature profiles (source identified), measured from ground level. If blank no value reported.

4] For complete reference see References Cited.

5] Identifies wells logged using conventional wireline tools in ice-bearing permafrost.

* See table II-4 for the depth to the base of the ice-bearing permafrost as determined from subsurface well-log data.

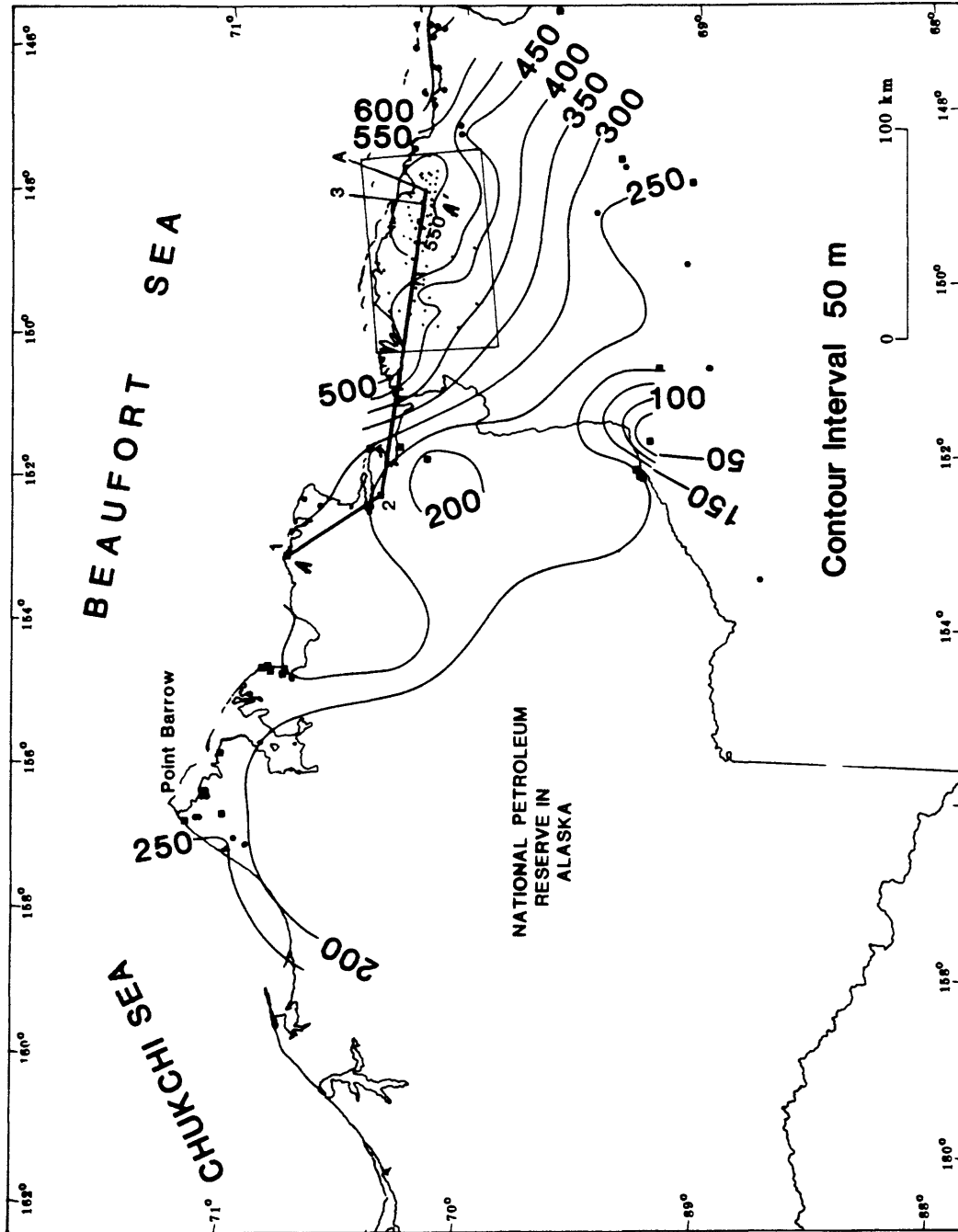


Figure II-2. Map of the depth to the base of the deepest ice-bearing permafrost on the North Slope of Alaska as determined from analysis of well log responses. Table II-4 lists wells and depths used in constructing this map.

problems such as: (1) Correcting seismic-reflection velocity data; (2) developing safe procedures for oil-well drilling, completion, and production in permafrost; (3) developing regional ground-water models; and (4) assessing the distribution of gas hydrates within or beneath the permafrost sequence.

Study of the thermal regime of North Slope permafrost using serial temperature profiles in wells dates from early days of exploratory drilling in this region. These data and permafrost thicknesses are reported by MacCarthy (1952), Brewer (1958), Ferrians (1965), Lachenbruch and others (1966), Lachenbruch and Marshall (1969), Stoneley (1970), Howitt (1971), Gold and Lachenbruch (1973), Lachenbruch and others (1982), Lachenbruch and others (1987). Temperature profiles from 46 wells that are near thermal equilibrium constitute the temperature data base for the North Slope (table II-2), and they show that permafrost ranges from 200 m to 660 m in thickness. The wells marked with an asterisk in Table II-2 have been used to interpret wire-line well-log responses and are described below.

ICE-RICH PERMAFROST

Lachenbruch and others (1982) noted a flexure or change in the trend of the temperature profiles at a depth of about 580 m and a temperature of approximately -1°C in a series of wells from the Prudhoe Bay area. They attributed the change in the temperature profile to a discontinuity in the thermal conductivity caused by ice-filled pores above 580 m and water-filled pores below that. This ice/water interface, as inferred from the gradient discontinuity in the temperature profiles, defines the base of ice-rich permafrost (Lachenbruch and others, 1987). The base of ice-rich permafrost will not coincide exactly with the base of the permafrost (0°C isotherm), but will usually be in equilibrium at temperatures lower than 0°C . The ice/water phase boundary was not observed in the recovered cores of the Prudhoe Bay wells; however, analysis of the retarding effects of latent heat on the dissipation of the drilling disturbance indicates that the discontinuity in recorded temperature profiles represents an ice/water interface (Lachenbruch and others, 1982). This observation is true only for the Prudhoe Bay area wells; the data are inconclusive for the NPRA. The depths to the base of an ice-rich layer were reported by Lachenbruch and others (1982), and Lachenbruch and others (1987) for 22 of the 46 wells listed in table II-2. These reported depths may in some cases represent the base of the deepest ice-rich layer, thus representing the base of ice-rich permafrost.

ICE-BEARING PERMAFROST

As defined earlier ice-bearing permafrost refers to strata containing a sufficient volume of ice to be detected on geophysical well logs without the aid of temperature data. The minimum amount of ice necessary for detection by well-logging devices is unknown. Well-log responses used to determine the base of the ice-bearing permafrost are summarized in table II-3.

The temperature at the base of ice-bearing permafrost is always at or below 0°C ; therefore, the depth to the base of the ice-bearing permafrost is always at or above the depth of the 0°C isotherm. Within the thick ice-bearing permafrost sequence, locally found on the North Slope, multiple frozen and thawed horizons are present. In this study, the base of the ice-bearing permafrost is interpreted as the deepest observed frozen-to-thawed phase boundary that may exist in any particular location.

Desai and Moore (1968) were the first to report that an ice-bearing horizon exhibits physical characteristics that can be detected with subsurface geophysical devices. They demonstrated that properties such as electrical resistivity and acoustic transit time are affected by the presence of ice within the sediment. Others have shown that the ice-bearing permafrost thickness can be determined from well logs (Stoneley, 1970; Howitt, 1971; Hoyer and others, 1975; Walker and Stuart, 1976; Hnatiuk and Randall, 1977; Osterkamp and Payne, 1981; Osterkamp and others, 1985); the term ice-bearing permafrost was used first by Osterkamp and Payne (1981). Their predecessors used the term permafrost to describe both temperature conditions and the presence of ice within pore spaces.

Desai and Moore (1968) demonstrated that the spontaneous potential, resistivity, and acoustic logs show significant deflections at the base of the ice-bearing permafrost (called permafrost by these authors) in an unidentified well on the North Slope of Alaska. They observed a significant increase in electrical resistivity, decrease in acoustic transit time, and a pronounced drift in spontaneous potential from less negative to increased negative values after crossing the boundary from non-ice-bearing to ice-bearing permafrost. Stoneley (1970) illustrated similar log responses in Put River-1 (well no. 18,

Table II-3. Comparison of well-log responses within ice-bearing permafrost (IBPF) with those below the base of IBPF in a porous sandstone lithology.

Well-log response	In IBPF	Below IBPF	Remarks
Resistivity (Res)--Substantial drop in resistivity; the long-normal curve separates from the short-normal curve within the IBPF.	>1000 $\Omega\cdot\text{m}$	5-15 $\Omega\cdot\text{m}$	-----
Acoustic Transit Time (ATT)--Significant increase in transit time.	80 ms/ft	130 ms/ft	-----
Caliper (Cal)--Often shows large variations above the IBPF.	larger	smaller	Relative change, dependent on engineering parameters.
Spontaneous Potential (SP)--Drift from negative to positive below the IBPF.	more negative	more positive	20 to 30 mV shift.
Drilling Rate (DR)--Increased drilling rate is often observed below the IBPF.	slower	faster	Relative rate depending on geologic conditions.
Gas Chromatograph (GC)--Anomalous pressures or a release of free-gas may be detected at base IBPF.	no gas	gas detection	Geologically dependent.
Density (Den)--Increase in recorded densities from above to below the IBPF.	2.1 gm/c ³	2.4 gm/c ³	-----
Neutron Porosity (NP)--Small to no reduction in calculated apparent porosities, often masked by geologic conditions.	25%	22%	-----
Gamma Ray (GR)--Small deflection to higher API values.	lower	higher	5- to 10-API unit deflection.

table II-4) in the Prudhoe Bay oil field, which he also attributed to the presence of ice. He based this interpretation on cores recovered from the BP 12-10-14A well which reportedly contained sandstone and conglomerates that were bounded by ice downward almost to the same depth as suggested by the well logs. Stoneley's (1970) observations of ice-bounded cores represent the only direct evidence that verifies the accuracy of well logs as ice-detection devices. Also, Howitt (1971) noted that the resistivity-log pick for the base of the ice-bearing permafrost in the Put River 19-10-15 well is at the same level as the flexure in the temperature profile representing the base of ice-rich permafrost.

Osterkamp and Payne (1981) examined electrical-resistivity and acoustic-transit-time well logs from 61 wells on the North Slope in order to develop a map of the depth to the base of the deepest ice-bearing permafrost. Their map indicates that the depth to the base of ice-bearing permafrost varies from more than 610 m in the Prudhoe Bay area to 120 m or less in the NPRA. The data used by Osterkamp and Payne (1981) are listed in the last column of table II-4.

INTERPRETATION OF WELL LOGS WITHIN THE ICE-BEARING PERMAFROST SEQUENCE

During drilling of exploratory and production wells on the North Slope, the well bore is surveyed with a series of well-logging devices that can be used to determine the physical state of the pore waters. Logs used in this study included resistivity, acoustic transit time, spontaneous potential, gamma ray, caliper, neutron porosity, density, and the drilling rate and gas chromatograph curves on the mud log. In many wells, the permafrost interval is logged with only one or two of these devices or not logged at all. The lack of well-log data limits the number of North Slope wells from which the base of ice-bearing permafrost can be determined. Each of the 156 wells selected for this project has at least a resistivity survey within the shallow substrate. The electrical-resistivity and acoustic-transit-time well logs were found to be the most useful in detecting the base of the ice-bearing permafrost. However, we do not have independent evidence that the well-log pick for the base of the ice-bearing permafrost is the depth of the actual phase boundary between the ice-bearing and water-saturated strata. Short descriptions of the well-log responses within and below the ice-bearing permafrost, in order of importance, are as follows:

Resistivity (Res)--The base of the ice-bearing permafrost commonly exhibits a substantial resistivity decrease from within to below the ice-bearing permafrost sequence. Ice exhibits relatively high electrical resistivity in comparison to water.

Acoustic transit time (ATT)--A significant transit time change generally marks the base of the ice-bearing permafrost. Ice is characterized by relatively high acoustic velocities in comparison to water.

Caliper (Cal)--The caliper log commonly indicates an enlarged bore hole within the permafrost horizon which can be attributed to caving associated with thawing of ice-bearing sediment.

Spontaneous potential (SP)--The spontaneous potential log generally shows a pronounced drift from negative in the ice-bearing permafrost sequence to positive below the base of ice-bearing permafrost. This drift can be attributed to the increased concentration of the remaining salt particles in the unfrozen pore spaces of the ice.

Drilling rate (DR)--In many wells a significant increase in the drilling rate occurs below the ice-bearing permafrost. Ice-bearing sediments apparently exhibit properties similar to a well-cemented rock unit with a relatively slow drilling rate.

Gas chromatography (GC)--Because of the relatively impermeable nature of the ice-bearing permafrost, free gas can be trapped at its base. This free-gas response was observed in 31 wells.

Density (Den)--The density log shows a slight decrease in density within ice-bearing permafrost relative to the section below. Ice has a lower density than water.

Neutron porosity (NP)--In several wells, the neutron porosity log shows a slightly lower recorded

Table II-4. Depth in meters to base of ice-bearing permafrost (IBPF) as inferred from well-log responses in North Slope wells. These wells (except unnumbered wells) were used to construct contour map of the base of ice-bearing permafrost (fig. II-2).

Well Index	Well Name	Location			API # ^{1]}	IBPF ^{2]} Interpreted	IBPF ^{3]} Corrected	IBPF ^{4]} Osterkamp & Payne (1981)
		Sec.	T.	R.				
1	Simpson Core Test 23	1	19N	11W	5002310002	130	129	
2	Simpson Core Test 24	6	19N	10W	5002310003	122	121	
	Arcon Barrow 1	22	23N	18W	5002310008			280
3°	South Barrow Test Well 3	24	21N.	18W.	5002310011	245	241	
4	South Barrow Test Well 4	14	22N	18W	5002310012	210	206	
5	Iko 1	16	21N	16W	5002320007	177	173	
6	South Barrow Test Well 13	14	22N	18W	5002320008	223	217	
7	South Barrow Test Well 14	25	22N	17W	5002320009	232	226	
8	South Barrow Test Well 17	30	22N	16W	5002320011	197	189	
9	Walakpa 1	9	20N	19W	5002320013	250	244	
10	South Barrow Test Well 20	26	22N	17W	5002320015	229	223	
11	South Barrow Test Well 15	23	22N	17W	5002320016	213	206	
12	South Barrow Test Well 18	24	22N	17W	5002320017	213	208	
13°	Tulageak 1	7	21N	14W	5002320018	174	169	
14	Walakpa 2	31	20N	19W	5002320019	195	190	
15	Prudhoe Bay 1	10	11N	14E	5002920001	575	571	561
16	Sag River 1	4	10N	15E	5002920002	588	583	583
17	Delta State 1	10	10N	15E	5002920004	583	578	583
	Toolik Federal 1	4	8N	15E	5002920005			624
18	Put River 1	27	11N	14E	5002920006	574	569	570
19	Socal 31-25	25	10N	14E	5002920007	557	550	
20	Kuparuk State 1	21	11N	12E	5002920008	520	516	
	Northwest Eileen State 1	28	12N	11E	5002920013			532
21	West Kuparuk 3-11-11	3	11N	11E	5002920014	529	524	529
22	Hemi 3-9-11	3	9N	11E	5002920018	522	521	519
23	Prudhoe Bay Unit J-1	9	11N	13E	5002920020	619	602	615
24	Kad River 1	4	8N	18E	5002920021	488	482	
25	Hurl 5-10-13	5	10N	13E	5002920027	613	607	613
26	Kavearak Point 32-25	25	13N	10E	5002320028	547	541	
27	Lake 79 Federal 1	1	8N	17E	5002920031	461	455	461
28	North Kuparuk 26-12-12	26	12N	12E	5002920032	636	630	462
29	Toolik Federal 2	5	8N	12E	5002920041	457	454	457
	Prudhoe Bay Unit M-1	1	11N	12E	5002920042			553
30	Prudhoe Bay Unit 1-1	8	10N	15E	5002920044	512	500	
31°	North Prudhoe Bay State 1	23	12N	14E	5002920049	560	550	560
32	Toolik Federal 3	4	8N	9E	5002920051	344	340	340
33	Mikkelsen Bay 13-9-19	13	9N	19E	5002920055	625	619	629
34	Kuparuk State 7-11-12	7	11N	12E	5002920062	591	571	
35	Kup Delta 51-1	11	12N	13E	5002920065	551	541	551
36	Milne Point 18-1	11	13N	10E	5002920069	521	512	514
37	Prudhoe Bay Unit 4-1	34	11N	15E	5002920078	579	567	
38°	BP 08-11-13	8	11N	13E	5002920079	591	585	590
39	Prudhoe Bay Unit F-1	2	11N	13E	5002920080	594	589	594
40	West Sak River State 1	2	11N	10E	5002920090	538	530	529
41	Prudhoe Bay Unit H-1	21	11N	13E	5002920099	588	583	591
42	Prudhoe Bay Unit A-1	35	11N	13E	5002920108	530	525	608
43	Prudhoe Bay Unit 4-6	34	10N	15E	5002920111	589	579	579
44	Northwest Eileen State 2	28	12N	11E	5002920117	532	525	
45	Prudhoe Bay Unit C-1	19	11N	14E	5002920121	582	577	575
46	North Franklin Bluffs 1	20	8N	14E	5002920122	512	504	506
47	West Sak River State 2	22	11N	10E	5002920134	487	481	
48	West Sak River State 3	26	11N	9E	5002920139	435	428	427
49	West Sak River State 5	11	10N	10E	5002920141	429	423	424

Table II-4. Depth in meters to base of ice-bearing permafrost (IBPF) as inferred from well-log responses in North Slope wells. These wells (except unnumbered wells) were used to construct contour map of the base of ice-bearing permafrost (fig. II-2).--Continued

Well Index	Well Name	Location			API # ^{1]}	IBPF ^{2]} Interpreted	IBPF ^{3]} Corrected	IBPF ^{4]} Osterkamp & Payne (1981)
		Sec.	T.	R.				
50	West Sak River State 6	29	11N	11E	5002920142	538	531	
51	Foggy Island Bay State 1	19	11N	17E	5002920146	530	522	519
52	Gwydyr Bay South 1	8	12N	13E	5002920149	564	557	
53	Niakuk 1-A	26	12N	15E	5002920156	540	530	532
54	Kuparuk 9-11-12	9	11N	12E	5002920158	568	562	562
55	Prudhoe Bay Unit E-1	6	11N	14E	5002920175	587	578	579
56	Sag Delta 33-12-16	4	11N	16E	5002920176	511	503	503
57	State 1	2	10N	13E	5002920177	576	570	
58	Prudhoe Bay Unit 6-4	2	10N	14E	5002920179	587	580	
59	Kuparuk 30-11-13	30	11N	13E	5002920191	625	618	627
60	Gull Island State 2	28	12N	15E	5002920195	540	534	533
61	Highland State 1	24	11N	11E	5002920199	571	564	549
62	Abel State 1	27	12N	14E	5002920200	558	551	553
63	Prudhoe Bay Unit NGI-7	12	11N	14E	5002920210	562	550	
64*	BP 12-11-13	12	11N	13E	5002920085	613	604	
65	Prudhoe Bay Unit 9-7	2	10N	15E	5002920223	566	554	555
66	Prudhoe Bay Unit 3-6	11	10N	15E	5002920224	601	589	
	Prudhoe Bay Unit G-4	2	10N	14E	5002920225			562
67	Sag Delta 3	35	12N	16E	5002920233	459	451	
68	Sag Delta 2	10	11N	16E	5002920234	575	568	
69	Kuparuk River Unit 1B-5	9	11N	10E	5002920237	505	497	494
70	Point McIntyre 2	16	12N	14E	5002920264	556	550	
71	Kuparuk River Unit 1D-8	23	11N	10E	5002920266	497	487	493
72	West Sak River State B-10	23	10N	9E	5002920267	487	476	
73	West Sak River State 9	3	11N	9E	5002920274	461	454	
74	West Sak River State 11	36	12N	8E	5002920275	468	462	
75	West Mikkelsen State 1	32	10N	19E	5002920278	608	600	
76	Duck Island Unit 1	8	11N	17E	5002920280	415	408	
77	Prudhoe Bay Unit 1-16	8	10N	15E	5002920288	607	597	595
78	Prudhoe Bay Unit 7-6	33	11N	14E	5002920294	589	582	
79	Kuparuk River Unit 1A-8	5	11N	10E	5002920313	480	470	450
80	Prudhoe Bay Unit Q-3	16	11N	13E	5002920322	616	608	
81	Prudhoe Bay Unit 13-2	14	10N	14E	5002920324	596	586	
82	Prudhoe Bay Unit 14-5	9	10N	14E	5002920327	585	573	
83	Reindeer Island STRAT TEST 1	18	13N	15E	5002920342	310	302	
84	West Sak River State 4	7	10N	9E	5002920343	470	462	
85	Niakuk 3	13	12N	15E	5002920350	477	466	
86	Prudhoe Bay Unit TERM-B	20	11N	13E	5002920355	616	608	
87	Prudhoe Bay Unit TERM-C	3	11N	12E	5002920356	604	596	
88	West Mikkelsen Unit 2	13	10N	19E	5002920357	571	560	
89	Gwydyr Bay State 1	9	12N	13E	5002920375	562	555	
90	Milne Point 1	23	13N	10E	502920376	521	510	
91	Prudhoe Bay Unit 12-3	18	10N	15E	5002920377	575	565	
92	Kuparuk River Unit CPF 1(23-9-11)	9	11N	10E	5002920378	547	534	
93	Prudhoe Bay Unit X-1	8	10N	14E	5002920390	549	540	
94	Kuparuk River Unit 1D-1	14	11N	13E	5002920393	516	501	
95	Prudhoe Bay Unit Y-1	34	11N	13E	5002920394	544	535	
96	Gwydyr Bay State Unit 1	2	12N	12E	5002920396	549	543	
97	Prudhoe Bay Unit TERM-A	33	12N	14E	5002920406	571	562	
98	Kuparuk River Unit 1D-5	23	11N	10E	5002920417	537	512	

Table II-4. Depth in meters to base of ice-bearing permafrost (IBPF) as inferred from well-log responses in North Slope wells. These wells (except unnumbered wells) were used to construct contour map of the base of ice-bearing permafrost (fig. II-2).--Continued

Well Index	Well Name	Location			API # ^{1]}	IBPF ^{2]} Interpreted	IBPF ^{3]} /IBPF ^{4]} Corrected	Osterkamp & Payne (1981)
		Sec	T.	R.				
99	West Sak River State 14	19	11N	9E	5002920419	463	454	
100	Nomination 1	34	11N	12E	5002920426	544	536	
101	Kuparuk River Unit 1E-1	16	11N	10E	5002920464	469	455	
102	Kuparuk River Unit 1B-1	9	11N	10E	5002920465	524	495	
103	Prudhoe Bay Unit 17-1	22	10N	15E	5002920476	586	574	
104	Prudhoe Bay Unit 11-4	34	11N	15E	5002920480	586	577	
105	Gwydyr Bay State 2	11	12N	13E	5002920491	571	564	
106	Prudhoe Bay Unit 16-11	24	10N	15E	5002920516	601	590	
107	Sag Delta 7	36	12N	16E	5002920518	444	433	
108	Sag Delta 8	27	12N	16E	5002920519	445	433	
109	Kuparuk River Unit 1C-1	12	11N	10E	5002920526	549	536	
110	Prudhoe Bay Unit TR 15-11-12	9	11N	12E	5002920524	575	565	
111	Sag Delta 5	36	12N	15E	5002920527	531	520	
112	MP Tract (43-31-11-13)	5	10N	13E	5002920536	617	608	
113	West Sak River Unit 16	36	11N	8E	5002920541	507	497	
114	West Sak River Unit 7	26	13N	9E	5002920542	521	512	
115	MP Tract (22-31-11-13)	30	11N	13E	5002920545	631	621	
116	MP Tract (32-30-11-13)	30	11N	13E	5002920546	638	628	
117	Prudhoe Bay Unit TR T-3C	17	11N	15E	5002920555	586	576	
118	Kuparuk River Unit 1C-8	12	11N	10E	5002920585	547	534	
119	West Sak River Unit 23	7	12N	9E	5002920669	472	461	
120	West Staines 1	18	9N	23E	5008920001	605	601	605
121	East Mikkelsen Bay 1	7	9N	21E	5008920002	594	586	
122	Alaska State A-1	27	10N	24E	5008920003	425	416	
123	West Staines State 2	25	9N	22E	5008920004	619	612	613
124	Point Thomson Unit 1	32	10N	23E	5008920005	602	596	
125	Point Thomson Unit 2	3	9N	22E	5008920006	604	598	
126	Point Thomson Unit 3	34	10N	23E	5008920007	555	549	
127	Alaska State C-1	16	9N	23E	5008920011	592	583	
128	Challenge Island 1	8	10N	22E	5008920012	491	483	
129*	Fish Creek 1	15	11N	1E	5010310001	186	182	
130	Colville Delta 1	9	13N	6E	5010320002	564	558	473
131	Cape Halkett 1	5	16N	2W	5010320004	311	304	304
132*	South Harrison Bay 1	6	12N	2E	5010320007	280	274	
133*	Atigaru Point 1	19	14N	2E	5010320008	299	293	293
134	West Fish Creek 1	11	11N	1W	5010320009	123	116	
135	W.T. Foran 1	13	17N	2W	5010320010	116	108	
136*	North Kalikpik 1	3	13N	2W	5010320011	127	120	
137	West Sak River Unit 15	5	10N	8E	5010320013	444	438	
138	West Sak River Unit 20	5	9N	8E	5010320018	418	409	
139	West Sak River Unit 18	16	11N	8E	5010320019	464	455	
140	East Kurupa Unit 1	9	7S	6W	5013720002	148	140	
	Kagrva 1	8	14N	26W	5016320002			207
141	Beli Unit 1	8	4N	23E	5017920002	512	504	
	Kavik Unit 3	8	3N	23E	5017920004			257
142	Canning River Unit B-1	32	4N	34E	5017920006	560	550	
143	Susie Unit 1	22	2N	13E	5022310001	258	253	254
144*	Echooka Unit 1	32	1N	16E	5022320008	261	254	247
145	Aufeis Unit 1	30	3S	11E	5022320010	181	174	
146	Ivishak Unit 1	6	1S	16E	5022320014	294	289	289
	Simpson Core Test 1	10	18N	13W	5027910001			310
147*	Simpson Core Test 13	24	19N	11W	5027910013	221	219	

Table II-4. Depth in meters to base of ice-bearing permafrost (IBPF) as inferred from well-log responses in North Slope wells. These wells (except unnumbered wells) were used to construct contour map of the base of ice-bearing permafrost (fig. II-2).--Continued

Well Index	Well Name	Location			API # ^{1]}	IBPF ^{2]} Interpreted	IBPF ^{3]} Corrected	IBPF ^{4]} Osterkamp & Payne (1981)
		Sec.	T.	R.				
148	Simpson Core Test 17	24	19N	11W	5027910018	91	90	
149	Simpson Core Test 20	18	19N	10W	5027910021	122	119	
150*	J.W. Dalton 1	14	18N	5W	5027920006	276	270	
	Drew Point 1	26	18N	8W	5027920002			247
151	East Simpson 2	23	19N	11W	5027920007	192	187	
	Umiat 1	35	1N	2W	5028710001			335
152	Umiat 2	2	1S	1W	5028710002	320	317	
153*	East Umiat 1	19	1S	2E	5028710016	174	169	
154	Shale Wall Unit 1	2	5S	5E	5028710017	83	79	
155*	Kuparuk Unit 1	1	2S	5E	5028710018	215	211	215
	Kaolak 1	25	7N	34W	5029710001			259
156	East Harrison Bayn State 1	10	13N	8E	5025020001	479	469	

1] American Petroleum Institute well identification number.

2] IBPF measured well-depth interpreted from all logs (this study).

3] IBPF depth corrected to ground surface by subtracting distance between kelly bushing and ground elevation from the interpreted IBPF well-log depth.

4] Wells without Map number were not used to contour.

* Temperatures measured after well bore reached near-thermal equilibrium conditions (see table II-2).

porosity in the ice-bearing permafrost, apparently because of the density difference between ice and water which translates to a hydrogen density difference between a unit saturated with water and one containing ice.

Gamma ray (GR)-- The gamma ray device shows a small deflection from lower values in ice-bearing permafrost to higher values below, apparently because of a high concentration of potassium ions in solution at the freezing front.

Idealized log responses at the base of ice-bearing permafrost are shown in figure II-3 in which a uniform sandstone lithology is assumed; the magnitude of log shifts are summarized in table II-3. The presence of interbedded shales within an ice-bearing permafrost sequence, however, affects the well-log responses, making the interpretation of the depth to the base of the ice-bearing permafrost difficult. The 156 wells and log-determined depths to the base of the ice-bearing permafrost shown on the map in figure II-2 are listed in table II-4.

RELATIONS OF PERMAFROST, ICE-BEARING PERMAFROST, AND ICE-RICH PERMAFROST

Physical factors that control the response of a well log within a stratigraphic section include mineralogy, porosity, temperature, pore fluids, and, of special concern for this study, the physical state of the pore fluids. The ability of a well-log device to indicate presence of ice within a rock mass is dependent on the sensitivity of the device to detect ice and the volume of ice within the rock. Observations made using well logs from the North Slope indicate that a substantially thick wedge of ice-laden strata is present in the Prudhoe Bay area (discussed below). The base of the ice-bearing permafrost in the high-porosity sandstone and conglomerate units of the Prudhoe Bay region is easily detected, and the log responses are similar to the idealized ones (fig. II-3). Here the depth of the 0^o C isotherm is at approximately the same depth as the base of ice-bearing permafrost. However, in many of the wells from the NPRA, in which the shallow, potentially ice-bearing sequences are characterized by siltstone and shale lithologies, the well logs fail to indicate the presence of ice, even though the depth of the 0^o C isotherm commonly extends deep into the lithologic section. Also many of the NPRA well-bore temperature surveys fail to reveal a discontinuity in the near-surface geothermal gradient like that observed in the Prudhoe Bay area. In these wells, either ice does not exist within the permafrost sequence (above the 0^o C isotherm), or the volume of the pore-filling ice and related physical characteristics were such that the well-logging devices did not respond as expected. Shales that have not been deeply buried generally have high porosity and fluid content; however, waters associated with shales are ionically bonded to the clays, preventing the formation of ice (Anderson and others, 1973; Osterkamp and Payne, 1981). Therefore, ice may not exist within a section where clay-rich rocks are found, even though water and sub-0^o C temperatures are present. The thick shale sections present within the shallow substrate of parts of the NPRA may affect pore-filling ice conditions, but currently there is no direct evidence to support this contention.

The lithologic variability that complicates selecting the base of ice-bearing permafrost from well logs is shown for 3 wells located across the North Slope (fig. II-4); each well is represented by a resistivity and gamma-ray log. The resistivity log was selected because of its ability to reveal the presence of ice; the gamma ray curve was used to add relative lithologic and stratigraphic data. The depth of the base of the ice-bearing permafrost, as picked from the well-log data (fig. II-4), was compared to the depth of the 0^o C isotherm.

In section A-A' (fig. II-4), the base of the ice-bearing permafrost has been identified in all 3 wells. In the BP12-10-14A the apparent base of the ice-bearing permafrost is interpreted to be at 562 m, near the base of a long transition zone from resistive to conductive strata. We have used recorded temperature data from 3 nearby wells to estimate the depth of the 0^o C isotherm in BP12-10-14A at 623 m. In South Harrison Bay-1 the base of ice-bearing permafrost is tentatively placed at the resistivity deflection at 275 m. The depth of the 0^o C isotherm is at 375 m. In J.W. Dalton-1 the base of the ice-bearing permafrost at 270 m appears to coincide with a distinct lithologic contact, and the depth of the 0^o C isotherm is at 410 m. The plot of the 0^o C isotherm on cross section A-A' reveals the discrepancy between the well-log pick for the base of the ice-bearing permafrost and the 0^o C equilibrium isotherm. The differences in thickness between these horizons are variable.

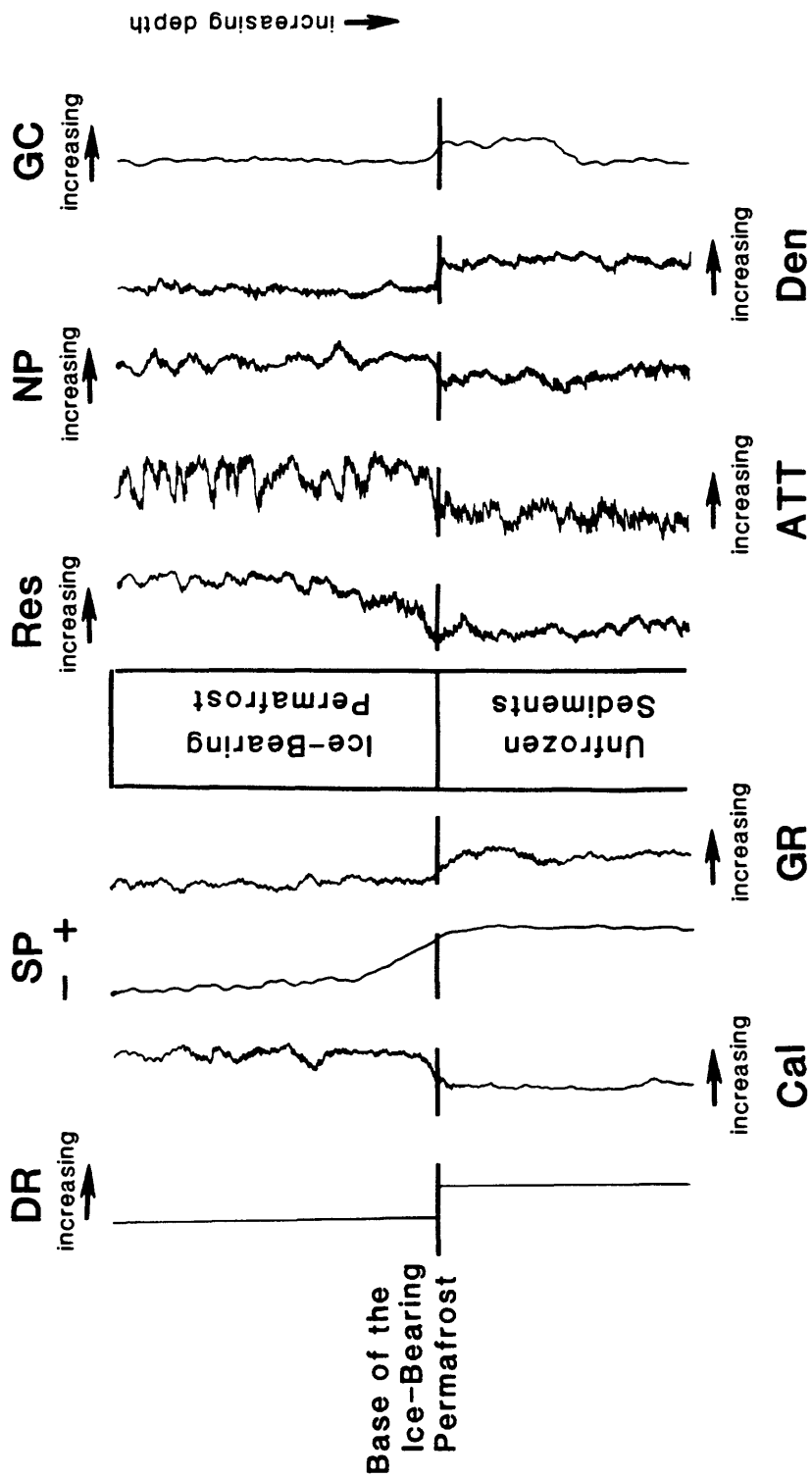


Figure II-3. Idealized log responses at the base of the ice-bearing permafrost assuming uniform sandstone lithology (see table II-3 for description).

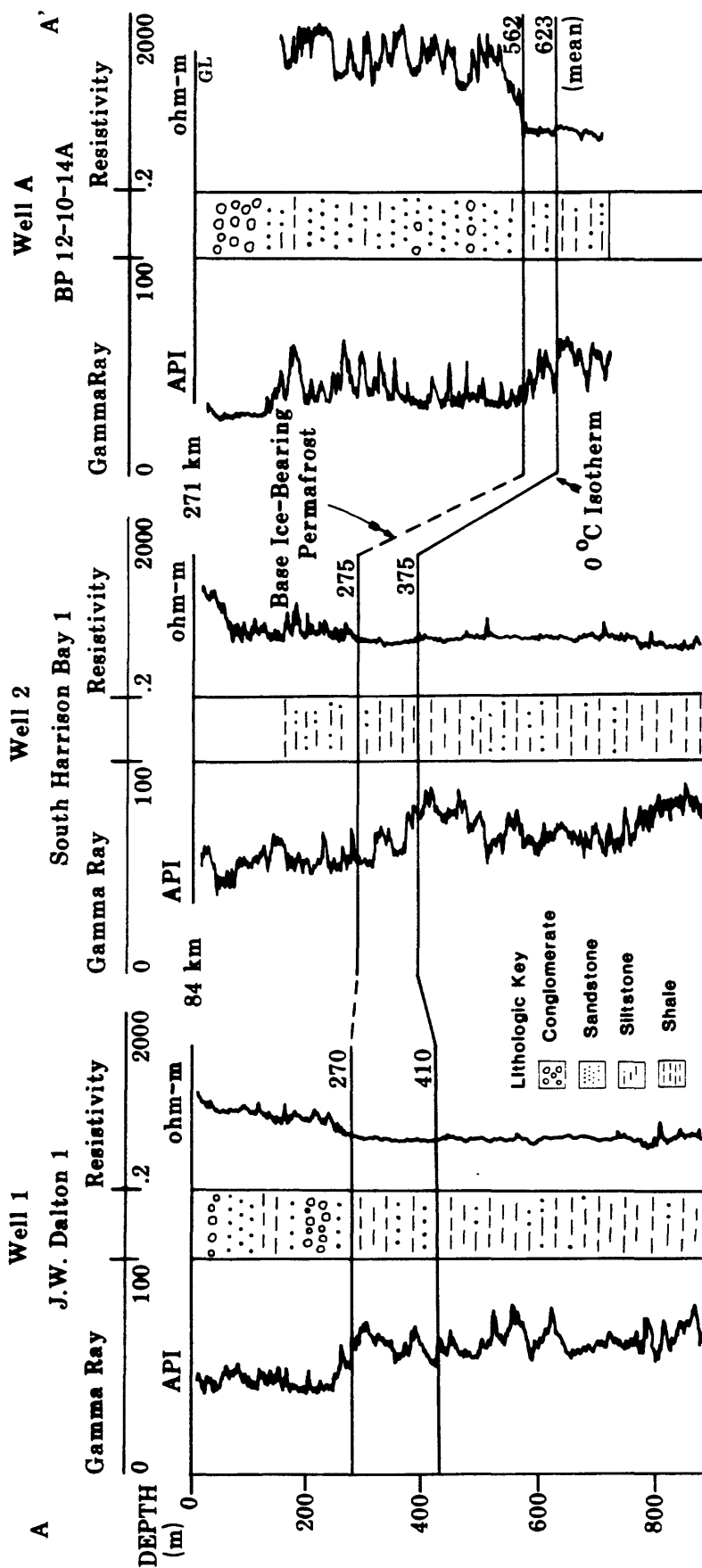


Figure II-4. Selected North Slope wells illustrating relationship of permafrost depth (0°C isotherm), base of ice-bearing permafrost (from resistivity-log response), and generalized interpreted lithologies. Depths measured from ground surface. Ice-bearing permafrost depths from table II-4. Depths of 0°C isotherm from table II-2, except for well A where depth is a mean value determined from 3 nearby wells. Well locations shown on figure II-2.

In BP12-10-14A, this difference is 61 m, but in J.W. Dalton-1, the difference is approximately 140 m. A summary list of all North Slope wells, where comparisons of this type can be made, is shown in table II-5, and, for 7 of the 14 wells the depths to the base of an ice-rich layer (IRL), as interpreted from temperature profiles (Lachenbruch and others, 1982; Lachenbruch and others, 1987), are indicated. BP12-10-14A is not included in table II-5, because the temperature data used to estimate the depth of the 0 °C isotherm was from nearby wells.

ICE-BEARING PERMAFROST THICKNESS

The wells used to map the base of the ice-bearing permafrost were selected on the basis of the quality of the log data and geologic information. Well localities are divided into (1) wells in which depths to the base of ice-bearing permafrost have been obtained (table II-4); (2) wells for which both well-log picks for ice-bearing permafrost and temperature surveys are available (tables II-2, II-4, and II-5); and (3) wells for which temperature profiles but no well-log picks are available (table II-2, not used to determine contours). Of the 46 wells listed in table II-2 only 14 have well-log picks for the base of the ice-bearing permafrost (table II-4), whereas the remaining 31 wells were not logged, or the confidence level was low in the selection of an accurate well-log pick for the base of ice-bearing permafrost.

The depths to the base of the ice-bearing permafrost as selected by Osterkamp and Payne (1981) (table II-4) compare closely with the depths we obtained in our study. However, 12 of 61 wells used by Osterkamp and Payne (1981) were not incorporated into our work because of lack of well data in our study or uncertain reliability of the well logs. In addition to the 49 wells used from Osterkamp and Payne (1981), we have added 107 wells to the data base which allowed us to reduce the contour interval from 200 m, as used by Osterkamp and Payne (1981), to 50 m (fig. II-2).

In the central and south-central parts of the NPRA, no ice-bearing permafrost depths could be determined because of problems in well-log interpretation. The presence of near-surface, thick shale sequences or highly compacted sandstone probably mask the base of the ice-bearing permafrost in the log data.

The pronounced linear trend of the contours (fig. II-2), which follows the coastline from the northeastern part of the NPRA eastward, shows that maximum ice-bearing permafrost thickness occurs a few miles inland from the coast, and the ice-bearing permafrost thins to the north (offshore) and south (onshore). Offshore thinning of the ice-bearing permafrost has been attributed to the presence of the overlying water column of the Arctic Ocean (Lachenbruch, 1957). In the Point Barrow and Cape Simpson areas, ice-bearing permafrost thins toward the south, similar to the situation in the Prudhoe Bay area. However, the suspected offshore thinning is not shown on the map because of the lack of offshore well data. The substantial thinning south and west of the Prudhoe Bay area is attributed to a change in the near-surface geology (Osterkamp and Payne, 1981; Lachenbruch and others, 1982). The shallow substrate of the Prudhoe Bay area is characterized by high porosity, coarse-grained sedimentary rocks that have relatively low geothermal gradients within the permafrost horizon. This low geothermal gradient corresponds to a thick ice-bearing permafrost sequence. Regions to the south and west into NPRA, however, are characterized by finer grained and (or) lower porosity sediments which exhibit relatively high geothermal gradients in the permafrost that correspond to a relatively thin or absent ice-bearing permafrost sequence. In this region, permafrost thickness is also influenced by an increase in mean annual surface temperature of approximately 5° C from Prudhoe Bay to the south into the northern foothills of the Brooks Range (Lachenbruch and others, 1987).

II.A.2. GEOTHERMAL GRADIENT

Accurate information on geothermal gradients is essential for determining the thickness of the gas-hydrate stability zone. On the North Slope, subsurface-temperature data come from high-resolution, equilibrated well-bore surveys in 46 wells, and from estimates based on identification of the base of ice-bearing permafrost in 98 other wells. The geothermal gradient discussion is divided into three sections depending on the source of the data. The first section will describe the history and use of temperature data collected from high-resolution, stabilized well-bore surveys. This section will be followed by a discussion of the use of well-log delineated ice-bearing permafrost depths to evaluate subsurface temperature conditions on the North Slope. The geothermal gradient discussion

Table II-5. North Slope wells in which temperature profiles and diagnostic well logs allow comparison of depths to base of permafrost ($^{\circ}\text{C}$), to base of an ice-rich layer (IRL), and to base of ice-bearing permafrost (IBPF).

Well index	Well name	API No. ^{1]}	Depth to 0 $^{\circ}\text{C}$ ^{2]} (m)	IRL ^{3]} (m)	IBPF ^{4]} (m)
3,F	South Barrow Test Well-3	5002310011	396		241
13,V	Tulageak-1	5002320018	305		169
31,O	ARCO N Prudhoe Bay St-1	5002920049	605	560	550
38,P	BP 08-11-13 (P.B.U. N-1)	5002920079	620	600	585
64,S	BP 12-11-13 (P.B.U. F-3)	5002920085	640	620	604
129,II	Fish Creek-1	5010310001	260	140	182
132,JJ	South Harrison Bay-1	5010320007	375		274
133,KK	Atigaru Point-1	5010320008	405	330	293
136,HH	North Kalikpik-1	5010320011	215		120
144,RR	Mobil Echooka-1	5022320008	280	260	254
147,A	Simpson Core Test-13	5027910013	320		219
150,X	J.W. Dalton-1	5027920006	410	310	270
153,H	East Umiat-1	5028710016	235		169
155,PP	Sinclair/BP Kuparuk-1	5028710018	300		211

1] American Petroleum Institute well identification number.

2] From table II-2.

3] Depth to base of IRL picked from temperature profiles by authors listed in table II-2. If blank, then no value given.

4] Well-log picks from table II-4.

will conclude with a detailed evaluation of both the measured and projected geothermal gradients.

MEASURED TEMPERATURES

Temperature disruptions in the borehole attributed to drilling can be both significant and long lasting. Lachenbruch and Brewer (1959) demonstrated in their analysis of the South Barrow-3 well that drilling operations acted as a positive heat source in the shallow permafrost horizon. This well is located 10 kilometers from the Arctic Coast near Barrow, Alaska, and was drilled to a depth of 884 m. The thermal disturbance at a depth of 181 m decreased from 20 °C to about 0.1 °C in a 6 year period following drilling.

Beginning in 1958, a series of 46 wells (table II-6; figures II-5 and II-6), considered to be in or near thermal equilibrium, have been surveyed with high-resolution temperature devices (MacCarthy, 1952; Brewer, 1958; Ferrians, 1965; Lachenbruch and others, 1982; Lachenbruch and others, 1987). Temperature and geothermal gradient data obtained from these high-resolution surveys are presented in table II-6 where the names of the 46 wells along with API numbers are listed. Data given in tables II-6 and II-7 denoted with the symbol ‡ indicates that the reported information was calculated and presented by other workers, and referenced either in the tables or the text of the report. Data not so marked have been calculated as part of this project.

Most of the published temperature gradients reveal a departure from the generalized temperature profile in the upper 200 m of the well. This departure has been attributed to a recent worldwide warming trend occurring over the last 100 years (Lachenbruch and others, 1982). It is possible, however, to project the undisturbed temperature profiles to the surface from surveyed depths where this warming trend has not affected equilibrium temperature conditions. Temperatures projected to the surface from the recorded high-resolution surveys are listed in column 5 of table II-6, and contoured in figure II-7 (modified from Lachenbruch and others, 1987); appropriate references are listed in column 11 of table II-6.

Depths to the base of the ice-bearing permafrost (discussed earlier) as determined from geophysical well logs for 32 of the 46 temperature-surveyed wells are given in column 6 of table II-6. Ice-bearing permafrost depths for 12 of the 32 wells in table II-6 are from the work presented in table II-5; our confidence level in these 12 well-log picks is high. In addition to these 12 wells, we have made log picks for the base of ice-bearing permafrost in an additional 20 wells (table II-6). These 20 new picks are not shown in tables II-2, II-4 or II-5, and were not used to contour the depth to the base of ice-bearing permafrost in the map of figure II-2. Confidence in these 20 new ice-bearing permafrost well-log picks is relatively low; most picks have been estimated from regional data and from poor quality well logs. The temperature at the base of the ice-bearing permafrost is always 0°C or less, which requires that the depth to the base of the ice-bearing permafrost must coincide with or be shallower than the 0°C isotherm. The base of ice-bearing permafrost, as determined from well logs, does not represent an isotherm. Nevertheless, ice-bearing permafrost depths can be used to project subsurface temperature profiles.

To further evaluate the temperature conditions at the base of the ice-bearing permafrost, the depths of the well-log picks for the base of the ice-bearing permafrost were plotted on the equilibrated temperature-depth profiles for the 32 wells denoted in column 6 of table II-6. The equilibrium temperatures at the base of ice-bearing permafrost as interpreted from these temperature profiles have been listed in column 7 of table II-6 and contoured in figure II-8. Figure II-9 shows the use of the resistivity and gamma-ray well logs and the recorded equilibrium temperature profile from the BP 08-11-13 well to determine the temperature at the base of the ice-bearing permafrost. The depth to the base of the ice-bearing permafrost of 585 m was selected from the resistivity log for this well. The recorded temperature profile indicates that at this depth the base of the ice-bearing permafrost is in equilibrium at a temperature of -0.6°C. As discussed in Collett and others (in press-b) and noted in figure II-8, equilibrium temperatures at the base of the ice-bearing permafrost on the North Slope range from -0.3°C in the Prudhoe Bay area to -4.8°C in the NPRA. Both the mean annual surface temperature map (fig. II-7) and the map of equilibrium temperatures at the base of the ice-bearing permafrost (fig. II-8) are used in this report to project geothermal gradients within the ice-bearing permafrost sequence.

Geothermal gradients needed to predict the depth and thickness of the gas-hydrate stability field can be interpreted directly from recorded equilibrium temperature profiles (table II-6).

Table II-6. Data from high-resolution temperature surveys combined with well-log-determined base of ice-bearing permafrost (IBPF) showing temperatures at that point, geothermal gradients above and below that point, and ratio of the geothermal gradients. Temperature surveys were conducted in wells considered to be in or near thermal equilibrium. Well locations shown on figures II-5 and II-6.

(1) Map Index	(2) Well Name and # and Number	(3) API Number	(4) Depth to 0°C (meters)	(5) Temperature at Surface °C	(6) Depth to Base of IBPF (meters)	(7) Temperature at Base IBPF °C	(8) Geothermal Gradient in IBPF (Gfr)	(9) Geothermal Gradient below IBPF (Gth)	(10) Ratio Gth/Gfr	(11) Source
A	Simpson Core Test 13	5027910013	320‡	-12.0	219	-3.8	3.99‡	3.48	0.87	Brewer, 1958
B	Simpson Core Test 21	5002310001	250‡	-12.0	-	-	5.14‡	5.23	1.02	do.
C	Simpson Core Test 28	5027910026	279‡	-12.0	198	-3.5	4.33‡	4.26	0.98	do.
D	Simpson Core Test 29	5027910027	290‡	-11.5	-	-	4.00‡	-	-	do.
E	South Barrow Test Well 1	5002310009	204‡	-08.8	-	-	4.23‡	-	-	MacCarthy, 1952
F	South Barrow Test Well 3	5002310011	396‡	-12.2	241	-4.8	3.12‡	-	-	do.
G	Umiat 11	5028710011	322‡	-08.0	238	-2.1	2.46	-	-	Ferrians, 1965
H	East Umiat 1	5028710016	235‡	-08.5	169	-2.4	3.62	-	-	do.
I	Topagoruk 1	5027910033	335‡	-10.2	-	-	3.24	-	-	do.
J	Kaolak 1	5029710001	299‡	-10.0	198	-3.4	3.34	-	-	do.
K	BP 33-12-13	5002920047	660‡	-11.4‡	620	-0.7	1.60‡	2.70‡	1.70‡	Lachenbruch and others, 1982
L	BP 04-11-13	5002920025	640‡	-11.1‡	620	-0.4	1.65‡	3.00‡	1.82‡	do.
M	BP 19-10-15	5002920035	595‡	-09.8‡	570	-0.4	1.55‡	2.75‡	1.77‡	do.
N	BP 23-11-13	5002920054	629‡	-11.0‡	605	-0.4	1.75‡	2.75‡	1.57‡	do.
O	ARCO N Prudhoe Bay St 1	5002920049	605‡	-12.0‡	550	-1.2	1.90‡	2.90‡	1.53‡	do.
P	BP 08-11-13	5002920079	620‡	-11.0‡	585	-0.6	1.70‡	3.00‡	1.76‡	do.
Q	BP 31-11-14	5002920059	650‡	-10.6‡	620	-0.5	1.50‡	2.90‡	1.93‡	do.
R	BP 11-11-13	5002920084	640‡	-11.0‡	620	-0.3	1.72‡	3.17‡	1.84‡	do.
S	BP 12-11-13	5002920085	640‡	-11.0‡	604	-0.5	1.72‡	3.11‡	1.81‡	do.
T	BP 27-11-14	5002920006	625‡	-10.7‡	574	-0.9	1.55‡	2.85‡	1.84‡	do.
U	ARCO E Bay St 1	5002920133	625‡	-10.6‡	580	-0.8	1.55‡	2.55‡	1.65‡	do.
V	Tulageak 1	5002320018	305‡	-12.5‡	-	-	4.10‡	4.25	1.04	Lachenbruch and others, 1987
W	West Dease 1	5002320014	280‡	-12.0‡	223	-2.5	4.29‡	4.36	1.02	do.
X	J.W. Dalton 1	5027920006	410‡	-12.0‡	270	-3.9	2.93‡	4.32	1.47	do.
Y	Tumalik 1	5030120001	290‡	-10.4‡	-	-	3.59‡	3.61	1.01	do.
Z	Peard Bay 1	5030120002	310‡	-10.3‡	270	-1.3	3.32‡	2.97	0.90	do.
AA	Kugrua 1	5016320002	282‡	-10.6‡	250	-1.2	3.76‡	3.41	0.91	do.
BB	South Meade 1	5016320001	200‡	-10.2‡	160	-2.0	5.10‡	4.21	0.83	do.
CC	Kuyanak 1	5016320003	330‡	-10.9‡	-	-	3.30‡	3.81	1.16	do.
DD	East Simpson 1	5027920005	370‡	-11.0‡	259	-3.3	2.97‡	3.52	1.19	do.
EE	Ikpikpak 1	5027920004	340‡	-10.6‡	280	-1.9	3.12‡	2.74	0.89	do.
FF	Drew Point 1	5027920002	325‡	-11.3‡	250	-2.6	3.48‡	4.08	1.17	do.
GG	East Teshekpuk 1	5010320006	265‡	-11.5‡	-	-	4.34‡	4.20	0.97	do.
HH	North Kalikpak 1	5010320011	215‡	-11.3‡	-	-	5.26‡	4.69	0.89	do.
II	Fish Creek 1	5010310001	260‡	-11.6‡	182	-3.5	4.46‡	3.89	0.87	do.
JJ	South Harrison Bay 1	5010320007	375‡	-11.4‡	274	-3.1	3.04‡	-	-	do.
KK	Atigaru Point 1	5010320008	405‡	-10.8‡	293	-3.0	2.67‡	5.24	1.96	do.
LL	Awuna 1	5015520001	295‡	-09.0‡	177	-3.6	3.05‡	3.03	0.99	do.
MM	Lisburne 1	5013720003	290‡	-06.2‡	-	-	2.14‡	2.14	1.00	do.
NN	Kohuktak 1	5011920001	290‡	-09.3‡	-	-	3.20‡	3.26	1.02	do.
OO	Seabee Test Well 1	5028720007	310‡	-08.9‡	-	-	2.87‡	1.64	0.57	do.
PP	Kuparuk 1	5028710018	300‡	-08.8‡	211	-2.6	2.93‡	2.74	0.94	do.
QQ	Lupine 1	5022320011	240‡	-04.6‡	-	-	1.92‡	1.92	1.00	do.
RR	Echocka 1	5022320008	280‡	-06.6‡	254	-0.6	2.36‡	2.11	0.89	do.
SS	Canning River A-1	5017920005	282‡	-08.3‡	-	-	2.94‡	2.98	1.01	do.
TT	Umiat 9	5028710009	356‡	-08.6‡	-	-	2.40‡	-	-	do.

(3) American Petroleum Institute unique well identification number (Alaskan Oil and Gas Conservation Commission, 3001 Porcupine Drive, Anchorage, Alaska, 99501).

(4) Depth from surface.

(5) Temperatures projected from the recorded well profiles.

(6) Depth from surface (Collett and others, in press - a).

(11) Data source (See References Cited).

(IBPF) Ice-Bearing Permafrost.

(‡) Data reported by referenced authors in column 11.

(-) No data

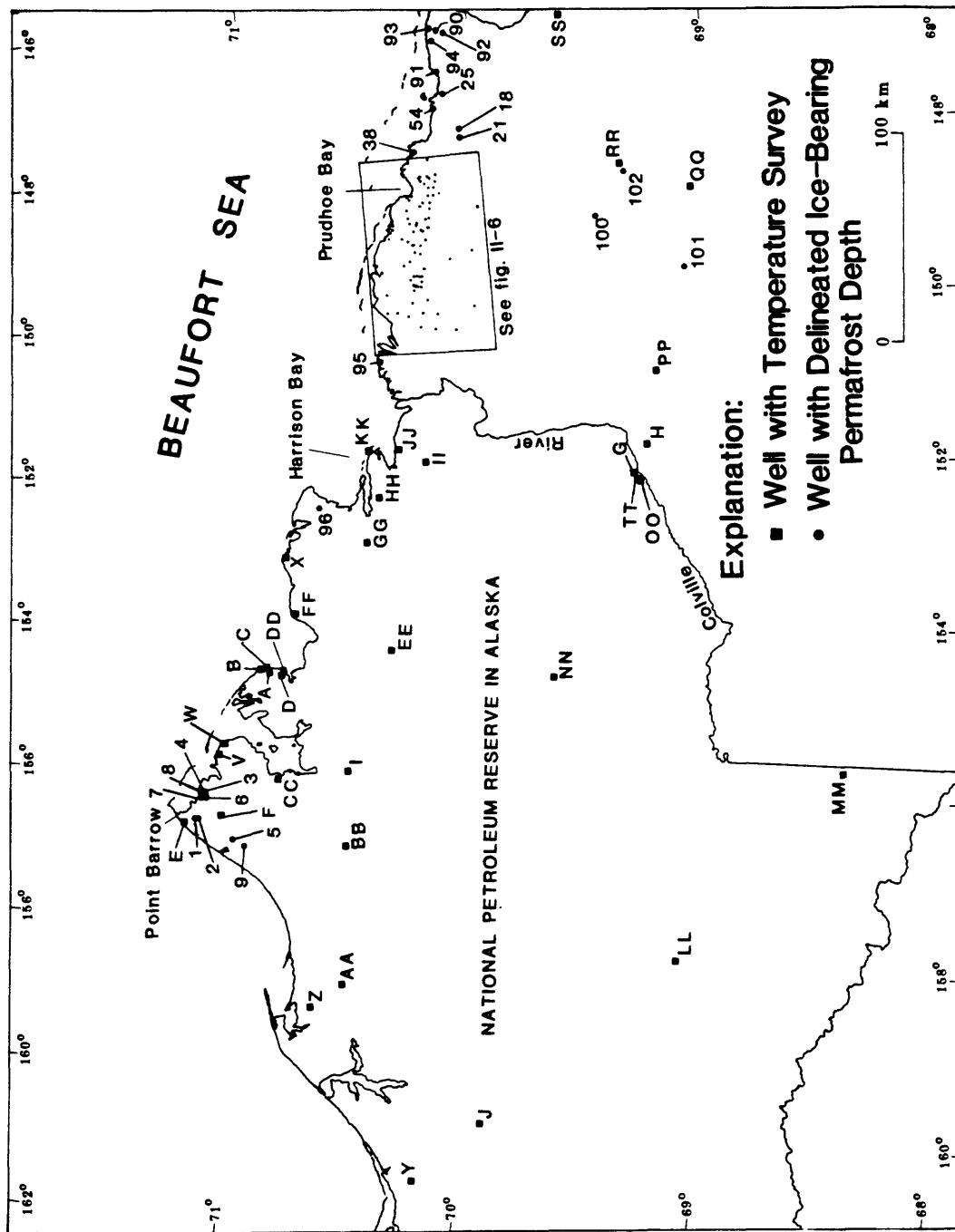
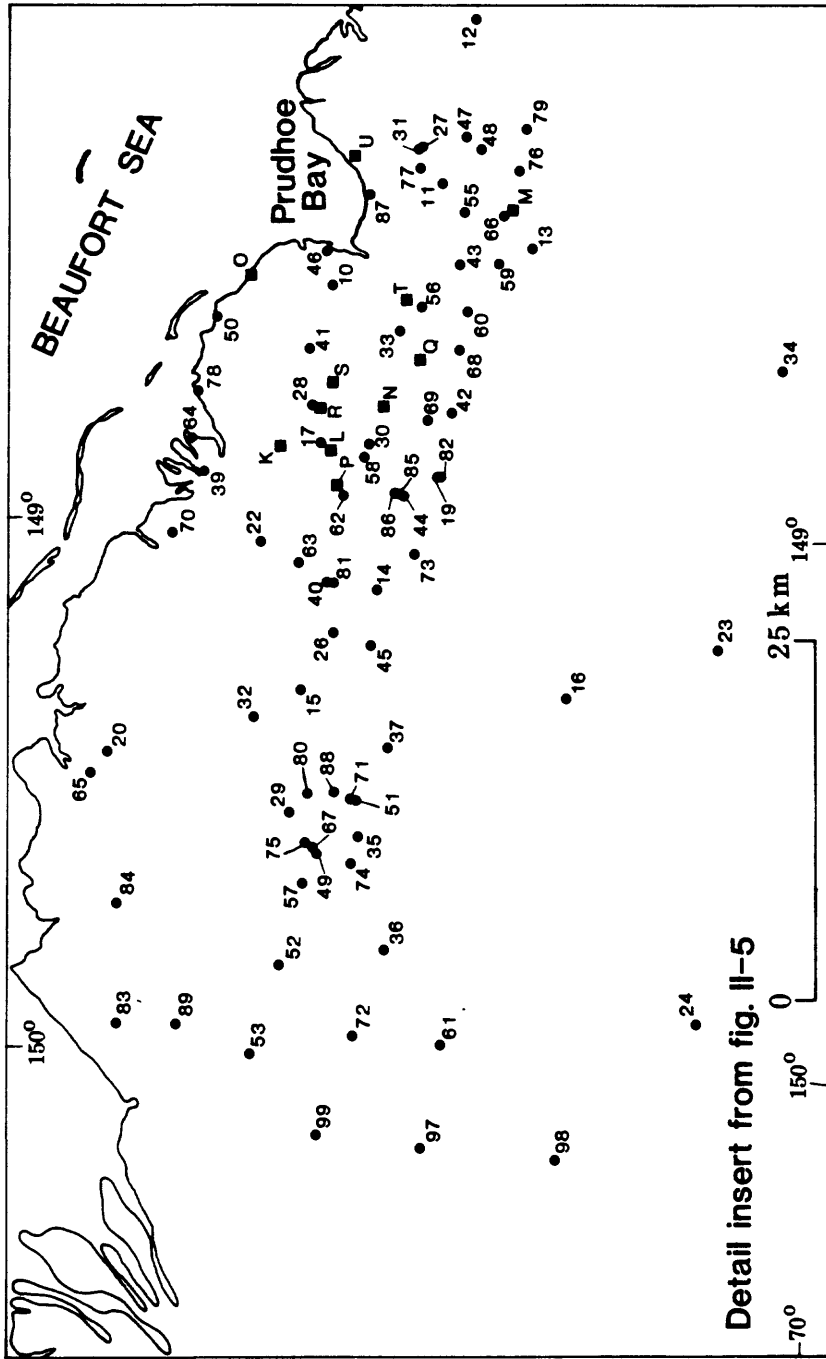


Figure II-5. Locations of North Slope wells in which subsurface temperature data have been acquired within the permafrost sequence. Data for these wells are listed in table II-6.



Detail insert from fig. II-5

Figure II-6. Detail insert of base-map in figure II-5.

Table II-7. North Slope wells with our log-determined base of ice-bearing permafrost (IBPF) in which we have estimated temperatures and geothermal gradients from regional North Slope trends estimated by 46 wells with high-resolution temperature surveys (table II-6, figures II-7, II-8, II-10, II-11, and II-12). Well locations shown in figures II-5 and II-6.

(1) Map No.	(2) Well Name and #	(3) Sec. Location T. R.	(4) API #	(5) Depth of IBPF (meters)	(6) Interpolated T _o at Surface °C	(7) Interpolated T _o at base IBPF °C	(8) Ratio Gtb/Gfr	(9) Projected Geothermal Gradient in IBPF (Gfr)	(10) Projected Geothermal Gradient below IBPF (Gtb)
1.	South Barrow 4	14 22N 18W	5002310012	206	-12	-4.5	1.1	3.64	4.00
2.	South Barrow 13	14 22N 18W	5002320008	217	-12	-4.5	1.1	3.46	3.81
3.	South Barrow 14	25 22N 17W	5002320009	226	-12	-4.5	1.1	3.32	3.65
4.	South Barrow 17	30 20N 16W	5002320011	189	-12	-4.5	1.1	3.97	4.37
5.	Walatpa 1	9 20N 19W	5002320013	244	-12	-4.5	1.1	3.07	3.38
6.	South Barrow 20	26 22N 17W	5002320015	223	-12	-4.5	1.1	3.36	3.70
7.	South Barrow 15	23 22N 17W	5002320016	206	-12	-4.5	1.1	3.64	4.00
8.	South Barrow 18	24 22N 17W	5002320017	208	-12	-4.5	1.1	3.59	3.95
9.	Walatpa 2	31 20N 19W	5002320019	190	-12	-4.0	1.1	4.21	4.63
10.	Pudhoe Bay 1	10 11N 14E	5002920001	571	-11	-0.5	1.7	1.84	3.13
11.	Sag River 1	4 10N 15E	5002920002	583	-11	-1.0	1.7	1.80	3.06
12.	Delta State 1	10 10N 15E	5002920004	578	-11	-1.0	1.7	1.73	2.94
13.	Socak 31-25	25 10N 14E	5002920007	516	-11	-1.0	1.6	1.82	2.91
14.	Kuparuk State 1	21 11N 12E	5002920008	516	-11	-0.5	1.8	2.03	3.65
15.	West Kuparuk 3-11-11	3 11N 11E	5002920014	524	-11	-0.5	1.8	2.00	3.60
16.	Hemi 3-9-11	3 9N 11E	5002920018	521	-11	-1.0	1.4	1.92	2.69
17.	Pudhoe Bay Unit J-1	9 11N 13E	5002920020	602	-11	-0.5	1.8	1.74	3.13
18.	Kad River 1	4 8N 18E	5002920021	482	-10	-1.5	1.7	1.76	2.99
19.	Hurt 5-10-13	5 10N 13E	5002920027	607	-11	-1.0	1.5	2.03	2.48
20.	Kavearak Point 32-25	25 13N 10E	5002920028	541	-12	-1.0	1.9	2.03	2.48
21.	Lake 79 Federal 1	1 8N 17E	5002920031	455	-10	-1.5	1.7	1.87	3.18
22.	North Kuparuk 26-12-12	26 12N 12E	5002920032	630	-11	-0.5	1.8	1.67	3.01
23.	Tootlik Federal 2	5 8N 12E	5002920041	454	-10	-1.5	1.2	1.87	2.24
24.	Tootlik Federal 3	4 8N 9E	5002920051	340	-10	-1.5	1.4	2.50	3.50
25.	Mikkelsen Bay 13-9-19	13 9N 19E	5002920055	619	-11	-1.5	1.7	1.53	2.60
26.	Kuparuk State 7-11-12	7 11N 12E	5002920062	571	-11	-0.5	1.8	1.84	3.31
27.	Pudhoe Bay Drill Site 4-1	34 11N 15E	5002920078	567	-11	-0.5	1.7	1.85	3.15
28.	Pudhoe Bay Unit F-1	2 11N 13E	5002920080	589	-11	-0.5	1.8	1.78	3.20
29.	West Sak River State 1	2 11N 10E	5002920090	530	-11	-1.0	1.8	1.89	3.40
30.	Pudhoe Bay Unit H-1	21 11N 13E	5002920099	583	-11	-0.5	1.8	1.80	3.24
31.	Pudhoe Bay Drill Site 4-6	34 10N 15E	5002920111	579	-11	-0.5	1.7	1.81	3.08
32.	Northwest Eileen State 2	28 12N 11E	5002920117	525	-11	-1.0	1.7	1.91	3.25
33.	Pudhoe Bay Unit C-1	19 11N 14E	5002920121	577	-11	-0.5	1.7	1.82	3.09
34.	North Franklin Bluffs 1	20 8N 14E	5002920122	504	-11	-1.5	1.8	1.69	3.04
35.	West Sak River State 2	22 11N 10E	5002920134	481	-11	-1.0	1.7	2.08	3.54
36.	West Sak River State 3	26 11N 9E	5002920139	428	-11	-1.0	1.7	2.34	3.98
37.	West Sak River State 6	29 11N 11E	5002920142	531	-11	-1.0	1.7	1.88	3.20
38.	Foggy Bay State 1	19 11N 17E	5002920146	522	-12	-1.0	1.6	2.11	3.38
39.	Gwydyr Bay South 1	8 12N 13E	5002920149	557	-12	-1.0	1.7	1.97	3.35
40.	Kuparuk 9-11-12	9 11N 12E	5002920158	562	-11	-0.5	1.8	1.87	3.37
41.	Pudhoe Bay Unit E-2	6 11N 14E	5002920175	578	-11	-0.5	1.7	1.82	3.09
42.	State 1	2 10N 13E	5002920177	570	-11	-1.0	1.3	1.76	2.29
43.	Pudhoe Bay Drill Site 6-4	2 10N 14E	5002920179	580	-11	-0.5	1.7	1.81	3.08

Table II-7. North Slope wells with our log-determined base of ice-bearing permafrost (IBPF) in which we have estimated temperatures and geothermal gradients from regional North Slope trends estimated by 46 wells with high-resolution temperature surveys (table II-6, figures II-7, II-8, II-10, II-11, and II-12). Well locations shown in figures II-5 and II-6.—Continued

(1) Map No.	(2) Well Name and #	(3) Sec. Location T.	(4) R. API #	(5) Depth of IBPF (meters)	(6) Interpolated T _o at Surface °C	(7) Interpolated T _o at base of IBPF °C	(8) Ratio CtH/GtH	(9) Projected Geothermal Gradient in IBPF (Gfr)	(10) Projected Geothermal Gradient below IBPF (Gth)
44.	Kuparuk 30-11-13	30	11N 13E	5002920191	-11	-1.0	1.6	1.62	2.59
45.	Highland State 1	24	11N 11E	5002920199	-11	-1.0	1.7	1.77	3.01
46.	Pudhoe Bay Unit NGI-7	12	11N 14E	5002920210	-12	-0.5	1.7	1.91	3.25
47.	Pudhoe Bay Drill Site 9-7	47	2 10N 15E	5002920223	-11	-1.0	1.7	1.80	3.06
48.	Pudhoe Bay Drill Site 3-6	11	10N 15E	5002920224	-11	-1.0	1.7	1.70	2.89
49.	Kuparuk River Unit 1B-5	9	11N 10E	5002920237	-11	-1.0	1.7	2.01	3.42
50.	Point McIntyre 2	16	12N 14E	5002920264	-12	-1.0	1.6	2.00	3.20
51.	Kuparuk River Unit 1D-8	23	11N 10E	5002920266	-11	-1.0	1.7	2.06	3.50
52.	West Sak 25645 9	3	11N 9E	5002920274	-11	-1.0	1.8	2.20	3.96
53.	West Sak 25548 11	36	12N 8E	5002920275	-11	-1.0	1.7	2.17	3.69
54.	West Mikkelsen State 1	32	10N 19E	5002920278	-12	-1.5	1.9	1.75	3.33
55.	Pudhoe Bay Drill Site 1-16	55	8 10N 15E	5002920288	-11	-1.0	1.6	1.68	2.69
56.	Pudhoe Bay Drill Site 7-6	33	11N 14E	5002920294	-11	-0.5	1.6	1.80	2.88
57.	Kuparuk River Unit A-8	5	11N 10E	5002920313	-11	-1.0	1.7	2.13	3.62
58.	Pudhoe Bay Unit Q-3	16	11N 13E	5002920322	-11	-0.5	1.8	1.73	3.11
59.	Pudhoe Bay Drill Site 13-2	14	10N 14E	5002920324	-11	-1.0	1.6	1.71	2.74
60.	Pudhoe Bay Drill Site 14-5	9	10N 14E	5002920327	-11	-1.0	1.6	1.75	2.80
61.	West Sak 25667 4	7	10N 9E	5002920343	-11	-1.5	1.5	2.06	3.09
62.	Pudhoe Bay Unit TERM B	20	11N 13E	5002920355	-11	-0.5	1.8	1.73	3.11
63.	Pudhoe Bay Unit TERM C	3	11N 12E	5002920356	-11	-0.5	1.8	1.76	3.17
64.	Gwydyr Bay State 1	9	12N 13E	5002920375	-12	-1.0	1.7	1.98	3.37
65.	Milne Point 1	23	13N 10E	5002920376	-12	-1.0	1.9	2.16	4.10
66.	Pudhoe Bay Drill Site 12-3	18	10N 15E	5002920377	-11	-1.0	1.7	1.77	3.01
67.	CPF 1(23-9-11-10)	9	11N 10E	5002920378	-11	-1.0	1.8	1.87	3.37
68.	Pudhoe Bay Unit X-1	8	10N 14E	5002920390	-11	-1.0	1.4	1.85	2.59
69.	Pudhoe Bay Unit Y-1	34	11N 13E	5002920394	-11	-1.0	1.4	1.87	2.62
70.	Gwydyr Bay State Unit 1	2	12N 12E	5002920396	-12	-1.0	1.7	1.84	3.13
71.	Kuparuk River Unit 1D-5	71	11N 10E	5002920417	-11	-1.0	1.7	1.95	3.32
72.	West Sak 25655 14	19	11N 9E	5002920419	-11	-1.0	1.7	2.20	3.74
73.	Nomination 1	34	11N 12E	5002920426	-11	-0.5	1.6	1.96	3.14
74.	Kuparuk River Unit 1E-1	16	11N 10E	5002920464	-11	-1.0	1.7	2.20	3.74
75.	Kuparuk River Unit 1B-1	9	11N 10E	5002920465	-11	-1.0	1.8	2.02	3.64
76.	Pudhoe Bay Drill Site 17-1	22	10N 15E	5002920476	-11	-1.0	1.7	1.74	2.96
77.	Pudhoe Bay Drill Site 11-4	34	11N 15E	5002920480	-11	-0.5	1.7	1.82	3.09
78.	Gwydyr Bay State 2	11	12N 13E	5002920491	-12	-1.0	1.6	2.04	3.26
79.	Pudhoe Bay Drill Site 16-11	24	10N 15E	5002920516	-11	-1.0	1.7	1.69	2.87
80.	Kuparuk River Unit 1C-1	12	11N 10E	5002920526	-11	-1.0	1.8	1.87	3.37
81.	Pudhoe Bay Unit TR 15-11-12	9	11N 12E	5002920524	-11	-0.5	1.8	1.86	3.35
82.	MP Tract (43-31-11-13)	5	10N 13E	5002920536	-11	-1.0	1.6	1.65	2.64
83.	West Sak 25523 16	36	11N 8E	5002920541	-11	-1.0	2.0	2.01	4.02
84.	West Sak 25519 17	26	13N 9E	5002920542	-11	-1.0	2.0	1.95	3.90
85.	MP Tract (22-31-11-13)	30	11N 13E	5002920545	-11	-0.5	1.8	1.69	3.04
86.	MP Tract (32-30-11-13)	30	11N 13E	5002920546	-11	-0.5	1.7	1.67	2.84

Table II-7. North Slope wells with our log-determined base of ice-bearing permafrost (IBPF) in which we have estimated temperatures and geothermal gradients from regional North Slope trends estimated by 46 wells with high-resolution temperature surveys (table II-6, figures II-7, II-8, II-10, II-11, and II-12). Well locations shown in figures II-5 and II-6.-Continued

(1) Map No.	(2) Well Name and #	(3) Location Sec. T. R.	(4) API #	(5) Depth of IBPF (meters)	(6) Interpolated T° at Surface °C	(7) Interpolated T° at base IBPF °C	(8) Ratio GtH/GtF	(9) Projected Geothermal Gradient in IBPF (GtF)	(10) Projected Geothermal Gradient below IBPF (GtH)
87.	Prudhoe Bay Unit TR T-3C	17 11N 15E	5002920555	576	-11	-0.5	1.7	1.82	3.09
88.	Kuparuk River Unit 1C-8	12 11N 10E	5002920585	534	-11	-1.0	1.8	1.87	3.37
89.	West Sak 25631 23	7 12N 9E	5002920669	461	-11	-1.0	1.9	2.17	4.12
90.	West Staines 1	18 9N 23E	5008920001	601	-11	-1.0	1.7	1.66	2.82
91.	East Mikkelsen Bay 1	7 9N 21E	5008920002	586	-11	-1.0	1.7	1.71	2.91
92.	West Staines Suite 2	25 9N 24E	5008920004	612	-11	-1.0	1.7	1.63	2.77
93.	Point Thomson Unit 1	32 10N 23E	5008920005	596	-12	-1.0	1.7	1.85	3.15
94.	Point Thomson Unit 2	3 9N 22E	5008920006	598	-11	-1.0	1.7	1.67	2.84
95.	Colville Delta 1	9 13N 6E	5010320002	558	-12	-1.5	2.0	1.88	3.76
96.	Cape Hallett 1	5 16N 2W	5010320004	304	-12	-3.5	1.7	2.80	4.76
97.	West Sak 25590 15	5 10N 8E	5010320013	438	-11	-1.5	1.5	2.17	3.26
98.	West Sak 25618 20	5 9N 8E	5010320018	409	-11	-1.5	1.4	2.32	3.25
99.	West Sak 25571 18	16 11N 8E	5010320019	455	-11	-1.5	1.6	2.09	3.34
100.	Susie Unit 1	22 2N 13E	5022310001	253	-8	-1.0	1.1	2.77	3.05
101.	Aufais Unit 1	30 3S 11E	5022320010	174	-6	-1.5	1.0	2.59	2.59
102.	Ivishuk Unit 1	6 1S 16E	5022320014	289	-7	-1.0	1.0	2.08	2.08

(4) Well API number: American Petroleum Institute unique well identification number (Alaska Oil and Gas Conservation Commission, 3001 Percepigne Drive, Anchorage, Alaska, 99501)

(5) Depths measured from ground level to the base of the ice-bearing permafrost (IBPF); (Collet and others, in press-a).

(6) Values interpolated from the map in figure II-7.

(7) Values interpolated from the map in figure II-8.

(8) Values interpolated from the map in figure II-12.

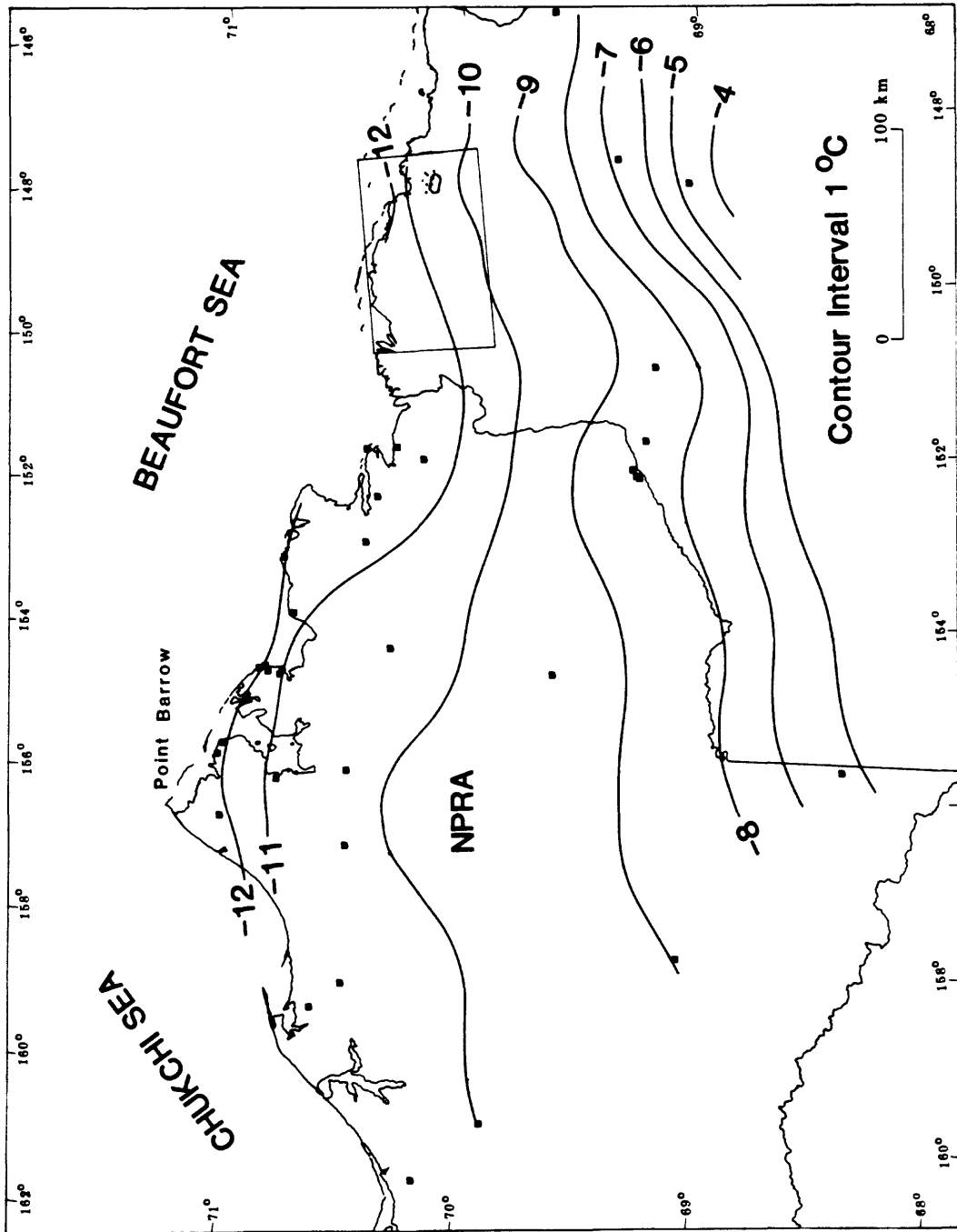


Figure II-7. Contour map of projected undisturbed surface temperatures ($^{\circ}\text{C}$) in the central North Slope (modified from Lachenbruch and others, 1987).

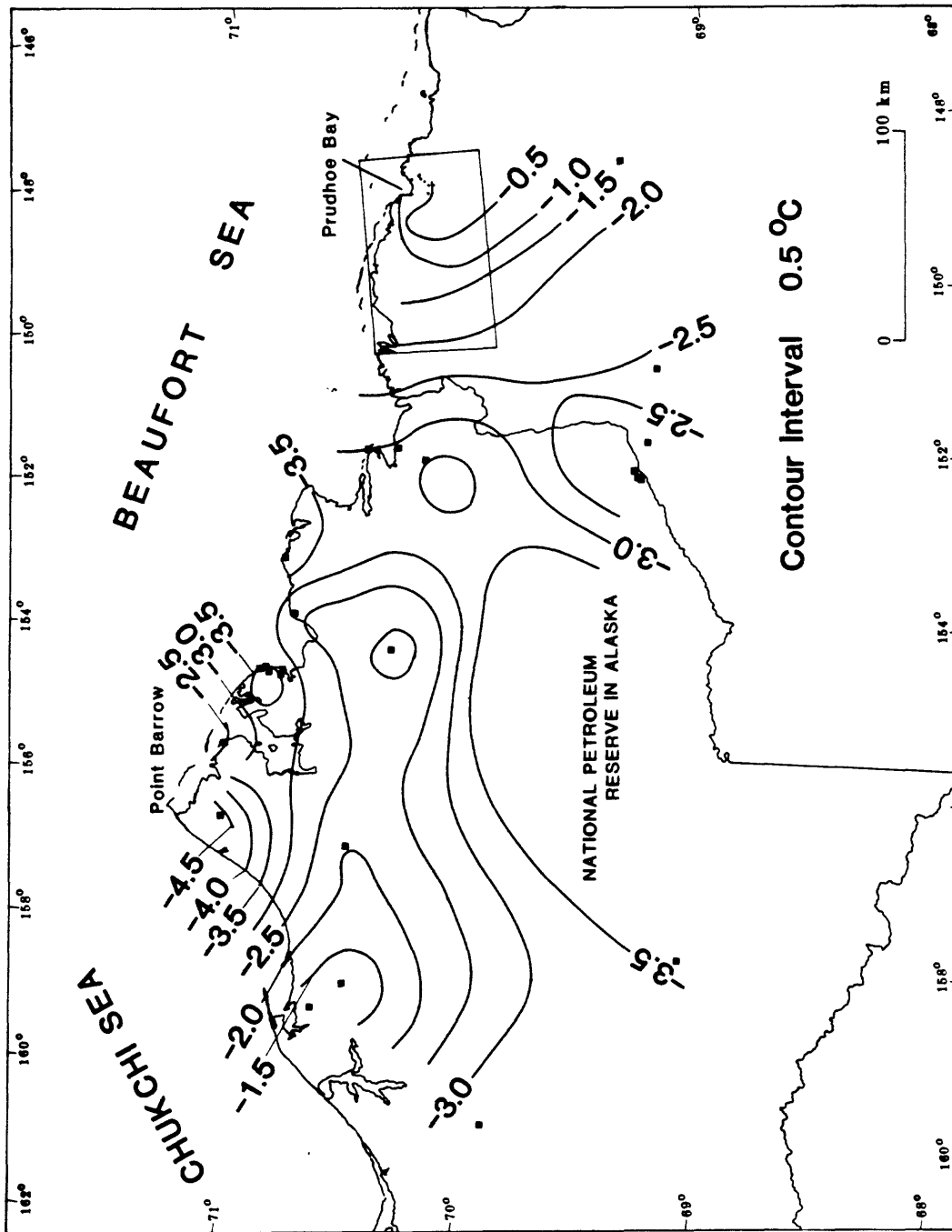


Figure II-8. Contour map of temperature ($^{\circ}\text{C}$) at the log-determined base of ice-bearing permafrost for the central North Slope. Wells identified in figures II-5 and II-6; temperature data tabulated in table II-6; method of determining temperature at base of ice-bearing permafrost illustrated in figure II-9.

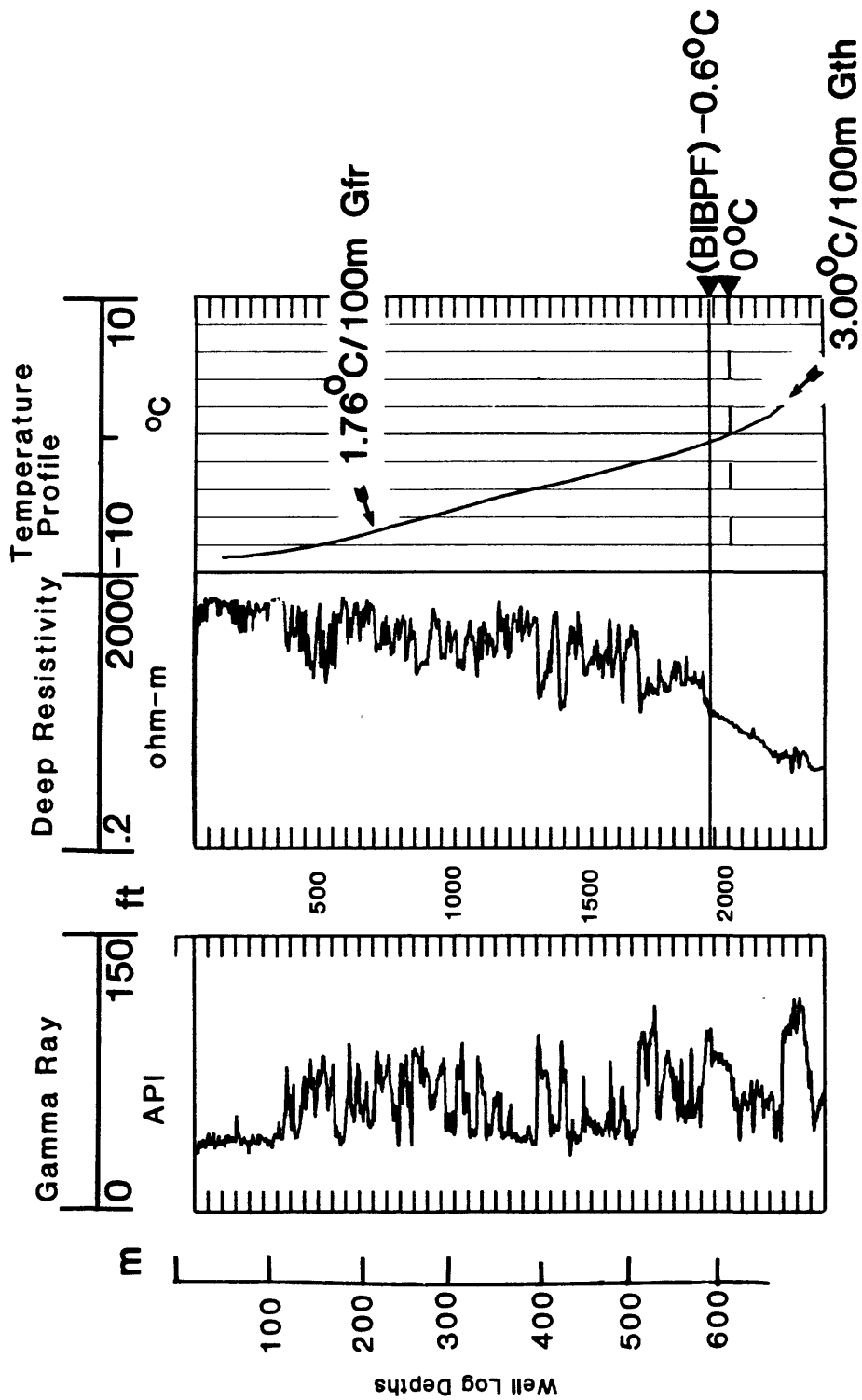


Figure II-9. Well logs from the BP 08-11-13 well (well P, table II-6) and recorded temperature profile from Lachenbruch and others, 1982. Base of ice-bearing permafrost is determined from the resistivity log at 585 m (measured from surface) where temperature is -0.6°C . Depth of the 0°C isotherm is 35 m deeper at 620 m. Lachenbruch and others (1982) calculate a geothermal gradient of $1.76^{\circ}\text{C}/100\text{m}$ in the permafrost interval and $3.00^{\circ}\text{C}/100\text{m}$ below the permafrost interval.

Geothermal gradients calculated from the temperature surveys within the ice-bearing permafrost section are listed in column 8 of table II-6 and presented along with projected geothermal gradients (to be discussed later) in figure II-10. Geothermal gradients below the base of the ice-bearing permafrost are listed in column 9 of table II-6 and contoured with 102 projected geothermal gradients in figure II-11. Nine of the 46 surveyed wells have no geothermal gradients reported below the base of the ice-bearing permafrost because of insufficient survey depths. In addition, the measured geothermal gradients noted in column 8 of table II-6 for Simpson Core Test-21 and East Simpson-1 were not used to contour the geothermal gradient in the ice-bearing permafrost sequence in figure II-10 due to regional discontinuities in the reported values.

Lachenbruch and others (1982) pointed out that the geothermal gradient changes abruptly at the base of the ice-bearing permafrost due to a change in thermal conductivity resulting from pores filled with ice in the ice-bearing permafrost sequence to pores filled with water below the base of ice-bearing permafrost. This change in the geothermal gradient can be seen by comparing the gradients listed in columns 8 and 9 of table II-6. The regional variation in the change of thermal conductivity from above to below the base of the ice-bearing permafrost can also be observed by comparing maps in figures II-10 and II-11. The ratios between the geothermal gradients from below the base of the ice-bearing permafrost (G_{th}) (column 9, table II-6) over the geothermal gradients from above the base of the ice-bearing permafrost (G_{fr}) (column 8, table II-6) are given in column 10 of table II-6 and contoured in figure II-12. This ratio (G_{th}/G_{fr}) represents the variation in the geothermal gradient from within to below the ice-bearing permafrost, and the map in figure II-12 shows that the ratio varies from values as low as 1 in NPRA to approximately 2 near Harrison Bay. Thus the geothermal gradient below and above the base of the ice-bearing permafrost is the same for much of NPRA; however, in the Harrison Bay region the geothermal gradient below the base of the ice-bearing permafrost may be two times greater than the geothermal gradient within the ice-bearing permafrost sequence. For 11 of the ratios listed in table II-6 the calculated values are less than 1. In theory, the geothermal gradient within the ice-bearing sequence should be lower than the geothermal gradient below the base of the ice-bearing permafrost if there is no change in lithology (uniform rock thermal conductivity). Therefore, no ratio less than 1 should exist. The reported values less than 1 generally range from 0.89 to 0.99 with one value of 0.57. The relative nearness of ten of these ratios to 1, and the locations of most of these eleven sites in the NPRA suggest that the geothermal gradient both above and below the base of the ice-bearing permafrost sequence are approximately the same in these wells. This variation in the reported values is possibly due to inconsistencies in the data and gradient calculations.

The high resolution temperature surveys have provided 39 geothermal gradients within the ice-bearing sequence and 35 gradients below the base of the ice-bearing permafrost. Thus a total of 74 geothermal gradient values are considered reliable. In addition, the recorded temperature profiles have been used to project mean annual surface temperatures, base of ice-bearing permafrost equilibrium temperatures, and ratios between the geothermal gradients from above to below the base of the ice-bearing permafrost sequence across the North Slope. However, specific evaluation of subsurface temperature conditions at any one particular site on the North Slope is difficult and subject to error because of the vastness of the study area and the limited number of equilibrated well-bore temperature surveys. Nevertheless, the temperature data obtained from the high-resolution surveys and known ice-bearing permafrost depths will be used in the next section of this report to project geothermal gradients within the near-surface sediment package.

PROJECTED TEMPERATURES

A method of evaluating local geothermal gradients has been developed (Collett and others, in press-a). This method uses known ice-bearing permafrost depths and regional temperature constants derived from stabilized well-bore temperature surveys (table II-6; figures II-7, II-8, and II-12). To refine the resolution of the geothermal gradient data for the North Slope, a series of well-log picks for the base of the ice-bearing permafrost from 102 wells have been used to extrapolate temperature data (table II-7). In column 5 of table II-7 are the depths to the base of the ice-bearing permafrost as determined from well logs. The maps in figures II-7, II-8, and II-12 have been used to interpolate regional constants at each well for the equilibrium surface temperatures (column 6, table II-7), temperatures at the base of ice-bearing permafrost (column 7, table II-7), and the ratios between the

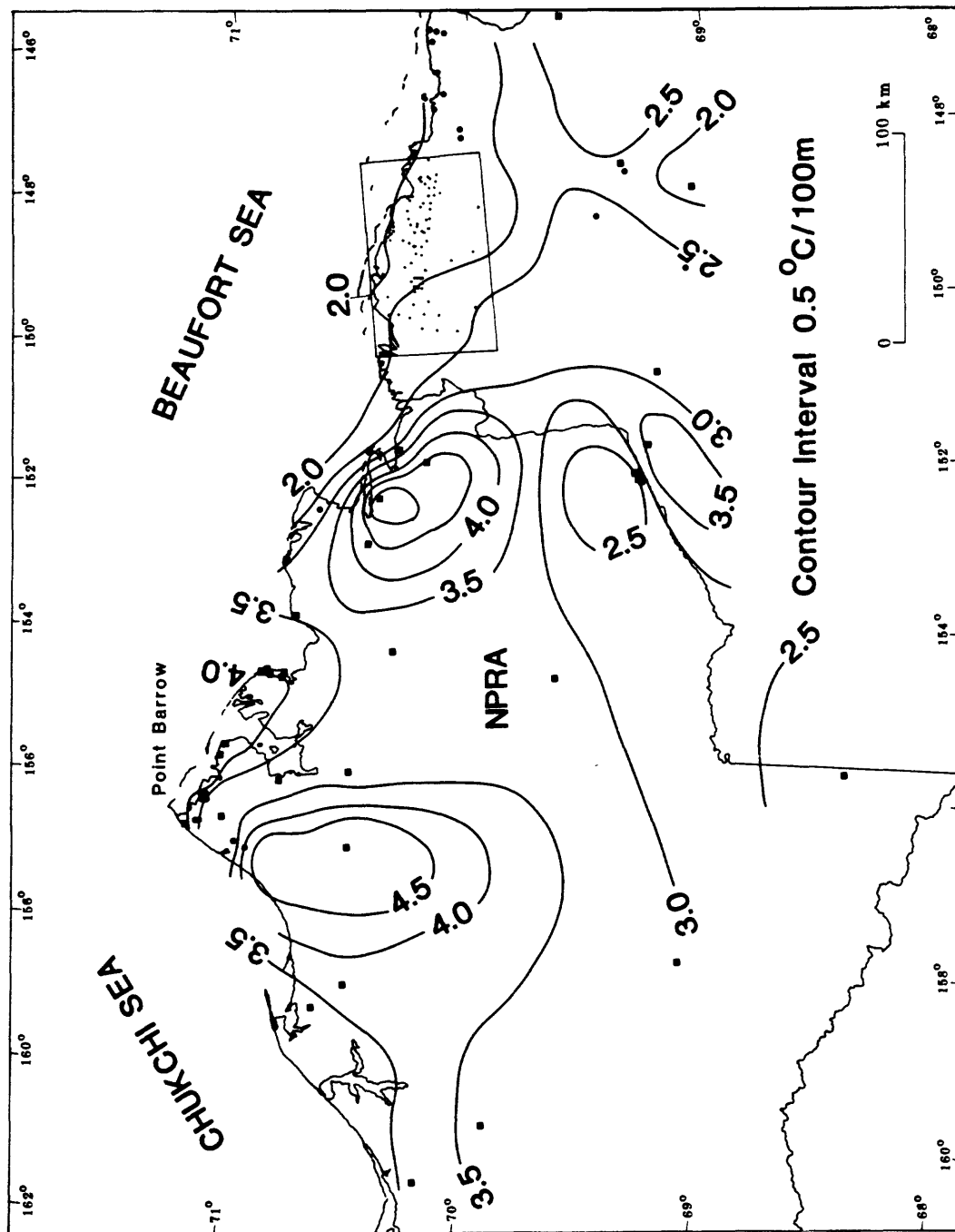


Figure II-10. Contour map of calculated and projected geothermal gradients ($^{\circ}\text{C}/100\text{m}$) above the base of ice-bearing permafrost for the central North Slope. Wells identified in figures II-5 and II-6; temperature data tabulated in tables II-6 and II-7.

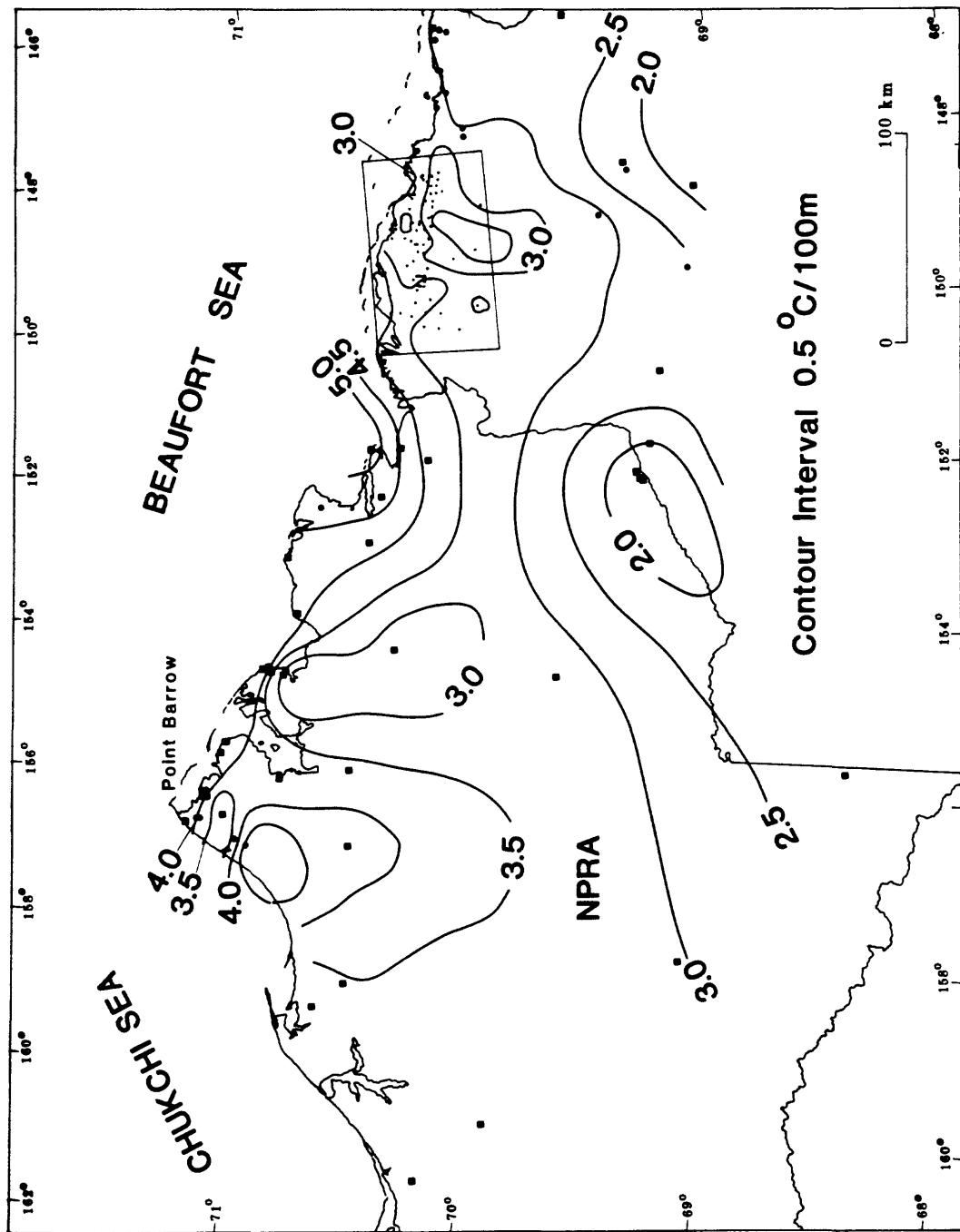


Figure II-11. Contour map of calculated and projected geothermal gradients ($^{\circ}\text{C}/100\text{m}$) below the base of ice-bearing permafrost for the central North Slope. Wells identified in figures II-5 and II-6; temperature data tabulated in tables II-6 and II-7.

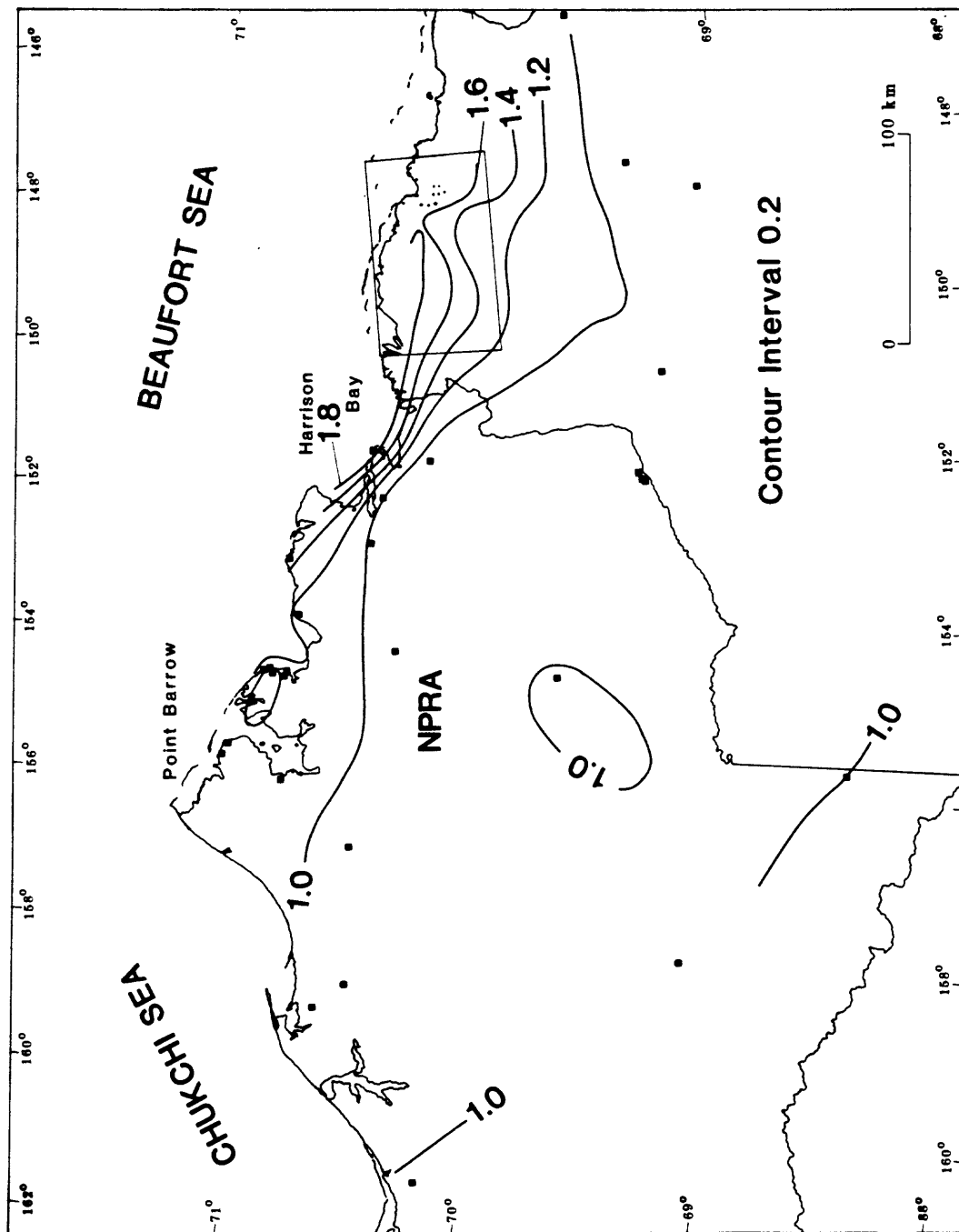


Figure II-12. Contour map of ratios of the calculated geothermal gradient from below ice-bearing permafrost to the geothermal gradient from within the ice-bearing permafrost (G_b/G_f) for the central North Slope. Wells identified in figures II-5 and II-6; temperature data tabulated in table II-6.

geothermal gradients above and below the base of the ice-bearing permafrost (column 8, table II-7).

For each of the wells listed in table II-7 a geothermal gradient was projected from equilibrium surface temperatures to the interpreted depth and temperature at the base of the ice-bearing permafrost (column 9, table II-7). As discussed earlier, the geothermal gradient changes abruptly in many places at the base of the ice-bearing permafrost due to a change in thermal conductivity. The interpolated ratios between the geothermal gradient above and below the base of the ice-bearing permafrost as determined from information on the map in figure II-12 are listed for all 102 wells (column 8, table II-7). These ratios were then used to relate the projected geothermal gradients within the ice-bearing permafrost (column 9, table II-7) to the projected geothermal gradients below the base of the ice-bearing permafrost (column 10, table II-7). The projected geothermal gradients, both above and below the base of the ice-bearing permafrost, have been combined with the geothermal gradients calculated from the high-resolution temperature surveys to construct maps of the geothermal gradient above (fig. II-10) and below (fig. II-11) the base of the ice-bearing permafrost on the North Slope. In the maps shown in figures II-10 and II-11, the wells with geothermal gradients calculated from the high-resolution temperature surveys have been noted with a ■, and wells with projected geothermal gradients are referenced with a • (see figures II-5 and II-6 for detail).

Figures II-9 and II-13 demonstrate the procedures for determining the equilibrium temperature conditions at the base of the ice-bearing permafrost (as discussed earlier), and for evaluating geothermal gradients projected from known ice-bearing permafrost depths. In figure II-9, the recorded temperature profile from the BP 08-11-13 well indicates that the base of the ice-bearing permafrost (585 m) is in equilibrium at -0.6°C , and the ratio is 1.8 between the recorded geothermal gradient below the base of the ice-bearing permafrost ($3.0^{\circ}\text{C}/100\text{m}$) and the geothermal gradient above the base of the ice-bearing permafrost ($1.7^{\circ}\text{C}/100\text{m}$). There are no temperature data available for the Prudhoe Bay Drill Site 14-5 (fig. II-13), but the depth to the base of the ice-bearing permafrost, as determined from well logs, is 573 m. For this site the interpolated mean annual surface temperature is -11.0°C (fig. II-7), and the base of the ice-bearing permafrost should be in equilibrium at -1.0°C (fig. II-8). This information enables us to project a geothermal gradient of $1.75^{\circ}\text{C}/100\text{m}$ from the surface to the base of the ice-bearing permafrost. The interpolated regional ratio between the geothermal gradients below and above the base of the ice-bearing permafrost is 1.8 (fig. II-12) for this location. Therefore, the geothermal gradient below the base of the ice-bearing permafrost at this site should be about $2.8^{\circ}\text{C}/100\text{m}$.

DISCUSSION OF NORTH SLOPE NEAR-SURFACE GEOTHERMAL GRADIENTS

A comparison of geothermal gradients calculated from the high-resolution temperature surveys and projected from known ice-bearing permafrost depths generally agree favorably over most of the North Slope with values in the ice-bearing sequence ranging from $1.55^{\circ}\text{C}/100\text{m}$ in the Prudhoe Bay area to $4.46^{\circ}\text{C}/100\text{m}$ at Fish Creek-1 in east central NPRA. Geothermal gradients calculated from a series of high-resolution temperature surveys conducted in 11 closely spaced Prudhoe Bay Unit wells (table II-6; wells K through U) show that local geothermal gradients range from 1.55 to $1.90^{\circ}\text{C}/100$ in the ice-bearing permafrost sequence, and from 2.55 to $3.17^{\circ}\text{C}/100\text{m}$ below the base of the ice-bearing horizons. Thus, there appears to be a local variation in the geothermal gradient as great as $0.62^{\circ}\text{C}/100\text{m}$ in a region that is characterized by generally uniform rock types and constant external temperature parameters. With our limited data base, it is impossible to evaluate this range in the calculated geothermal gradients; the range could be due to differences in subsurface rock types, porosities, water content, or unknown parameters. An unexplained variation in the geothermal gradient of $0.62\text{C}/100\text{m}$ over such a limited area indicates that great care must be employed when using the reported gradients, and further highlights the need for additional high-resolution equilibrated temperature surveys.

II.A.3. GAS CHEMISTRY

The next step required before proceeding with the determination of the zone of gas-hydrate stability is the selection of a gas hydrate stability curve which best represents the gas chemistry of the in-situ gas hydrates. The analysis of mud-log gas-chromatographic data from 320 wells suggest that methane is the dominant gas in the near-surface (0-1,500 m) sediments of the North Slope. However, analysis of the gas believed to be evolved from the hydrates in the Northwest Eileen State-2 well

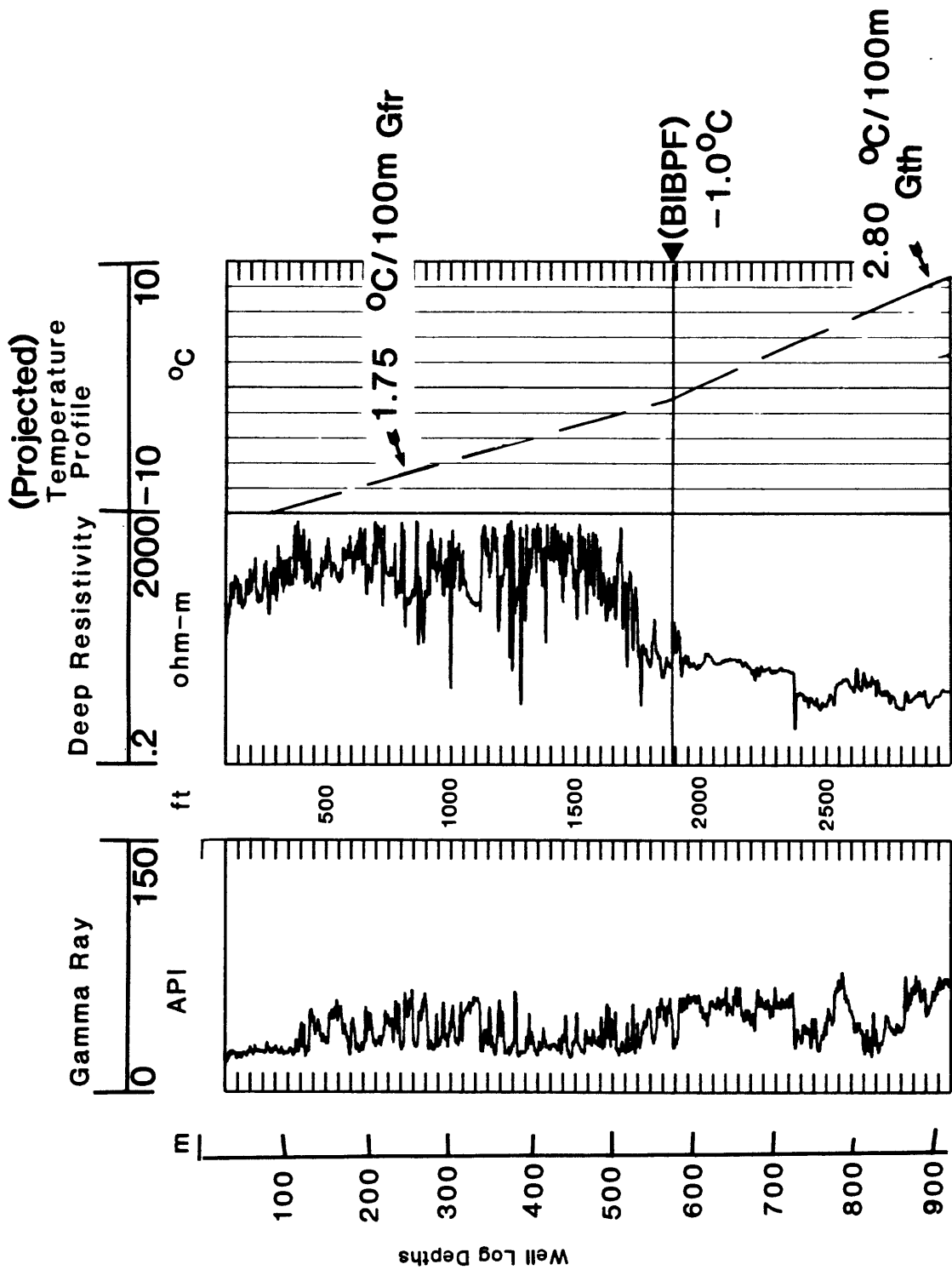


Figure II-13. Well logs from Prudhoe Bay Unit 14-5, and projected temperature profile with a geothermal gradient of $1.75^{\circ}\text{C}/100\text{ m}$ in the permafrost sequence (G_r) and $2.80^{\circ}\text{C}/100\text{ m}$ below the permafrost sequence (G_{th}). Base of ice-bearing permafrost is determined from the resistivity log at 573 m (measured from surface).

(Collett, 1983a) reveals a more complex gas chemistry than pure-methane (table II-8). In several analyses nitrogen was detected; this gas inhibits gas-hydrate formation. Repeat analyses of the same samples reveal almost a 100% methane composition. The validity, therefore, of the gas analyses from the Northwest Eileen State-2 well is uncertain.

In figure II-14, three different gas-hydrate stability curves have been displayed with the projected geothermal gradient for the Placid State-1 well to show the potential effect of nitrogen on the depth and thickness of the gas-hydrate stability field. The three stability curves represent gas hydrates with three different gas chemistries: (1) 100% methane; (2) 93% methane, 7% nitrogen; (3) 86% methane, 14% nitrogen. The stability curves have been generated by three, fourth-order polynomials calculated by D. Sloan, Colorado School of Mines, Golden, Colorado. The addition of 7% nitrogen to the pure methane gas mixture would shift the stability curve to the left approximately -1.0°C , and the addition of 14% nitrogen would shift the curve -2.0°C . For example, the base of the pure methane-hydrate stability field would be at 1,320 m in the Placid State-1 well, the addition of 7% nitrogen would shift the base of the gas hydrate stability field up 30 m, to a depth of 1,290 m. The addition of 14% nitrogen would shift the stability boundary up approximately 120 m, to 1,200 m. Because of the lack of data and the uncertainty in reported geochemical analyses, the gas-hydrate stability calculations in this paper have been made assuming a pure-methane chemistry.

II.A.4. PORE-WATER SALINITY

Fluid and rock properties are known to affect the temperature at which water freezes in the subsurface. For example, the base of the ice-bearing permafrost on the North Slope is not in equilibrium at 0°C but at a lower temperature (Collett and others, in press-a). This freezing-point depression may be attributed to the presence of dissolved salts in the unfrozen pore fluids, or to non-standard pore-pressures, or to the presence of clays which exhibit high surface areas (Osterkamp and Payne, 1981). These physical parameters that collectively suppress the freezing point of water may have an effect on gas hydrate equilibrium as previously discussed. Listed in table II-9 are 31 wells from which near-surface (0-1,500 m) formation-water samples have been obtained from drill-stem and production tests, or for which salinity calculations have been made from the available well log data. Locations of the wells are shown in figure II-15. Analyses of the recovered waters indicate that the pore-fluid salinities are low, ranging from 0.5 to 18.1 ppt. To further evaluate reservoir fluid salinities, and to verify the reported analyses, salinity calculations have been made from the spontaneous-potential well logs within the intervals listed in table II-9. These calculations were made by using conventional well-log interpretation procedures in which the electrical resistivity of the formation waters are calculated from the spontaneous-potential device and from which the dissolved salt content is estimated (Schlumberger and others, 1934; Wyllie, 1949; Gondouin and others, 1957). In general, the well-log-derived salinities agree closely with the analysis of the recovered samples.

The spontaneous-potential well logs for 14 of the wells listed in table II-9 (noted with an †) have been used to generate a series of pore-fluid-salinity profiles within the near-surface sediments, similar to the three profiles illustrated in figure II-16 from the J.W. Dalton-1, South Harrison Bay-1, and Prudhoe Bay Unit N-1 wells. Uncorrected log-calculated salinities from within ice-bearing permafrost and clay-rich horizons are not valid because of the effect of ice and clay on the electrochemical potential of a water-rock system. Therefore, only sub-permafrost clean sandstone units have been examined. The salinities obtained from the profiles fall within the range of values reported from the analysis of the recovered samples, with a maximum calculated salinity of 18.0 ppt. The maximum recorded salinity of 18.0 ppt would shift the methane hydrate stability curve approximately -1.0°C , which would correspond to a 30 m upward shift in the base of the methane-hydrate stability field in Placid State-1 (from 1,320 m to 1,290 m). In addition to reporting the calculated salinities in table II-9, the thermal-effect on gas-hydrate equilibrium of each referenced salinity has been listed. The overall thermal-effect of the dissolved salts on gas-hydrate stability on the North Slope can generally be considered negligible and was not included in the gas-hydrate stability determinations.

II.A.5. PORE-PRESSURE

Most gas-hydrate stability studies assume that the subsurface pore-pressure gradient is hydrostatic (9.795 kPa/m; 0.433 psi/ft). Pore-pressure gradients greater than hydrostatic will

Table II-8. Gas analyses from cores and flow tests in Northwest Eileen State-2 (Collett, 1983a). Cored interval 665-667 m is inferred from pressure data to contain natural gas hydrates and the cored interval is interpreted as gas hydrate bearing from well-log responses (fig. I-2).

Sample Type	Depth Interval (m)	Carbon Dioxide %	Oxygen %	Nitrogen %	Methane %	Ethane %	Propane %
Core	577-580	-	1.26	14.70	84.04	Trace	-
Core	577-580	Trace	0.14	2.26	97.60	Trace	-
Core	577-580	Trace	0.15	1.09	98.76	Trace	-
Core	577-580	-	0.40	2.01	97.59	Trace	-
Core	664-667	-	0.52	12.53	86.95	Trace	-
Core	664-667	-	0.02	0.84	99.14	Trace	-
Core	664-667	-	0.03	0.80	99.17	Trace	-
Core	664-667	-	0.05	1.46	98.49	Trace	-
Flow Test	663-671	Trace	-	7.19	92.79	0.02	Trace
Flow Test	663-671	Trace	-	7.23	92.76	0.01	Trace

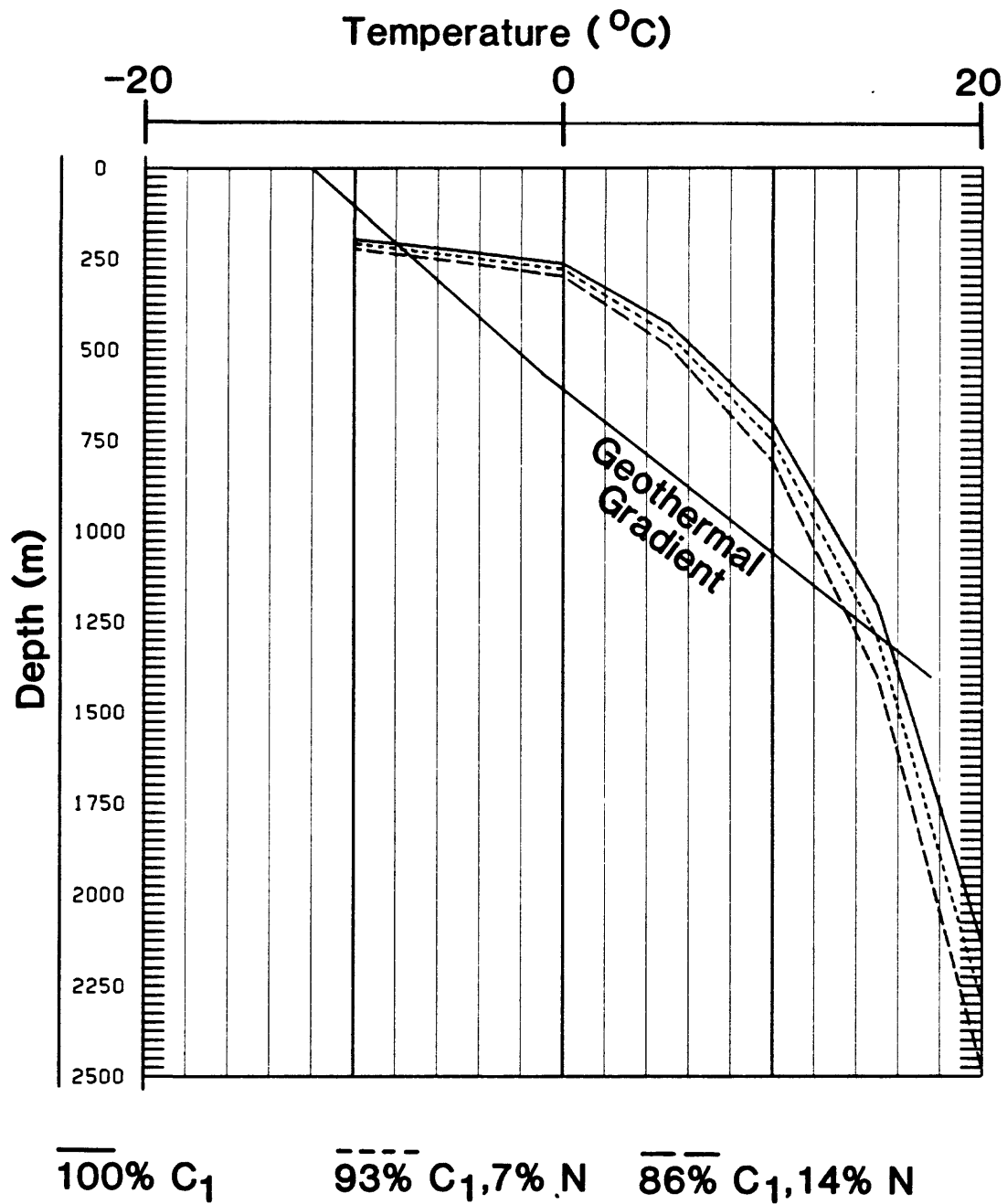


Figure II-14. Gas hydrate phase diagram for the Placid State-1 well shown with three different gas-hydrate stability curves, each representing a different gas chemistry.

Table II-9. Near surface (0-1,500 m) pore-water salinity data. Sources include analysis of 52 water samples recovered from drill-stem and production tests, 14 spontaneous potential well-log calculated salinity profiles, and well log calculated salinities from 36 selected horizons in 18 wells (see fig. II-15 for location of wells).

Well Name and Number	API Number	Depth ^{1]} (m)	Salinity ^{2]} (ppt)	Temperature ^{3]} effect (°C)	Salinity ^{4]} (ppt)	Temperature ^{5]} effect (°C)	Rock Formation sampled		
Kuparuk River Unit 1B-1	5002920645	553	1.1	0.07	3.0	0.17	Sagavanirktok		
		553	0.9	0.06	2.5	0.14	Sagavanirktok		
Northwest Eileen State 2	5002920117	610	1.2	0.08	-	-	Sagavanirktok		
		663-671	0.9	0.06	-	-	Sagavanirktok		
		663-671	0.9	0.06	-	-	Sagavanirktok		
		663-671	3.5	0.20	-	-	Sagavanirktok		
		663-671	3.5	0.20	-	-	Sagavanirktok		
		663-671	1.2	0.08	-	-	Sagavanirktok		
		663-671	0.9	0.06	-	-	Sagavanirktok		
		229-411†	-	-	(1.0-3.0)	(0.07-0.17)	Sagavanirktok		
Bush Federal 1	5022320004	1518-1707	2.7	0.15	8.0	0.43	Sagavanirktok		
Kuparuk 1	5028710018	836-839	1.7	0.10	6.0	0.33	Sagavanirktok		
Prudhoe 1	5002920796	1110-1113	1.8	0.11	6.0	0.33	Sagavanirktok		
		1128-1156	0.8	0.06	8.30	0.43	Sagavanirktok		
		1314-1320	5.0	0.28	5.5	0.30	Sagavanirktok		
		762-1524†	-	-	(6.0-15.0)	(0.33-0.81)	Sagavanirktok		
Kuparuk River Unit 1B-5	5002920237	962-1148	2.6	0.14	3.5	0.20	Sagavanirktok		
Northwest Eileen State 1	5002920013	1248-1259	18.1	0.98	6.0	0.33	Sagavanirktok		
		640-1524†	-	-	(3.5-9.0)	(0.20-0.49)	Sagavanirktok		
Grandstand 1	5005710001	254-263	0.9	0.06	3.5	0.20	Nanushuk		
		264-274	1.5	0.09	5.0	0.28	Nanushuk		
		591-595	1.5	0.09	2.5	0.14	Nanushuk		
		1191-1201	1.8	0.11	2.0	0.12	Nanushuk		
		91-1189†	-	-	(2.0-5.0)	(0.12-0.28)	Nanushuk		
Square Lake 1	5011910007	502-511	15.7	0.85	-	-	Nanushuk		
		563-573	5.6	0.31	-	-	Nanushuk		
		572-578	5.4	0.30	-	-	Nanushuk		
		924-935	0.5	0.04	-	-	Nanushuk		
Wolf Creek 3	5011910010	621-633	5.6	0.31	7.0	0.38	Nanushuk		
		16-277	9.0	0.49	-	-	Nanushuk		
Knifblade	5011910012	16-381	7.3	0.40	-	-	Nanushuk		
		16-381	7.3	0.40	-	-	Nanushuk		
		369-418	11.6	0.63	-	-	Nanushuk		
Umiat 2	5028710002	230-251	5.4	0.30	6.5	0.37	Nanushuk		
Umiat 7	5028710007	365-376	6.0	0.33	8.0	0.43	Nanushuk		
Umiat 11	5028710011	639-654	7.8	0.42	5.5	0.30	Nanushuk		
		724-735	2.9	0.17	5.0	0.28	Nanushuk		
		746-750	4.9	0.27	7.5	0.40	Nanushuk		
		858-863	6.0	0.33	8.0	0.43	Nanushuk		
		863-869	6.0	0.33	9.0	0.49	Nanushuk		
		399-412	0.6	0.04	1.5	0.09	Colville Group		
Gubik 2	5028710014	413-427	0.6	0.04	1.0	0.07	Colville Group		
		436-458	0.6	0.04	1.0	0.07	Colville Group		
		458-474	0.6	0.04	0.5	0.04	Colville Group		
		510-529	0.6	0.04	1.5	0.09	Colville Group		
		588-605	4.5	0.25	2.0	0.12	Colville Group		
		1052-1066	8.8	0.48	1.0	0.07	Nanushuk		
		1152-1161	14.1	0.76	1.0	0.07	Nanushuk		
		1180-1186	1.8	0.11	1.5	0.09	Nanushuk		
		1231-1238	0.6	0.04	1.5	0.09	Nanushuk		
		1290-1299	1.4	0.09	1.0	0.07	Nanushuk		
		0-1402†	-	-	(0.2-2.0)	(0.02-0.12)	Nanushuk		
		South Barrow 8	5002320002	660-718	2.3	0.13	2.5	0.14	Barrow SS
		South Barrow 5	5002310014	701-749	17.0	0.92	-	-	Barrow SS
South Barrow 7	5002320001	503-683	12.8	0.69	5.5	0.30	Barrow SS		
East Umiat 1	5028710016	546-914	7.5	0.40	10.0	0.54	Sagavanirktok		
Kuparuk River Unit 1B-5	5002920237	1072-1148	1.9	0.13	5.0	0.28	Sagavanirktok		
Kuparuk River Unit 2D-15	5002921184	30-1219†	-	-	(1.0-8.0)	(0.07-0.43)	Sagavanirktok		
Point Thomson Unit 1	5008920005	366-1524†	-	-	(5.0-15.0)	(0.28-0.81)	Sagavanirktok		
West Sak 7	5010320014	61-1372†	-	-	(0.5-5.0)	(0.04-0.28)	Sagavanirktok		
Prudhoe Bay Unit 2-14	5002920446	488-1372†	-	-	(2.0-9.0)	(0.12-0.49)	Sagavanirktok		
West Sak 1	5002920090	427-1524†	-	-	(2.0-8.0)	(0.12-0.43)	Sagavanirktok		
Kuparuk River Unit 1B-1	5002920465	152-975†	-	-	(1.0-9.0)	(0.07-0.49)	Sagavanirktok		
J.W. Dalton 1	5027920006	270-890†	-	-	(2.0-18.0)	(0.12-0.98)	Nanushuk		
South Harrison Bay 1	5010320007	270-600†	-	-	(5.0-18.0)	(0.28-0.98)	Nanushuk		
Prudhoe Bay Unit N-1	5002920079	650-1100†	-	-	(5.0-17.0)	(0.28-0.92)	Sagavanirktok		

1] Measured well depth of sampled or evaluated interval.

2] Pore-water salinity analysis of samples collected during drill-stem or production test.

3] Thermal depression effect on the stability of gas hydrate attributed to the analyzed salt concentrations listed in the previous column.

4] Pore-water salinities calculated from the spontaneous potential well log.

5] Thermal depression effect on the stability of gas hydrate attributed to the calculated salt concentrations listed in the previous column.

† Salinity profiles from spontaneous-potential well-log calculations.

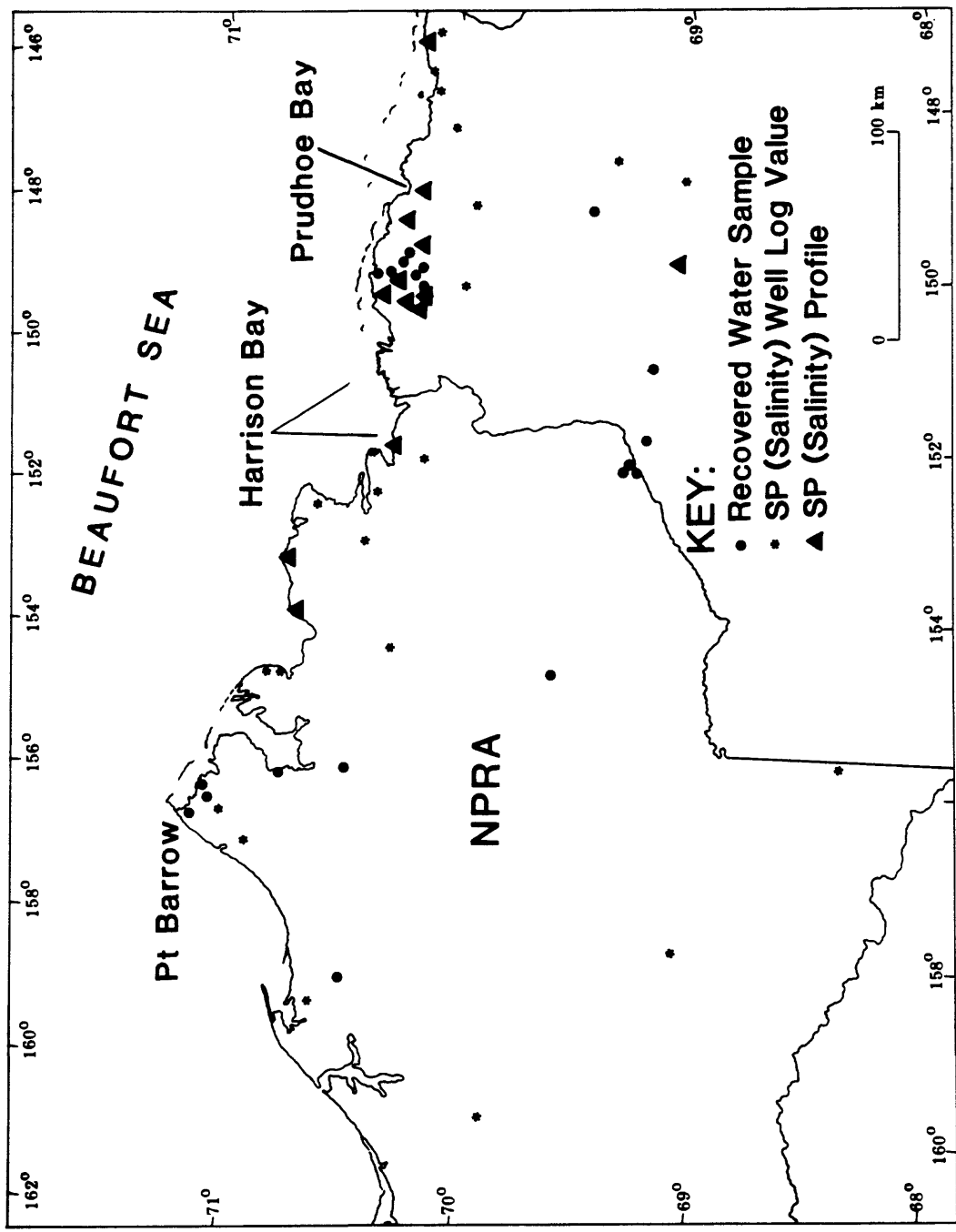


Figure II-15. Location of central North Slope wells from which pore-water salinity data have been obtained. Salinities are from analysis of recovered samples and well log calculations (table II-9).

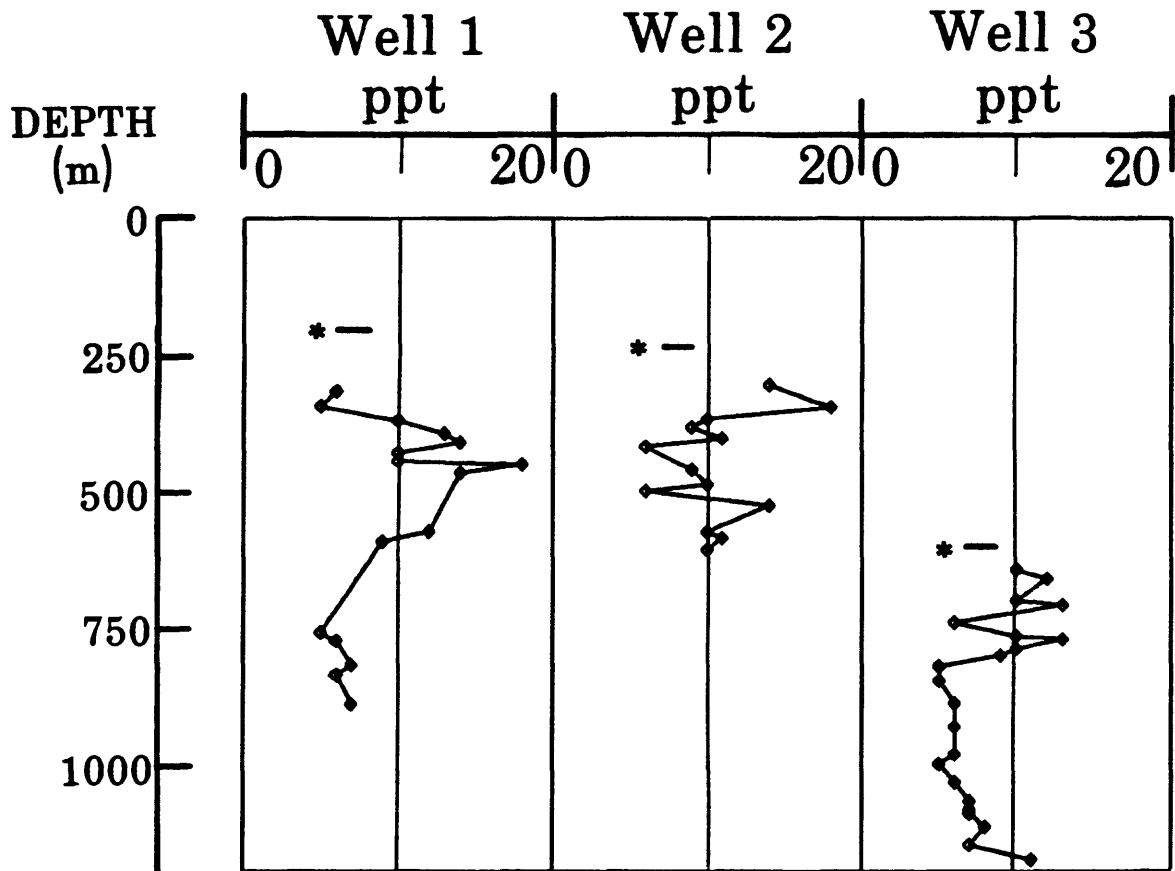


Figure II-16. Calculated pore-water salinity profiles using the spontaneous-potential log method beneath the ice-bearing permafrost in selected North Slope wells (Well 1, J.W. Dalton-1; Well 2, South Harrison Bay-1; Well 3, Prudhoe Bay Unit N-1). See figure II-2 for well locations. Only clean-sandstone units have been utilized in calculations. No well log corrections have been used (* denotes base of ice-bearing permafrost).

correspond to relatively higher pore-pressures with depth and a thicker gas-hydrate stability field. Listed in table II-10 and denoted on the map in figure II-17 are 17 wells from which recorded pressure data have been used to calculate pore-pressure gradients within the near-surface sediments. The wells in table II-10 are divided into three groups based on their location (fig. II-18). For the eight wells from the Eastern Coastal Plain Province the average pore-pressure gradient is 9.817 kPa/m (0.434 psi/ft), near hydrostatic. However, in the Western Coastal Plain Province and in the Northern Foothills Province, the calculated pore-pressure gradients are greater than hydrostatic, with values as high as 13.414 kPa/m (0.593 psi/ft). These higher pore-pressure gradients may be due to rapid regional uplift and local tectonic activity. The observed pore-pressure gradients in the near-surface sediments of the North Slope range from a minimum of 9.433 kPa/m (0.417 psi/ft) to a maximum 13.414 kPa/m (0.593 psi/ft). A low pore-pressure gradient of 9.433 kPa/m (.417 psi/ft) would correspond to a -0.4°C temperature shift of the methane-hydrate stability curve, and a 13.414 kPa/m (.593 psi/ft) gradient would shift the stability curve $+2.3^{\circ}\text{C}$. In the Placid State-1 well, a -0.4°C stability curve shift would move the base of the methane-hydrate stability field up approximately 20 m. However, a $+2.3^{\circ}\text{C}$ shift would increase the depth of the methane-hydrate stability field 120 m, to a depth of 1,440 m.

To examine further the regional distribution of non-standard pore-pressures, well-log data from 18 wells were considered (table II-11). Because rocks, particularly shales, are subjected to increasing over-burden pressures, they are compacted, and consequent transit-time velocities and gamma-ray values increase with depth due to formation density changes. However, if a rock interval is overpressured it will resist compaction, and this effect can be identified from the recorded sonic transit-times and gamma-ray log data (Whittaker, 1985). For example, the gamma ray, resistivity, and transit-time plots in figure II-19 from West Sak River State-1 reveal that the pore-pressure within the near-surface sediment (0-1,500 m) is at or near hydrostatic. However, at approximately 1,700 m the plotted log values deviate from the expected trend with depth, suggesting the presence of overpressured shales. A review of all the available pressure data suggests that the pore-pressures within the near-surface sediments for most of the Coastal Plain Province are at or near hydrostatic. The over-pressured horizons appear to be limited to the Foothill Province. Because most of the study area is within the Coastal Plain Province, the gas-hydrate stability determinations assumed a hydrostatic pore-pressure gradient of 9.795 kPa/m (0.433 psi/ft).

II.A.6. PARTICLE GRAIN-SIZE

Many workers including Anderson and others (1973), Pusch (1979), and Osterkamp and Payne (1981) have shown that rock grain size (grain surface area) affects the freezing point of water. However, the quantification of the freezing-point depression attributed to the presence of high-surface-area matrix material, such as clay, is difficult. Anderson and others (1973) suggested that a pure-clay could suppress the freezing-point of water several degrees Celsius. Conversely, Anderson and others (1973) showed that the soil/rock particle effect in silt and coarse-grained mediums is negligible. In addition, Pusch (1979) demonstrated that variations in clay microstructure can affect the volume of unfrozen water, thus further complicating freezing-point depression calculations. However, it is not known if high-surface-area rock material will affect the thermal equilibrium of gas hydrate in a manner similar to that of ice. Therefore, it is impossible to quantify the effect of grain size on gas-hydrate equilibrium conditions on the North Slope. It is possible, however, to speculate on regions which may be affected by grain-size variations by evaluating local rock types. Figure II-20 is a generalized geologic map of the major rock types within the near-surface sediments of the North Slope. Depicted on the map are two relatively coarse-grained sediment packages: one in west-central NPRA; the second extends from Harrison Bay to Canada. Within coarse-grained sediment, grain size should not affect gas-hydrate stability. However, in eastern NPRA and along the mountain-front to the east, a thick section of Cretaceous shale occurs near the surface, and these shales may significantly affect gas-hydrate stability. In addition, local geologic features, such as the shale-filled Cretaceous Simpson Canyon, may affect stability conditions.

Table II-10. Pore-pressure data from North Slope wells obtained from drill-stem or production tests. The calculated pore-pressure gradients are shown in kPa/m, and are grouped by location (fig. II-18).

Well Name and Number	API Number	Depth Interval (m)	Pore-Pressure gradient kPa/m
Eastern Coastal Plain Province			
West Sak 1	5002920090	990-997	10.089
East Ugnu 1	5002920052	1050-1061	9.682
		917-931	9.953
		927-931	9.930
		953-994	9.885
Hurl State 5-10-13	5002920027	953-994	9.840
		1272-1283	(9.998-9.908)
		1299-1309	(9.863-9.795)
Kuparuk 26-12-12	5002920032	1130-1136	9.433
Placid State 1	5002920667	1238-1244	9.546
Milne Point 2	5002920490	1146-1206	9.455
Ravik 1	5002920888	1193-1198	10.270
West Sak 23	5002920669	707-713	(9.795-9.704)
Northern Foothills Province			
Aufeis 1	5022320010	841-1036	11.672
Gubik 1	5028710013	1044-1204	(12.215-10.586)
		410-440	(11.197-10.428)
		410-440	(11.175-10.405)
		500-516	(13.210-12.962)
		504-516	(13.391-13.097)
		506-516	(13.414-13.165)
		507-510	(12.871-12.781)
Shale Wall 1	5028720017	533-535	(11.446-11.423)
		344-347	(10.835-10.722)
Seabee 1	5028720007	808-812	(10.813-10.767)
Western Coastal Plain Province			
South Barrow 4	5002310012	328	9.840
South Barrow 9	5002320009	707-746	(9.908-9.478)
South Barrow 17	5002320011	669-715	11.401
		671-709	10.044
		675-687	(9.591-9.433)
East Topagoruk 1	5027910034	675-687	(9.591-9.433)
Tulageak 1	5002320018	1149-1166	(11.220-11.061)

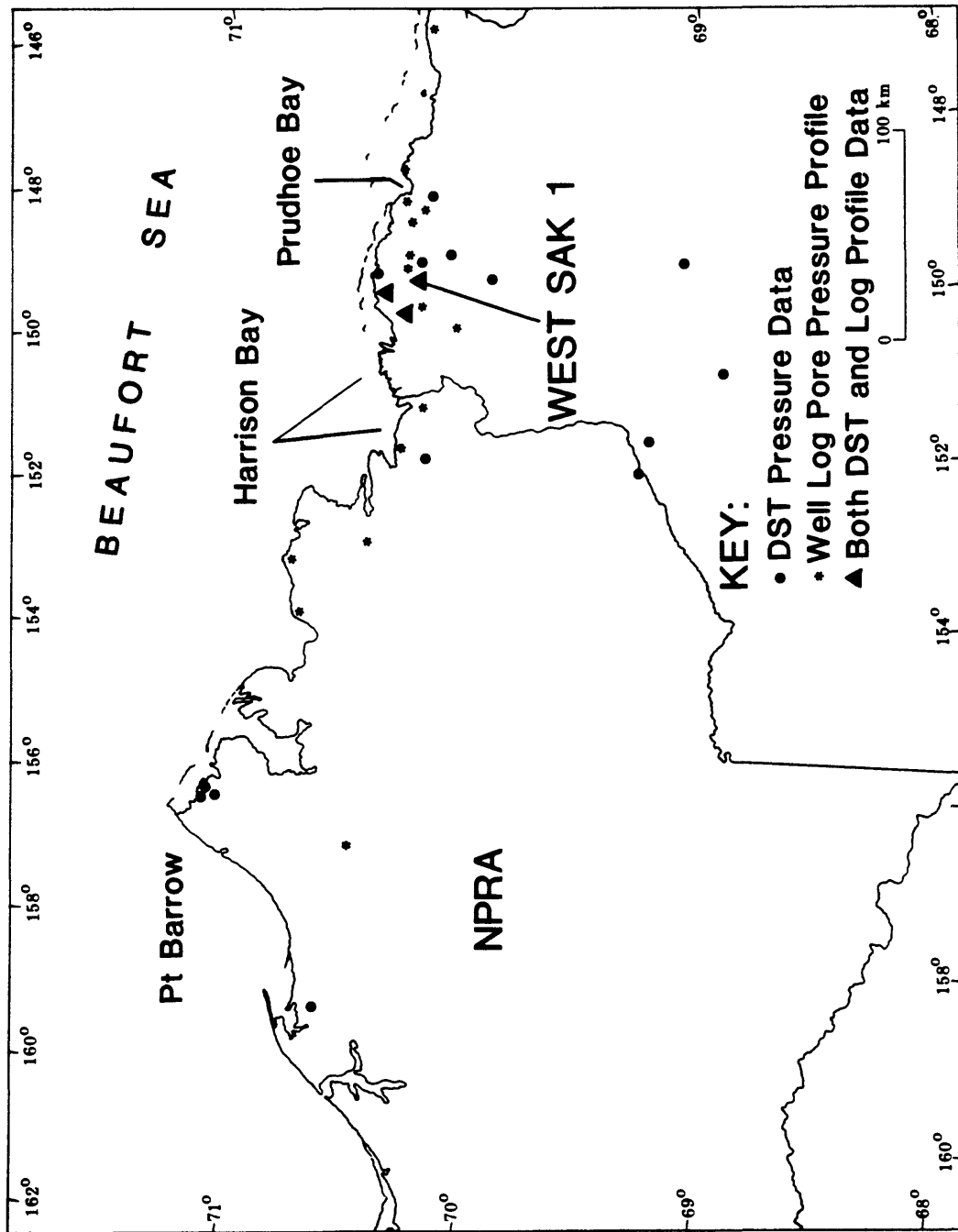


Figure II-17. Locations of central North Slope wells in which pore-pressure gradients have been determined. Data sources include drill-stem test pressure measurements and wire-line well log calculations (tables II-10 and II-11).

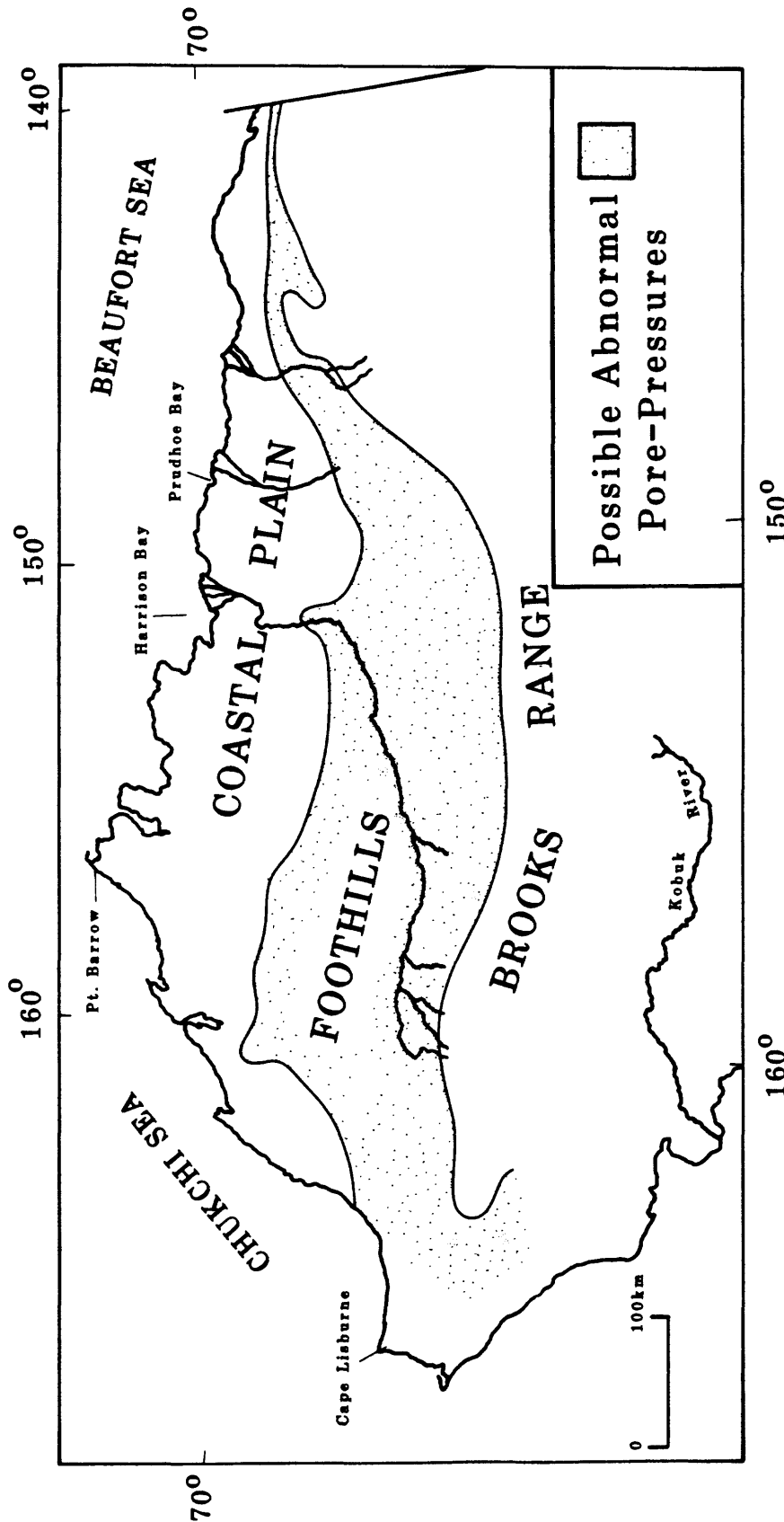


Figure II-18. General map of the physiographical provinces of the North Slope, showing the region of possible abnormal pore-pressures within the near-surface (0-1,500 m) sediments (table II-10).

Table II-11. North Slope wells in which wire-line logs have been used to evaluate formation pore-pressures (see fig. II-17 for location of wells).

Well Names and Numbers	API #
Point Thomson Unit 2	5008920006
West Sak River State 1	5002920090
Prudhoe Bay Unit 14-5	5002920327
Prudhoe Bay Unit 17-1	5002920476
Foggy Island Bay Unit 1	5002920146
South Meade 1	5016320001
Tunalik 1	5030120001
Prudhoe Bay State 1	5002920001
Nechelik 1	5010320020
South Harrison Bay 1	5010320007
J.W. Dalton 1	5027920006
Cape Halkett 1	5010320004
West Sak River State 14	5002920419
Kuparuk River Unit 1D-8	5002920266
East Ugnu 1	5002920052
Itkillik River Unit 1	5010320003
West Sak River State 23	5002920378
Kuparuk River Unit 1B-5	5002920237

WEST SAK 1

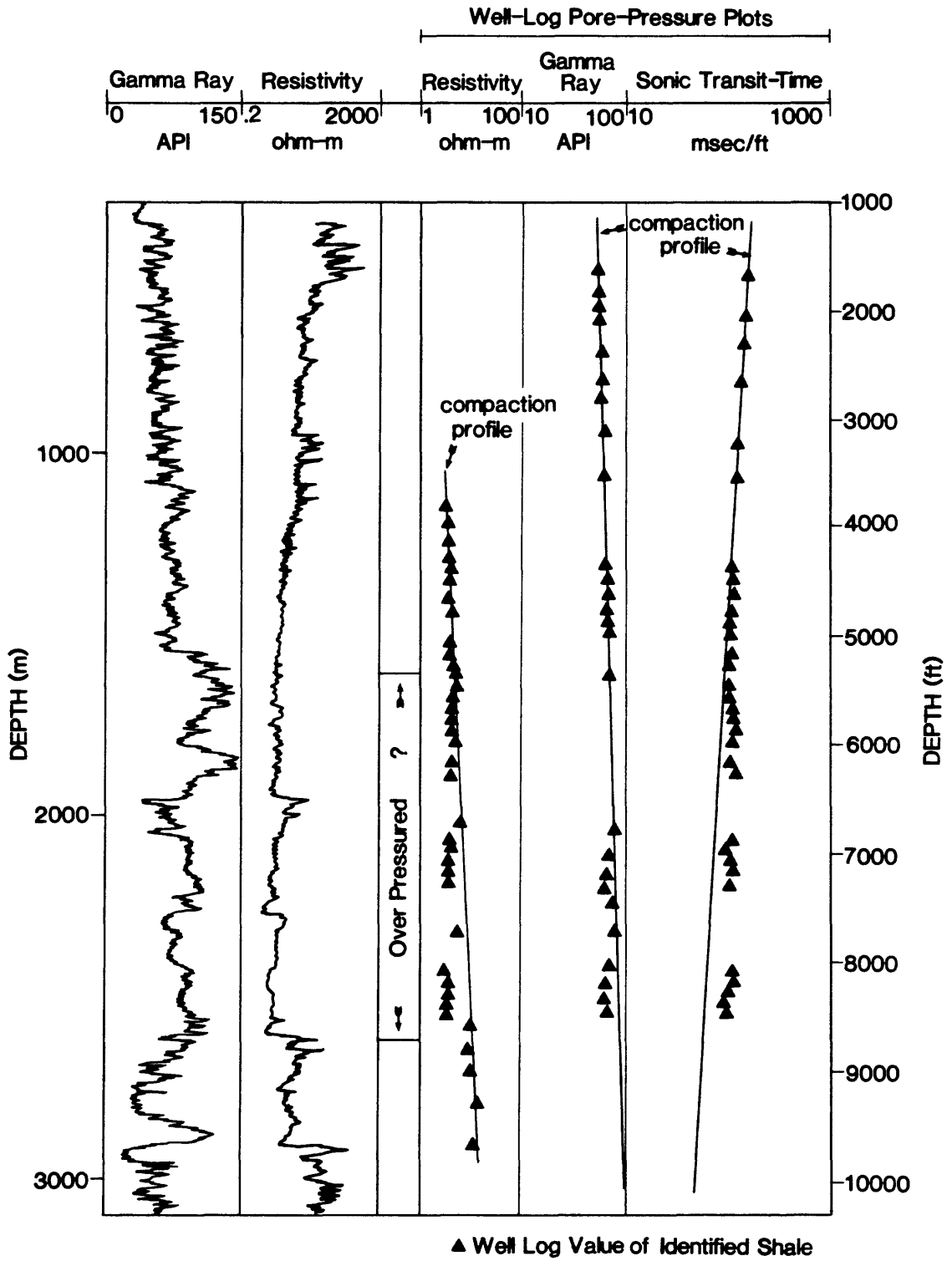


Figure II-19. Well log compaction (pore-pressure) profiles from West Sak River State-1 (table II-11).

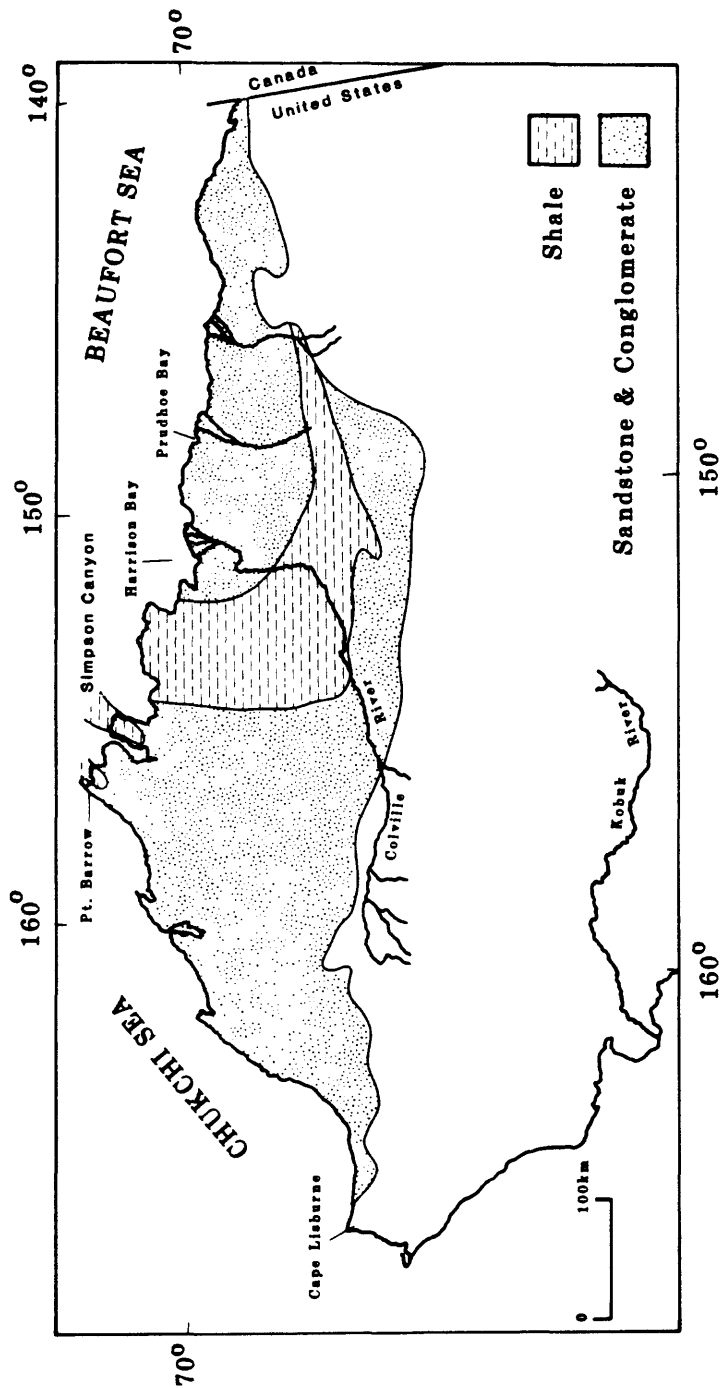


Figure II-20. Generalized bedrock geologic map of the North Slope coastal plain and northern foothills provinces showing the distribution of major rock types. Stippled pattern indicates bedrock composed of significant but highly variable amounts of sandstone with some conglomerate. Dashed pattern indicates bedrock composed mostly of shale and siltstone.

II.B. DISTRIBUTION OF THE GAS-HYDRATE STABILITY FIELD

Table II-12 presents a summary of the assumptions we have made in determining the extent of the zone of gas-hydrate stability. The methane-hydrate stability curve used for this study was based on a stability model and experimental results published by Lewin and Associates, Inc., (1983). The stability curve has been simplified as a function of temperature into two equations;

$$P(\text{kPa})=\exp[14.7170+1886.79/T^{\circ}\text{K}] \text{ (From 248 to 273 K or -25 to 0}^{\circ}\text{C)}$$

$$P(\text{kPa})=\exp[38.9803+8533.80/T^{\circ}\text{K}] \text{ (From 273 to 298 K or 0 to 25}^{\circ}\text{C)}$$

The $P(\text{kPa})$ represents the dissociation or formation pressure in kilopascals of a methane hydrate at a given temperature T (K). For the purpose of calculating subsurface gas-hydrate stability conditions, the variable T (K) represents the equilibrium temperature in Kelvin at any given depth. The depth values of the stability curve can be calculated by means of the equation by converting the derived pressure $P(\text{kPa})$ using the local pore-pressure gradient. As previously noted, the regional pore-pressure gradient is near hydrostatic in the near-surface sediment of the North Slope, and for the purpose of this study, a pore-pressure gradient of 9.795 kPa/m (0.433 psi/ft) was used.

A computer program was written to facilitate calculations of the limits of the gas-hydrate stability zone. The gas-hydrate stability program requires as input the mean annual surface temperature (table II-13, column 6), the depth to the base of the ice-bearing permafrost (table II-13, column 5), the temperature at the base of the ice-bearing permafrost (table II-13, column 7), and the ratio between the geothermal gradient from above to below the base of the ice-bearing permafrost (table II-13, column 8). These data were obtained by interpolation from the maps discussed earlier. The program will project the geothermal gradient above and below the base of the ice-bearing permafrost (table II-13, columns 9 and 10) and calculate the depths of the upper and lower intersections of the methane-hydrate stability curve and the projected geothermal gradient (table II-13, columns 11 and 12). In addition, the program will allow the user to input geothermal gradients from other sources.

Depths of the calculated upper and lower boundaries of the methane-hydrate stability field for the 124 wells considered are listed in columns 11 and 12 of table II-13. The depth to the top of the methane-hydrate stability field (table II-13, column 11) has been contoured in figure II-21, and the depth to the base of the stability field (table II-13, column 12) is shown in figure II-22. In addition, the calculated total thickness of the methane-hydrate stability field within each well is listed in column 13 of table II-13 and isopached in figure II-23. Figure II-23 reveals that the methane-hydrate stability field on the North Slope is thickest in the Prudhoe Bay area, with calculated values slightly greater than 1,000 m.

Table II-12. Summary of the physical parameters that control gas-hydrate stability and the assumptions that we made to calculate the thickness of the gas hydrate stability field on the North Slope.

1. GAS CHEMISTRY

Assumed 100% methane

2. GEOTHEMAL GRADIENT

Within Ice-Bearing Permafrost:
1.55°C/100 m to 4.46°C/100 m
(Tables II-6 and II-7)

Below Ice-Bearing Permafrost:
2.08°C/100 m to 4.76°C/100 m
(Tables II-6 and II-7)

3. PORE-FLUID SALINITY

Calculated range of 0.5 to 18.0 ppt
(assumed fresh water; no thermal effect)

4. PORE-PRESSURE

Assumed hydrostatic pore-pressure gradient of 9.795 kPa/M (0.433 psi/ft)

5. ROCK GRAIN-SIZE

Assumed sand size or larger
(no thermal effect)

Table II-13. Wells and data used to calculate and map the depth and thickness of the methane-hydrate stability field on the North Slope of Alaska (figures II-21, II-22 and II-23).

(1) Well Index	(2) Well Name	(3) API Number	(4) Location Sec. T. R.	(5)	(6)	(7)	(8)	(9)	(10)	(11)	(12)	(13)
1.	South Barrow Test Well 4	5002310012	14 22N 18W	206	-12.0	-4.5	1.10	3.64	4.00	231	480	249
2.	South Barrow Test Well 13	5002320008	14 22N 18W	217	-12.0	-4.5	1.10	3.46	3.81	227	530	303
3.	South Barrow Test Well 14	5002320009	25 22N 17W	226	-12.0	-4.5	1.10	3.32	3.65	225	570	345
4.	Walakpa 1	5002320013	9 20N 19W	244	-12.0	-4.5	1.10	3.07	3.38	221	654	433
5.	West Dease 1	5002320014	21 21N 14W	223	-12.0	-2.5	1.00	4.29	4.36	242	383	141
6.	South Barrow Test Well 20	5002320015	26 22N 17W	223	-12.0	-4.5	1.10	3.36	3.70	226	557	331
7.	South Barrow Test Well 15	5002320016	23 22N 17W	206	-12.0	-4.5	1.10	3.64	4.00	231	482	251
8.	South Barrow Test Well 18	5002320017	24 22N 17W	208	-12.0	-4.5	1.10	3.59	3.95	230	489	259
9.	Walakpa 2	5002320019	31 20N 19W	190	-12.0	-4.0	1.10	4.21	4.63	243	360	126
10.	Prudhoe Bay 1	5002920001	10 11N 14E	571	-11.0	-0.5	1.70	1.84	3.13	210	1019	809
11.	Sag River 1	5002920002	4 10N 15E	583	-11.0	-0.5	1.70	1.80	3.06	209	1053	844
12.	Delta State 1	5002920004	10 10N 15E	578	-11.0	-1.0	1.70	1.73	2.94	208	1098	890
13.	BP 27-11-14	5002920006	27 11N 14E	574	-10.7	-0.9	1.84	1.55	2.85	210	1040	830
14.	Socal 31-25	5002920007	25 10N 14E	550	-11.0	-1.0	1.60	1.82	2.91	210	1064	854
15.	West Kuparuk 3-11-11	5002920014	3 11N 11E	524	-11.0	-0.5	1.80	2.00	3.60	212	873	661
16.	Hemi 3-9-11	5002920018	3 9N 11E	521	-11.0	-1.0	1.40	1.92	2.69	211	1085	874
17.	Prudhoe Bay Unit J-1	5002920020	9 11N 13E	602	-11.0	-0.5	1.80	1.74	3.13	209	1062	853
18.	Kad River 1	5002920021	4 8N 18E	482	-10.0	-1.5	1.70	1.76	2.99	215	968	753
19.	BP 04-11-13	5002920025	4 11N 13E	620	-11.1	-0.4	1.82	1.65	3.00	208	1083	875
20.	Huzi 5-10-13	5002920027	5 10N 13E	607	-11.0	-1.0	1.50	1.65	2.48	208	1288	1080
21.	Kavearak Point 32-35	5002920028	25 13N 10E	541	-12.0	-1.0	1.90	2.03	3.86	206	883	677
22.	Lake 79 Federal 1	5002920031	1 8N 17E	455	-10.0	-1.5	1.70	1.87	3.18	217	887	670
23.	North Kuparuk 26-12-12	5002920032	26 12N 12E	630	-11.0	-0.5	1.80	1.67	3.01	208	1132	924
24.	BP 19-10-15	5002920035	19 10N 15E	570	-09.8	-0.4	1.77	1.55	2.75	215	1062	847
25.	Toolik Federal 2	5002920041	5 8N 12E	454	-10.0	-1.5	1.20	1.87	2.24	217	1191	974
26.	BP 33-12-13	5002920047	33 12N 13E	620	-11.4	-0.7	1.70	1.60	2.70	206	1144	938
27.	North Prudhoe Bay State 1	5002920049	23 12N 14E	550	-12.0	-1.2	1.53	1.90	2.90	205	1051	846
28.	BP 23-11-13	5002920054	23 11N 13E	605	-11.0	-0.4	1.57	1.75	2.75	209	1157	948
29.	BP 31-11-14	5002920059	31 11N 14E	620	-10.6	-0.5	1.93	1.50	2.90	210	1087	877
30.	Kuparuk State 7-11-12	5002920062	7 11N 12E	571	-11.0	-0.5	1.80	1.84	3.31	210	986	776
31.	Prudhoe Bay Drill Site 4-1	5002920078	34 11N 15E	567	-11.0	-0.5	1.70	1.85	3.15	210	1012	802
32.	BP 08-11-13	5002920079	8 11N 13E	585	-11.0	-0.6	1.76	1.70	3.00	209	1045	836
33.	Prudhoe Bay Unit F-1	5002920080	2 11N 13E	589	-11.0	-0.5	1.80	1.78	3.20	209	1031	822
34.	BP 11-11-13	5002920084	11 11N 13E	620	-11.0	-0.3	1.84	1.72	3.17	208	1071	863
35.	West Sak River Unit 1	5002920090	2 11N 10E	530	-11.0	-1.0	1.80	1.89	3.40	211	935	724
36.	Prudhoe Bay Unit H-1	5002920099	21 11N 13E	583	-11.0	-0.5	1.80	1.80	3.24	209	1014	805
37.	Prudhoe Bay Drill Site 4-6	5002920111	34 10N 15E	579	-11.0	-0.5	1.70	1.81	3.08	210	1041	831
38.	Northwest Eileen State 2	5002920117	28 12N 11E	525	-11.0	-1.0	1.70	1.91	3.25	211	955	744
39.	Prudhoe Bay Unit C-1	5002920121	19 11N 14E	577	-11.0	-0.5	1.70	1.82	3.09	210	1036	826
40.	North Franklin Bluffs 1	5002920122	20 8N 14E	504	-10.0	-1.5	1.80	1.69	3.04	214	992	778
41.	East Bay State 1	5002920133	15 11N 15E	580	-10.6	-0.8	1.65	1.55	2.55	211	1131	920
42.	West Sak River State 2	5002920134	22 11N 10E	481	-11.0	-1.0	1.70	2.08	3.54	213	840	627
43.	West Sak River State 3	5002920139	26 11N 9E	428	-11.0	-1.0	1.70	2.34	3.98	217	707	490
44.	West Sak River State 6	5002920142	29 11N 11E	531	-11.0	-1.0	1.70	1.88	3.20	211	972	761
45.	Foggy Island Bay State 1	5002920146	19 11N 17E	522	-12.0	-1.0	1.60	2.11	3.38	207	927	720
46.	Gwydyr Bay South 1	5002920149	8 12N 13E	557	-12.0	-1.0	1.70	1.97	3.35	205	980	775
47.	Kuparuk 9-11-12	5002920158	9 11N 12E	562	-11.0	-0.5	1.80	1.87	3.37	210	963	753
48.	State 1	5002920177	2 10N 13E	570	-11.0	-1.0	1.30	1.76	2.29	209	1316	1107
49.	Prudhoe Bay Drill Site 6-4	5002920179	2 10N 14E	580	-11.0	-0.5	1.70	1.81	3.08	210	1045	835
50.	Highland State 1	5002920199	24 11N 11E	564	-11.0	-1.0	1.70	1.77	3.01	209	1058	849
51.	Prudhoe Bay Unit NGI-7	5002920210	12 11N 14E	550	-12.0	-0.5	1.70	1.91	3.25	207	917	710
52.	BP 12-11-13	5002920085	12 11N 13E	604	-11.0	-0.5	1.81	1.72	3.11	208	1086	878
53.	Prudhoe Bay Drill Site 9-7	5002920223	2 10N 15E	554	-11.0	-1.0	1.70	1.80	3.06	209	1034	825
54.	Prudhoe Bay Drill Site 3-6	5002920224	11 10N 15E	589	-11.0	-1.0	1.70	1.70	2.89	208	1127	919
55.	Kuparuk River Unit 1B-5	5002920237	9 11N 10E	497	-11.0	-1.0	1.70	2.01	3.42	212	883	671
56.	Point McIntyre 2	5002920264	16 12N 14E	550	-12.0	-1.0	1.60	2.00	3.20	206	998	792
57.	Kuparuk River Unit 1D-8	5002920266	23 11N 10E	487	-11.0	-1.0	1.70	2.06	3.50	213	855	642
58.	West Sak River State 9	5002920274	3 11N 9E	454	-11.0	-1.0	1.80	2.20	3.96	215	745	530
59.	West Sak River State 11	5002920275	36 12N 8E	462	-11.0	-1.0	1.70	2.17	3.69	215	791	576
60.	West Mikkelsen State 1	5002920278	32 10N 19E	600	-12.0	-1.5	1.90	1.75	3.33	203	1066	863
61.	Prudhoe Bay Drill Site 1-16	5002920288	8 10N 15E	597	-11.0	-1.0	1.60	1.68	2.69	208	1197	989
62.	Prudhoe Bay Drill Site 7-6	5002920294	33 11N 14E	582	-11.0	-0.5	1.60	1.80	2.88	209	1092	883
63.	Kuparuk River Unit 1A-8	5002920313	5 11N 10E	470	-11.0	-1.0	1.70	2.13	3.62	214	814	600
64.	Prudhoe Bay Unit Q-3	5002920322	16 11N 13E	608	-11.0	-0.5	1.80	1.73	3.11	208	1077	869
65.	Prudhoe Bay Drill Site 13-2	5002920324	14 10N 14E	586	-11.0	-1.0	1.60	1.71	2.74	208	1167	959

Table II-13. Wells and data used to calculate and map the depth and thickness of the methane-hydrate stability field on the North Slope of Alaska (figures II-21, II-22 and II-23).—Continued

(1) Well Index	(2) Well Name	(3) API Number	(4) Location Sec. T. R.	(5)	(6)	(7)	(8)	(9)	(10)	(11)	(12)	(13)
66.	Prudhoe Bay Drill Site 14-5	5002920327	9 10N 14E	573	-11.0	-1.0	1.60	1.75	2.80	209	1130	921
67.	West Sak River 4	5002920343	7 10N 9E	462	-11.0	-1.5	1.50	2.06	3.09	213	917	704
68.	Prudhoe Bay Unit TERM B	5002920355	20 11N 13E	608	-11.0	-0.5	1.80	1.73	3.11	208	1076	868
69.	Prudhoe Bay Unit TERM C	5002920356	3 11N 12E	596	-11.0	-0.5	1.80	1.76	3.17	209	1047	838
70.	Gwydyr Bay State 1	5002920375	9 12N 13E	555	-12.0	-1.0	1.70	1.98	3.37	206	974	768
71.	Milne Point 1	5002920376	23 13N 10E	510	-12.0	-1.0	1.90	2.16	4.10	208	811	603
72.	Prudhoe Bay Drill Site 12-3	5002920377	18 10N 15E	565	-11.0	-1.0	1.70	1.77	3.01	209	1061	852
73.	West Sak CPF 1(23-9-11-10)	5002920378	9 11N 10E	534	-11.0	-1.0	1.80	1.87	3.37	210	943	733
74.	Prudhoe Bay Unit X-1	5002920390	8 10N 14E	540	-11.0	-1.0	1.40	1.85	2.59	210	1143	933
75.	Prudhoe Bay Unit Y-1	5002920394	34 11N 13E	535	-11.0	-1.0	1.40	1.87	2.62	210	1129	919
76.	Gwydyr Bay State Unit 1	5002920396	2 12N 12E	543	-12.0	-1.0	1.70	1.84	3.13	206	943	737
77.	Kuparuk River Unit 1D-5	5002920417	23 11N 10E	512	-11.0	-1.0	1.70	1.95	3.32	212	921	709
78.	West Sak River 14	5002920419	19 11N 9E	454	-11.0	-1.0	1.70	2.20	3.74	215	771	556
79.	Nomination 1	5002920426	34 11N 12E	536	-11.0	-0.9	1.60	1.96	3.14	212	969	757
80.	Kuparuk River Unit 1E-1	5002920464	16 11N 10E	455	-11.0	-1.0	1.70	2.20	3.74	215	775	560
81.	Kuparuk River Unit 1B-1	5002920465	9 11N 10E	495	-11.0	-1.0	1.80	2.02	3.64	212	847	635
82.	Prudhoe Bay Drill Site 17-1	5002920476	22 10N 15E	574	-11.0	-1.0	1.70	1.74	2.96	209	1085	876
83.	Prudhoe Bay Drill Site 11-4	5002920480	34 11N 15E	577	-11.0	-0.5	1.70	1.82	3.09	210	1036	826
84.	Gwydyr Bay State 2	5002920491	11 12N 13E	564	-12.0	-1.0	1.60	2.04	3.26	205	1034	829
85.	Prudhoe Bay Drill Site 16-11	5002920516	24 10N 15E	590	-11.0	-1.0	1.70	1.69	2.87	208	1181	923
86.	Prudhoe Bay Unit TR 15-11-12	5002920524	9 11N 12E	565	-11.0	-0.5	1.80	1.86	3.35	210	970	760
87.	Kuparuk River Unit 1C-1	5002920526	12 11N 10E	536	-11.0	-1.0	1.80	1.87	3.37	210	948	738
88.	MP Tract (43-31-11-136)	5002920536	5 10N 13E	608	-11.0	-1.0	1.60	1.65	2.64	208	1229	1021
89.	West Sak River 16	5002920541	36 11N 8E	497	-11.0	-1.0	2.00	2.01	4.02	212	801	589
90.	West Sak River 17	5002920542	26 13N 9E	512	-11.0	-1.0	2.00	1.95	3.90	212	836	624
91.	MP Tract (22-31-11-13)	5002920545	30 11N 13E	621	-11.0	-0.5	1.80	1.69	3.04	208	1109	901
92.	MP Tract (32-30-11-13)	5002920546	30 11N 13E	628	-11.0	-0.5	1.70	1.67	2.84	208	1168	960
93.	Prudhoe Bay Unit TR T-3C	5002920555	17 11N 15E	576	-11.0	-0.5	1.70	1.82	3.09	210	1035	825
94.	Kuparuk River Unit 1C-8	5002920585	12 11N 10E	534	-11.0	-1.0	1.80	1.87	3.37	210	943	733
95.	West Sak River 23	5002920669	7 12N 9E	461	-11.0	-1.0	1.90	2.17	4.12	215	741	526
96.	West Staines 1	5008920001	18 9N 23E	601	-11.0	-1.0	1.70	1.66	2.82	208	1160	952
97.	East Mikkelsen Bay 1	5008920002	7 9N 21E	586	-11.0	-1.0	1.70	1.71	2.91	208	1119	911
98.	West Staines 2	5008920004	25 9N 24E	612	-11.0	-1.0	1.70	1.63	2.77	207	1191	984
99.	Point Thomson Unit 1	5008920005	32 10N 23E	596	-12.0	-1.0	1.70	1.85	3.15	204	1077	873
100.	Point Thomson Unit 2	5008920006	3 9N 22E	598	-11.0	-1.0	1.70	1.67	2.84	208	1151	943
101.	Fish Creek 1	5010310001	15 11N 1E	182	-11.6	-3.5	0.87	4.46	3.89	247	393	146
102.	Colville Delta 1	5010320002	9 13N 6E	558	-12.0	-1.5	2.00	1.88	3.76	204	936	732
103.	Cape Halkett 1	5010320004	5 16N 2W	304	-12.0	-3.5	1.70	2.80	4.76	217	535	318
104.	South Harrison Bay 1	5010320007	6 12N 2E	274	-11.4	-3.1	1.00	3.04	3.04	225	711	486
105.	Atigaru Point 1	5010320008	19 14N 2E	293	-10.8	-3.0	1.96	2.67	5.24	223	472	249
106.	West Sak River 15	5010320013	5 10N 8E	438	-11.0	-1.5	1.50	2.17	3.26	215	846	631
107.	West Sak River 20	5010320018	5 9N 8E	409	-11.0	-1.5	1.40	2.32	3.25	217	803	586
108.	West Sak River 18	5010320019	16 11N 8E	455	-11.0	-1.5	1.60	2.09	3.34	213	855	642
109.	Awana 1	5015520001	30 3S 25W	177	-09.0	-3.6	0.99	3.05	3.03	243	556	313
110.	South Moede 1	5016320001	31 15N 19W	160	-10.2	-2.0	0.83	5.10	4.21	0	0	0
111.	Kugrua 1	5016320002	8 14N 26W	250	-10.6	-1.2	0.91	3.76	3.41	244	468	224
112.	Susie Unit 1	5022310001	22 2N 13E	253	-08.0	-1.0	1.10	2.77	3.05	245	526	281
113.	Echocka 1	5022320008	32 1N 16E	254	-06.6	-0.6	0.89	2.36	2.11	248	838	590
114.	Ivishak Unit 1	5022320014	6 1S 16E	289	-07.0	-1.0	1.00	2.08	2.08	240	963	723
115.	Simpson Core Test 13	5027910013	24 19N 11W	219	-12.0	-3.8	0.87	3.99	3.48	232	596	364
116.	Drew Point 1	5027920002	26 18N 8W	250	-11.3	-2.6	1.17	3.48	4.08	233	467	234
117.	Ikpikuk 1	5027920004	25 13N 10W	280	-10.6	-1.9	0.89	3.12	2.74	232	719	487
118.	East Simpson 1	5027920005	18 18N 10W	259	-11.0	-3.3	1.19	2.97	3.52	226	589	363
119.	J. W. Dalton 1	5027920006	14 18N 5W	270	-12.0	-3.9	1.47	2.93	4.32	219	547	328
120.	Umiat 11	5028710011	27 1N 1W	238	-08.0	-2.1	1.00	2.46	2.46	240	754	514
121.	East Umiat 1	5028710016	19 1S 2E	169	-08.5	-2.4	1.00	3.62	3.62	0	0	0
122.	Kuparuk 1	5028710018	1 2S 5E	211	-08.8	-2.6	0.94	2.93	2.74	242	632	390
123.	Koolak 1	5029710001	25 7N 34W	198	-10.0	-3.4	1.00	3.34	3.34	240	273	33
124.	Poard Bay 1	5030120002	25 16N 28W	270	-10.3	-1.3	0.90	3.32	2.97	238	597	359

(5) Depth to the base of ice-bearing permafrost (m), (Collett and others, in press-a).

(6) Surface temperature (°C), (Collett and others, in press-b).

(7) Temperature at the base of ice-bearing permafrost (°C), (Collett and others, in press).

(8) Ratio between the geothermal gradient below the base of the ice-bearing permafrost over the geothermal gradient above the base of the ice-bearing permafrost (Collett and others, in press-b).

(9) Geothermal gradient within the ice-bearing permafrost (°C/100m), (Collett and others, in press-b).

(10) Geothermal gradient below the base of the ice-bearing permafrost (°C/100m), (Collett and others, in press-b).

(11) Calculated depth to the top of the methane hydrate stability field (m).

(12) Calculated depth to the base of the methane hydrate stability field (m).

(13) Calculated total thickness of the methane hydrate stability field (m).

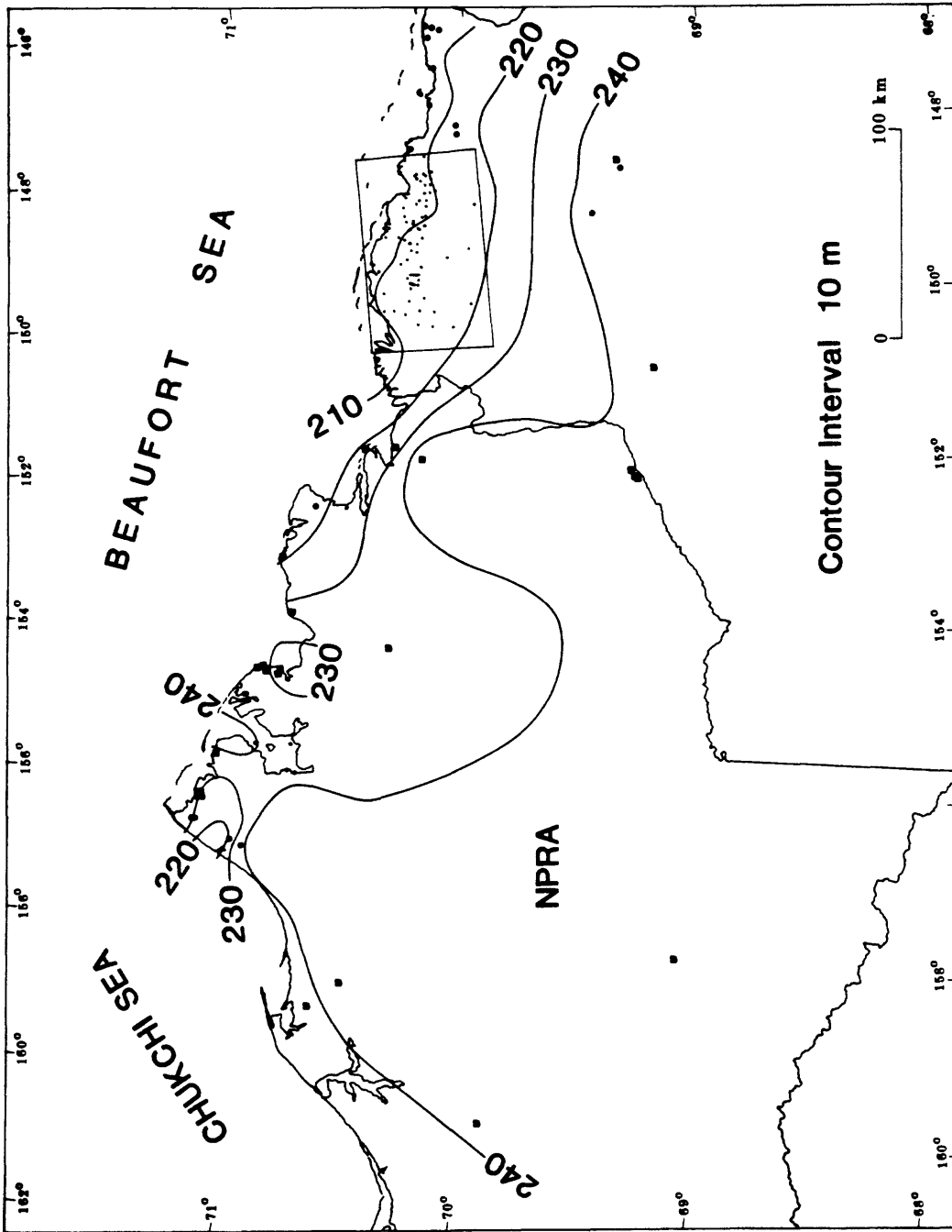


Figure II-21. Contour map of the central North Slope showing depth (in meters) to the top of the methane-hydrate stability field based on data in table II-13.

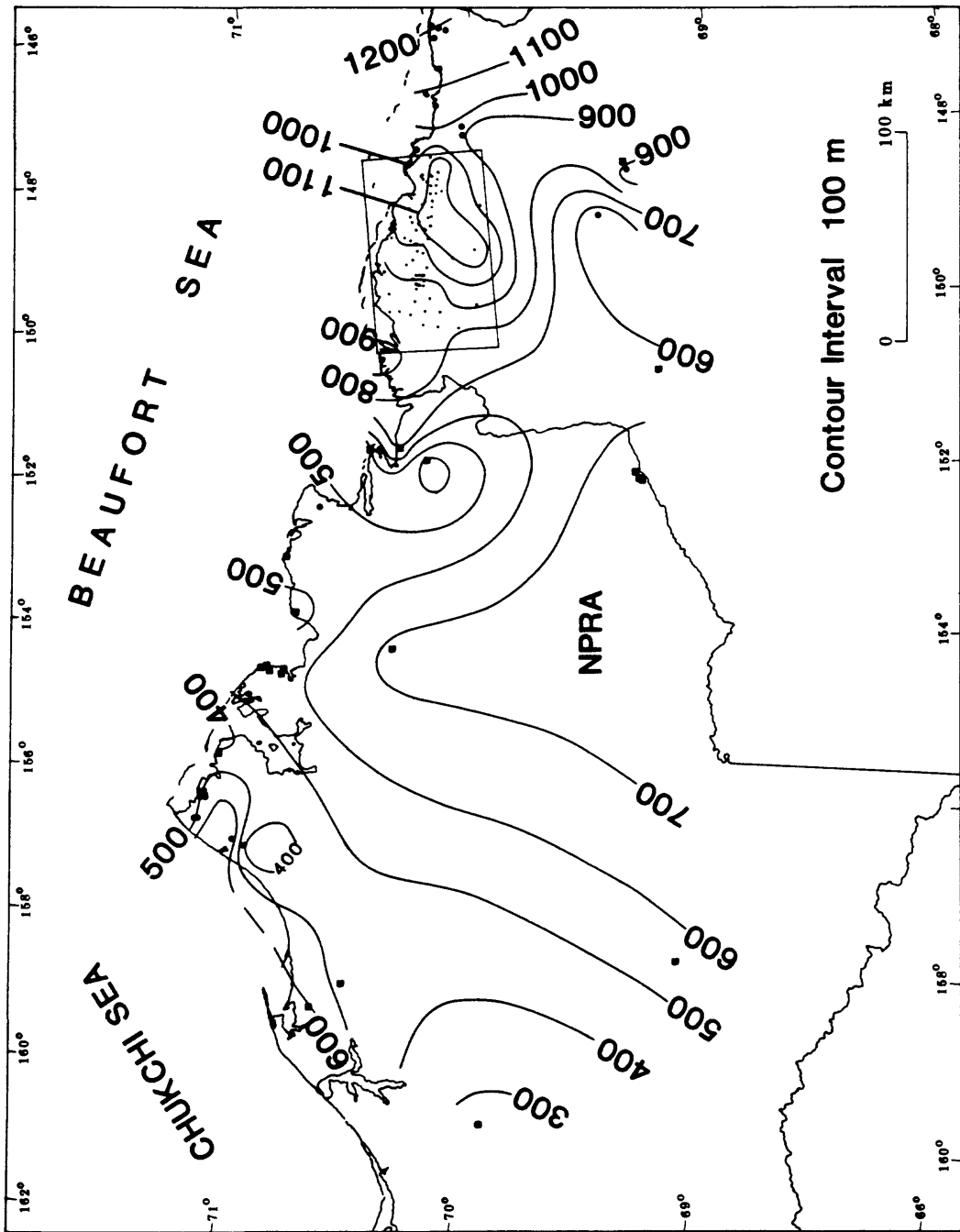


Figure II-22. Contour map of the central North Slope showing depth (in meters) to the base of the methane-hydrate stability field based on data in table II-13.

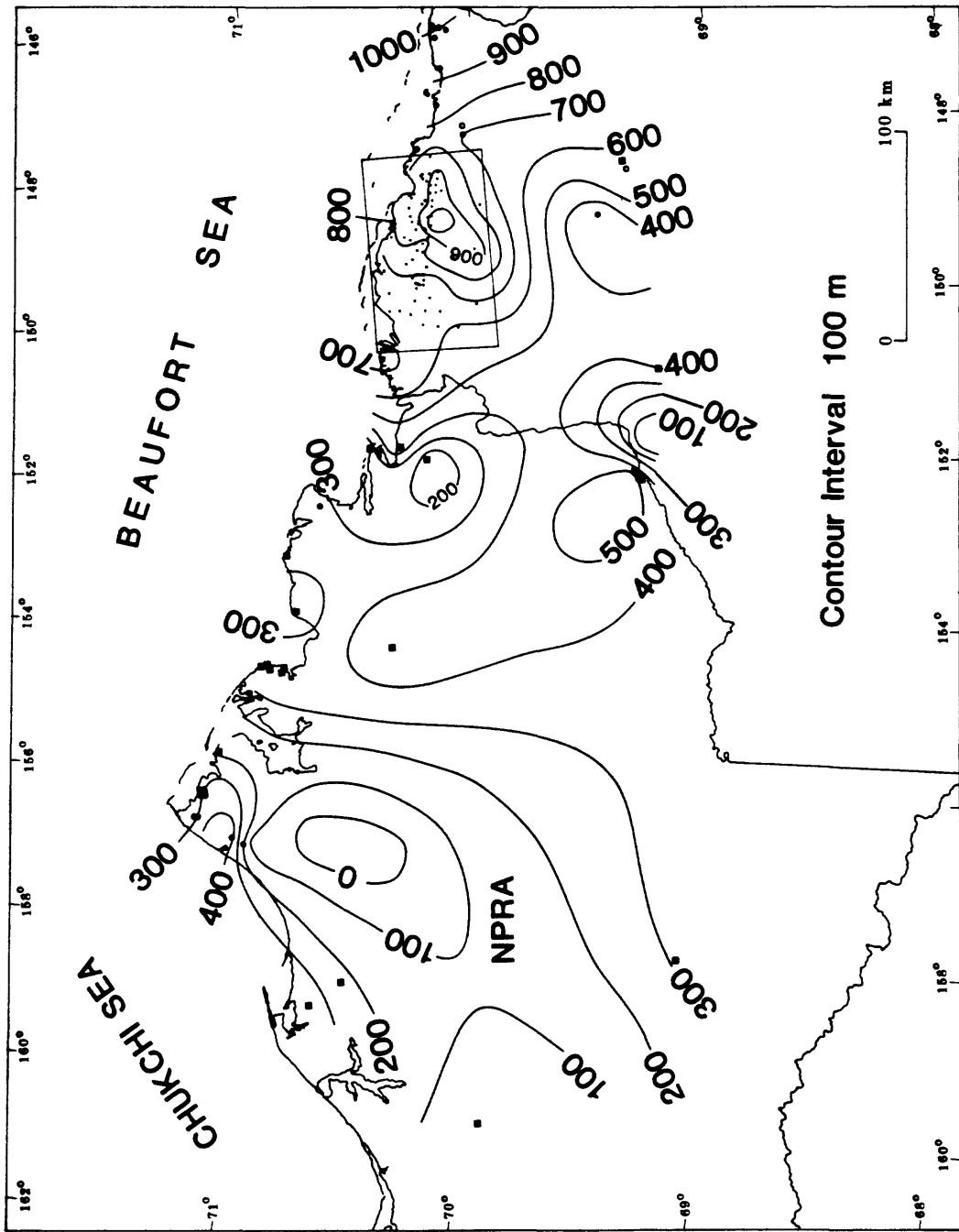


Figure II-23. Isopach map of the central North Slope showing thickness (in meters) of the methane-hydrate stability field based on data in table II-13.

CHAPTER III. GEOLOGIC SETTING

III.A. REGIONAL GEOLOGY

This chapter on geologic setting is divided into two sections: Section "A" deals with a review of the regional geology of the study area. In Section "B" the local structural-stratigraphic framework in the Prudhoe Bay and Kuparuk River area is described.

The North Slope of Alaska, one of several petroleum-bearing areas bordering the Arctic Ocean (fig. III-1), encompasses all of the land north of the Brooks Range drainage divide and is generally subdivided into three physiographic provinces, from south to north: the Brooks Range, the foothills, and the coastal plain (fig. III-2). Oriented in a subparallel east-west direction, these provinces reflect underlying geologic trends. The three main structural elements that compose the North Slope are the Brooks Range orogen, the Colville trough, and the Barrow arch, all of which correspond generally to the respective physiographic provinces (fig. III-3).

The Barrow arch is a broad regional basement high that separates the Colville trough from the present Arctic Ocean basin. The basement, at relatively shallow depths along the Barrow arch, slopes gently southward and reaches a depth of about 10,000 m in the Colville trough. The southern part of the trough is overridden by the Brooks Range orogen, which contains basement and younger rocks. These structural relations are diagrammatically illustrated in a cross section trending north through Point Barrow (fig. III-4).

Much new information on the stratigraphic and petroleum geology of the North Slope has been published since the summary by Brosge and Tailleir (1971). This new information includes publications on the NPRA by Carter and others (1977), Bird (1978), Bird and others (1978), Ahlbrandt (1979), Magoon and Claypool (1979), and Bird (1986); on the Prudhoe Bay area by the Alaska Geological Society (1972, 1977, 1979), Jones and Speers (1976), Bird and Jordan (1977), USGS (1978), and Molenaar and others (1986); and on the Arctic National Wildlife Range (ANWR) area by Reiser and others (1978), Armstrong and Mamet (1975), Detterman and others (1975), Sable (1977), Grantz and Mull (1978), Kososki and others (1978), Palmer and others (1979), Bird and Magoon (1987), and Tailleir and Weimer (1987). The tectonic setting of the North Slope in relation to adjacent offshore areas has been summarized in Grantz and others (1975, 1982), and Grantz and May (1983).

The bedded rocks of the North Slope can be conveniently grouped into three sequences that reflect major episodes in the tectonic development of the region and, to a degree, its lithologic character. Defined on the basis of source area, these sequences, proposed by Lerand (1973) and applied to northern Alaska by Grantz and others (1975) are, in ascending order, the Franklinian (Cambrian through Devonian), the Ellesmerian (Mississippian through Jurassic), and the Brookian (Cretaceous to Holocene). The areal distribution of these sequences and significant structural trends on the North Slope are shown on the map in figure III-5. Figures III-6 and III-7 separately summarize these sequences and their component formations for the western and eastern regions of the North Slope.

FRANKLINIAN SEQUENCE

The Franklinian (pre-Mississippian) sequence is generally considered nonprospective for petroleum in the western North Slope area. This sequence is best known in the northern Brooks Range, where it consists of a variety of deformed and mildly metamorphosed clastic and carbonate geosynclinal rocks (Reiser and others, 1978; Armstrong and Mamet, 1975). Most wells drilled into this sequence have penetrated argillite. Ordovician and Silurian graptolites and chitinozoans have been recovered from this argillite at Point Barrow and Prudhoe Bay (Carter and Laufeld, 1975). Late Devonian orogenic uplift in what is now northern Alaska shed large amounts of clastic debris southward. Thick clastic wedges, composed mainly of quartz and chert (the Kanayut Conglomerate and its marine equivalent, the Hunt Fork Shale), are present in the Brooks Range. Subsequent erosion and subsidence of the Devonian orogen provided a platform for deposition of the Ellesmerian sequence.

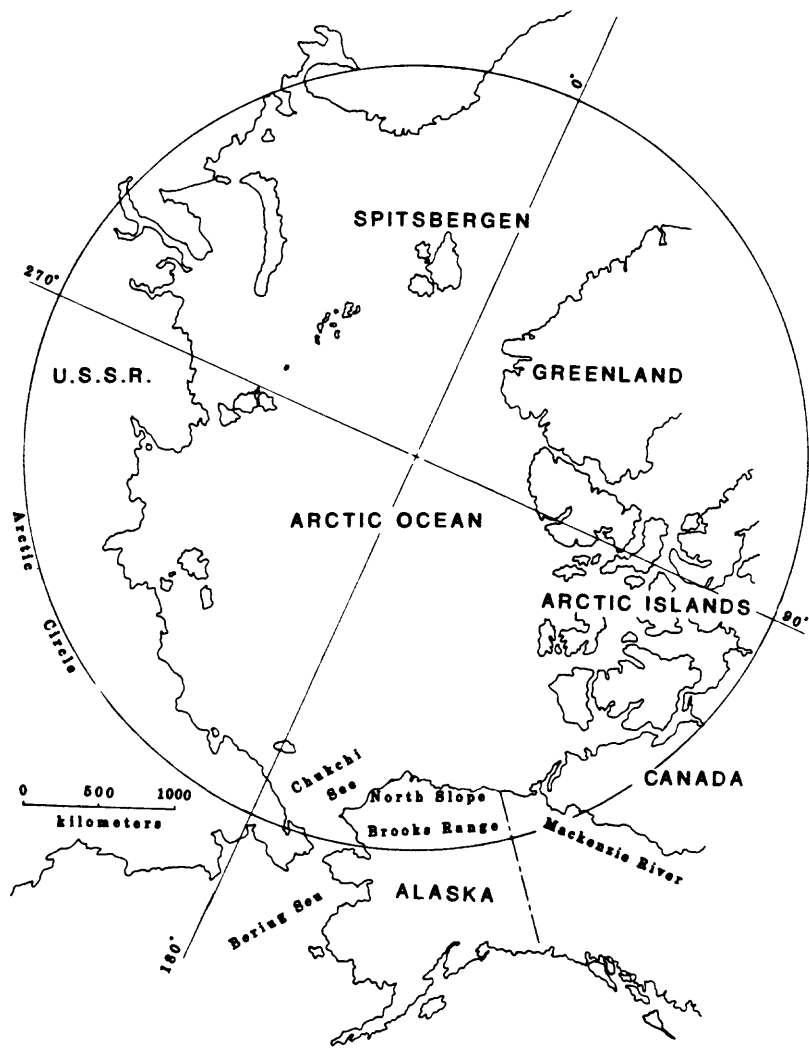


Figure III-1. Location of the North Slope of Alaska in relation to other circum-Arctic lands. Other petroleum-bearing areas include Arctic USSR, Mackenzie Delta, and Canadian Arctic Islands.

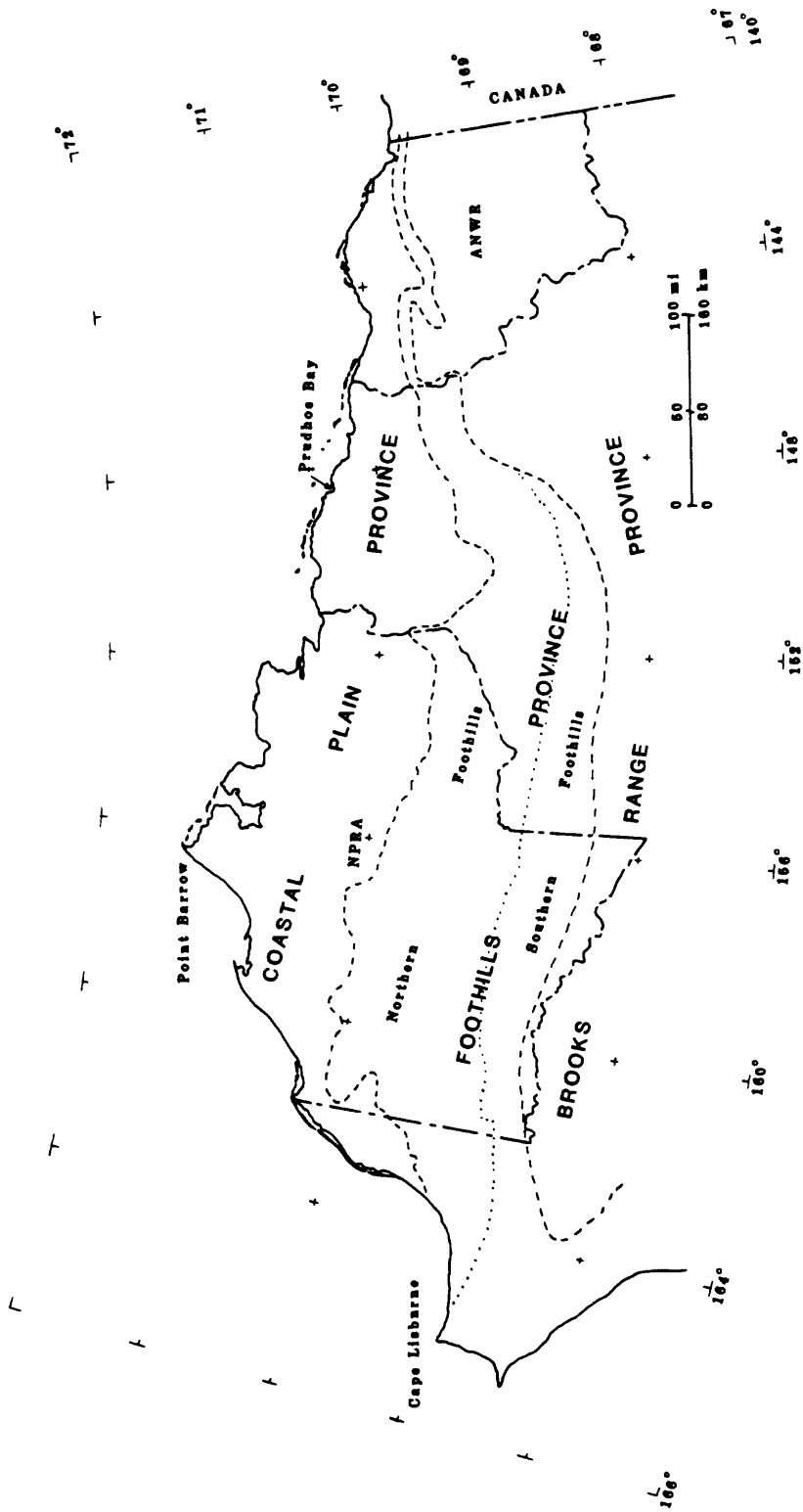


Figure III-2. Physiographic provinces of the North Slope.

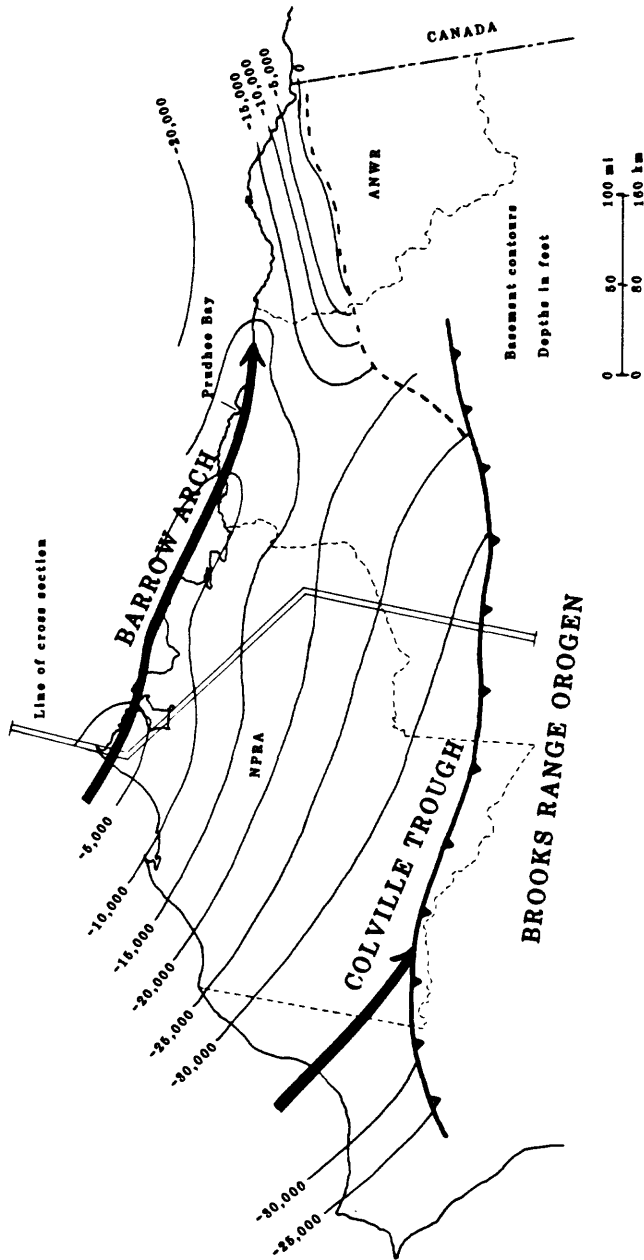


Figure III-3. Major tectonic features of North Slope in Alaska.

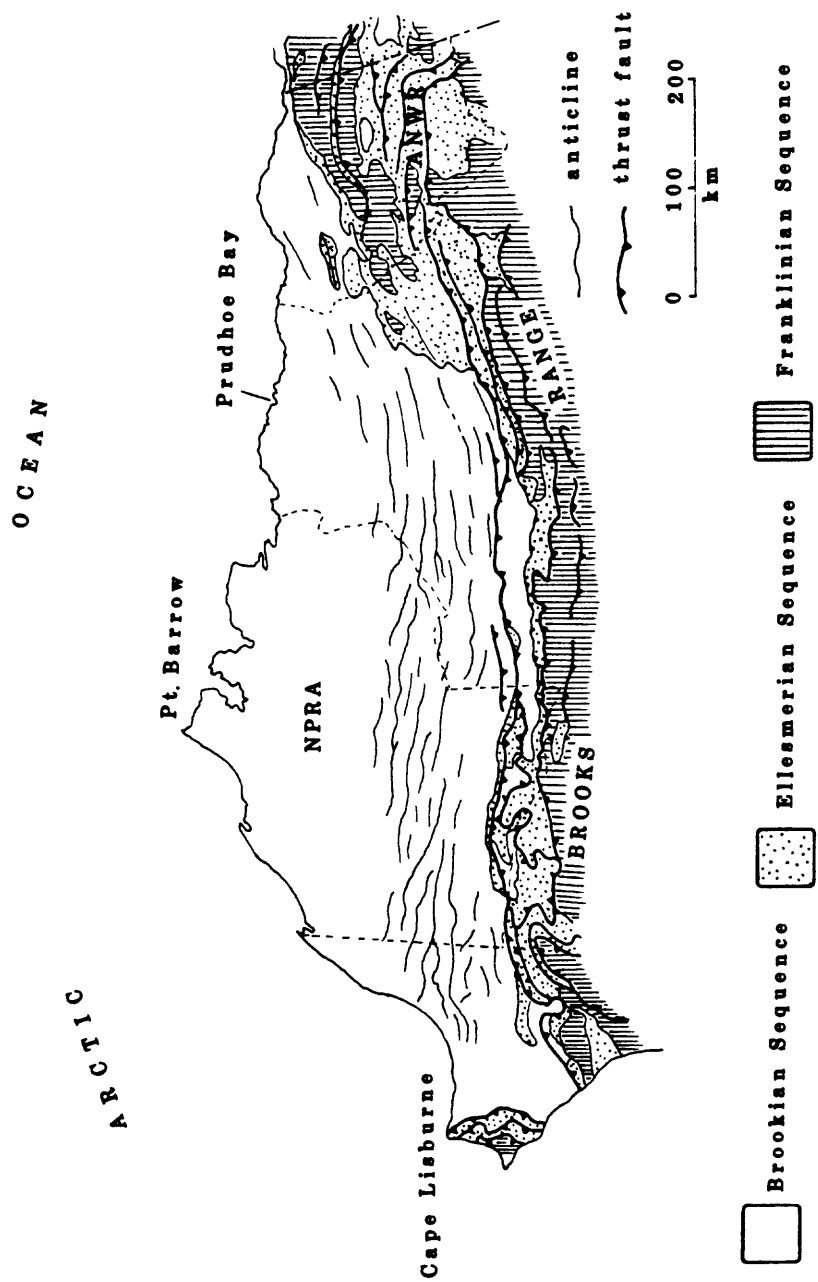


Figure III-5. Generalized geologic map of North Slope showing distribution of major rock sequences, thrust faults, and anticlines.

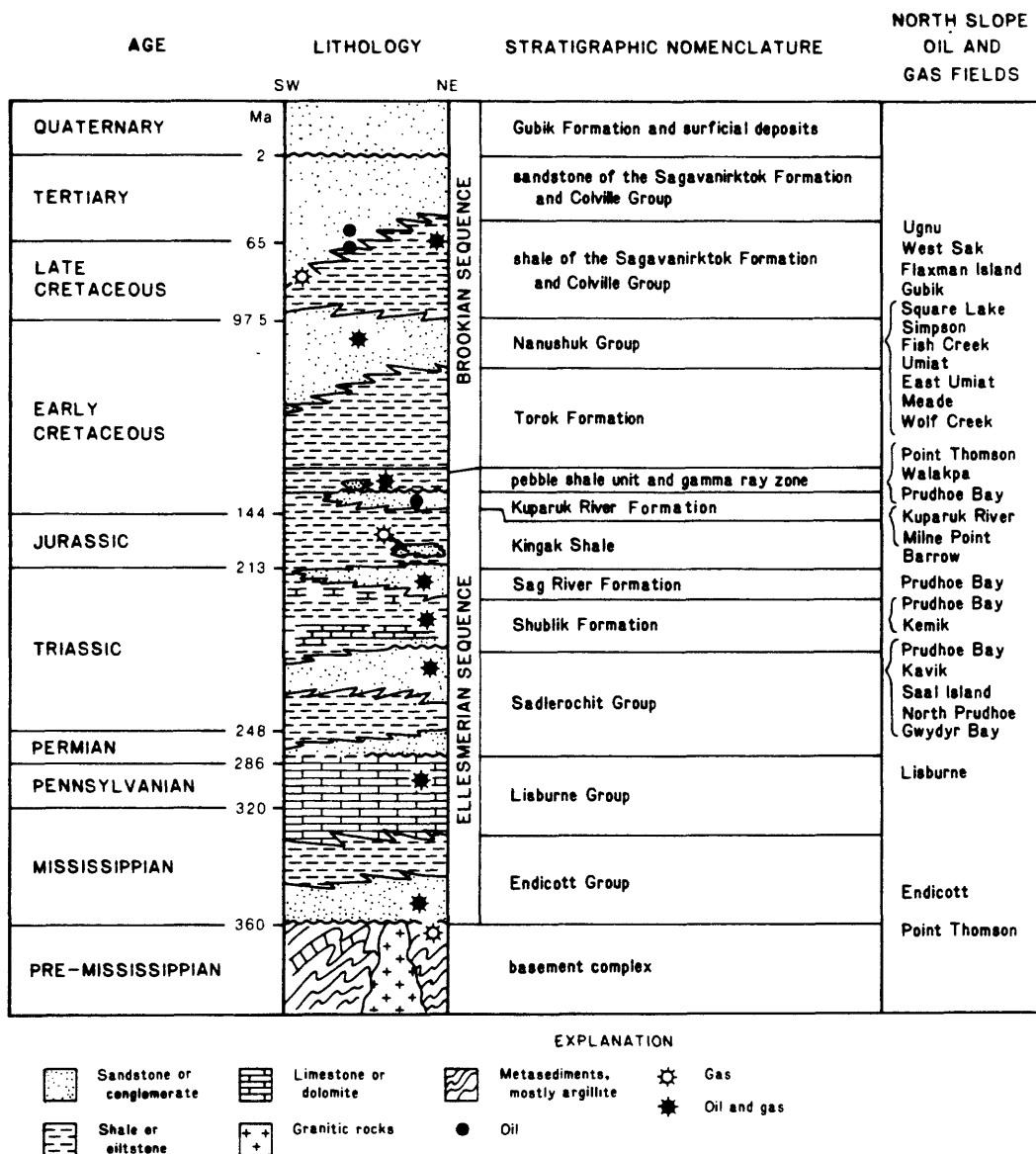


Figure III-6. Generalized stratigraphic column for western North Slope, exclusive of the allochthonous rocks in the Brooks Range, showing stratigraphic locations of petroleum-bearing formations (Bird, 1986).

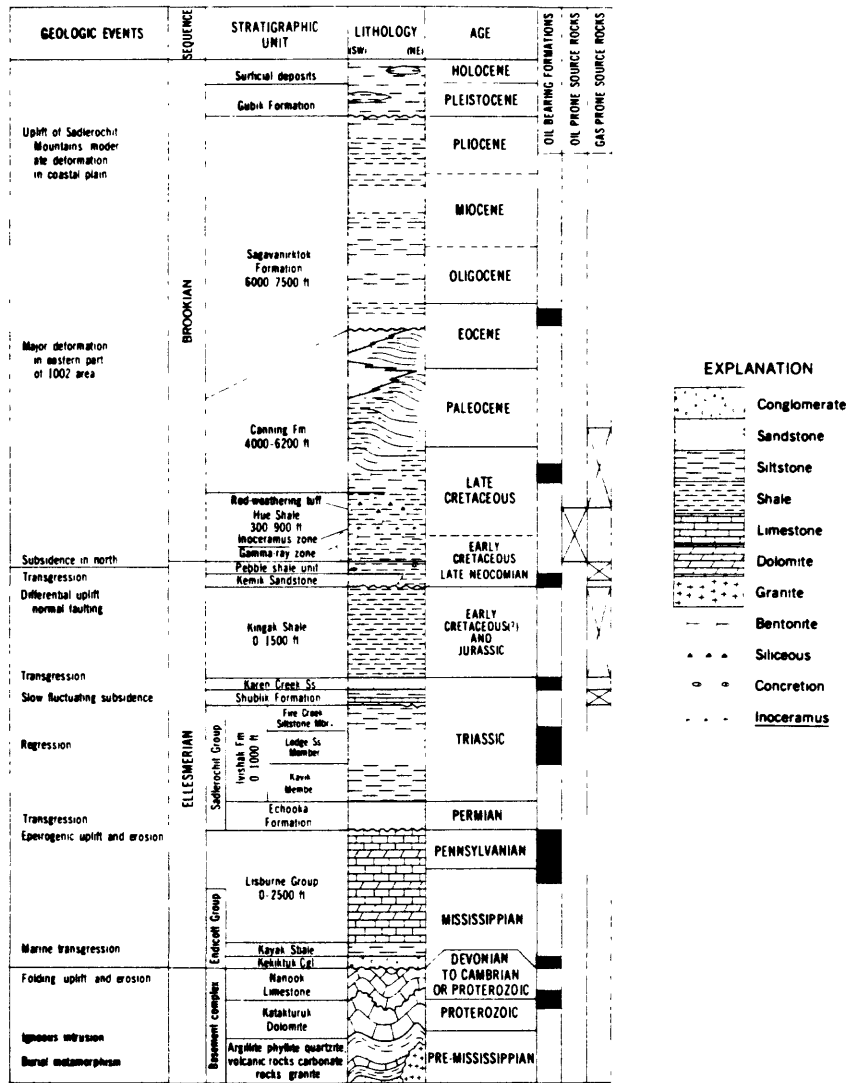


Figure III-7. Generalized stratigraphic column for northern part of the ANWR showing oil-bearing formations west of ANWR and potential source rocks. Vertical scale is not uniform (Bird and Magoon, 1987).

ELLESMERIAN SEQUENCE

The Ellesmerian (Mississippian to Early Cretaceous) sequence records a major northward advance of the sea. The sequence consists of shallow-marine and nonmarine clastic rocks, composed predominantly of quartz and chert, and of platform carbonate rocks. Such features in the rocks as northward onlap, increasing grain size, decreasing stratigraphic thickness, and numerous unconformities suggest that the ancient shoreline lay near the present coast and that the open ocean was to the south. Periods of mild tectonic activity and local volcanism are represented in the lower part of the sequence (Reiser and others, 1979). Differential subsidence accompanied by faulting created local basins (for example, the Ikpikpuk and Meade basins) containing as much as 5,000 m of Carboniferous and Permian rock. By Triassic time, most deformation ended and consequent local variations in sedimentary thickness were eliminated.

Mississippian clastic rocks and coal of the Endicott Group unconformably overlie steeply dipping, mildly metamorphosed basement rocks of the Franklinian sequence. The clastic rocks grade upward and laterally into shallow-marine carbonates of Carboniferous and Permian age (the Lisburne Group). Southward retreat of the sea during Permian time terminated carbonate deposition and created a regional unconformity that truncates older sedimentary deposits in the north. After the northward readvance of the sea, clastic sedimentation predominated. Important sandstone reservoir rocks were deposited during the Permian and Triassic (the Sadlerochit Group), Late Triassic (the Sag River Sandstone), Middle Jurassic (unnamed sandstone), and Early Cretaceous (the Kuparuk River Sandstone). All sandstone units are of limited areal extent and grade southward (down-dip) into siltstone and shale that are potential source rocks. Important petroleum-source-quality shale was deposited during transgressions in the Middle to Late Triassic (the Shublik Formation), Jurassic and Early Cretaceous (the Kingak Shale), and Early Cretaceous (pebble shale unit).

The following differences in the Ellesmerian sequence on the Barrow arch between the NPRA and the Prudhoe Bay area are noteworthy. In the NPRA the Ellesmerian sequence displays successively northward onlapping rock units. In contrast, at Prudhoe Bay and eastward, very little onlap is evident; instead, the entire sequence is truncated and over-lapped by Cretaceous marine shale. This truncation by Late Jurassic-Early Cretaceous subaerial erosion, related to rift-margin uplift, is postulated to have improved the porosity of exposed Ellesmerian reservoir rocks by leaching (Melvin and Knight, 1984). Overlap of the truncated sequence by Cretaceous seas juxtaposed potential (Cretaceous) source rocks and reservoir rocks. This relation of rich Cretaceous source rocks to porosity-enhanced reservoir rocks occurs only locally and on a small scale in the NPRA.

In the Brooks Range, the Ellesmerian sequence consists of a variety of rock types that have been juxtaposed by faulting; these rock types include Mississippian shallow-marine clastic rocks (the Endicott Group and the Nuka Formation), shallow- to deep-marine carbonate rocks (the Lisburne Group), Pennsylvanian through Jurassic siliceous shale, chert, and minor amounts of limestone, local oil shale of Mississippian, Triassic, and Jurassic age (Tailleur, 1964), and intrusive and extrusive basic igneous rocks are known from the Mississippian, Permian, and Jurassic age (Ellaersieck and others, 1979; Reiser and others, 1979).

BROOKIAN SEQUENCE

The Brooks Range orogeny drastically changed the paleogeography of Arctic Alaska. Northern sources were replaced by southern sources--the ancestral Brooks Range. Initially, however, sediment was supplied from both northern (Ellesmerian) and southern (Brookian) sources. As the Brooks Range was uplifted, regional subsidence immediately to the north formed the Colville trough. Subsidence of the rifted northern land area took place by northward downwarping and by normal faulting concentrated along a linear zone approximately parallel to the present shoreline. The resulting structure, the Barrow arch, is a linear basement ridge plunging to the southeast. Numerous oil and gas fields, including the Prudhoe Bay field, are situated along the crest of this feature. Grantz and others (1979) postulated that the Barrow arch is but one of three segments of contrasting structure and stratigraphy that make up the continental margin north of Alaska.

Present-day landforms and most structures on the North Slope are related to the Brooks Range orogeny. The driving force for that widespread and long-lasting period of deformation is considered by many to be rifting and rotation of northern Alaska away from the continental margin of northern Canada (Grantz and others, 1979). Deformation in much of the Brooks Range is characterized by

east-trending, low-angle, northward-yielding thrust faults. Aggregate shortening by 100 to 500 km is postulated for those faults in the western part of the range (Snelson and Tailleur, 1968; Tailleur, 1969; Martin, 1970; and Mayfield and others, 1983). A comparable amount of shortening is postulated for the central Brooks Range (Butler and others, 1985). In the northeastern part of the range, however, deformation is characterized more by vertical uplift and folding, and by high-angle reverse faulting. In the southern foothills immediately north of the Brooks Range, structural style resembles that of the range itself; deformation diminishes northward in a series of linear detachment folds (fig. III-5).

Throughout the orogeny, large volumes of clastic debris were shed from the rising Brooks Range northward (and probably southward as well) into a foredeep. Older uplifted sedimentary rocks to the southwest and younger deeply buried sedimentary deposits to the northeast indicate that the orogen and foredeep migrated northeastward. The oldest Brookian orogenic deposit (Neocomian) is a flysch-like sequence of turbidites (the Okpikruak Formation) exposed in the Brooks Range and southern foothills. To the north, in the subsurface, is the pebble shale unit, slightly younger than the Okpikruak Formation. This black marine shale, partly of northern derivation, forms part of a sequence of Cretaceous shale units.

Throughout the remainder of Cretaceous and Tertiary time, periodic influxes of coarse terrigenous debris accumulated in thick clastic wedges in the Colville trough. Prominent among these deposits are the Lower Cretaceous Fortress Mountain Formation, the Upper Lower and lower Upper Cretaceous Nanushuk Group, and the Upper Cretaceous to Tertiary Sagavanirktok Formation (figure III-8). Periods of relative basin subsidence separated these wedges with thick marine shale sections; the depocenter of each wedge is successively farther northeast. The depocenter in the middle part of Cretaceous time was southwest of the NPRA, whereas depocenters in Late Cretaceous and Tertiary time was near Prudhoe Bay and partly offshore. Most oil and gas fields in the NPRA and several of the latest discoveries east of Prudhoe Bay are in Brookian rocks.

III.B. GEOLOGY OF THE PRUDHOE BAY AND KUPARUK RIVER AREA

Preliminary review of all geologic data, including drilling plans, well histories, daily drilling reports, mud reports, coring information, and geophysical well logs, indicate that in-situ gas hydrates occur only in the Prudhoe Bay and Kuparuk River area of the North Slope (to be discussed in Chapter IV). Therefore, in this section of Chapter III the local geology within the Prudhoe Bay--Kuparuk River area is described. The distribution of the major oil and gas accumulations is characterized, followed by a description of the near-surface stratigraphic framework developed as part of this project. This chapter will conclude with descriptions of the potential gas-hydrate reservoir rocks, and a characterization of possible hydrocarbon traps within the Prudhoe Bay--Kuparuk River area.

The Prudhoe Bay--Kuparuk River area shown on the map in figure III-9 and in the cross sections of figures III-10 and III-11 encompasses six known oil accumulations including the super-giant Prudhoe Bay oil field (1) with production from the Sadlerochit Group. The second largest producing oil accumulation is within the Kuparuk River Formation, with production in the Kuparuk River (field no. 2, fig. III-9) and Milne Point (field no. 3, fig. III-9) oil fields. Other, deeper, reservoirs recently brought on-line are within the Lisburne (4) and Endicott (5) Groups (see Bird and Magoon, 1987, for complete references). Reservoired within 1,400 m of the surface in the Sagavanirktok Formation of the Kuparuk River area is an estimated 26 to 44 billion barrels of heavy-oil and tar (Werner, 1987). These oils are reservoired within a series of sandstone units which have been grouped into two packages informally referred to by ARCO Alaska as the West Sak and Ugnu sands. These oil bearing sands are of particular interest because some of the oil is reservoired within the zone of methane-hydrate stability, as described in Chapter II and shown in figure III-11. This relation will be further explored in Chapter IV.

The zone of methane-hydrate stability in the Prudhoe Bay--Kuparuk River area is limited to the Brookian sequence of rocks, as shown in figures III-10 and III-11. Therefore, the remainder of this chapter will deal with the development of a stratigraphic-structural framework in the Brookian rocks.

III.B.1. Stratigraphic Framework

To investigate possible geologic controls on the occurrence of in-situ gas hydrate, well-log data from 106 wells have been used to construct ten detailed geologic cross sections (locations shown on

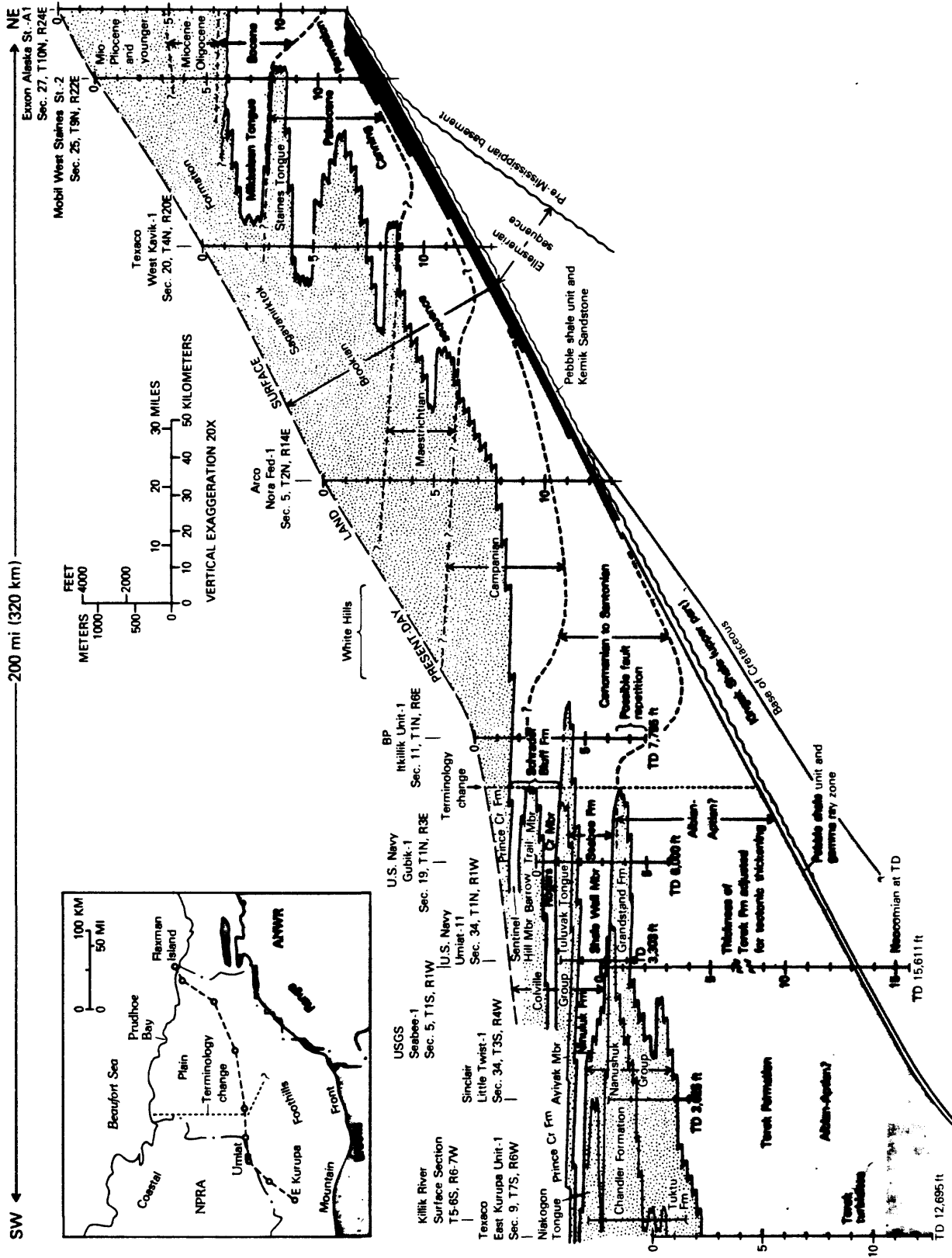


Figure III-8. Regional stratigraphic cross section of Cretaceous and Tertiary rocks from central North Slope to northeastern North Slope. Series and stage boundaries (short dashed lines) are approximate. Well depths are in thousands of feet (Molenaar and others, 1986).

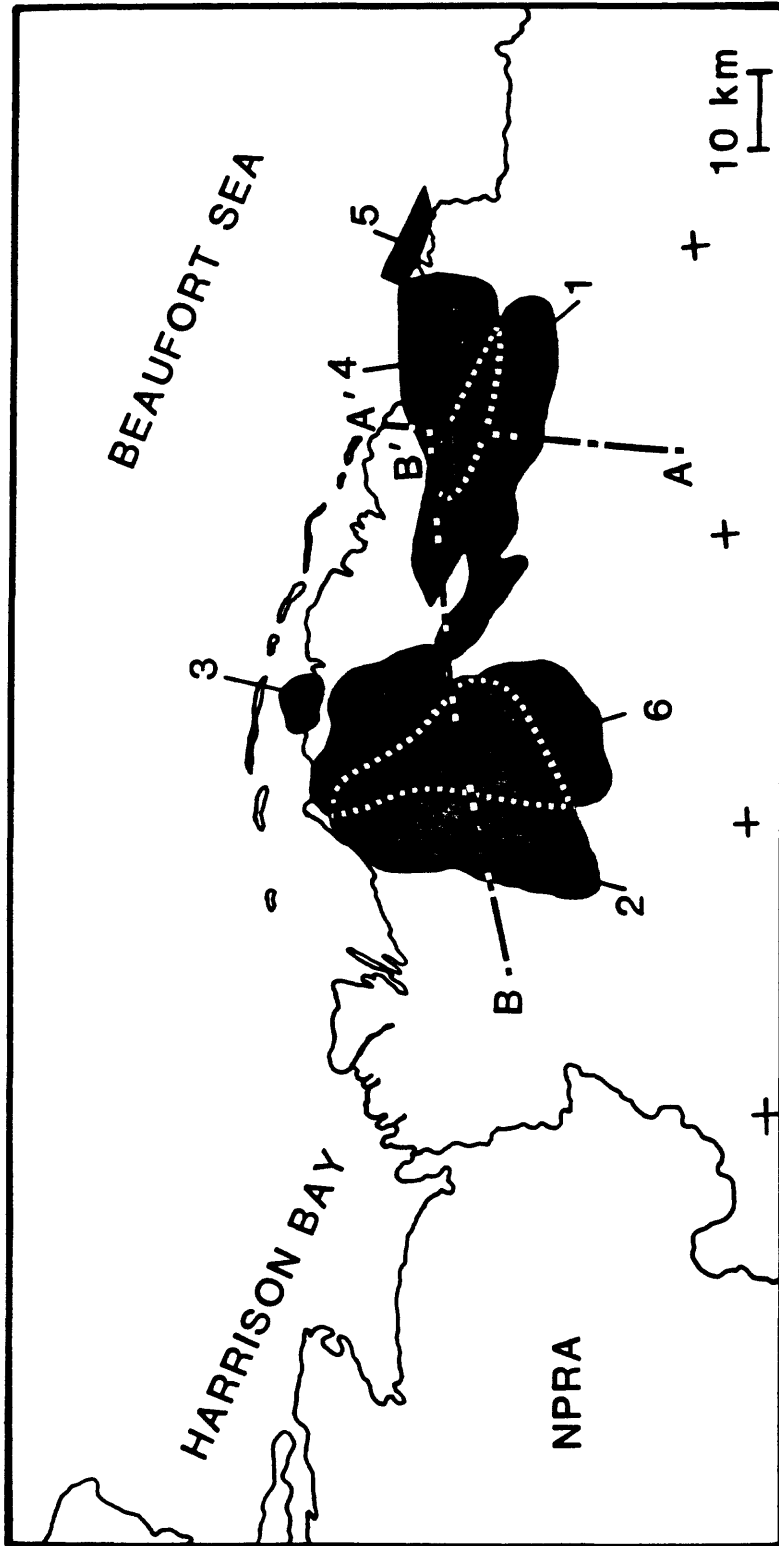


Figure III-9. Distribution of oil accumulations in the Prudhoe Bay--Kuparuk River area: 1) Prudhoe Bay (production from Sadlerochit Group), 2) Kuparuk River (production from Kuparuk River Formation), 3) Milne Point (production from Kuparuk River Formation), 4) Lisburne (production from Lisburne Group), 5) Endicott (production from Endicott Group), and 6) West Sak-Ugnu sands (production from Sagavanirktok Formation). Also shown are the location of the cross sections in figures III-10 (A-A') and III-11 (B-B').

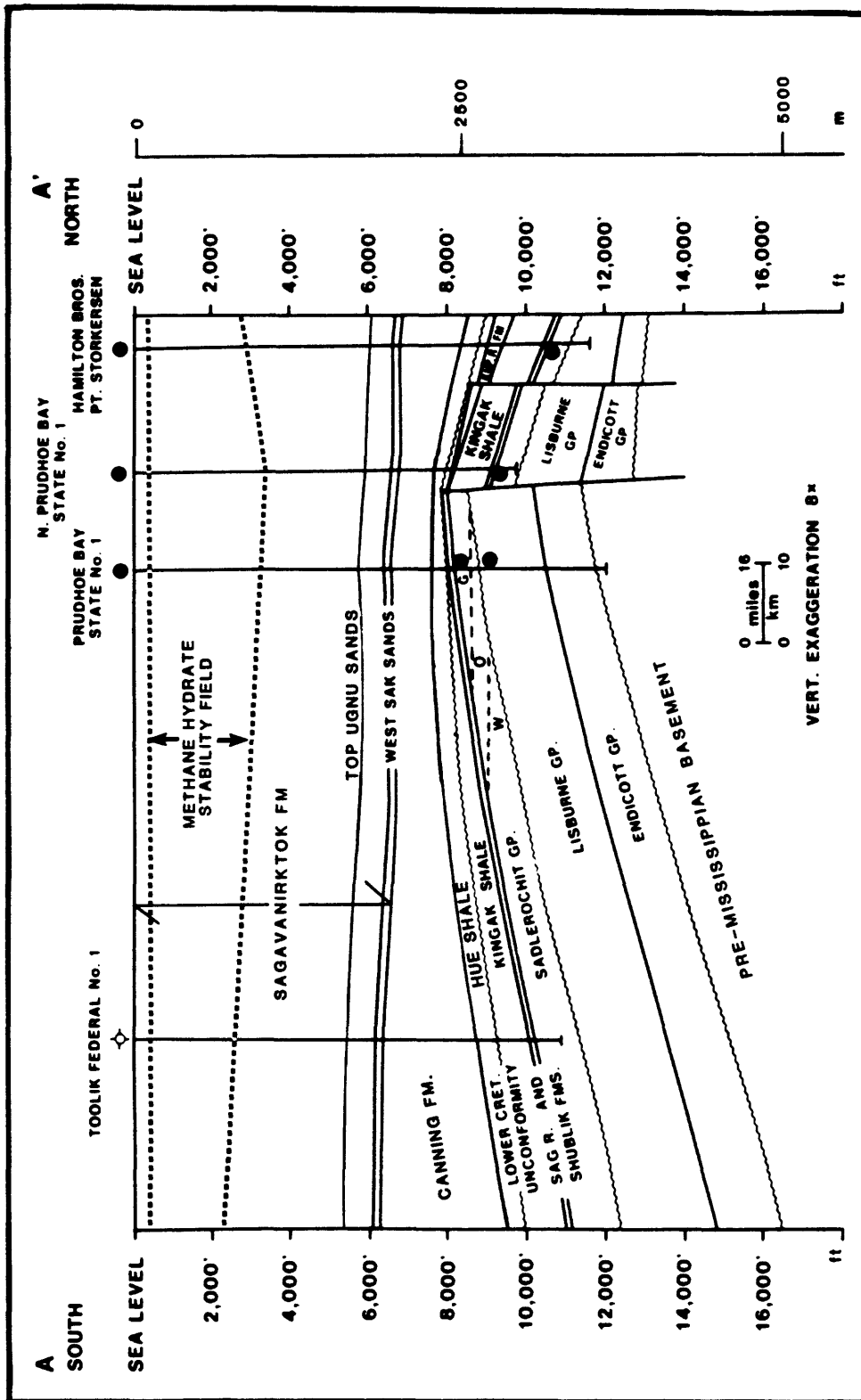


Figure III-10. Cross section through the Prudhoe Bay area illustrating the relation of the gas-hydrate stability field to the stratigraphic framework. For location, see figure III-9. (Adapted from Jamison and others, 1980, fig. 7).

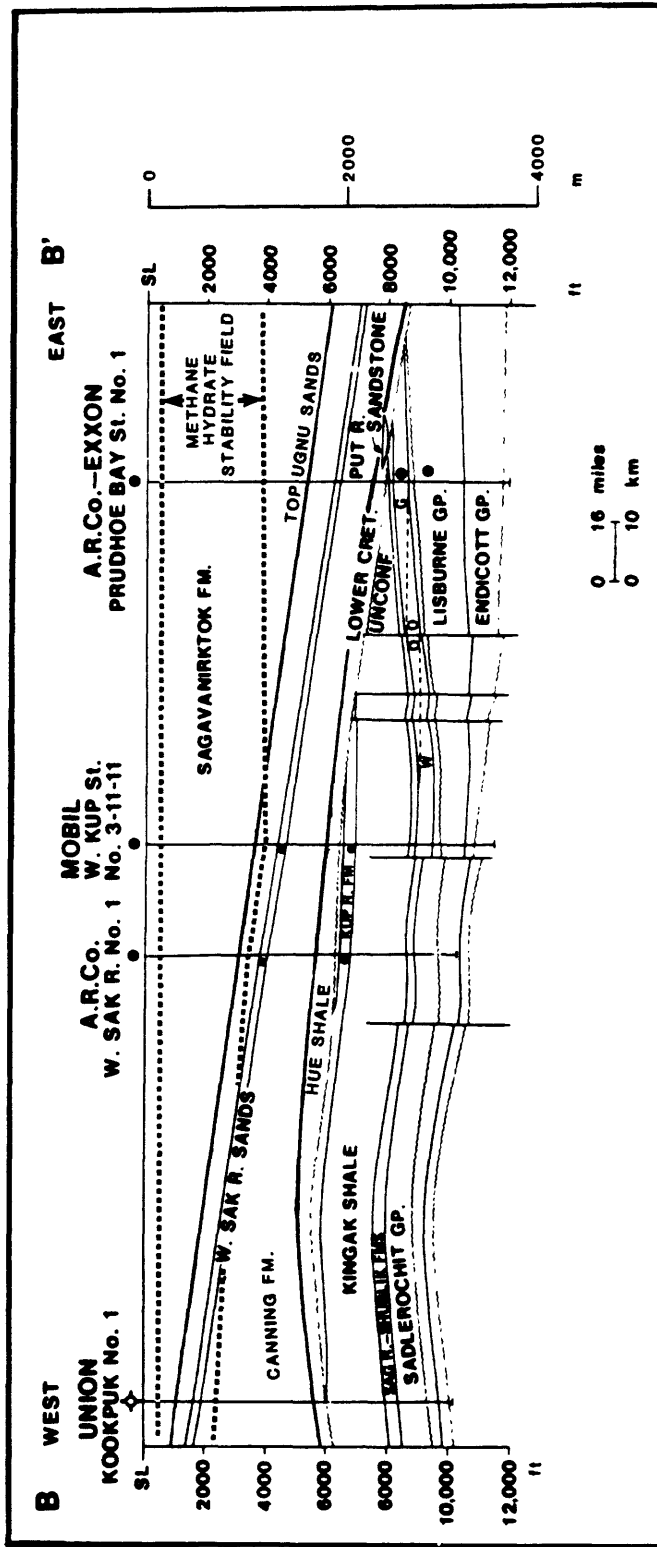


Figure III-11. Cross section through the Prudhoe Bay area illustrating the relation of the gas-hydrate stability field to the stratigraphic framework. For location, see figure III-9. (Adapted from Jamison and others, 1980, fig. 8).

the map in figure III-12) within the upper 2,000 m of sediment in the Prudhoe Bay--Kuparuk River area. The stratigraphic framework developed from these cross sections is based on 22 markers picked from the gamma ray and electrical resistivity well logs. Each log marker represents an abrupt lithologic change that produces a notable characteristic response on the logs. The 22 markers are laterally persistent and were used to define the upper and lower boundaries of stratigraphic units. To summarize the regional stratigraphic relations developed in these cross sections, eight of the wells used to construct the geologic-framework have been displayed in three correlation sections in figures III-13, III-14, and III-15.

The remainder of this discussion on the stratigraphic-framework in the Prudhoe Bay--Kuparuk River area is limited to a description of the rock units above the Lower Cretaceous Unconformity (LCU) (Marker 1 of this study; table III-1). Locally, the Lower Cretaceous unconformity cuts into the Kingak Shale, and is overlain by the pebble shale unit. However, in the Kuparuk River area the pebble shale unit may conformably and gradationally overlie the Kuparuk River Formation without a break in sedimentation. All of the rocks above the pebble shale unit are assigned to the Brookian sequence, a thick, northeasterly prograding, basinal, basin-slope, shallow-marine, and nonmarine group of shelf deposits derived from the ancestral Brooks Range orogenic belt to the south and southwest. Conformably overlying the pebble shale unit is the Hue Shale (Molenaar and others, 1987). The base of the Hue Shale is placed at the base of the bentonite beds above the non-bentonitic pebble shale. This lithologic change also coincides with greatly increased gamma radiation, the gamma-ray zone (GRZ). The top of the Hue Shale west of the Kuparuk River oil field area coincides with the top of the GRZ (Marker 5). In this area, the pebble shale unit is overlain by shales of the Torok Formation, which grades up into interbedded sandstones and shales of the overlying Nanushuk Group. The Torok-Nanushuk package represents a northeast prograding marine to nonmarine deltaic sequence. The Kuparuk River oil field area represents a transition area where the Torok-Nanushuk sediments thin rapidly eastward to a thin, distal shale sequence within the Hue Shale. Therefore, Markers 2, 3, and 4 (table III-1) represent markers equivalent to the base of the Torok, top of the Torok-base of the Nanushuk, and top of the Nanushuk; Marker 5 identifies the top of the Hue Shale.

The Canning Formation was named by Molenaar and others (1987) for a thick, dominantly shale unit that conformably overlies the Hue Shale and gradationally underlies thick, deltaic deposits of the Sagavanirktok Formation. It was not surprising then that for most of the Prudhoe Bay--Kuparuk River area, we were unable to identify a distinct lithologic marker to represent the contact between the Canning and Sagavanirktok formations. No formal terminology is used in this report to describe the rocks within these two formations.

Overlying the top of the Hue Shale (Marker 5) is a relatively thick bentonitic shale with minor thin sand beds. The top of this predominant shale sequence is marked by a distinct gamma ray log break (Marker 6) which appears to represent a basin-wide marine transgression. This sequence is generally considered to be a basin or slope deposit. Between Marker 6 and the surface is a thick, shallow-marine and nonmarine, sandstone and siltstone sequence which can be identified on the well logs as a distinct coarsening-upward deposit. The sandstone sequence conformably overlies the shale on most of the North Slope, but in several wells east of Prudhoe Bay there is an unconformity at the base of the sandstone. In the area of the unconformity, a conglomeratic sandstone rests directly on marine shale with no angular discordance.

The first laterally persistent identifiable markers within the sandstone sequence (Markers 7 through 11) delineate the heavy-oil- and tar-bearing West Sak and Ugnu sands. These two sands are interpreted as Upper Cretaceous and Tertiary shallow marine and nonmarine deltaic deposits, respectively. The West Sak interval represents a transition from inner-shelf deposition for the lower member to delta-front deposition for the upper member (Werner, 1987). The top of the West Sak (Marker 9) is separated from the base of the overlying Ugnu (Marker 10) by a regionally extensive shale and mudstone ranging in thickness from 30 to 45 m in the Kuparuk River oil field area. The Lower Ugnu sands, as described by Werner (1987), apparently span the Cretaceous-Tertiary boundary with the basal part of the Lower Ugnu sands being Late Cretaceous (Maestrichtian) and the upper part of the Lower Ugnu being Paleocene in age. Stratigraphic relationships indicate that the Cretaceous-Tertiary boundary is conformable.

The rock package overlying the Ugnu sands, Marker 11 to Marker 16, is characterized by numerous coarsening-upward and fining-upward sandstone and siltstone sequences. In general, the

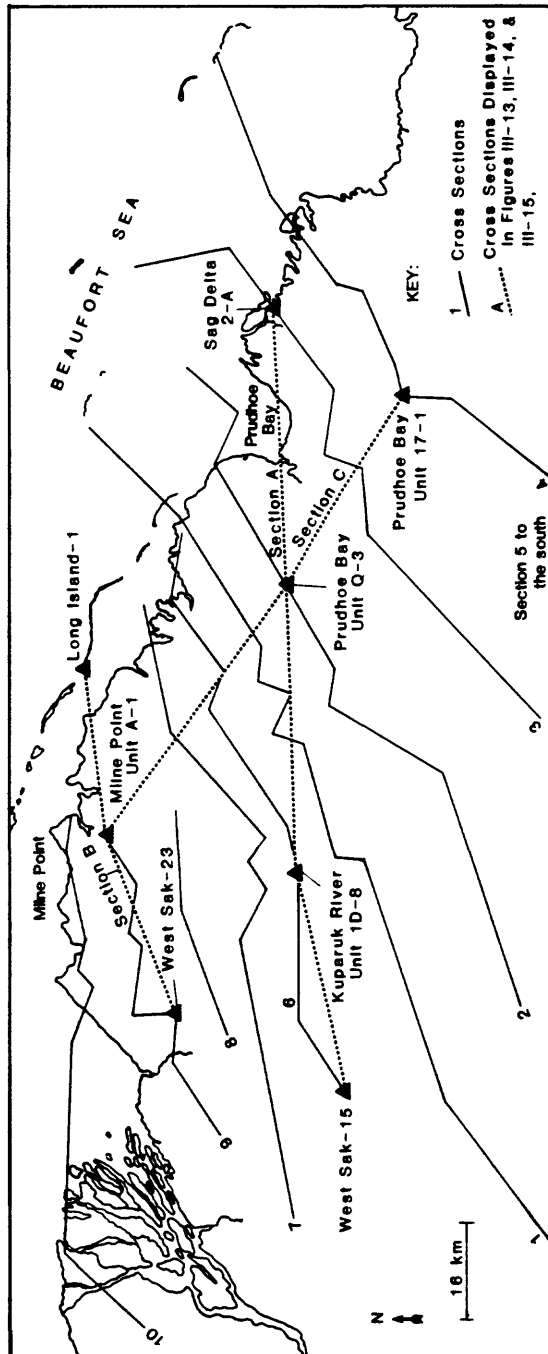


Figure III-12. Map of the Prudhoe Bay-Kuparuk River area showing the location of the ten cross sections (solid lines) used to construct the near-surface stratigraphic framework. Also shown (dashed lines) are correlation sections A, B, and C from figures III-13, III-14 and III-15; ▲, wells used in correlation sections.

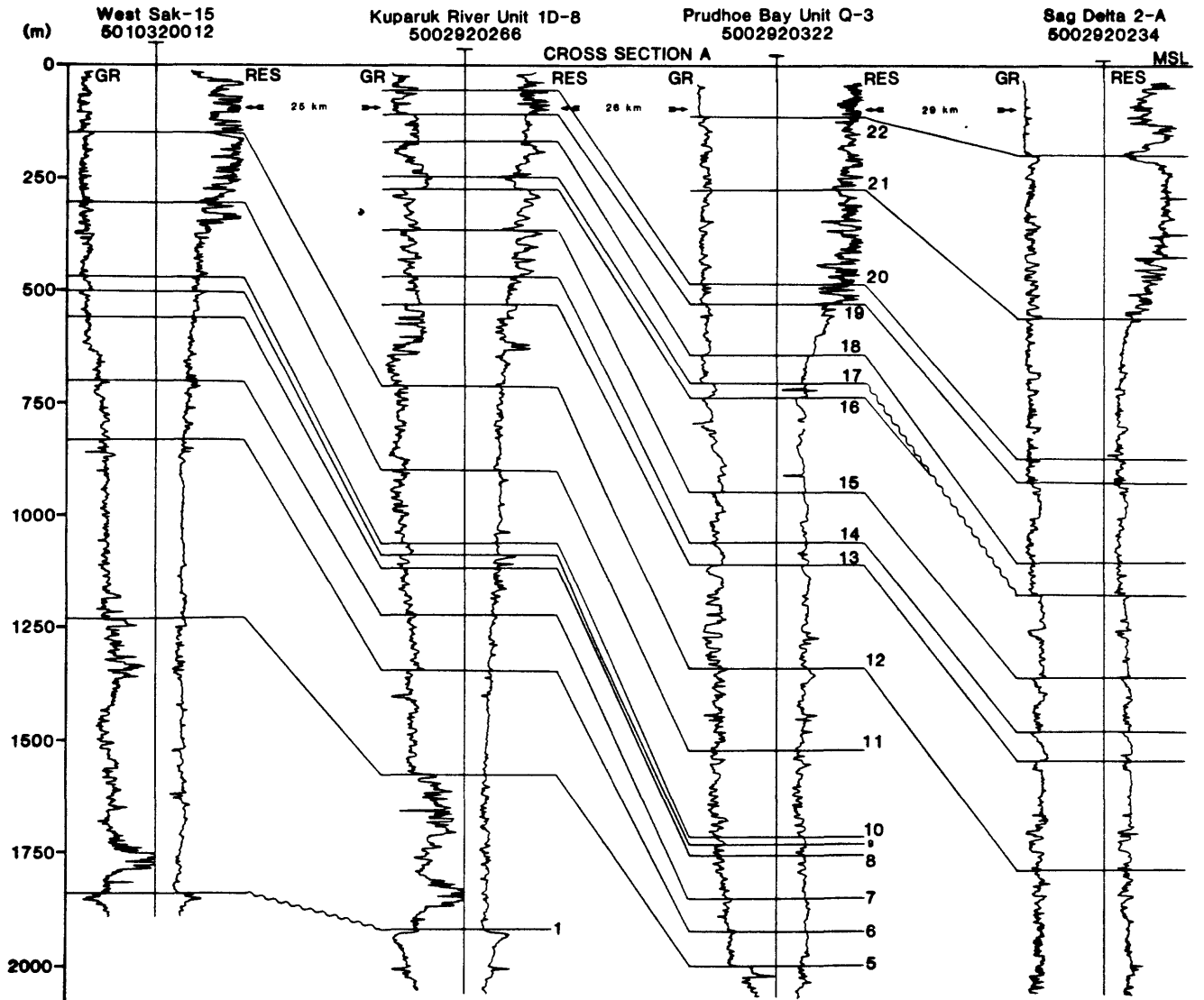


Figure III-13. Four-well correlation section across the Kuparuk River--Prudhoe Bay region illustrating stratigraphic relations in the Brookian sequence. See figure III-12 for location of section.

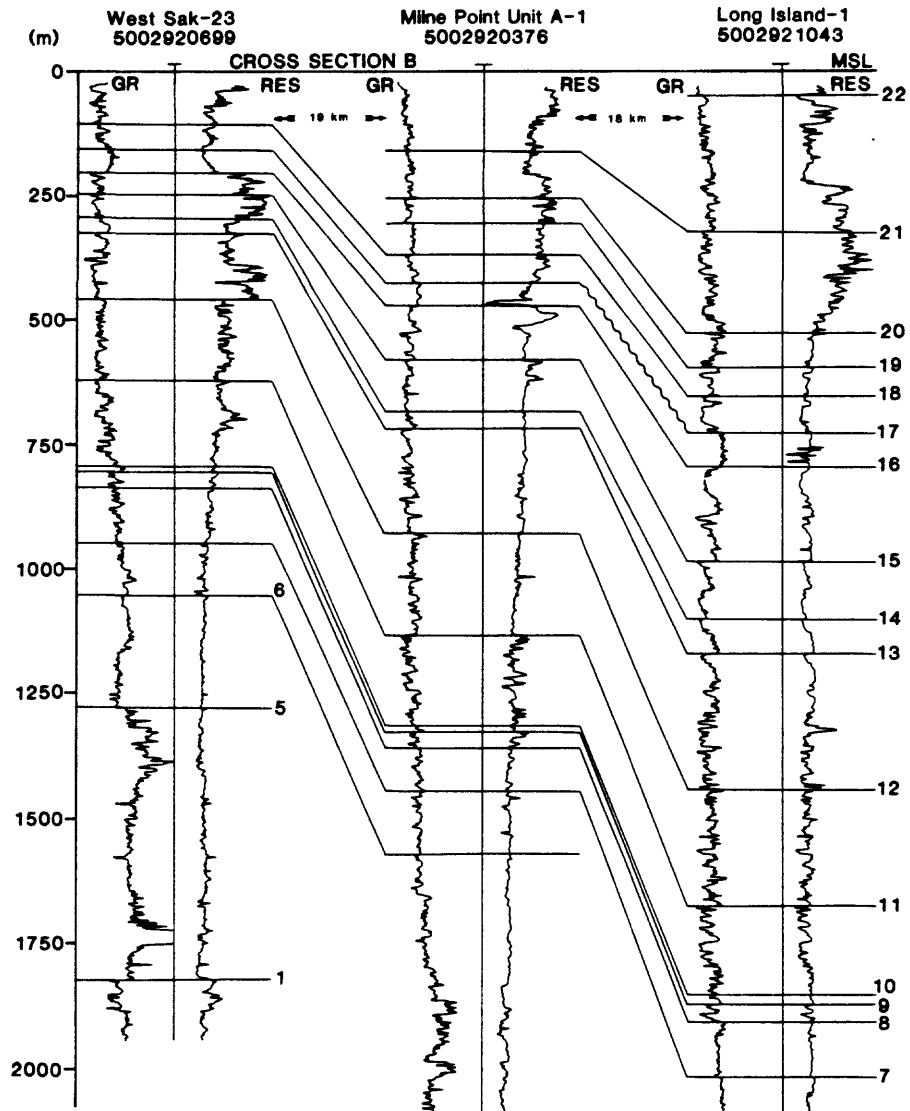


Figure III-14. Three-well correlation section across the Kuparuk River--Prudhoe Bay region illustrating stratigraphic relations in the Brookian sequence. See figure III-12 for location of section.

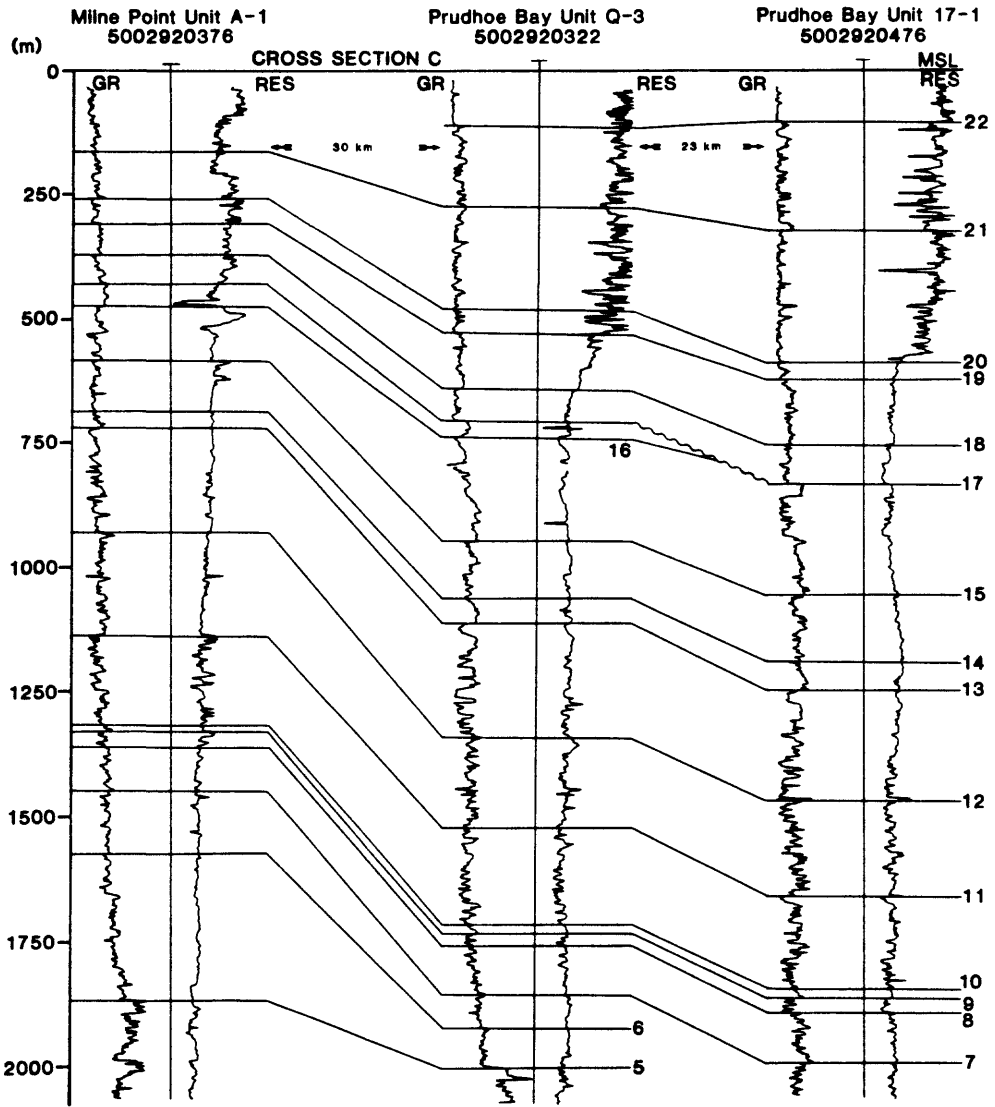


Figure III-15. Three-well correlation section across the Kuparuk River--Prudhoe Bay region illustrating stratigraphic relations in the Brookian sequence. See figure III-12 for location of section.

Table III-1. Listing of geologic Markers 1 through 22 used to construct the stratigraphic framework in the Prudhoe Bay--Kuparuk River area and their stratigraphic equivalents.

Marker Number	Stratigraphic Equivalents
22	
21	
20	
19	
18	
17	Eocene unconformity
16	Base Eocene marine transgression
15	
14	
13	
12	
11	Top Ugnu sands
10	Base Ugnu sands
9	Top Upper West Sak sands
8	Base Upper West Sak/Top Lower West Sak sands
7	Base Lower West Sak sands
6	
5	Top of High Gamma Ray + (Top Hue Shale)
4	Top Nanushuk Group
3	Base Nanushuk Group/Top Torok Formation
2	Base Torok Formation
1	Lower Cretaceous unconformity

coarsening-upward sequences are thicker than the fining-upward units. The coarsening-upward units may be distributary mouth bar deposits, and it is likely the fining-upward sequences are channel and overbank deposits. Overlying this nonmarine deltaic package (top: Marker 16) is a marine siltstone and mudstone. This unit was likely deposited during a basin-wide marine transgression in the Eocene. In general, the unit thins from the northeast to the southwest and laterally coarsens to a sandstone in the eastern part of the Kuparuk River Oil Field area. In most of the Prudhoe Bay--Kuparuk River area, the upper-boundary of the siltstone and mudstone unit (Marker 17) is an erosional unconformity. This unconformity appears to be an erosional remnant of a northeasterly migrating deltaic channel sequence which has cut into the underlying marine sequence. East of Prudhoe Bay, near the Sagavanirktok Delta, this unconformity (Marker 17) has eroded all of the marine siltstone and mudstone sequence and has removed Marker 16 and an undetermined volume of underlying sediments. However, to the west and southwest into the Kuparuk River area, this Eocene unconformity appears to become a conformable contact.

The rocks overlying Marker 17 are generally of uniform composition both laterally and vertically in the section and appear to have been deposited in a delta-platform environment. The relative thicknesses of the rock units defined by Markers 17, 18, 19, 20, 21, and 22 significantly change laterally from southwest to northeast. In the Kuparuk River area, the individual thicknesses of these units range from 30 to 80 m, whereas near Prudhoe Bay their thicknesses range from 60 to 300 m. Stratigraphic thickening of the delineated rock units to the east may possibly represent the northeast prograding deltaic depocenter. Other unconformities may occur above Marker 17; however, with our present well log data base we are unable to identify any additional depositional hiatuses. It is possible that the pronounced thinning of some intervals, such as 21-22 near the east end of figure III-13, may be an indication of an unconformity.

III.B.2. Potential Gas-Hydrate Reservoirs

In considering the possible geologic controls on the occurrence of gas hydrate, we have included in this section of Chapter 3 a description of the potential gas-hydrate reservoir rocks within the Prudhoe Bay--Kuparuk River area. Both rock descriptions and pertinent reservoir data are included.

MARKER 7 THROUGH 11

As discussed earlier, Markers 7 through 11 delineate a series of shallow, oil-bearing horizons referred to as the West Sak and Ugnu sands (fig. III-16). These oil-bearing horizons have been extensively described by Werner (1987), and most of the information that follows is taken directly from this source. Locally, these horizons are potential gas-hydrate reservoirs. The West Sak (Marker 7 to 9) consists of very fine- to fine-grained sandstone and silty sandstone with interbedded siltstone and mudstone. Sand grains consist of quartz, lithic rock fragments, and feldspar with a trace-to-common amounts of mica and glauconite. Clay matrix ranges from 5 to 30 percent and consists of chlorite, illite, kaolinite and a trace of smectite. West Sak sands generally lack cementation and are very friable. They are classified as litharenites and lithic wackstones. Core data show that total porosities range from 25 to 35 percent, and horizontal air permeabilities range from 10 to 800 millidarcies in the sands. Upper (Marker 8 to 9) and lower (Marker 7 to 8) members are recognized in the Kuparuk River area (fig. III-16). The lower member consists of thin-bedded sands characterized by ripple bedding and hummocky cross stratification with interbedded bioturbated siltstone and mudstone. The upper West Sak consists of two distinct and laterally extensive sand packages. Sedimentary structures include massive bedding, planar bedding and planar cross bedding. Burrowing and bioturbation are common.

The West Sak sands are oil bearing primarily in the Kuparuk River and Milne Point areas at depths from 610 to 1,370 m (figures III-17 and III-18). The oil in the West Sak sands ranges from 16 to 22 degrees API gravity and contains methane through pentane gases in solution. Based on viscosity and gravity data, the West Sak oil is an intermediate-to-less heavy (Class I Heavy Crude Oil) crude.

The Ugnu sands (Marker 10 to 11) are predominantly fine- to medium-grained and well sorted. Composition of the sands is mostly quartz, chert, and volcanic rock fragments with a trace to common amounts of epidote and mica. Interstitial clay is rare in the sands, usually less than 5 percent. Clay types are similar to those in the West Sak sands and consist of chlorite, kaolinite, illite, and smectite.

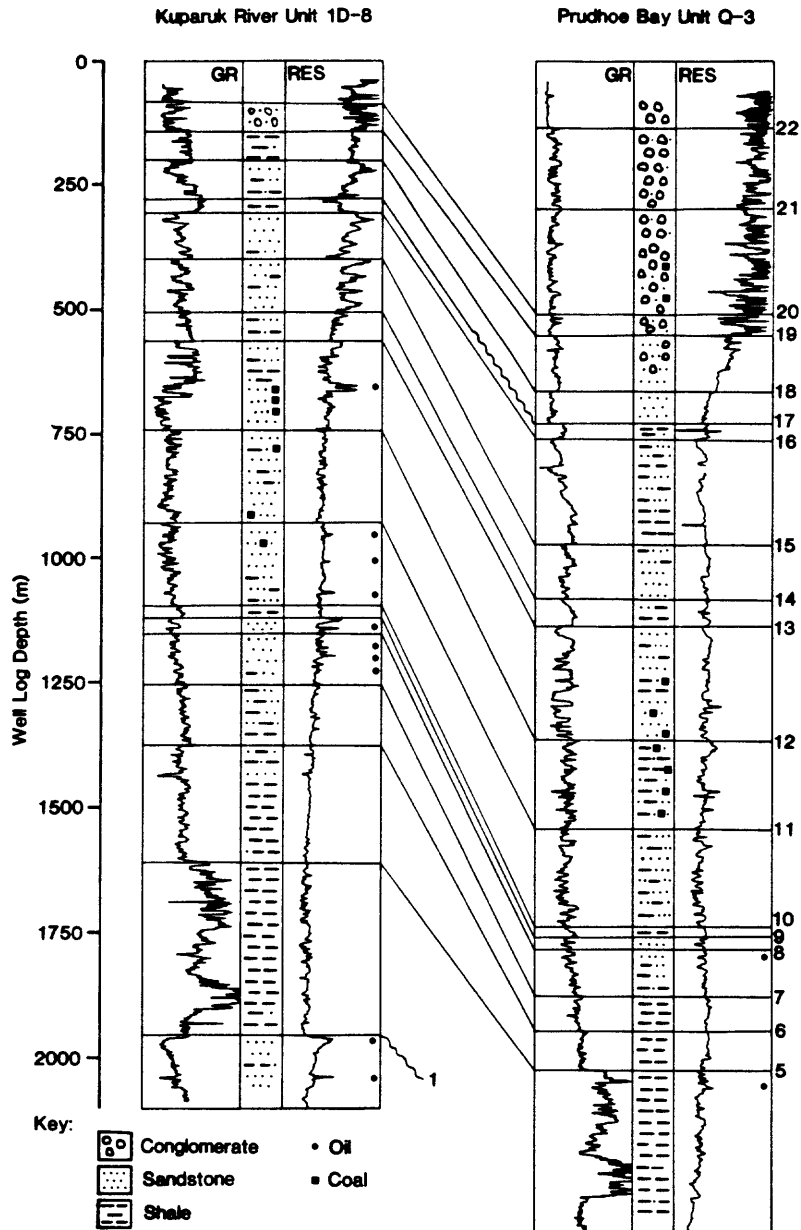


Figure III-16. Gamma ray, electrical resistivity, and lithologic log for Kuparuk River Unit 1D-8 and Prudhoe Bay Unit Q-3. Also shown are the geologic markers (table III-1) used to construct the stratigraphic framework in the Prudhoe Bay--Kuparuk River area (well log depth scale from the Kelley bushing).

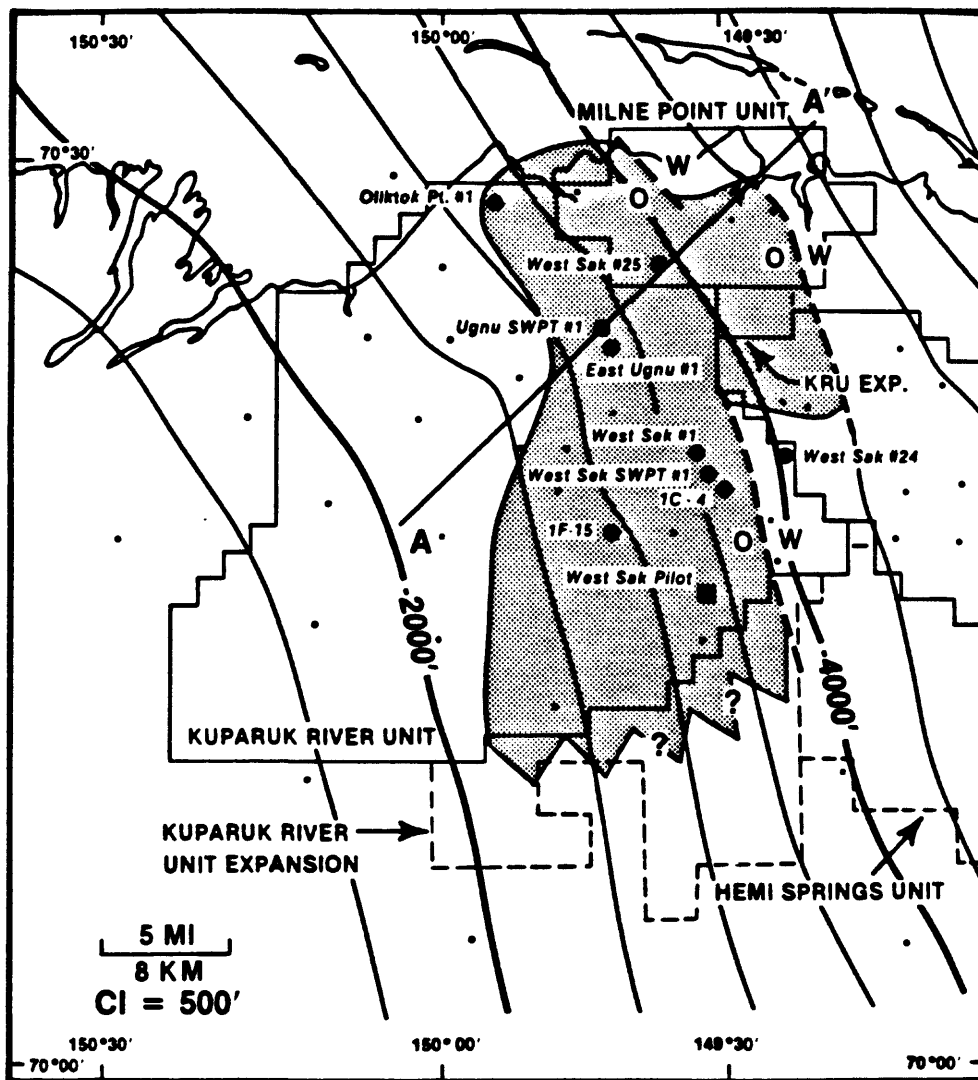


Figure III-17. Structure on top of West Sak Sands. Dots represent the well log data base. Stippled area is where both the upper and lower West Sak sands are oil-bearing; thick dashed lines are postulated oil/water contacts. Cross section line refers to figure III-18 (Werner, 1987).

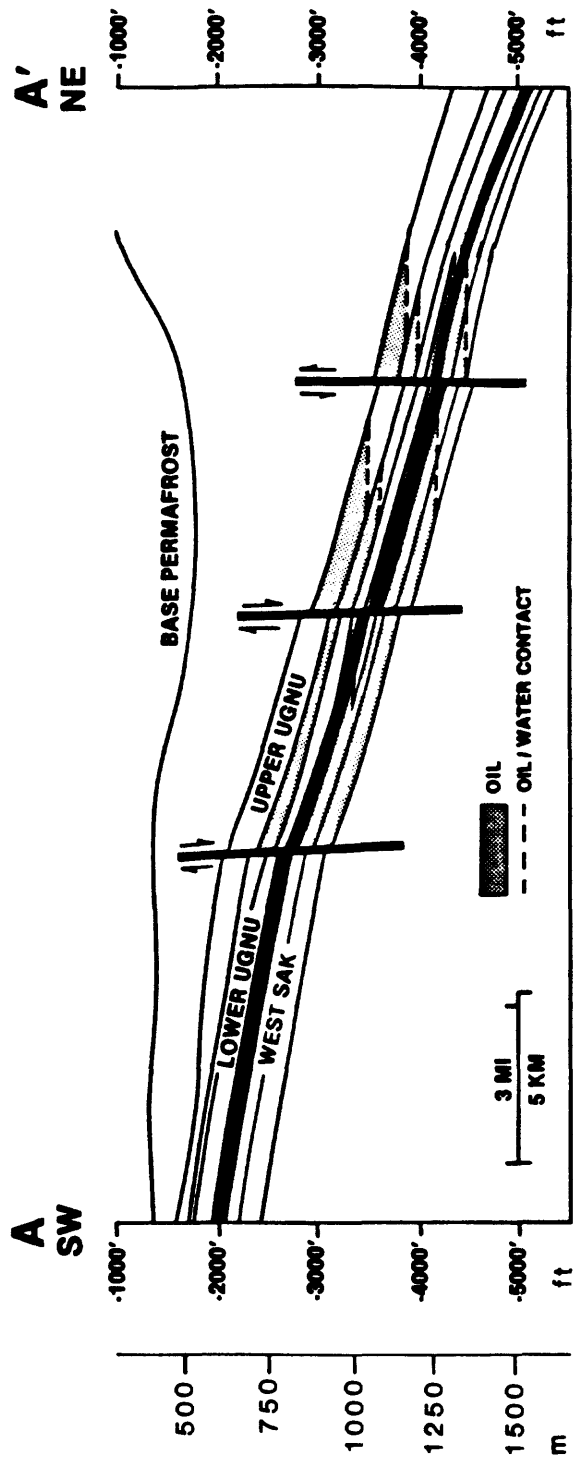


Figure III-18. Generalized structure section of shallow sand reservoirs in the northern Kuparuk River Unit with major faults indicated. Black marker bed is the regionally extensive shale which overlies the West Sak. See figure III-17 for location (Werner, 1987).

Interbedded coal, in one- to two-foot thick seams, occur locally, but coalified fragments of wood and other plant debris are common throughout. The sands are unconsolidated, and no significant cement or evidence of diagenesis has been observed.

The lower Ugnu oil accumulation occurs in the northern half of the Kuparuk River Unit (figures III-18 and III-19). Oil in the top-most sands of the lower Ugnu ranges from 8 to 12 degrees API gravity, and methane is the only gas in solution. Oil in the more discontinuous basal sands of the lower Ugnu is intermediate in both gravity and types of gas between the West Sak sand below and the upper Ugnu reservoir above.

Geochemical work, summarized by Carman and Hardwick (1983), indicates that crude oils from these shallow sands probably have the same source as the oil in the deeper Kuparuk, Sadlerochit, and Lisburne reservoirs, but are biodegraded. Carman and Hardwick (1983) postulated that the mid-to-late Tertiary regional tilting, which reduced the amount of original closure on the Prudhoe Bay Sadlerochit structure, "spilled" hydrocarbons to the west towards the shallower reservoirs. This secondary migration probably accounts for most of the oil in the shallow sands.

MARKER 11 THROUGH 16

The sediments between Markers 11 and 16 (fig. III-16) primarily consist of fine- to coarse-grained sandstone and conglomerate. Due to the lack of core data, little is known about these units. Our analysis of drill-cuttings suggests that the sand-grains consist of subangular to rounded quartz, chert, and rock fragments. Mica, bedded coal, and disseminated carbonaceous material are common throughout the section. No information is available on the clay matrix. Well-log calculated porosities range from 30 to 40 percent. Significant occurrences of oil and methane gas have been detected on numerous mud logs from wells in the Kuparuk River area. The lateral extent of these hydrocarbon occurrences is not known.

MARKER 17 THROUGH 22

This shallowest potential gas-hydrate reservoir (fig. III-16) consists of predominately medium- to coarse-grained sandstone and conglomerate. Examination of the mud log and drill-cuttings indicates that the sandstone and conglomerate are made up of poorly sorted, angular to rounded, chert and quartz clasts. Wood, carbonaceous material, and pyrite are common; coal is relatively rare. Well-log calculated porosities range from 25 to 40 percent. Within the Prudhoe Bay--Kuparuk River area there is no evidence of hydrocarbons in this sequence.

III.B.3. Potential Gas-Hydrate Traps

Werner (1987) felt that the oil accumulations in both the West Sak (Marker 7 through 9) and Ugnu sands (Marker 10 through 11) are the result of a combination of stratigraphic and structural traps. He described the regional structure on the tops of all the shallow oil zones as a monocline with strikes to the northwest and gentle 1 to 2 degree dips to the northeast (25 m/km). This surface is cut by north-south-trending faults which generally are downthrown to the east in the Kuparuk River area. Throw on the faults ranges from 15 to 60 m. The present northeast dip is believed to be the result of regional tilting. It has been proposed that tilting was the result of sedimentary loading as the deltaic depocenter prograded to the northeast (Carman and Hardwick, 1983). The shallow faulting may have been concurrent with tilting. Dewatering and compaction may also have induced faulting.

According to Werner (1987), in the area of the Kuparuk River Oil Field, faulting and lateral facies changes control the distribution of hydrocarbons in the West Sak to the north, whereas faulting alone seems to be the principal trapping mechanism to the south and west. Within the West Sak sands several oil/water contacts occur in the Kuparuk River and Milne Point areas. The different oil/water contacts are thought to be due to variations in seal efficiency and spill-point geometry. Faulting and facies changes associated with the delta plain environment are the trapping mechanisms for hydrocarbons in the lower Ugnu sands. As with the West Sak sands, several oil/water contacts are recognized in the lower Ugnu sands. Little is known about the distribution of oil within the upper Ugnu sands.

Due to the lack of confidence in the available data, Werner (1987) only showed the general location of several major faults within the West Sak and Ugnu sands (fig. III-18). There are only a few seismic surveys from the Prudhoe Bay--Kuparuk River area in the public domain; therefore, it is

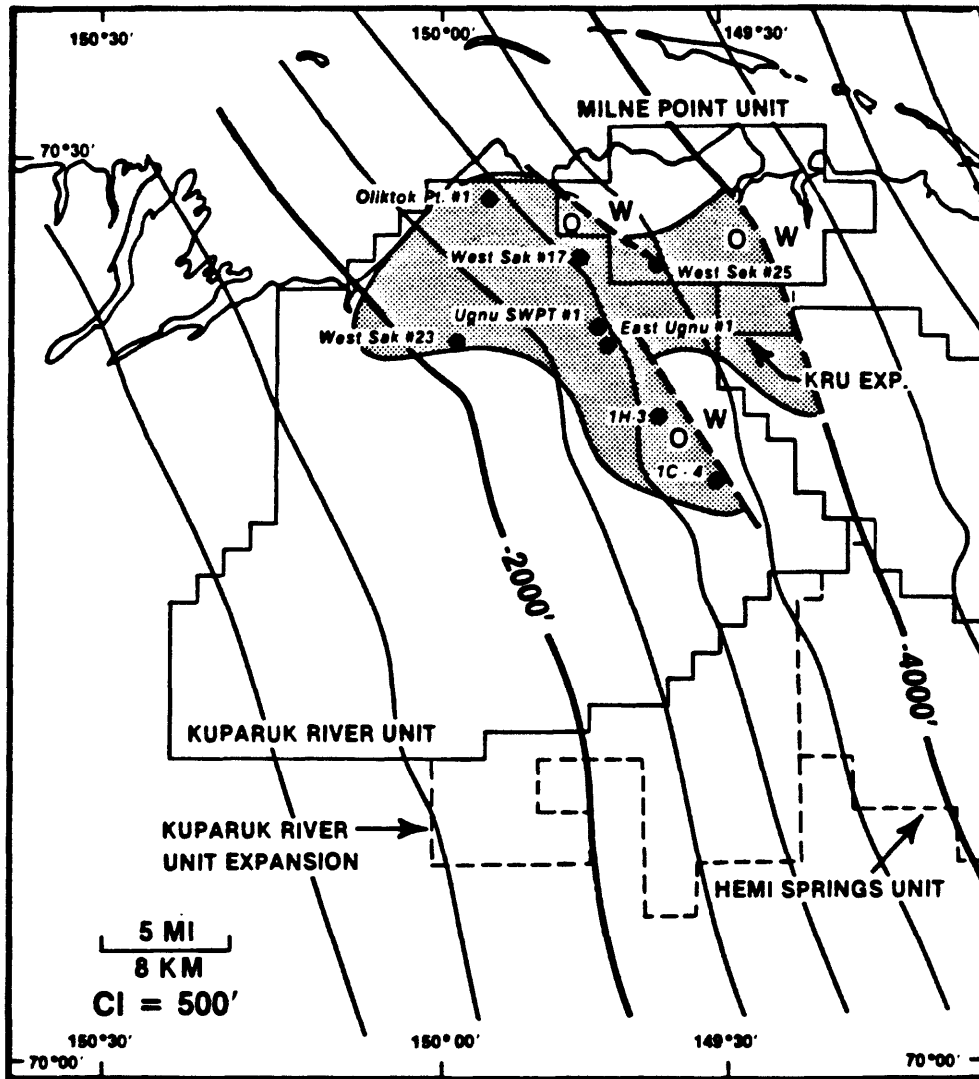


Figure III-19. Structure on top of Lower Ugnu Sands. See figure III-17 for explanation. Occurrence of oil in the Upper Ugnu generally is coincident with the eastern half of the Lower Ugnu oil accumulation (Werner, 1987).

impossible for us to map faults within the near-surface sediments. However, it is possible to map regional fault systems by using published data from deeper reservoirs (Alaska Oil and Gas Conservation Commission, 1984; Carman and Hardwick, 1983). Figure III-20 is a composite of two fault maps; the fault traces in the western half of the map are faults that transect the Kuparuk River Formation (Carman and Hardwick, 1983), and the traces in the east cut the deeper Sadlerochit Group (Alaska Oil and Gas Conservation Commission, 1984). In general, normal faults cross the Prudhoe Bay--Kuparuk River oil fields in two distinct trends. One set, oriented northeast-southwest, occurs along the northern edge of the Prudhoe Bay field and is downthrown to the north by as much as 300 m. A second set of faults of lesser magnitude, oriented northwest-southeast, occurs south and west of the Prudhoe Bay oil field. It is possible that the north-south-trending faults, which control the distribution of hydrocarbons in West Sak and Ugnu sands (Werner, 1987) may be reactivation faults or extensions of the deeper northwest-southeast-trending faults mapped in figure III-20.

In the reservoir rocks above the Ugnu sands, little is known about potential hydrocarbon traps. For instance, it is not known if the faults described by Werner (1987) extend into overlying horizons. Most of these near-surface stratigraphic units were deposited in a delta plain environment in which stratigraphic traps are common. Therefore, it is possible that lateral facies changes may provide hydrocarbon traps within these horizons; however, due to the unconsolidated nature of these rocks the efficiency of a seal may be reduced.

Two additional trapping mechanisms not previously discussed are relatively specialized. Permafrost (ice-bearing permafrost) is believed to be an effective impermeable barrier to migrating gas and liquids (Downey, 1984). Therefore, the base of ice-bearing permafrost could act as a hydrocarbon seal, but ice-bearing permafrost is not believed to be a present-day trap for the West Sak or Ugnu oils (Werner, 1987). Ice-bearing permafrost hydrocarbon traps may exist, however, within the reservoir rocks overlying the Ugnu sands. In addition to the permafrost hydrocarbon traps, it is possible for gas hydrate to form its own trap in a reservoir. As gas migrates into the zone of gas-hydrate stability (Chapter II), it may interact with the available pore-water to generate gas hydrate. With the appropriate volumes of gas and water, the pore-space within the reservoir rock could be completely filled, thus making the reservoir impermeable to further hydrocarbon migration. The plugging of gas pipelines and production tubing by gas hydrates is an example of its sealing potential.

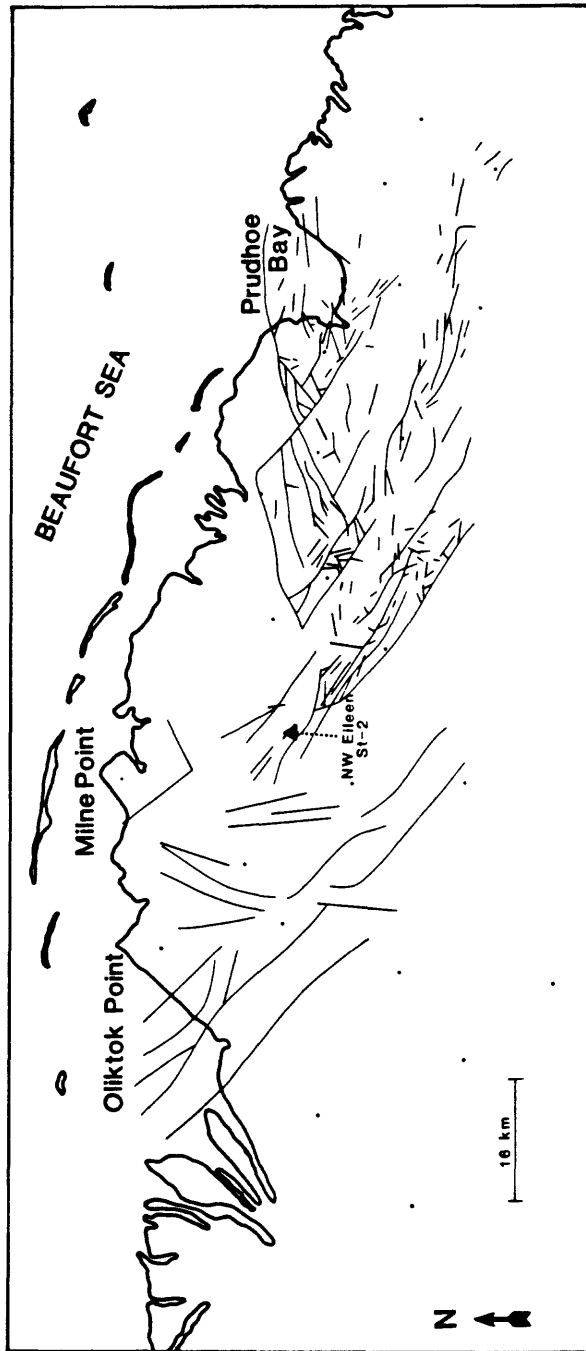


Figure III-20. Composite fault map of the Prudhoe Bay--Kuparuk River area. The fault traces in the western half of the map are faults that transect the Kuparuk River Formation (Carman and Hardwick, 1983) and the traces in the east cut the deeper Sadlerochit Group (Alaska Oil and Gas Conservation Commission, 1984).

CHAPTER IV. GAS-HYDRATE OCCURRENCES

IV.A. WELL-LOG EVALUATION

Chapter IV is divided into three sections: Section "A" is a review of the well-log interpretation techniques used to identify and evaluate in-situ gas-hydrate occurrences; in Section "B" the in-situ gas-hydrate occurrences in the Prudhoe Bay--Kuparuk River area have been mapped; and in Section "C" several gas hydrate reservoir properties are discussed.

Bily and Dick (1974) studied naturally occurring gas hydrates in the subsurface of the Mackenzie Delta, thus providing one of the few papers dealing with the detection of gas hydrates using wireline well logs. They discovered that when a gas hydrate was penetrated during drilling, there was a marked increase in the amount of gas in the drilling mud. These gas-hydrate bearing units produced a relatively high resistivity on the dual induction log and a slight negative spontaneous potential deflection in comparison to an interval containing free gas. In addition, acoustic logs indicated an increase in acoustic velocity for gas-hydrate bearing intervals.

The work of Galate and Goodman (1982) in the NPRA is one of only two gas-hydrate studies completed on the North Slope of Alaska. For this study, they used all available records including drilling plans, well histories, daily drilling reports, geologic data for the area, core information, and wireline well logs. Of the 17 wells investigated, they identified eight as showing evidence of gas hydrates.

Work in the Prudhoe Bay and Kuparuk River oil fields (Collett, 1983b) suggests the existence of six stratigraphically controlled gas-hydrate bearing units. In this previous study, two well logging devices were consistently used to identify potential gas-hydrate occurrences. They were the dual-induction and acoustic transit-time logs. The dual-induction and acoustic transit-time logs behave similarly within a unit either saturated with gas hydrate or ice. Hence, the occurrence of gas shows on the mud log produced from a decomposing gas hydrate often provides the only means of conclusively differentiating a gas hydrate from ice.

The remainder of Section "A" is divided into three major parts, the first consists of a general review of probable well-log responses within a gas hydrate. This review will be followed by a detailed discussion on the neutron-porosity and acoustic transit-time responses. This section will conclude with an analysis of a series of crossplots used to examine and identify suspected gas-hydrate occurrences.

WELL-LOG RESPONSES

The responses of the commonly available logs within the cored gas-hydrate interval of the Northwest Eileen State-2 well (fig. IV-1) are summarized below.

1. *Mud Log*: On a mud log there is a pronounced gas kick associated with a gas hydrate due to decomposition during drilling. However, if cold drilling fluids are used there may be minimal decomposition of the gas hydrates and little free-gas liberated.
2. *Dual Induction Log*: There is a relatively high electrical-resistivity deflection on this log in a gas-hydrate zone, in comparison to that in a free-gas saturated horizon. The deep-induction resistivity curve is separated from the shallower-reading laterolog-8 resistivity curve, apparently due to gas-hydrate decomposition next to the well-bore. If a unit were gas-hydrate saturated within the ice-bearing permafrost sequence, the resistivity response on the dual-induction log for the gas hydrate would not be significantly different from that in the surrounding ice-bearing permafrost. Below the base of the ice-bearing permafrost, however, the high-resistivity deflection associated with gas hydrate is distinct from the surrounding non-ice-bearing zones.
3. *Spontaneous Potential (SP)*: There is a relatively lower (less negative) spontaneous-potential deflection in a gas-hydrate bearing zone when compared to that associated with a free-gas bearing zone. The solid gas hydrate limits the penetration of mud-filtrate, thus reducing the negative spontaneous potential. The spontaneous-potential

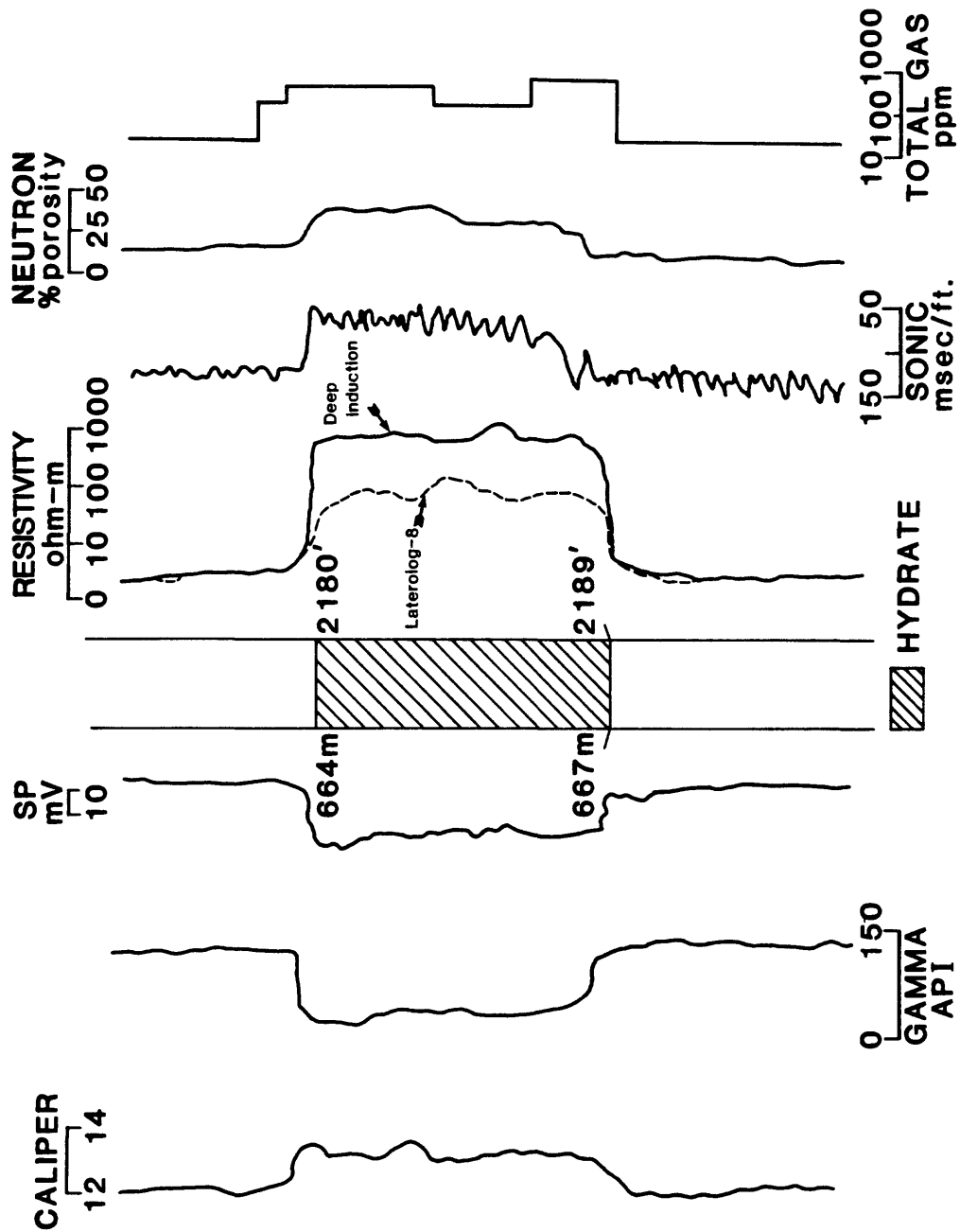


Figure IV-1. Well log responses within the cored gas-hydrate interval in the Northwest Eileen State-2 well, on the North Slope of Alaska.

curve for a gas-hydrate saturated unit within the ice-bearing permafrost sequence would be similar to that in the surrounding ice-bearing units where the mud-filtrate penetration is similarly limited.

4. *Caliper Log*: The caliper log in a gas-hydrate interval usually indicates an oversized well bore due to spalling associated with the decomposition of the gas hydrate. Because the caliper also indicates an enlarged borehole in ice-bearing permafrost, it is useful only in detecting gas hydrates below the base of the ice-bearing permafrost.
5. *Acoustic Transit-Time Log*: Within a gas hydrate there is a decrease in acoustic transit-time in comparison to a unit saturated with either water or free-gas. Because the acoustic transit-time of ice is similar to that of gas hydrate (Osterkamp and Payne, 1981), the acoustic log cannot be used alone to detect gas hydrates within the ice-bearing permafrost sequence. The acoustic transit-time response within gas hydrate will be discussed in detail later in this section.
6. *Neutron Porosity*: In a gas hydrate there is an increase in the neutron porosity; this response contrasts with the apparent reduction in neutron porosity in a free-gas zone. This relation and the neutron-porosity-device response to other pore-space constituents is examined later in this section.
7. *Density Log*: Within a gas hydrate there is a decrease in density in comparison to a unit saturated with water. Because the density of ice is similar to that of gas hydrate (Lewin and Associates, Inc., 1983), the density log cannot be used independently to identify a gas hydrate within ice-bearing permafrost.
8. *Drilling Rate*: In a gas hydrate the relative drilling rate decreases, due to the solid nature of the gas hydrate. There is a similar drilling rate response within ice-bearing permafrost, and, therefore, drilling rate change is not useful as a gas hydrate detector within the ice-bearing permafrost sequence.

NEUTRON POROSITY AND ACOUSTIC TRANSIT-TIME EVALUATION

The neutron-porosity log measures the attenuation in the passage of neutrons as emitted by the logging tool into the rock sequence. This response is a measure of the hydrogen content of the formation. Because the size of the hydrogen atom and the energy level of a neutron are similar, the hydrogen atom will capture neutron particles when encountered. Thus, a decrease in the number of captured neutrons would indicate a decrease in hydrogen content. The amount of hydrogen in a rock is related to the amount of water and hydrocarbons, including natural-gas hydrates, that is present. Through the aid of stoichiometric chemistry, we have calculated the amount of hydrogen present in one cubic centimeter of pore volume of the following constituents: water, pure methane, ice, structure I and structure II gas hydrates (table IV-1).

The neutron-log response to increasing hydrogen content indicates an increase in apparent porosity. Conversely a decrease in hydrogen content relates to a reduction in the recorded porosity. From this relation and the calculated hydrogen content of each possible pore-filling constituent listed in table IV-1, we make the following assumptions about the neutron-porosity-log response within a rock saturated with either free methane gas, water, ice, or gas hydrate. Assuming a constant porosity, a rock saturated with a gas hydrate of structure II would have the highest apparent porosity, and a free-gas saturated unit would exhibit the lowest apparent porosity, followed by proportionately higher porosities within ice- or water-saturated units. This relation can also be seen in figure IV-2 in which a neutron porosity log from the Kuparuk River Unit 1B-1 production well has been plotted. By using well-log interpretation techniques described earlier in the paper it is possible to identify a series of gas-hydrate, ice-bearing permafrost, and water-saturated units in the Kuparuk River Unit 1B-1 well; several distinct units have been noted in figure IV-2. Even though the apparent porosity differences between the different units are slight, they do prove to be useful in the identification of the pore-space constituents. The crossplotting of data from the neutron porosity device and the acoustic log aids in

Table IV-1. Comparison of hydrogen content of potential pore-filling substances (Collett and others, 1984).

CH ₄ (free gas)	$.01076 \times 10^{22}$	(atoms of hydrogen/cc)
Ice (pure H ₂ O) (density of 0.50 gm/cc)	3.75×10^{22}	(atoms of hydrogen/cc)
Ice (pure H ₂ O) (density of 0.72 gm/cc)	4.8×10^{22}	(atoms of hydrogen/cc)
Water	6.7×10^{22}	(atoms of hydrogen/cc)
Hydrate I*	7.18×10^{22}	(atoms of hydrogen/cc)
Hydrate II*	7.55×10^{22}	(atoms of hydrogen/cc)

* Definition after Makogon (1981).

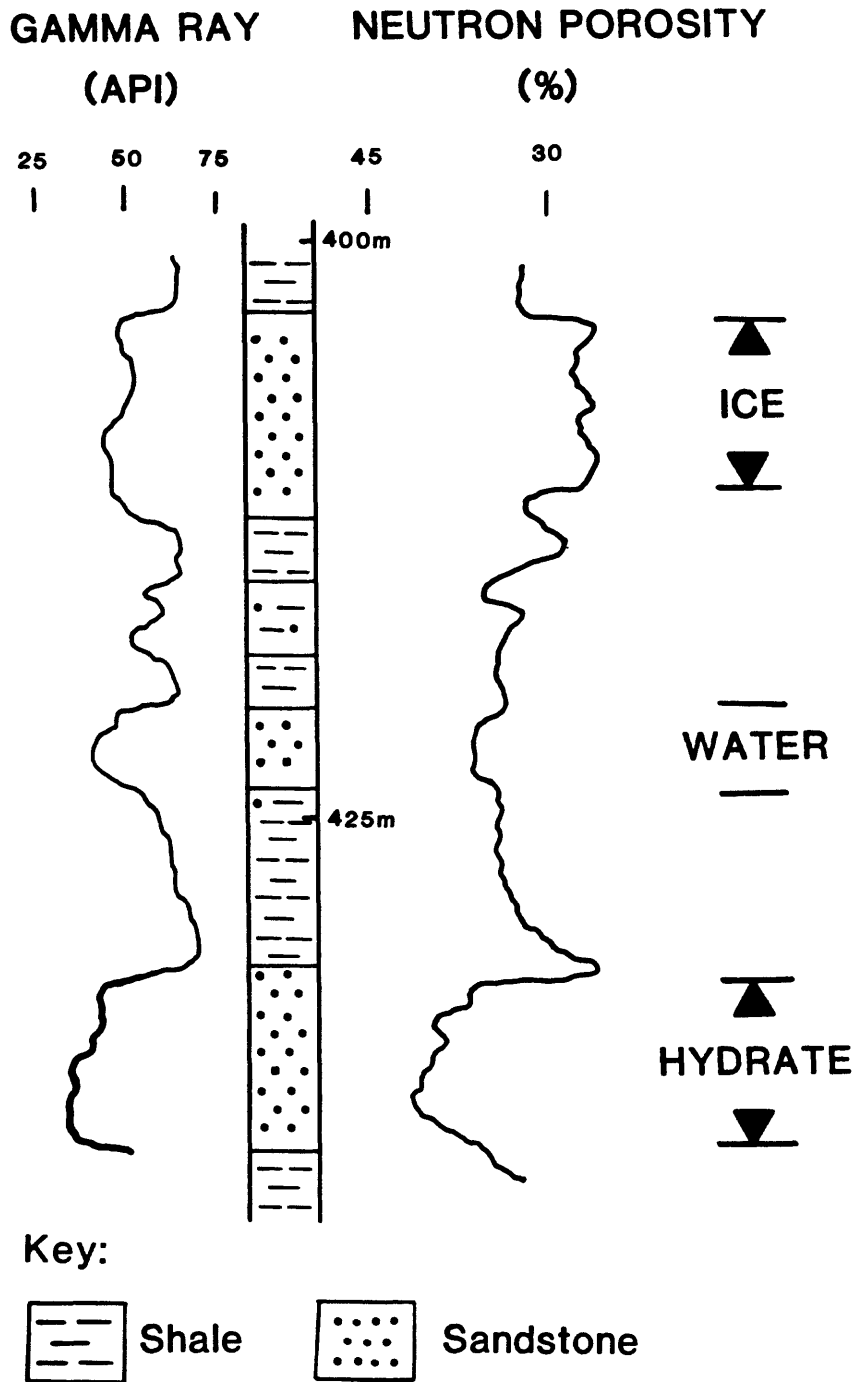


Figure IV-2. Neutron porosity and gamma ray well-log response for gas hydrate, ice, and water in the Kuparuk River Unit 1B-1 production well, North Slope of Alaska.

the identification of the gas hydrates. A detailed discussion of this procedure is included at the end of this section.

Accurate porosity data are required for resource estimates; however, obtaining accurate porosities in a gas-hydrate horizon is difficult. By making several assumptions about borehole conditions and taking into account the hydrogen pore-volume content for different constituents (table IV-1), it is possible to correct the neutron-porosity data within a gas-hydrate interval. Common well-log evaluation procedures assume that the pore-volume of a rock unit is occupied by hydrocarbons or water. Certain empirical equations used to calculate formation factors, such as porosity, are based on this assumption. However, due to the relatively high concentration of hydrogen atoms in a gas-hydrate saturated unit, the empirical equations used to evaluate the neutron-log responses within a water- or free-gas-bearing unit would lead to erroneous values if employed to examine a gas-hydrate interval. By assuming constant porosity between two units, one saturated with structure I gas hydrate and the second with water, it is possible to determine the following ratio:

$$\frac{\text{Amount of Hydrogen present in 1cc of water}}{\text{Amount of Hydrogen present in 1cc of gas hydrate (I)}} = \frac{6.7 \times 10^{22} \text{ (atoms of hydrogen/cc)}}{7.18 \times 10^{22} \text{ (atoms of hydrogen/cc)}} = 0.93$$

This ratio can be employed as a neutron-porosity log correction factor within any gas-hydrate saturated reservoir in order to obtain accurate porosities and thus better resource estimates. As an example, in the Kuparuk River Unit 1B-1 well (fig. IV-2) there is a probable gas hydrate occurrence at a depth of 433 m, and the compensated neutron response indicates an apparent porosity of 45 percent. If we assume this unit to be 100 percent saturated with a gas hydrate of structure I (methane) and use the correction factor calculated above, the actual porosity within the gas-hydrate saturated unit would be 42 percent.

The standard neutron log has a number of limitations, one of which is its sensitivity to borehole conditions. The enlargement of the borehole due to decomposing gas hydrates directly affects the recorded neutron-porosity data and is normally corrected for during standard well-logging procedures when a caliper is run along with the neutron device. The enlarged borehole, which may result from a decomposing gas hydrate or thawing ice, would be recorded as an apparent increase in the neutron porosity. For this reason only the compensated neutron log (compensated for borehole size) should be used during any evaluation within a gas-hydrate bearing horizon.

The maximum sensing depth of the compensated neutron device ranges from 5 to 15 centimeters. With drilling procedures employed on the North Slope, a gas hydrate may decompose to a depth of 3 to 6 centimeters into the formation from the borehole (Galate and Goodman, 1982). The vacated pore-space within the decomposed zone can be occupied by a wide array of constituents, including drilling fluids and free-gas from gas-hydrate dissociation. Both constituents can directly affect the neutron log response. Unrecognized changes in lithology may also result in erroneous interpretations.

As noted earlier, acoustic transit-time is shorter within a gas hydrate than in either free-gas or water. The acoustic log measures the shortest time required for a compressional wave to travel through the formation adjacent to the wellbore. The travel-time can be related to porosity when the lithology is known. In addition, the interval acoustic travel-time of the pore-fluids is required for accurate calculations of porosities. Compressional and shearwave velocities of a formation are not only properties of the matrix and pore fluid velocities but are also affected by the temperature of the formation and the salinity of the pore-fluids (Pandit and King, 1979).

In normal formation evaluation procedures, the empirical Wyllie equation (Wyllie, 1949) is used to relate travel time and porosity. In its original form this relation is given as:

$$\phi = \frac{t - t_{ma}}{t_f - t_{ma}}$$

ϕ is porosity in percent
 t is the formation travel time
 t_{ma} is the matrix travel time
 t_f is the fluid travel time
 (units: microseconds per foot)

The Wyllie equation does not account for the effect on the acoustic device of free-gas in a formation. However, an empirical correction factor for the free-gas effect has been calculated (Hilchie, 1982). Similarly, the effect of gas hydrate on the velocity device can be determined, and an empirical correction factor can be calculated.

In order to develop a gas hydrate correction factor for the acoustic measurements, it is necessary to calculate an acoustic transit-time relation between a formation saturated with water and a second saturated with gas hydrate in which all other parameters are constant or controlled. Pandit and King (1979) conducted a series of experiments to study the effect of pore water salinity changes on elastic-wave velocities at a wide range of temperatures (fig. IV-3). They noted that an increase in salinity decreases the compressional velocities below 0 °C, the effect being most pronounced close to 0 °C below the ice point. They also suggested that differences in velocities above 0 °C are probably due to slight differences in microstructure of the samples and differences in salinities. They conducted their experiments with a series of three rock types. One of these types, the Boise sandstone, with a measured porosity of 25 percent, is the best representative of the actual lithologic characteristics of North Slope gas-hydrate saturated units. However, the experimental 25 percent porosity of the Boise sandstone is much lower than the recorded porosities within the upper units of the North Slope.

In order to determine the expected acoustic velocity of a rock saturated with gas hydrate, the theoretical velocity constants (fig. IV-3) of Pandit and King (1979), calculated at known temperatures and pore-fluid salinities, have been employed in conjunction with the work of Whiffen and others (1982). With the aid of Brillouin spectroscopy, Whiffen and others (1982) were able to measure the sonic velocity of a pure-methane hydrate. They determined that the acoustic velocity of a gas hydrate of structure I is approximately 0.88 that of ice. By taking this experimentally derived relation between the acoustic velocity of gas hydrate and that of ice, along with the work of Pandit and King (1979), it is possible to calculate an acoustic velocity relation between a water-saturated unit and a gas-hydrate saturated unit. As noted earlier, acoustic velocities are also affected by the salinity of the pore filling constituents. In order to evaluate pore-fluid salinities within these upper units of the Prudhoe Bay region, 160 spontaneous potential logs were examined from a series of 32 wells. The pore fluid salinities within these upper units were determined to range from 0.5 to 18 parts per thousand. Howitt (1971) and Osterkamp and Payne (1981) noted salinity values associated with the permafrost of the North Slope in the range of 5 to 14 parts per thousand, similar to our calculated values. In order to avoid the large variations in acoustic velocities near 0 °C (Pandit and King, 1981), the theoretical transit time constant will be calculated for a series of temperatures well below 0 °C.

Taking the above assumptions into account, we have calculated a series of acoustic velocities for the Boise Sandstone described by Pandit and King (1981). In each case the core was assumed to be 100 percent saturated with a known, pore-filling constituent (gas hydrate, ice, free-gas), and the effects of other physical constants (temperature, pore-fluid salinities) were also considered (table IV-2).

As in the case of the neutron porosity correction factor determined earlier, it is possible to calculate a correction factor for the acoustic transit-time measurements in a gas hydrate. If the constant porosity of the Boise Sandstone is assumed, then the following relation can be written for the acoustic velocity characteristics of structure I gas hydrate and water within a given pore volume:

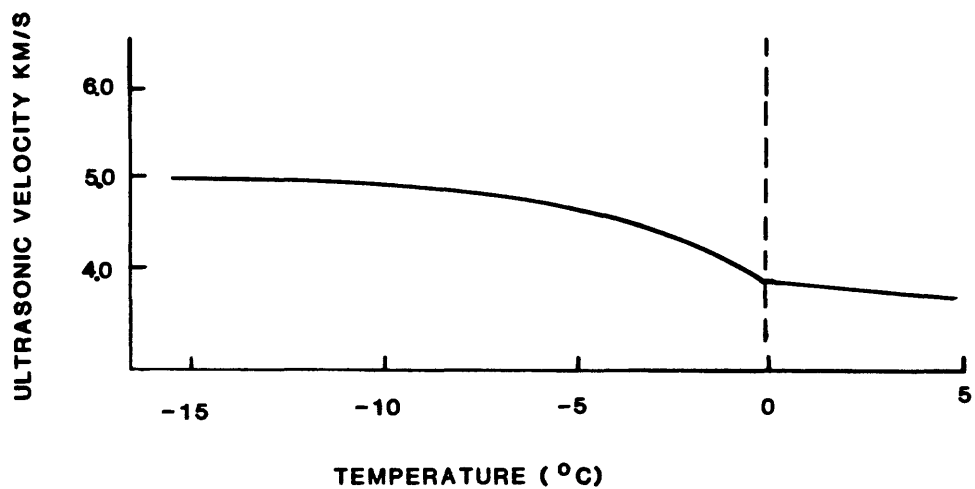


Figure IV-3. Compressional wave velocities as a function of temperature for the Boise Sandstone (Pandit and King, 1979).

Table IV-2. Acoustic velocities of the Boise Sandstone when occupied by various pore-filling constituents (Collett and others, 1984).

Pore filling Substance	Temperature	Acoustic Velocity
Water	(+0°C, salinity 0.1M)	3,500 meters/sec.
Hydrate I	(-5°C, salinity 0.1M)	4,048 meters/sec.
Hydrate I	(-15°C, salinity 0.1M)	4,224 meters/sec.
Ice	(-5°C, salinity 0.1M)	4,600 meters/sec.
Ice	(-15°C, salinity 0.1M)	4,800 meters/sec.

Velocity of Boise Sandstone saturated with hydrate I (-5°C)

----- =
Velocity of Boise Sandstone saturated with water

4,048 meters/sec

= 1.16

3,500 meters/sec

In order to correct for the porosity calculations made from the acoustic transit-time device, the ratio of 1.16 can be utilized as an empirical correction factor. For example, a gas hydrate has been inferred to be present within the Kuparuk River Unit 1B-1 well with a recorded acoustic transit-time of 100 microseconds per foot. Assuming a slow matrix transit time (55.5 microseconds per foot), the calculated apparent porosity would be approximately 33 percent. In order to correct this value for the gas-hydrate effect, the apparent porosity is multiplied by the previously calculated acoustic velocity ratio of gas hydrate to free-water in the Boise Sandstone. The corrected porosity for this unit would be 38 percent.

CROSSPLOTS

Crossplots can be used in well log interpretation to highlight certain formation characteristics. Recent work with acoustic velocities of gas hydrates by Whiffen and others (1982) and the detailed evaluation of the neutron-porosity device within this paper has enabled the development of an acoustic transit-time, neutron porosity crossplot to identify gas-hydrate occurrences. In the following example (fig. IV-4) from the Kuparuk River Unit 1B-1 production well, a series of neutron porosities and acoustic transit-times for 18 horizons were plotted. Through the use of previously described well-log evaluation procedures, nine of the units were determined to be gas-hydrate saturated, five were considered to be ice-bearing, and four water-bearing. Due to the relatively high apparent neutron porosity of gas hydrate in comparison to units saturated with either ice or free-water, there is a grouping of intervals with similar pore-space constituents. As noted in figure IV-4, the inferred gas-hydrate saturated units group in the lower left corner of the graph, with units saturated with ice or free-water plotting in other distinct groups. If a free-gas zone is encountered, the plotted values should be in the upper right corner of the graph.

In Collett and others (1984) it was assumed that a Pickett crossplot, which is commonly used to determine oil saturations in oil/water systems, could be used to determine the degree of gas-hydrate saturation in a gas-hydrate- and water-bearing rock unit. The accuracy of this procedure to determine gas-hydrate saturation is not known. No laboratory or core studies have been conducted to test the usefulness of the Pickett crossplots relative to gas-hydrate research. However, there is no evidence to indicate that they yield incorrect gas-hydrate saturation values. A Pickett crossplot is based on the following logic: If a unit is 100 percent saturated with water, the deep-resistivity device will record the resistivity of the 100 percent water-saturated unit. The water-saturated unit is considered a relative base line from which hydrocarbon saturations can be determined. If the salinity of the pore-fluids is known within the units being studied, the recorded resistivity measurements can be plotted on a Pickett crossplot, and any deviation from the known 100 percent water-saturated resistivity measurement would indicate the presence of hydrocarbons. Similarly, the recorded resistivity values for a gas-hydrate saturated unit would vary substantially from the known water-saturated unit, and this difference can be used to calculate gas-hydrate saturation. Plotted on the Pickett crossplot in figure IV-5 are the deep resistivities and corrected neutron porosities for the previously identified gas hydrate units in the Kuparuk River Unit 1B-1 well (fig. IV-2). On the crossplot for this well, there is a distinct grouping of the gas-hydrate intervals around the 10 percent water saturation line, indicating a potential gas hydrate saturation of approximately 90 percent for the identified horizons. In figure IV-5, the formation water resistivity line was constructed with a R_w of 0.4 ohm-m. A 0.4 ohm-m resistivity in a water-saturated unit for these shallow horizons would suggest pore-fluid salinities in the range of 10 to 15 parts per thousand which corresponds with the salinity values calculated earlier.

The Pickett crossplotting technique is susceptible to erroneous assumptions and interpretations. The incorrect identification of a potential gas-hydrate occurrence or the wrong selection of a pore-water resistivity (R_w) can alter the final saturation calculations. In addition, crossplot methods

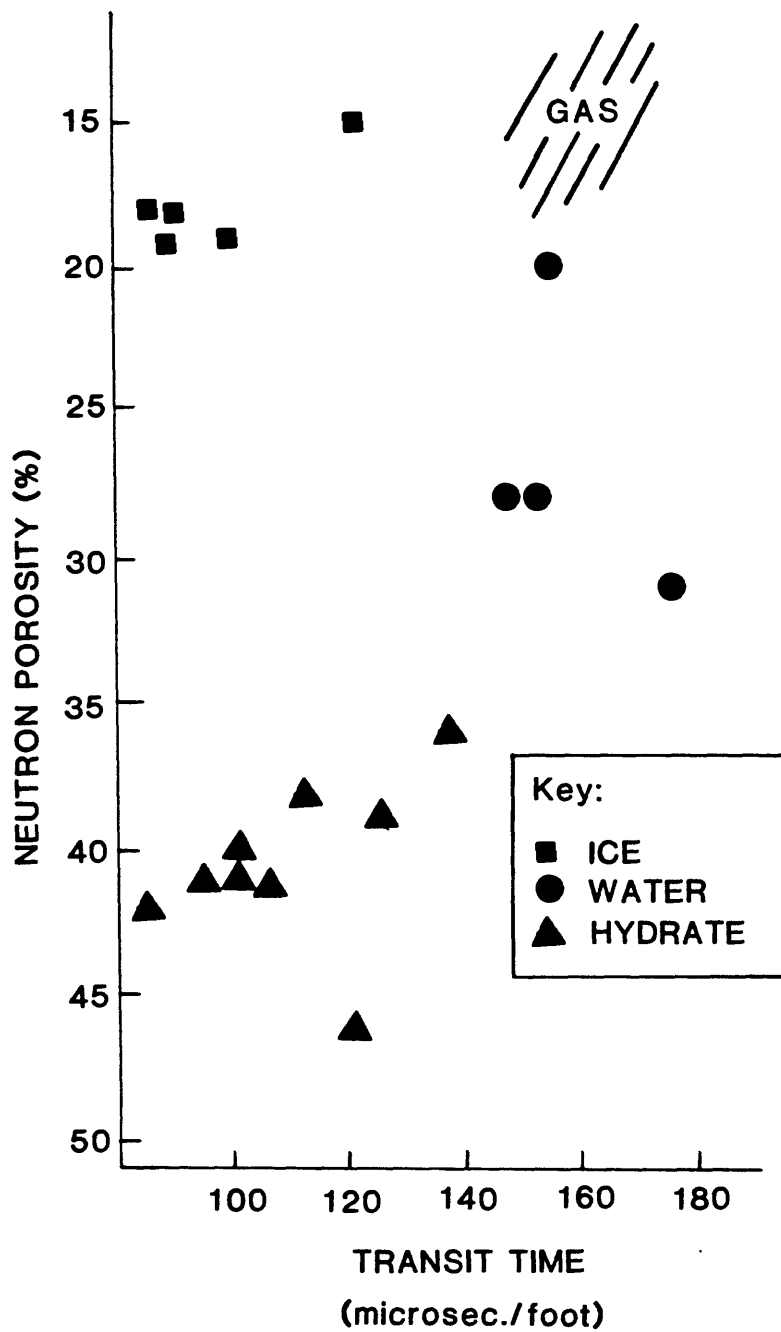


Figure IV-4. Crossplot of neutron porosity and transit time for 18 horizons in the Kuparuk River Unit 1B-1 production well.

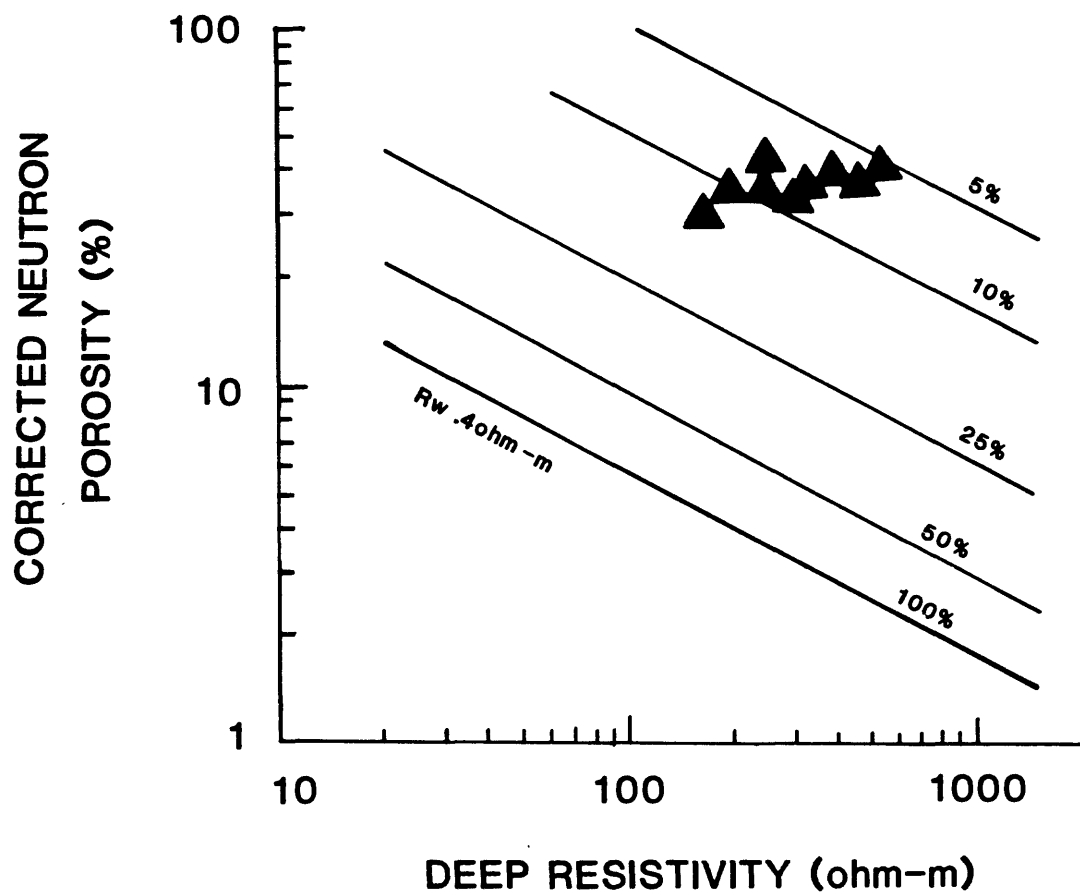


Figure IV-5. Pickett crossplot showing gas hydrate saturation in several horizons from the Kuparuk River Unit 1B-1 production well. The line noted as 100% is the 100 percent water saturation line (R_w is assumed to be 0.4 ohm-m).

employed to determine gas-hydrate saturation can only be used for a gas-hydrate interval below the base of the ice-bearing permafrost. Because of the relatively high resistivity of ice within the permafrost sequence, the comparison of a gas-hydrate saturated unit to an ice-saturated unit will result in an erroneous gas-hydrate saturation value. In using the crossplot-method to determine gas-hydrate saturation, it is assumed that the non-gas-hydrate saturated pore-space within a gas hydrate is occupied by free-water and not ice (i.e.; below the base of the ice-bearing permafrost).

IV.B. GAS HYDRATE DISTRIBUTION

Four-hundred and forty-five North Slope wells were examined for potential gas-hydrate occurrences. Most of the wells are from the Prudhoe Bay--Kuparuk River area; however, all wells from NPRA and most of the exploratory wells to the south and east of Prudhoe Bay have been reviewed. Data reviewed included well logs, well-histories, drilling-reports, core descriptions, and production tests. This review of all available data sources revealed that gas hydrates occur in 39 of the surveyed wells, all from the Prudhoe Bay--Kuparuk River area (tables IV-3 and IV-4). As in Collett (1983a), the resistivity, acoustic transit-time well logs, and the gas chromatograph on the mud log proved to be the most useful tools for identifying in-situ gas hydrates. One-hundred and thirty-four (30 percent) of the wells reviewed had resistivity, acoustic transit-time, and mud logs available within the zones of interest.

Because gas hydrates can not be conclusively identified with well logs, our evaluation procedures must be qualified. We have assigned four qualifiers which must be met before a particular horizon is identified as gas-hydrate bearing. These include (1) high resistivity relative to water (approximately 50 times greater); (2) short acoustic transit-times relative to water (an increase of approximately 40 microseconds per foot); (3) significant release of free-gas during drilling (recognized on the gas chromatograph of the mud log) with volumes of gas in the range of 30 to 100 parts per thousand; (4) a unit that is suspected of being gas-hydrate bearing must be laterally continuous in two or more wells. This last qualifier was only used in areas with a high density of wells. These qualifiers were selected because the cored gas hydrate in the Northwest Eileen State-2 well, discussed in Chapter 1, exhibited similar well log responses and appears to be laterally continuous in several surrounding wells.

All of the gas hydrates occur below the well-log identified geologic Marker 16 and above Marker 12 (see Chapter 3). As discussed previously, Marker 16 is the base of a siltstone unit that was deposited during a basin-wide marine transgression in the Eocene. All of the known and suspected gas hydrates occur in sandstone reservoirs. These sandstones were deposited as point- and distributary mouth-bars in a delta-plain environment. Most of the gas hydrates occur in six laterally continuous sandstone and conglomerate units and are geographically restricted to the east end of the Kuparuk River Unit and the west end of the Prudhoe Bay Unit (figures IV-6 and IV-7). The gas hydrates occur within relatively porous, discrete rock units. Many wells have multiple gas-hydrate bearing units, with individual occurrences ranging from 2 to 28 meters thick. The boundaries of the six delineated gas-hydrate bearing units in figure IV-7 have been interpolated between well locations at which in-situ gas hydrates have been determined to be either present or absent. Thus, the mapped positions of the gas-hydrate unit boundaries (fig. IV-7) are open to interpretation. Of the 34 wells with inferred gas-hydrate occurrences (table IV-3), 14 have the depths listed of the identified gas-hydrate occurrences. These 14 wells have been used to show the lateral and vertical extent of the identified gas-hydrate occurrences. The six, laterally continuous, discrete gas-hydrate bearing rock units have each been assigned a reference letter, with Unit A being stratigraphically the deepest (table IV-3; fig. IV-6). The depth of the identified gas hydrate occurrences in 20 of the wells from table IV-3 are not given; however, the Units (A through F) that are thought to be gas-hydrate bearing in each well have been noted with the symbol x. Data from these 20 wells were not used to describe the in-situ gas-hydrate occurrences for one of two reasons. Most of the omitted wells are regionally located near one of the 14 wells (table IV-3) for which depth intervals have been listed; these omissions reduce the chance of skewing the regional averaging of reservoir parameters, such as porosity; only a few wells, therefore, have been used to describe the gas hydrate occurrences. The second reason for the omission is the lack of confidence in the available well-log data for several of the wells.

The well log responses within the suspected gas-hydrate occurrences of NPRA as described by

Table IV-3. North Slope wells with inferred gas hydrate occurrences. The depth of the gas hydrate occurrences and the base of the ice-bearing permafrost have been listed for 14 of the wells (measured from mean-sea-level). The map location of the 14 referenced wells are shown in figure IV-7. The units believed to be gas-hydrate-bearing in the 20 wells with no depth intervals given have been denoted with an (x), wells with unknown ice-bearing permafrost depths have been denoted with a (-) in the last column.

Well Name and Number	API # 50029-	Reservo Interval (figure IV-6)						Depth to the Base of Ice-bearing Permafrost (m)
		Unit A	Unit B	Unit C	Unit D	Unit E	Unit F	
		(m)	(m)	(m)	(m)	(m)	(m)	(m)
Kuparuk State-1	20008			x	x			-
West Kuparuk 3-11-11	20014			664-681	613-631	567-582		524
Kavearak Point 32-25	20028			x	x			-
Beechy Point-1	20048			831-854	791-798			-
SOCAL 33-29E	20060			x	x	x		-
Kuparuk 7-11-12	20062		848-863	769-784	693-708			571
Milne Point 18-1	20069					x		-
Northwest Eileen State-2	20117			640-669	592-599	552-569		525
West Sak-3	20139	318-346						498
West Sak-6	20142	704-721						531
Kuparuk River Unit 1D-8	20266	610-627						486
Milne Point Unit A-1	20376			609-618	580-598			510
Kuparuk River Unit 1D-5	20417	x						-
Nomination RD-1	20426			807-814	775-783			536
Milne Point Unit B-1	20490			x	x			-
PBU TR 18-11-12	20511		x	x	x			-
Kuparuk River Unit 1C-1	20526		x	x	x	x	x	-
Kuparuk River Unit 1C-2	20532		x	x	x	x	x	-
Kuparuk River Unit 1C-3	20535		x	x	x	x	x	-
Kuparuk River Unit 1C-4	20547		x	x	x	x	x	-
Kuparuk River Unit 1C-5	20550		x	x	x	x	x	-
Kuparuk River Unit 1C-6	20564		x	x	x	x	x	-
Kuparuk River Unit 1C-7	20569		x	x	x	x	x	-
Kuparuk 28243-1	20573	x						-
Kuparuk River Unit 1C-8	20585		590-593	480-493	419-441	386-395	316-328 338-348 357-361	534
Milne Point C-1	20663						x	-
Milne Point D-1	20664				614-618	560-564		522
West Sak-25	20719			504-518	459-468			536
West Sak-24	20723	760-769	662-676					528
Kuparuk River Unit 1H-6	20741	580-588			371-390	344-354		497
Prudhoe-1	20796			x	x			-
Kuparuk River Unit 1F-5	20807	x						-
West Sak Pilot-5	21099	x						-
Kuparuk River Unit 2D-15	21184	x						-
Mean Thickness		15.8	10.3	15.9	11.7	11.0	NA	NA
Thickness Range		8-28	3-15	7-29	4-22	4-17	4-12	NA

Table IV-4. North Slope outlying wells in which gas hydrates may exist, there is no evidence of gas hydrates in adjacent wells; thus not meeting one of our gas-hydrate identification qualifiers.

Well	API #	Sec.	Location T.	R.	Depth ^{1]} (from MSL) (m)	Evidence for Gas Hydrate
West Sak B-10	5002920267	23	10N	9E	288-309	Gas show, high Resistivity & Δt
East Harrison Bay ST-1	5070320001	10	13N	8E	(150-750) ^{1]}	Gas show
Kuparuk River Unit 2V-6	5002921054	8	11N	9E	354-377	Gas show, high Resistivity & Δt
West Sak 16	5002920541	36	13N	8E	750-757 (Ugnu sands)	Gas show, high Resistivity & Δt
West Sak 15	5010320012	5	10N	8E	499-506 (West Sak sands)	Gas show, high Resistivity & Δt

Δt Acoustic Velocity

1] Depths of possible gas hydrate occurrences, measured from mean sea level in meters.

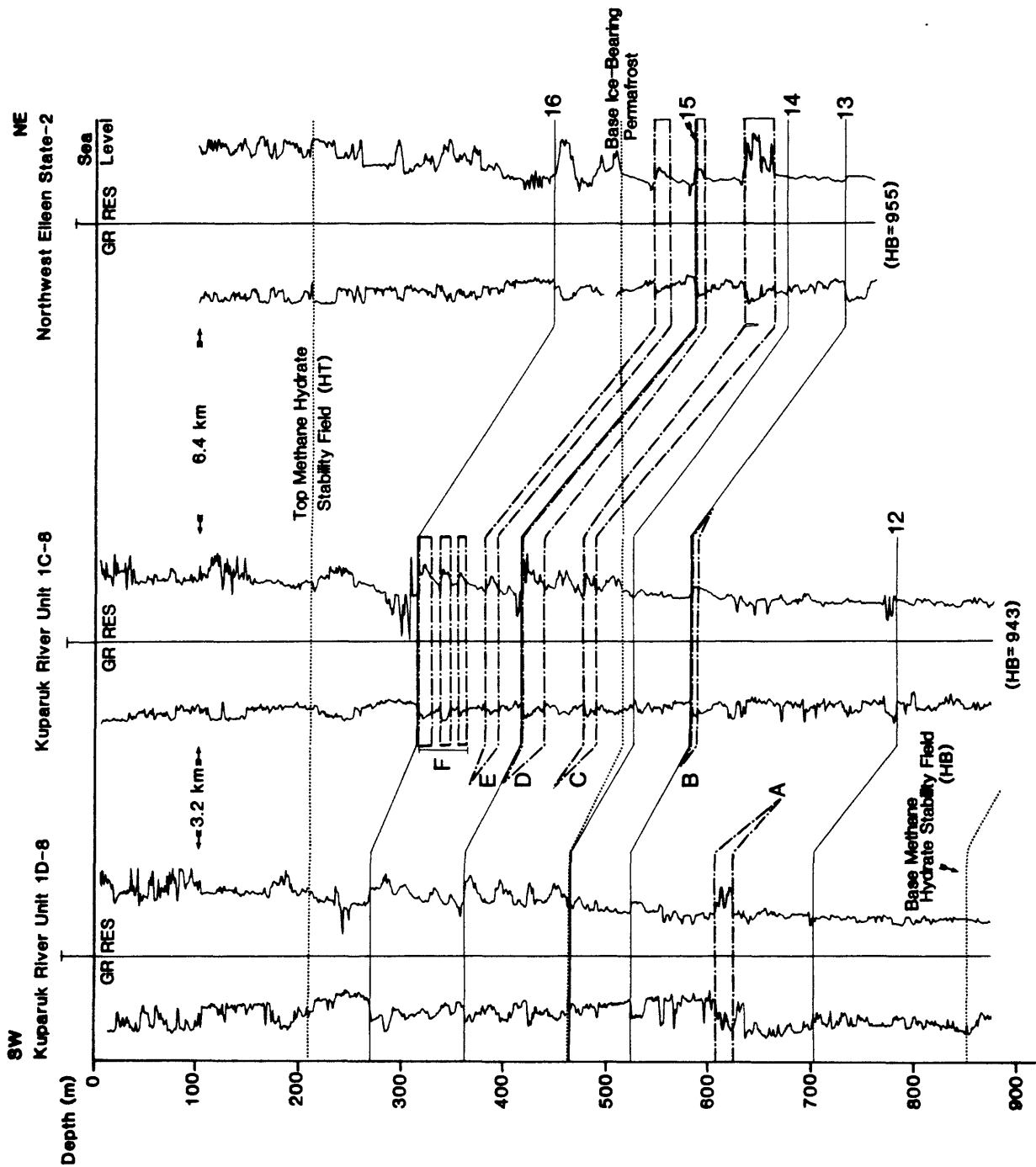


Figure IV-6. Three well cross-section showing the lateral and vertical extent of gas hydrates in the Prudhoe Bay--Kuparuk River area. See figure IV-7 for location of cross-section. Numbers indicate log markers (table III-1). Letters are informally designated gas-hydrate-bearing reservoirs.

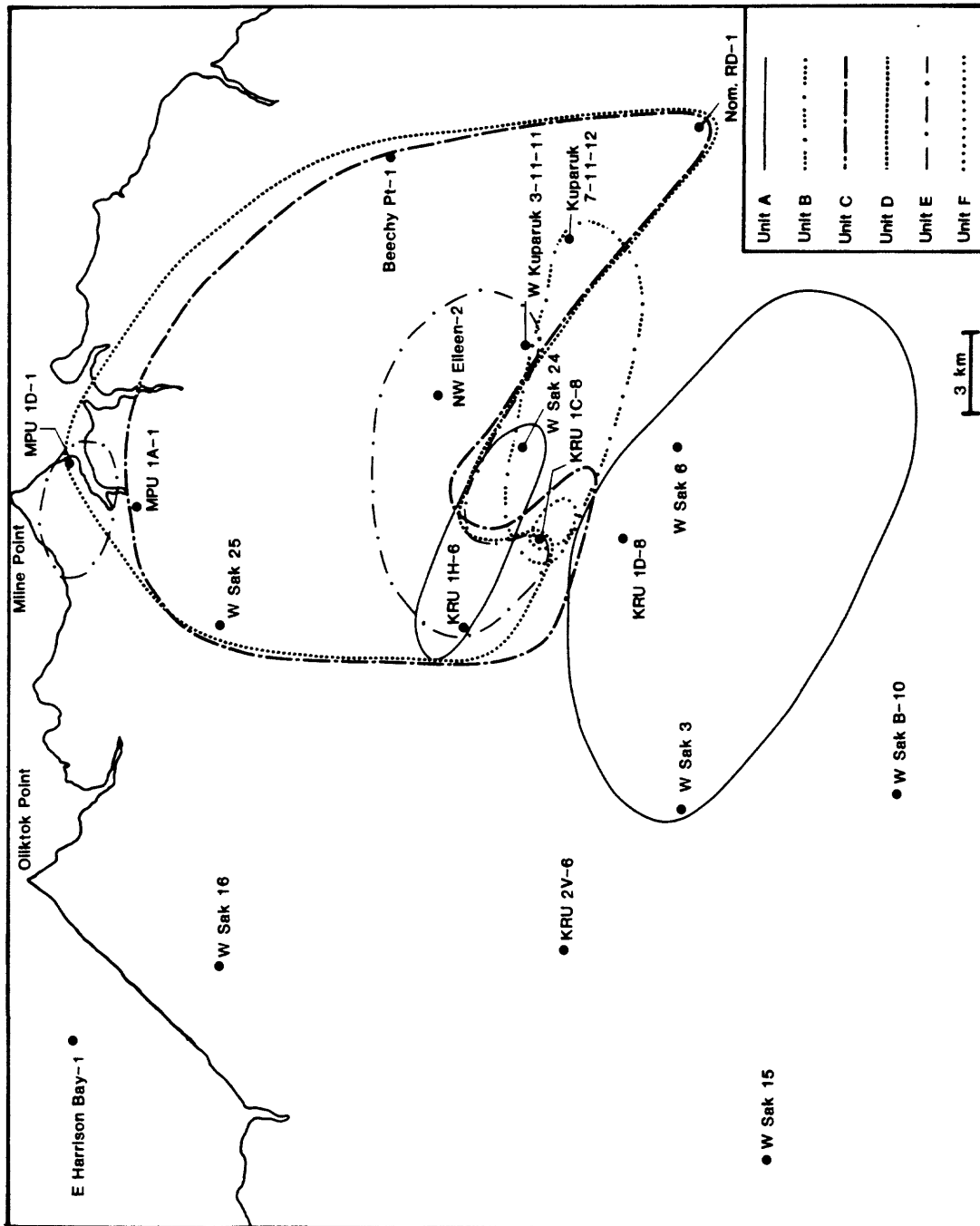


Figure IV-7. Geographic distribution of gas hydrates in the Prudhoe Bay--Kuparuk River area (table IV-3).

Galate and Goodman (1982) (Chapter 1) do not compare favorably with the well log responses within the cored gas-hydrate occurrence of the Northwest Eileen State-2 well. None of their suspected gas-hydrate occurrences meet the four gas hydrate identification qualifiers previously discussed in this section; therefore, we do not believe that gas hydrates occur within most of the wells discussed by Galate and Goodman (1982).

Examination of figure IV-7 shows that Unit A is gas-hydrate bearing in two separate areas of the Kuparuk River Unit. The total area in which Unit A is gas-hydrate bearing is approximately 82 km². The thickness of the gas hydrate deposit in Unit A ranges from 8 to 28 m, with an average thickness of 15.8 m. In the well log display of figure IV-8 from the Kuparuk River Unit 1D-8 well, Unit A is inferred to be gas-hydrate saturated from 642 to 659 m. Also reservoired in Unit A is a significant volume of oil, both in the Kuparuk River and Prudhoe Bay areas. Well log and drill-cuttings analyses have also revealed the presence of several thick coal seams (fig. IV-8). Most of the gas hydrates of Unit A occur below the base of ice-bearing permafrost. However, the mud log indicates that the up-dip portion of Unit A in West Sak-3 (fig. IV-7) appears to be gas-hydrate bearing above the base of ice-bearing permafrost.

The gas hydrates of Unit B have a total areal distribution of approximately 18 km² and thicknesses ranging from 3 to 15 m. In figure IV-9, Unit B is inferred to be gas hydrate bearing from a depth of 869 to 884 m in the Kuparuk 7-11-12 exploratory well. Coal is also abundant in Unit B; there is no evidence of reservoired oil. All the gas hydrates in Unit B occur below the base of ice-bearing permafrost.

The gas hydrates of Units C and D are the most laterally extensive and exhibit similar reservoir rock properties. The gas hydrates of Unit C have a total areal distribution of approximately 122 km², and the total lateral extent of the gas hydrates in Unit D is approximately 130 km². Unit C is the cored gas-hydrate bearing unit in the Northwest Eileen State-2 well, discussed in Chapter 1. In the well-log display of figure IV-10 from Northwest Eileen State-2, Units C and D are shown to be gas-hydrate bearing from a depth of 659 to 688 m and from 611 to 618 m, respectively. Relative to Units A and B, coal is scarce in Units C and D. The southern- and western-most gas hydrates in Units C and D occur within the ice-bearing permafrost sequence (fig. IV-7), with several occurrences more than 150 m above the base of ice-bearing permafrost.

Unit E is shown to be gas-hydrate bearing in two distinct areas near the boundary of the Kuparuk River Unit and at Milne Point (fig. IV-7). The total areal distribution of the gas hydrates in Unit E is approximately 30 km². Reservoir rock properties of Unit E are similar to those in Units C and D. Unit E is inferred to be gas-hydrate bearing in the well-log display of figure IV-10 from Northwest Eileen State-2. Gas hydrates of Unit E also appear to transect the base of ice-bearing permafrost with the farthest south-western up-dip extension of the gas hydrates more than 160 m above the base of ice-bearing permafrost.

Gas hydrates of Unit F are a composite of three gas-hydrate bearing rock units drilled in several wells from the Kuparuk River 1C production pad (fig. IV-7). These gas hydrate occurrences were first recognized during drilling when a significant volume of gas leaked from around the outside of the casing into the basement of the drilling rig. It appears that the free gas was from a series of gas hydrate- and coal-bearing units within 390 m of the surface, all within the ice-bearing permafrost sequence. Apparently drilling activity had dissociated the gas hydrates near the wellbore, and the free-gas migrated along the outside of the casing into the drilling rig. In the well-log display in figure IV-11 from the Kuparuk River Unit 1C-8 well, there are three inferred gas-hydrate-bearing units which we collectively refer to as Unit F. The combined total thicknesses of these units range from 4 to 12 m, and they are geographically restricted to the immediate area of the Kuparuk River 1C production pad. The total surface area of these occurrences is approximately 1 km².

Well-log data from five wells in the Kuparuk River Unit (table IV-4), located west of the delineated gas-hydrate occurrences (fig. IV-7), suggest that gas hydrates may be locally present. However, the well-log data are inconclusive, and there is no evidence of gas hydrates in surrounding wells.

Little is known about the lateral nature of the gas-hydrate deposits delineated in figure IV-7. It is speculated that within these units, gas hydrates are laterally continuous. However, due to the scarcity and the poor quality of the well logs, it is difficult to completely determine the lateral extent

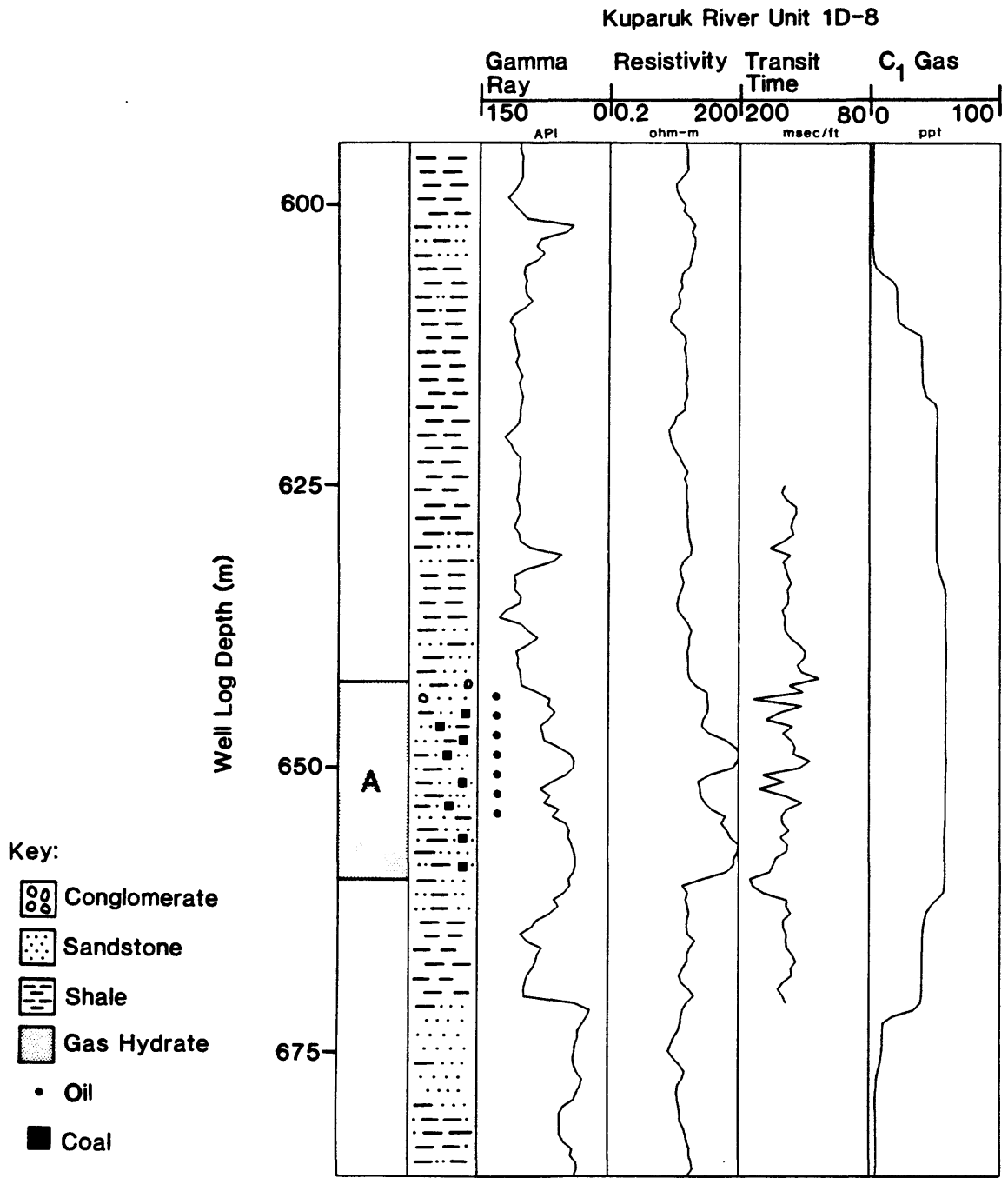


Figure IV-8. Well log display from Kuparuk River Unit 1D-8, Unit A is inferred to be gas hydrate bearing from 642 to 659 m (see figure IV-7 for location).

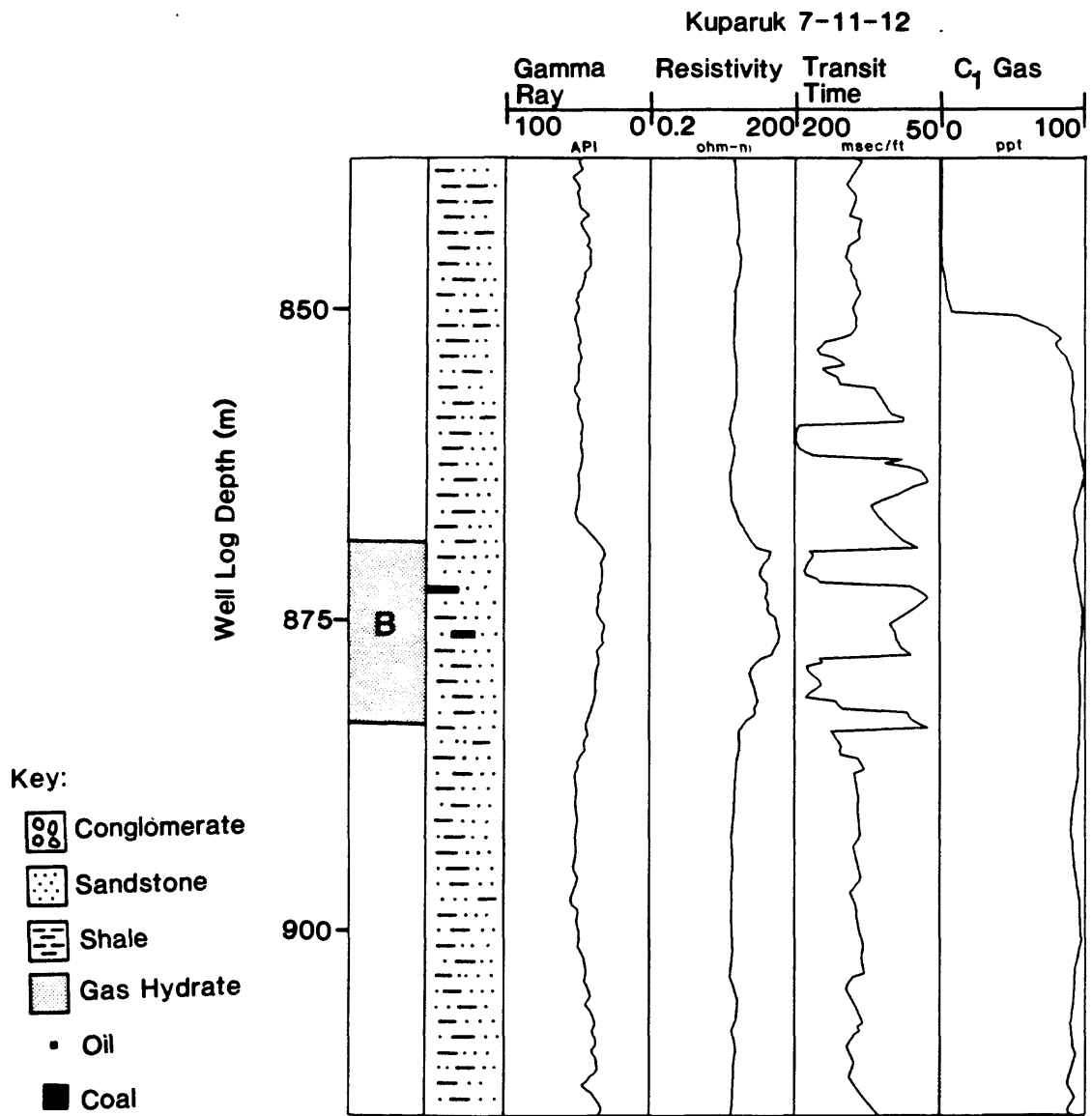


Figure IV-9. Well log display from Kuparuk 7-11-12, Unit B is inferred to be gas hydrate bearing from 869 to 884m (see figure IV-7 for location).

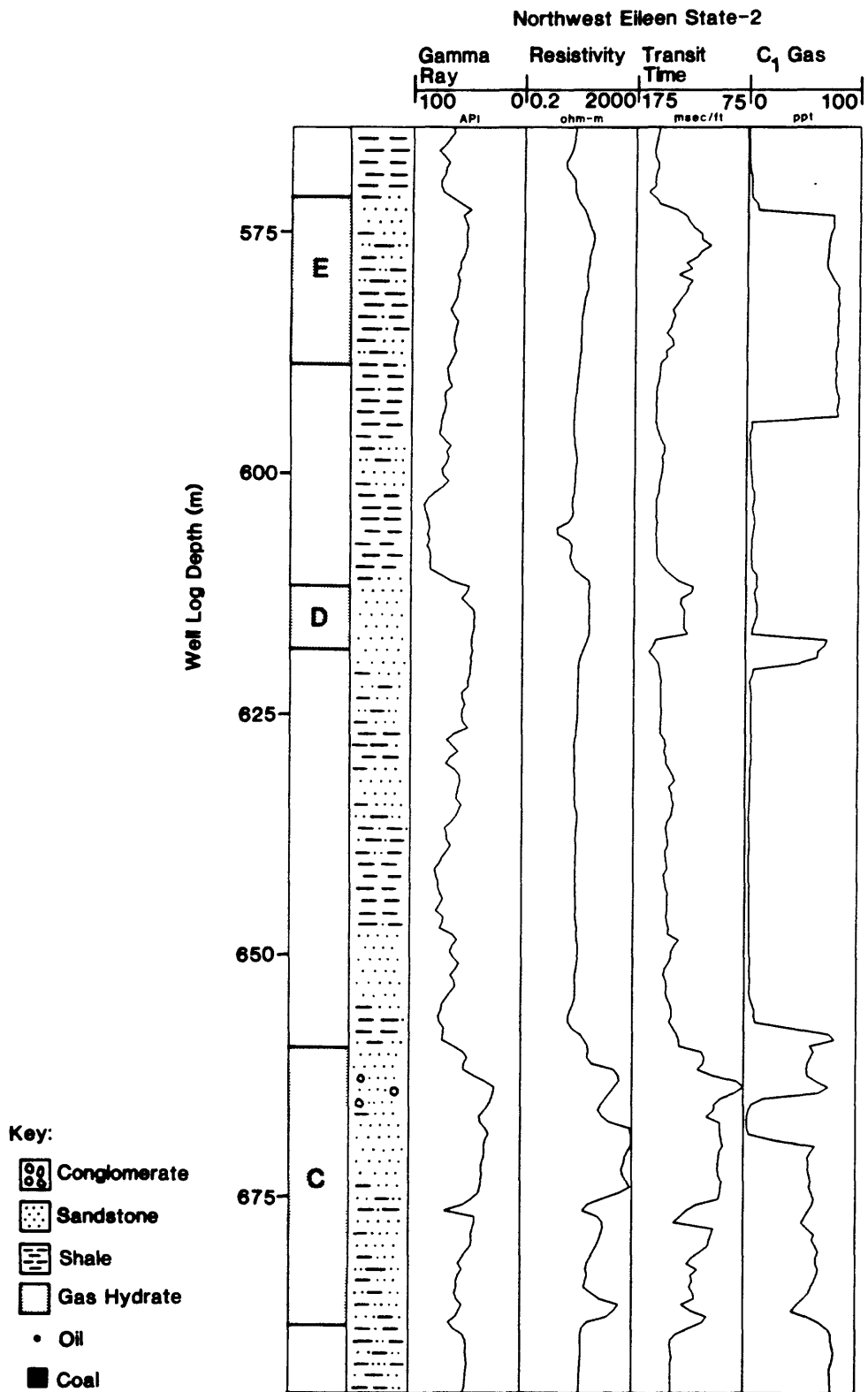


Figure IV-10. Well log display from Northwest Eileen State-2, Units C, D, and E are inferred to be gas hydrate bearing from 659 to 688 m, 611 to 618 m, and 570 to 588 m, respectively (see figure IV-7 for location).

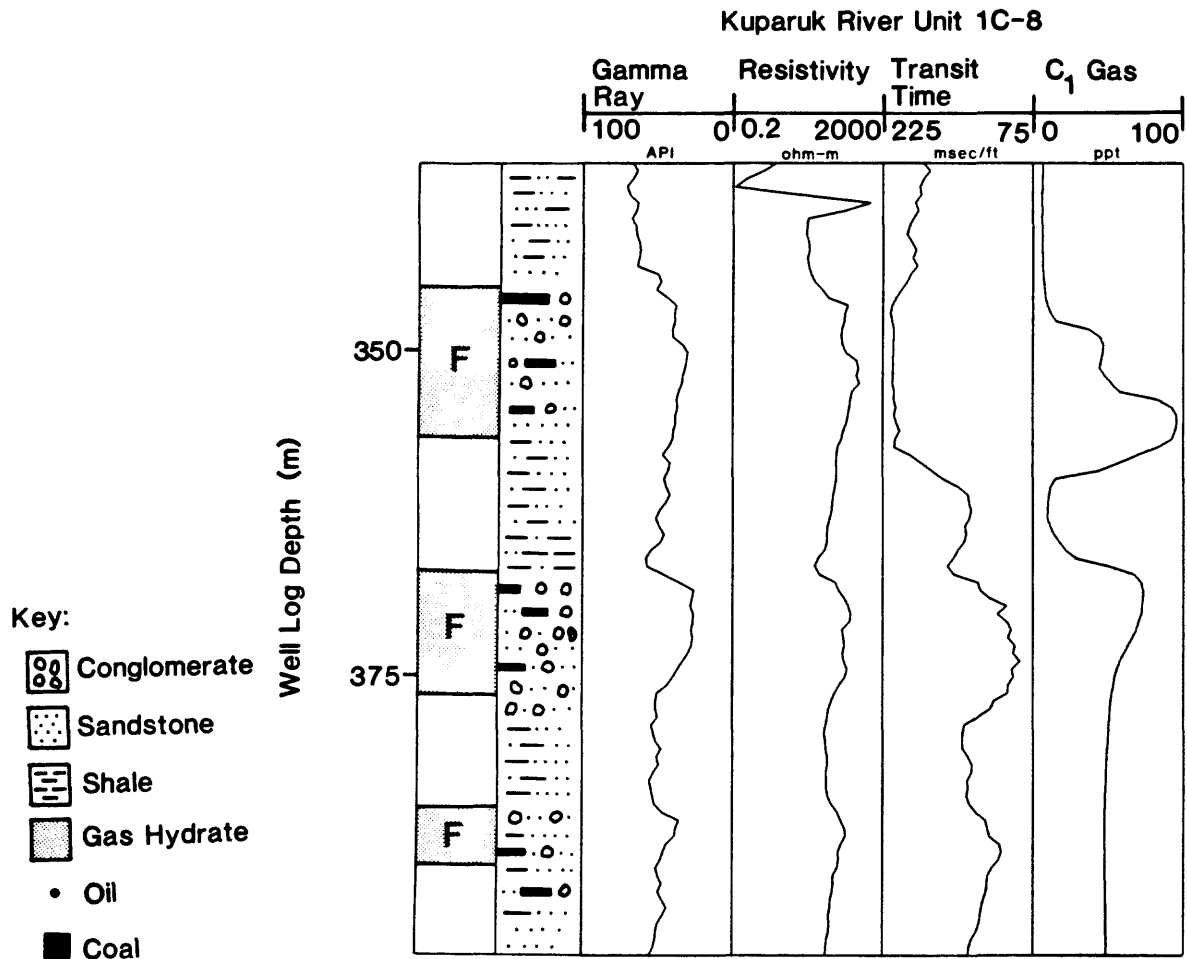


Figure IV-11. Well log display from Kuparuk River Unit 1C-8. Unit F is inferred to be gas hydrate bearing from 345 to 357 m, 367 to 377 m, and 385 to 389 m (see figure IV-7 for location). The acoustic transit-time device within the shallowest gas hydrate occurrence (345-357) did not behave as expected; the observed low acoustic velocities may be due to the presence coal or free-gas within the rock formation.

of the gas hydrates. For example, well-log data indicate that there is no gas hydrate in West Sak-1, but logs from the surrounding wells suggest that gas hydrates should be present in Units C, D, and E. In this particular case, the log data from West Sak-1 is generally of good quality; therefore, it is speculated that there is an unrecognized, localized geologic control limiting the occurrence of gas hydrates in this well. New data are required to determine accurately the lateral extent of the in-situ gas hydrates on the North Slope.

IV.C. GAS-HYDRATE RESERVOIR PROPERTIES

Two of the most difficult gas-hydrate reservoir properties to determine accurately are reservoir porosity and the degree of gas-hydrate saturation. The primary reason for this difficulty is the lack of previous field and laboratory studies. In Section "A" of this chapter, we have described several well-log-evaluation techniques that can be used to estimate porosity and gas-hydrate saturation within suspected gas-hydrate occurrence. In this section we have reviewed all available data sources to determine the reservoir porosity and the degree of gas-hydrate saturation within the six gas-hydrate bearing units (A through F) in the Prudhoe Bay--Kuparuk River area.

RESERVOIR POROSITY

Well logs serve as a source of porosity data; however, the determination of porosity with well logs in gas-hydrate or ice-bearing horizons is subject to significant error. Our work shows that calculations from the acoustic log in a gas-hydrate or ice-bearing unit can underestimate porosities from 16 to 20 percent. Porosity within a gas-hydrate bearing reservoir is most reliably derived with a borehole-compensated neutron device which will be in error by only 3% (Collett and others, 1984). To determine the porosities of the gas-hydrate reservoir rocks, 71 neutron-porosity calculations were made within the identified gas hydrates in seven of the wells. These porosity values, which range from 22 to 48 percent, are plotted in figure IV-12. Because of significant scatter in the calculated neutron porosities, the suspected neutron porosity error of 3% is negligible. An average trend-line, fitted to the calculated porosities, (figure IV-12) shows a 3% decrease per 1,000 m. Also shown are core-derived porosity trend-lines for rocks in this area. Howitt (1971) reported measured porosities ranging from 40 to 45 percent within the permafrost sequence (0-610 m) of the Prudhoe Bay area, and Werner (1984) showed that the West Sak sands have porosities ranging from 25 to 35 percent below the permafrost sequence (1,000-1,300 m) in the Kuparuk River area. The core- and the log-calculated porosity trends show remarkably close agreement (fig. IV-12). Presumably, this porosity reduction with depth is caused exclusively by compaction. A best-fit porosity trend-line was projected through the core- and log-derived porosities (fig. IV-12). This porosity curve (3% porosity decrease per 1,000 m) was used to calculate the average porosity of the identified gas-hydrate reservoirs. These calculations were made by comparing the depth interval of each gas-hydrate occurrence with the porosity trend-line in figure IV-12. For example, Unit A is gas-hydrate bearing from a depth of 318 m in West Sak-3, to a maximum depth of 769 m in West Sak-24 (table IV-5). The midpoint depth of the gas hydrate occurrence of Unit A is at 544 m. In figure IV-12 at a depth of 544 m, the expected porosity projected from the trend-line is 39%; thus, the average porosity of Unit A is estimated at 39%. The average porosity of the five remaining gas-hydrate occurrences have been similarly calculated (table IV-5). Subsequently, the total porosity volume (cubic meters) within each gas-hydrate reservoir has been calculated in Chapter VI.

GAS HYDRATE SATURATION

A series of Pickett crossplots were used to calculate gas hydrate saturation in four of the six delineated gas-hydrate occurrences (Units B, C, D, and E). As discussed previously in this chapter, the crossplot procedure for determining gas-hydrate saturation is not valid when ice or other hydrocarbons are present. Therefore, only sub-permafrost, non-oil-bearing gas hydrates were considered. Because Unit A is oil-bearing and all of Unit F is within the permafrost sequence, these units have been omitted from the saturation calculations.

In the Pickett crossplots of figures IV-13 through IV-16, the corrected neutron-porosity and resistivity log values have been plotted for twenty-seven gas-hydrate occurrences. Each crossplot represents one of the four delineated gas-hydrate units (Units B, C, D, and E). The crossplot in figure

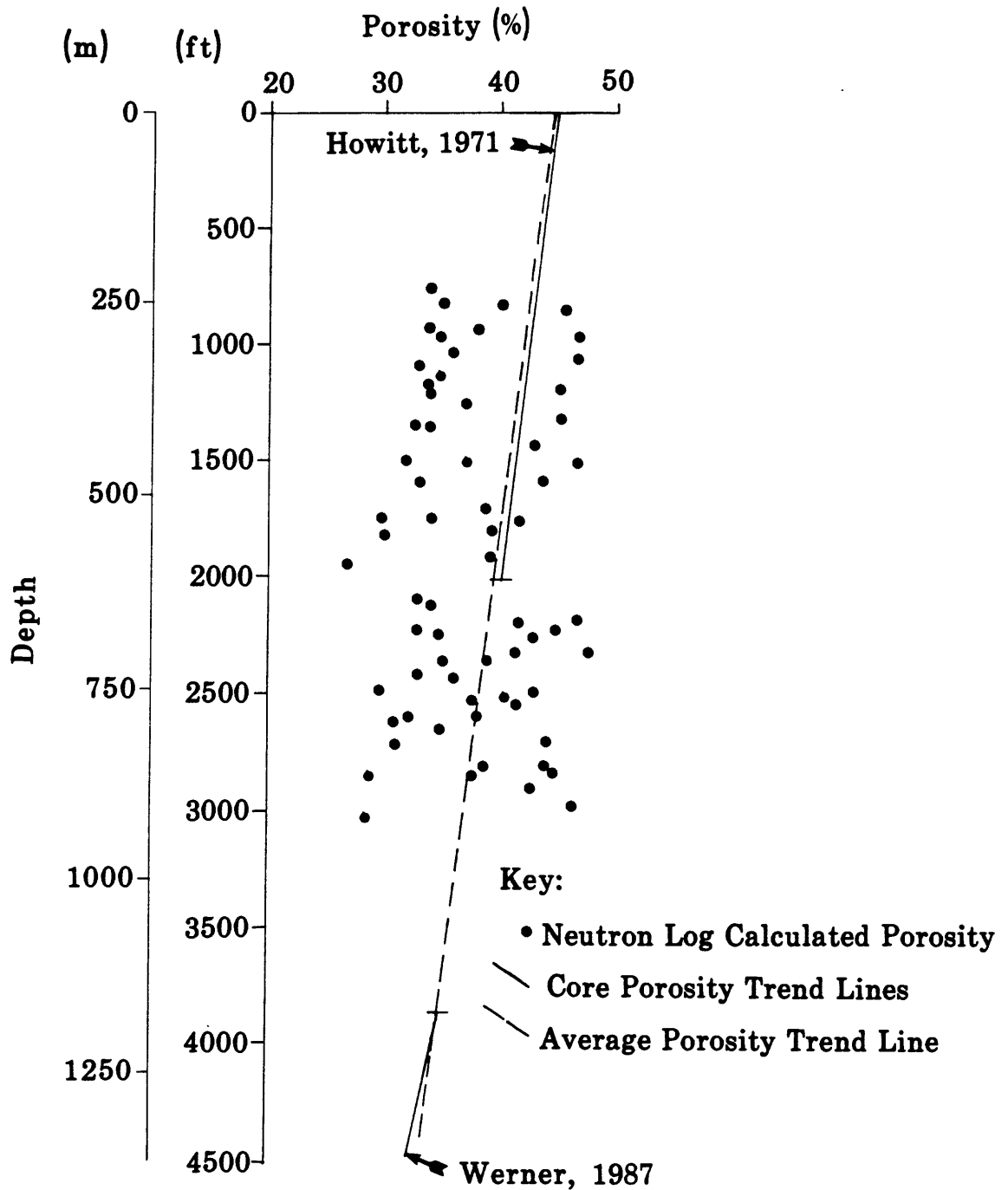


Figure IV-12. Plot of 71 log calculated neutron porosities (•) from within the gas hydrate occurrences in seven wells, and trends of referenced core-derived porosities for the Prudhoe Bay--Kuparuk River area (Werner, 1987; Howitt, 1971). Average porosity trend-line is based on both the log- and core-derived porosities.

Table IV-5. Average reservoir porosities estimated for gas hydrate Units A, B, C, D, E, and F utilizing the porosity trend-line in figure IV-12.

(1) Hydrate Bearing Unit	(2) Shallowest Gas Hydrate Occurrence (m)	(3) Deepest Gas Hydrate Occurrence (m)	(4) Mid-Point Depth of Gas Hydrate Occurrence (m)	(5) Average ϕ
A	318	769	544	39
B	590	863	727	38
C	480	854	667	38
D	371	798	585	39
E	344	582	463	40
F	316	361	339	41

- (1) Unit Index letter (figure IV-7)
- (2) Depth of the shallowest identified gas-hydrate occurrence (table IV-3).
- (3) Depth of the deepest identified gas-hydrate occurrence (table IV-3).
- (4) Average mid-point depth of the delineated gas-hydrate occurrence.
- (5) Porosity of the mid-point depth, projected from the porosity trend-line in figure IV-12.

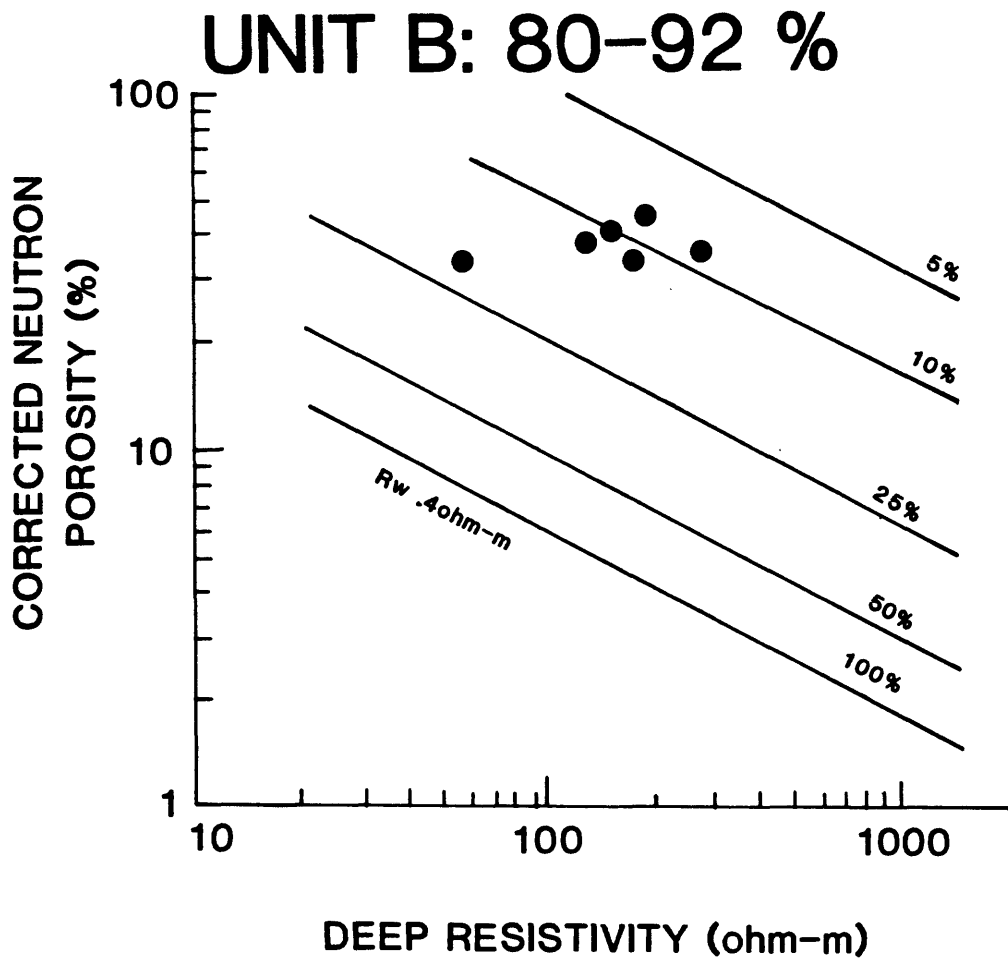


Figure IV-13. Pickett crossplot for gas-hydrate-bearing Unit B showing gas-hydrate saturation ranging from 80 to 92 percent (table IV-6).

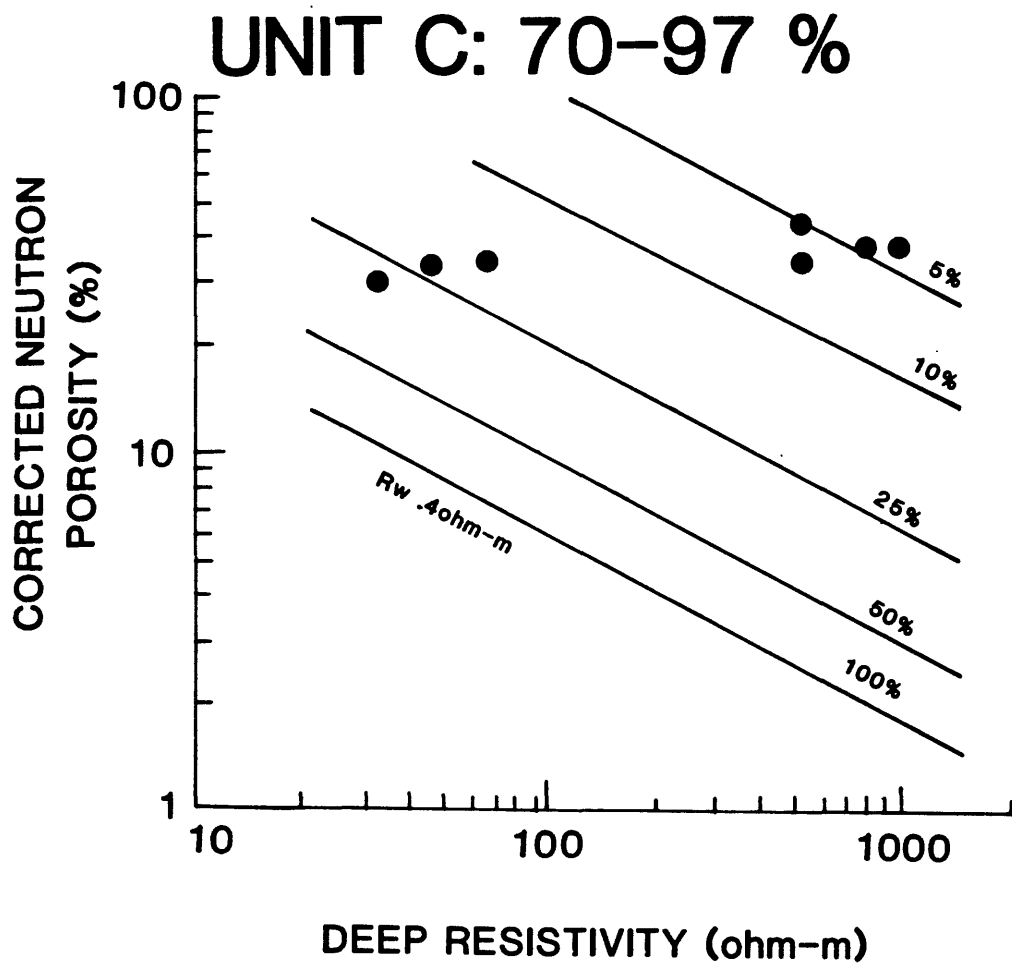


Figure IV-14. Pickett crossplot for gas-hydrate-bearing Unit C showing gas-hydrate saturation ranging from 70 to 97 percent (table IV-6).

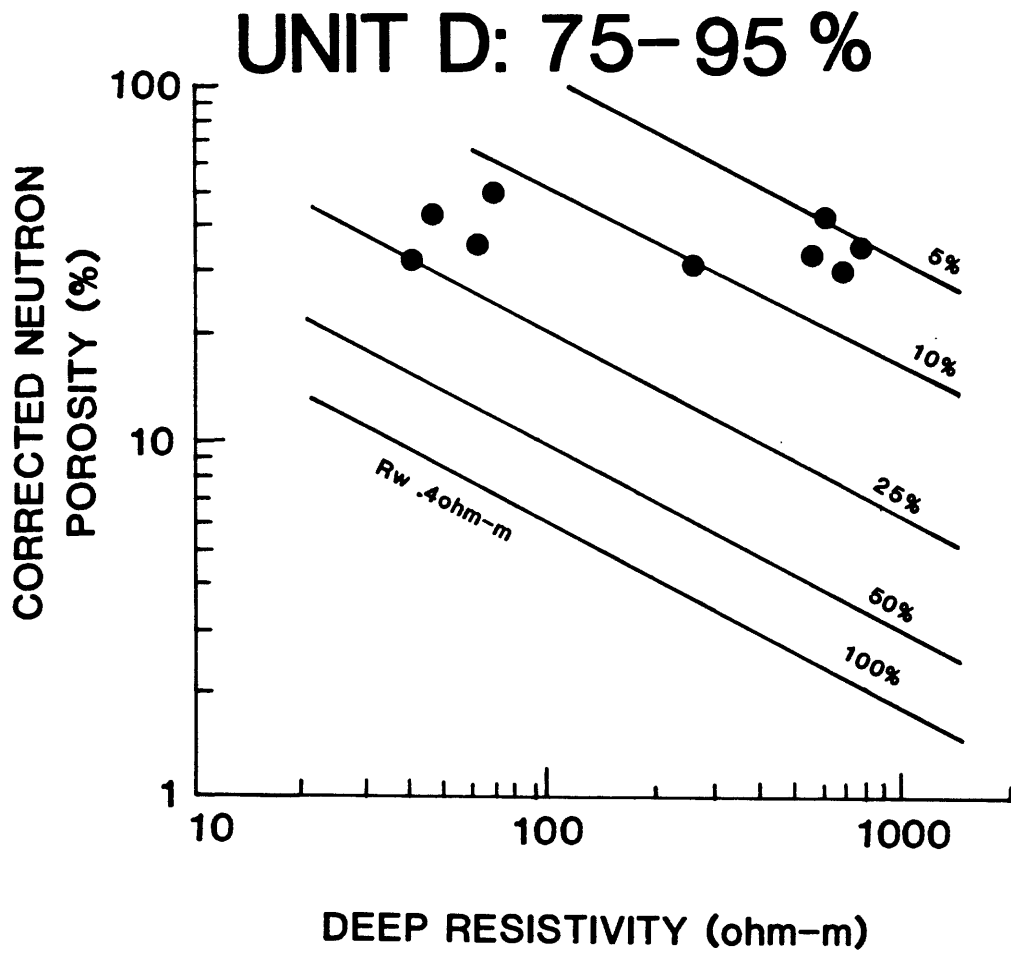


Figure IV-15. Pickett crossplot for gas-hydrate-bearing Unit D showing gas-hydrate saturation ranging from 75 to 95 percent (table IV-6).

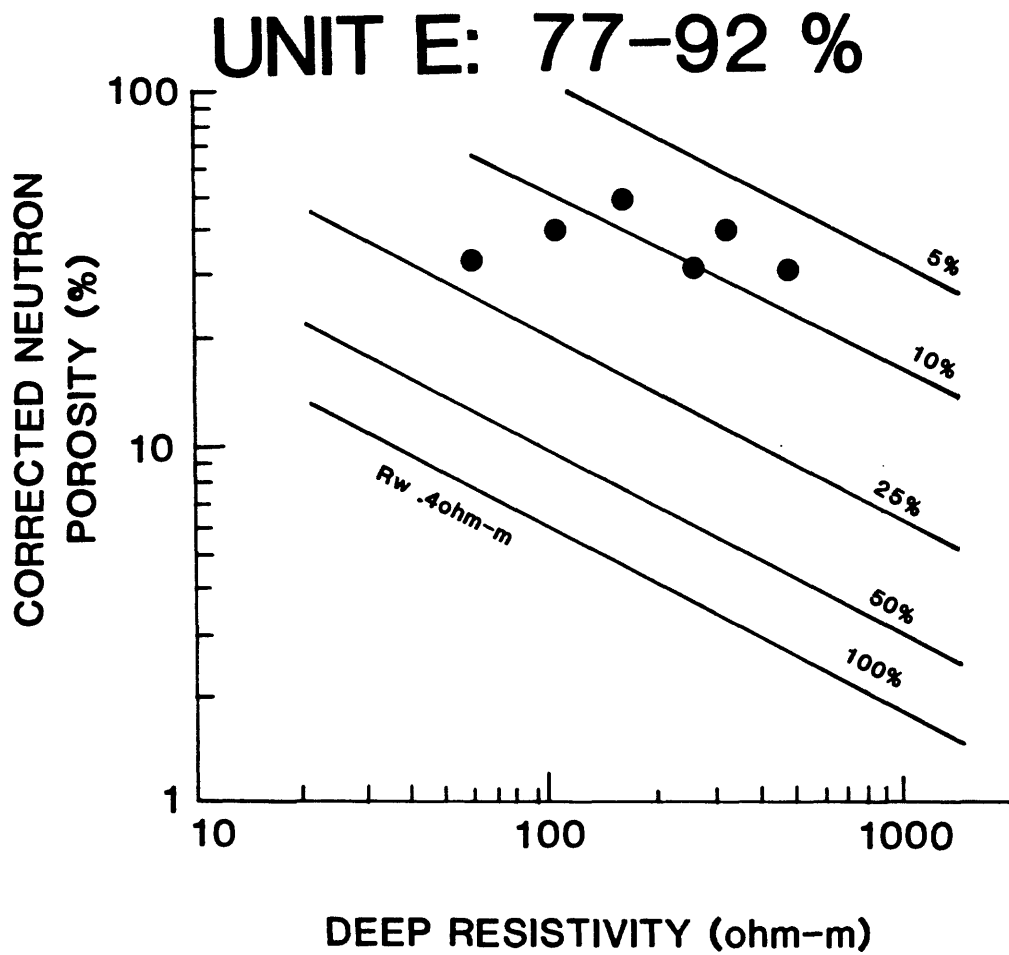


Figure IV-16. Pickett crossplot for gas-hydrate-bearing Unit E showing gas-hydrate saturation ranging from 77 to 92 percent (table IV-6).

IV-13 shows that gas-hydrate saturation in Unit B ranges from 80 to 92 percent, and averages approximately 86%. Similarly, the crossplots for Units C, D, and E (figures IV-14, IV-15, and IV-16) show that gas-hydrate saturation ranges from 70 to 95 percent and generally averages 85%. Because of the lack of data, we have assumed the degree of gas-hydrate saturation for Units A and F to also be 85%. Listed in table IV-6 are the ranges and average gas-hydrate saturations determined from the Pickett-Crossplots for Units B, C, D, and E.

Table IV-6. Gas-hydrate saturation data for Units A, B, C, D, E, and F as interpreted from the Pickett crossplots in figures IV-13 through IV-16.

(1) Hydrate Bearing Unit	(2) Gas Hydrate Saturation Range %	(3) Gas Hydrate Saturation Average %
B	80-92	86
C	70-97	84
D	75-95	85
E	77-92	85
Average	76-94	85
A	-	85*
F	-	85*

* Estimated Values.

(1) Unit Index letter (figure IV-7).

(2) Gas hydrate saturation range (figures IV-13 through IV-16).

(3) Average gas hydrate saturations (figures IV-13 through IV-16).

CHAPTER V. GAS-HYDRATE FORMATION MODELS

V.A. THEORETICAL MODELS

This chapter deals with the development of a model that describes the possible origin of gas hydrate on the North Slope. In Section A of this chapter we have described two highly-generalized models for gas-hydrate formation. Section B deals with the development of a gas-hydrate formation model specifically for the North Slope.

Various mechanisms for gas-hydrate formation have been postulated as discussed by Pratt (1979) and Makogon (1981). One theory suggests that gas hydrates could be part of a pre-existing gas reservoir, later solidified in place. A second theory suggests that a gas-hydrate accumulation could form by a flow of free gas into the zone of gas-hydrate stability. It is also possible that migrating free gas may be trapped at the base of the ice-bearing permafrost and converted to gas hydrate. In addition, gas hydrates are sometimes found closely associated with decaying biomatter, such as coal, which may serve as a gas source. These various schemes of gas hydrate formation can be grouped into two end-member models.

MODEL 1. The conversion of a pre-existing gas field into a gas hydrate with a favorable change in temperature or pore-pressure (fig. V-1a).

MODEL 2. Formation of gas hydrate by continuous migration of either microbial or thermogenic gas from below into the zone of gas-hydrate stability (fig. V-1b).

V.B. NORTH SLOPE MODEL

Before proceeding with the development of a model to describe the possible origin of gas hydrate on the North Slope of Alaska, it is useful to list several observations pertaining to the distribution of the gas hydrates: (1) All of the gas hydrates occur near the eastern boundary of the Kuparuk River Unit and extend into the west end of the Prudhoe Bay Unit, an area cut by faults extending deep into the stratigraphic section; (2) gas hydrates occupy a series of sandstone units which gently dip to the northeast; (3) all of the gas hydrates occur below Marker 16, which is the base of a relatively impermeable marine siltstone sequence; (4) the areal distributions of the individual gas-hydrate occurrences are irregular in shape and size; (5) gas hydrates are commonly reservoided near coal sequences; (6) oil and tar are reservoided with one inferred gas hydrate occurrence; (7) methane is the predominant gas in the near-surface sediments (0-1,500 m).

Carman and Hardwick (1983) postulated that the oil within West Sak and Ugnu sands migrated along faults from the underlying Prudhoe Bay oil field. If this theory is correct, free gas from within the Sadlerochit reservoir and dissolved gas associated with the oils would also have migrated into the overlying sediments. As shown in figures III-17, III-19, and IV-7, most of the gas hydrates and shallow-heavy-oils occur either up-dip from, or near to, the Eileen fault zone. This fault zone, therefore, may have acted as a conduit for free-gas and oil migration from deeper hydrocarbon accumulations. The gas within the gas cap of the Sadlerochit reservoir of the Prudhoe Bay oil field is composed primarily of methane along with small quantities of ethane and propane (table V-1).

However, solution gas from the oil has 13 to 19 percent CO² (Rickwood, 1970) which was not observed, for example, in gas samples from the Northwest Eileen State-2 well (table II-8). If gas within the near-surface sediments migrated from deeper structures, these shallow gases should have geochemical constituents similar to those of the deep gases. All of the chemical components known to be in Sadlerochit gases are present within gases of the West Sak sands (Werner, 1987). Outside of the scope of this report, we have conducted isotopic analyses of gases associated with inferred gas-hydrate occurrences. Preliminary results suggest that methane within the gas-hydrate bearing sequences is from both thermogenic and microbial sources. At this time, it is not known which source supplied the greatest volume of gas. However, the presence of thermogenic gas supports the theory that gas has migrated into these units from the underlying accumulations, possibly along the Eileen or related faults. In addition, one gas-hydrate unit (Unit A) is associated with a significant volume of oil which must have migrated from the underlying Prudhoe Bay or Kuparuk oil fields. A second

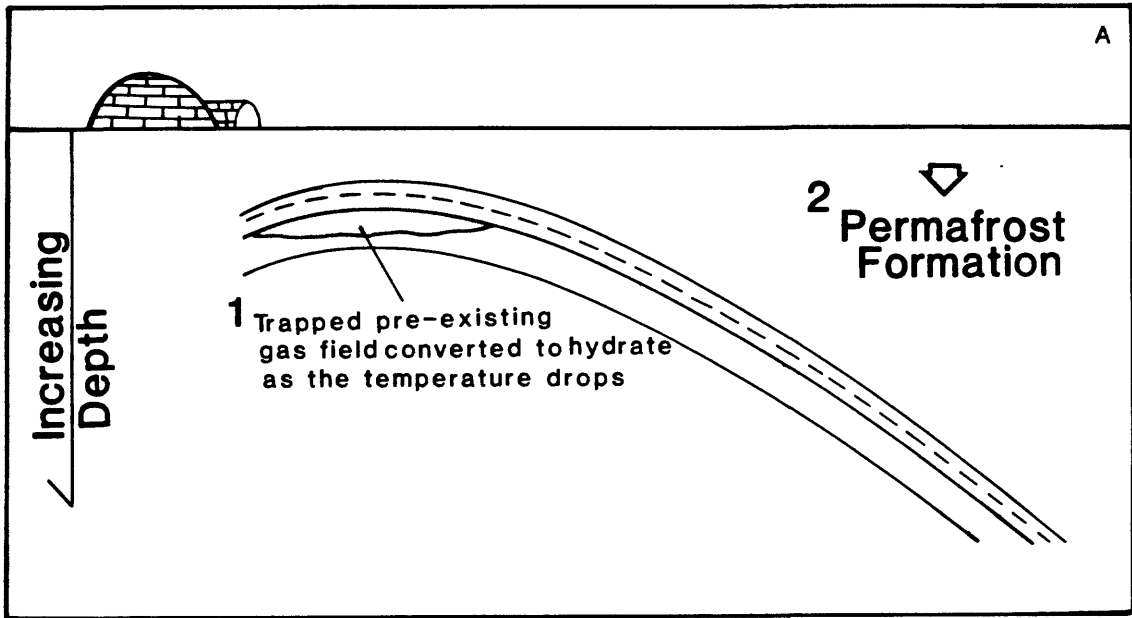


Figure V-1a. Example of Model 1: The conversion of a pre-existing free-gas field (1) into a gas-hydrate accumulation with a decrease in temperature (2).

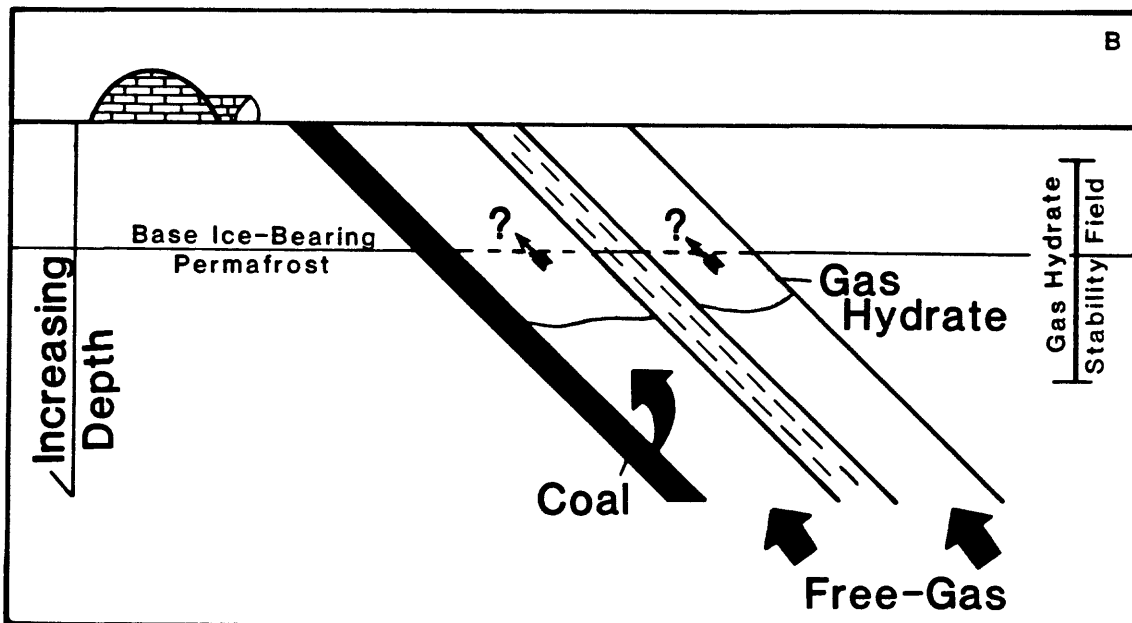


Figure V-1b. Example of Model 2: Formation of gas hydrate by migration of microbial or thermogenic gas into a pre-existing pressure-temperature regime in which gas hydrates are stable.

Methane	85.11
Ethane	7.70
Propane	3.99
l-butane	0.50
n-butane	0.73
l-pentane	0.11
n-pentane	0.09
Hexane	0.02
Heptanes plus	0.00
Carbon dioxide	1.00
Nitrogen	0.75

Table V-1. Composition of the gases from the gas cap of the Prudhoe Bay oil field (O'Donnell, 1976).

geochemical feature of gas hydrates that may be important is the relationship between coal and gas. Gas hydrates are known to occur in close proximity to several thick coal sequences in the Kuparuk River area. It is possible that alteration of these coals may have generated a significant volume of methane gas which has been converted to gas hydrate.

To describe the history of gas-hydrate formation, we have adapted a generalized cross-section from Carman and Hardwick (1983) to discuss possible gas-hydrate formation scenarios (figure V-2). As gas moved up along the Eileen fault and encountered relatively porous and permeable northeast-dipping sandstone units, some of the gas may have been rechanneled up-dip along these beds. The up-dip migrating gas may have collected in structural or stratigraphic traps where subsequent temperature changes deepened the permafrost sequence and converted the trapped gas into gas hydrate. Conversely, it may be possible that the up-dip migrating gas was converted to gas hydrate upon entering the pressure-temperature regime of gas-hydrate stability, thus forming its own trap. Because so little is known about the history of temperatures on the North Slope and the presence of traps for free gas in this area, either of these scenarios is applicable. However, it is speculated that gas hydrates presently occur more than 160 m above the base of ice-bearing permafrost which is assumed to be impermeable (see Chapter IV). Therefore, when gas migrated into these upper horizons, the base of the ice-bearing permafrost must have been at least 160 m shallower than today.

Since the onset of gas migration into these near-surface horizons (mid-Tertiary), temperatures have fluctuated significantly. Regional temperature changes during the last 2 to 3 million years have been great enough to repeatedly thicken and thin the zone of gas-hydrate stability; however, the magnitude of these changes is not known. In addition, we know that a surface water-body of depth sufficient to prevent complete freezing inhibits or prevents the formation of permafrost. Therefore, it is necessary to consider the paleo-positions of the coastline of the Arctic Ocean. Certainly more work is needed to establish the history of subsurface temperatures on the North Slope.

An additional observation which strengthens the idea that migrating gas was involved with gas-hydrate formation, is that all of the gas hydrates occur regionally below a marine siltstone sequence (base Marker 16). This relatively impermeable rock sequence may act as a barrier to vertical gas migration, thus controlling the distribution of gas hydrate. This potential vertical gas migration barrier may explain why no gas hydrates are present in the eastern part of the Prudhoe Bay Drilling Unit. Because of the regional northeastward dip, all potential gas hydrate-bearing units in the Prudhoe Bay area (units below Marker 16) occur below the zone of gas-hydrate stability. Thus, no gas hydrates are present in the subsurface at Prudhoe Bay because of a limited supply of gas within the zone of gas hydrate stability.

Figure IV-7 shows that the regional distribution of the delineated gas hydrate occurrences are of irregular shapes and sizes. The reasons for these irregularities are not known. A comparison of the gas hydrate distribution map in figure IV-7 with the West Sak and Ugnu sands oil distribution maps in figures III-17 and III-19 reveals several similarities. These gas hydrate and oil distribution maps (Units C, D, and E) exhibit similar irregularities near the West Sak-24 well at the eastern boundary of the Kuparuk River Unit. Werner (1987) suggested that faults control the distribution of oil within the West Sak and Ugnu sands, and it is possible that an unmapped fault near West Sak-23 has affected the shallow oil reservoirs. The same fault may control the distribution of the gas hydrates in the overlying rock units. The relative effect of faults on gas-hydrate formation is not understood because of insufficient data.

Given our present understanding, the most likely explanation for the origin of the gas hydrates we infer to be present in the Kuparuk-Prudhoe area is as follows: (1) Migration of thermogenic solution- and free-gas from reservoirs of the Prudhoe Bay Oil Field upward along the Eileen and related faults into the overlying sediments, and (2) the concentration of the gas in structural/stratigraphic traps as shallow free-gas pools, with later conversion of free-gas to gas hydrate in response to climatic cooling; or conversion of migrating gas to gas hydrate upon entering the zone of gas-hydrate stability.

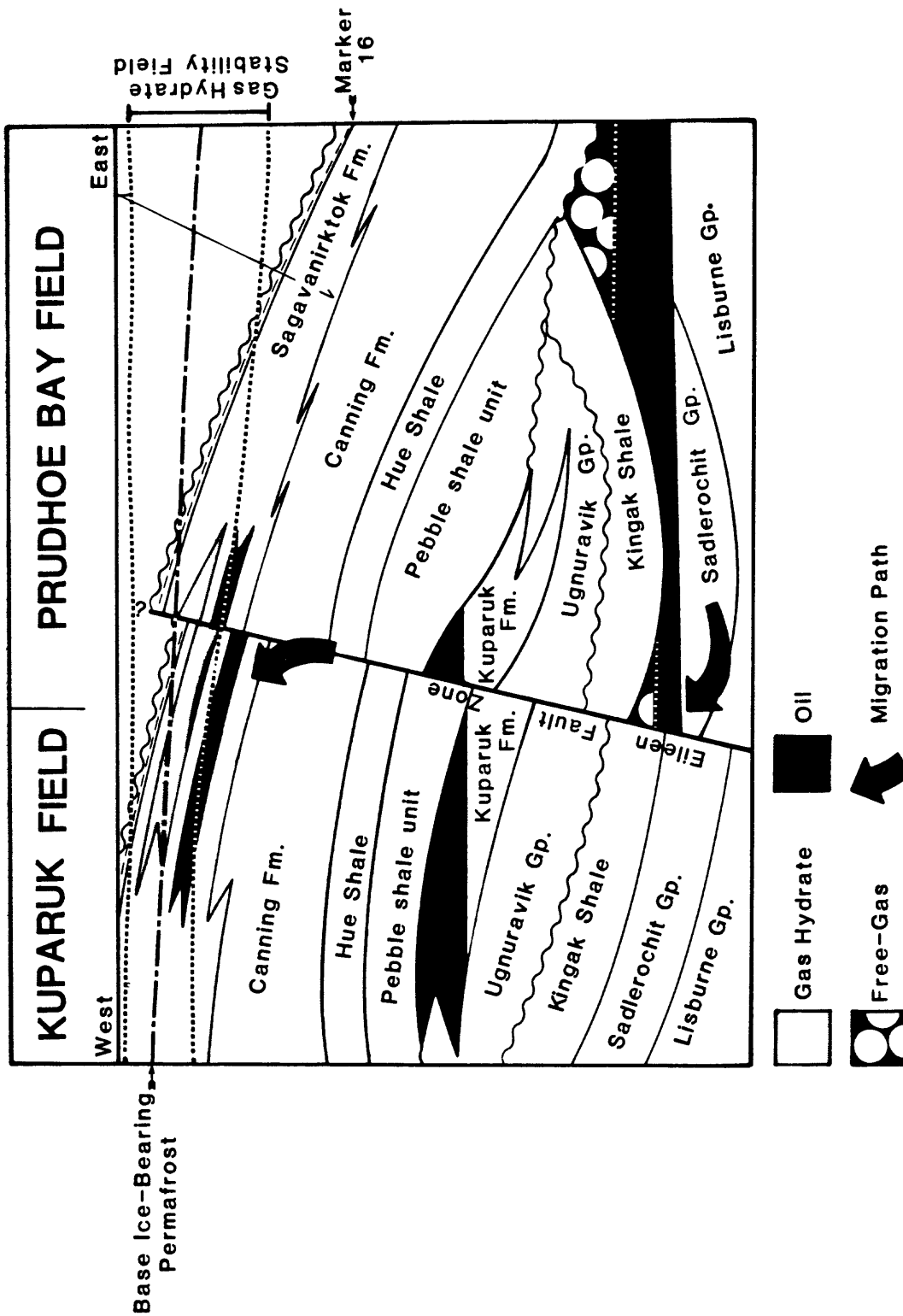


Figure V-2. Generalized west to east cross section through the Kuparuk-Prudhoe area illustrating possible gas migration roots and spatial relations between gas hydrates the Eileen Fault, oil, base of ice-bearing permafrost, gas-hydrate stability field, and geologic Marker 16. (Adapted from Carman and Hardwick, 1983, fig. 13).

CHAPTER VI. ESTIMATED RESOURCE VOLUME

Previous estimates of the gas volume that may be attributed to gas hydrates on the North Slope range from 3.1×10^{11} to $7,100.0 \times 10^{11}$ m³ [approximately 11 to 25,000 trillion ft³ (tcf) of gas], and world-wide estimates of gas hydrate resources in permafrost areas range from 140×10^{11} to $340,000 \times 10^{11}$ m³ [approximately 490 to 1,200,000 tcf of gas] (Potential Gas Agency, 1981). The broad range of these estimates demonstrates a general lack of knowledge pertaining to actual gas-hydrate occurrence and distribution; however, estimates of this magnitude are of interest especially when compared to the proved recoverable world resource of conventional natural gas of only 680×10^{11} m³ [approximately 2,400 tcf of gas] (Parent, 1984).

Most of the published estimates of gas volumes from gas hydrates have of necessity been made by broad extrapolation of only general knowledge of local geologic conditions that control the distribution and volume of in-situ gas hydrates. Gas volumes that may be attributed to gas hydrates in a permafrost setting are dependent on five reservoir properties: (1) areal extent of the gas-hydrate occurrences, (2) reservoir thickness, (3) porosity, (4) hydrate number, and (5) the degree of gas-hydrate saturation (table VI-1). In this chapter each parameter is reviewed for the North Slope, and a gas (hydrate) resource estimate is made.

AREAL EXTENT OF GAS HYDRATES

As described in Chapter IV, all identified gas hydrates on the North Slope occur in the Prudhoe Bay-Kuparuk River area, in six delineated gas-hydrate units (Units A through F; fig. IV-7). The total areal distribution of the in-situ gas-hydrate occurrences have been determined and listed in column 2 of table VI-2. The two most extensive gas-hydrate reservoirs are Units C and D, with an areal extent of approximately 120 and 130 square kilometers, respectively. The most limited occurrence is that of Unit F, which has a total areal distribution of approximately 1 square kilometer. The total mapped area of all six gas-hydrate occurrences is about 380 square kilometers, with the areal extent of the individual units ranging from 1 to 130 square kilometers.

GAS HYDRATE (RESERVOIR) THICKNESS

The thicknesses of the gas-hydrate occurrences (described in Chapter IV) in Units A through F are listed in column 3 of table VI-2. The thickest gas-hydrate occurrences are those of Units A and C, with an average thickness of 16 meters. The total thickness of the gas hydrates in Unit F (26 m) is greater than the hydrates of Units A or C, but Unit F is a composite of three separate intervals. The thinnest gas-hydrate sequence is that of Unit B, with an average thickness of 10 meters. As shown in table IV-3, the thicknesses of the individual gas-hydrate occurrences are regionally variable. More drilling and new well-log data are required to evaluate the discontinuities in the thickness of the gas hydrate occurrences. In this resource estimate, only average values of thickness are used (table VI-2).

RESERVOIR POROSITY

Porosities of potential gas-hydrate reservoirs can be calculated from a number of sources (see Chapter IV). The average porosity of each gas-hydrate reservoir (Units A through F), calculated in Chapter IV, are listed in table VI-2. As shown in figure IV-12 the calculated porosities of the gas-hydrate reservoir rocks range from 28 to 48 percent, and average approximately 39%. By using the estimates of the areal extent, average thickness, and rock-porosity of each gas-hydrate occurrence, the total porosity volume (cubic meters) within each gas-hydrate reservoir has been determined and listed in table VI-2.

*HYDRATE NUMBER (*n*)*

The hydrate number can be visualized as a factor describing how much of the clathrate-cage-structure is filled with gas. If the clathrate structure of a methane hydrate is saturated (100% gas filled), the gas hydrate would have a hydrate number of 5.8 (Lewin and Associates, Inc., 1983). However, it is believed that a 100% gas-filled clathrate is not likely to be found in nature. On the other hand, gas hydrates are not stable if the clathrate cages are less than 70% occupied by gas. For the purpose of this study, the gas-hydrate volume calculations were conducted assuming two

Table VI-1. Geologic data required to conduct a gas hydrate resource estimate and a list of potential data sources.

Variables	Data Sources
Areal Extent of Reservoir	Well logs, drill-cuttings, cores, seismic survey
Reservoir Thickness	Well logs, drill-cuttings, cores, seismic survey
Porosity ϕ	Well logs, drill-cuttings, cores, borehole gravity
Hydrate Number (n)	Theoretical calculations, laboratory measurements
Gas Hydrate Saturation	Well logs, cores, theoretical calculations

Table VI-2. Reservoir data from gas-hydrate-bearing Units A, B, C, D, E, and F in the Prudhoe Bay--Kuparuk River area, North Slope, Alaska.

(1) Hydrate Bearing Unit	(2) Average Area (km ²)	(3) Average Thickness (m)	(4) Average Porosity (%)	(5) Total m ³ of Porosity ×10 ⁶	(6) Average Gas Hydrate Saturation (%)
A	80	16	39	499.2	85
B	20	10	38	76.0	86
C	120	16	38	729.6	84
D	130	12	39	608.4	85
E	30	11	40	132.0	85
F	1	(26)	41	10.7	85
	≈ Total 380	Total ≈ 91	Average ≈ 39	Total ≈ 2055.9	Average ≈ 85

- (1) Unit index letter (fig. IV-7).
- (2) Total areal distribution of gas hydrate.
- (3) Average thickness of gas hydrate units.
- (4) Average porosity of gas hydrate units (see table IV-5).
- (5) Total volume of porosity in the mapped gas hydrate occurrences.
- (6) Average value of gas hydrate saturation (see table IV-6).

conditions; the clathrate is 90% filled (hydrate number=6.325) or the clathrate is 70% filled (hydrate number=7.475) (Lewin and Associates, Inc., 1983). This range in the hydrate number will fully represent the likely minimum and maximum values that occur in nature.

The volume of free-methane (scf) present in one cubic foot of methane hydrate may be calculated from the following equation (Lewin and Associates, Inc., 1983; published in non-metric units).

$$\frac{\text{gas(scf)}}{\text{ft}^3 \text{ hydrate}} = \frac{379}{n} \times \frac{\text{water density (lb/ft}^3\text{)}}{\text{water mole-weight (lb)}} \times \frac{1 \text{ (ft}^3\text{ water)}}{E \text{ (ft}^3\text{ hydrate)}}$$

In this equation at standard temperature and pressure conditions (STP) of 60°F and 14.7 psia (15.6°C and 101.4 kPa) it is assumed that one pound-mole of methane (i.e. 16 lbs of CH₄) is equivalent to 379 cubic feet (10.7 cubic meters) of free methane gas, and the water density is 62.4 lb/ft³ (1000 kg/m³) at a water mole-weight of 18 lb. E represents the gas-hydrate expansion factor which is 1.28 for a Structure I gas hydrate (Lewin and Associates, Inc., 1983), and n is the hydrate number. A cubic foot (0.028 m³) of methane hydrate with a hydrate number (n) of 6.325 (90% gas filled structure) would yield 162.3 cubic feet (4.6 cubic meters) of methane gas (at STP). One cubic foot (0.028 m³) of methane hydrate with a hydrate number (n) of 7.475 (70% gas filled structure) would yield 137.3 cubic feet (3.9 cubic meters) of methane gas. To maintain consistency the yield factors have been converted to metric units. One cubic meter of methane hydrate with a hydrate number (n) of 6.325 yields 164 cubic meters of methane (at STP). One cubic meter of methane hydrate with a hydrate number (n) 7.475 yields 139 cubic meters of methane (at STP). These gas hydrate yield factors are used in the following sections to determine the total volume of gas that may be contained within the in-situ gas hydrates.

GAS-HYDRATE SATURATION

The last variable required for a resource estimate is gas-hydrate saturation. In Chapter IV it was shown that well-log calculations of gas-hydrate saturations are similar to calculating common hydrocarbon saturations. The average degree of gas-hydrate saturation within each delineated reservoir (Units A through F), calculated in Chapter IV, are listed in table VI-2. As shown in table IV-6, and figures IV-13 through IV-16 gas-hydrate saturation ranges from 70 to 97 percent, and averages approximately 85%.

CALCULATIONS SUMMARY

For each inferred gas-hydrate bearing unit, we have calculated the areal extent (column 2, table VI-2), average stratigraphic thickness (column 3, table VI-2), average porosity (column 4, table VI-2), total volume of porosity within the delineated occurrences (column 5, table VI-2), and the average degree of gas hydrate saturation. In table VI-3, the theoretical minimum (n=6.325) and maximum (n=7.475) hydrate numbers have been used to estimate the volume of gas that may be attributed to the identified gas hydrates. These calculations suggest that the potential volume of gas within the identified gas hydrates of the North Slope is approximately 2.4 x 10¹¹ to 2.9 x 10¹¹ m³ (STP) [approximately 8 to 10 tcf of gas].

Our gas-hydrate resource estimate compares favorably with the low end of the range of values previously reported for the onshore North Slope (3.1 x 10¹¹ to 7,100.0 x 10¹¹ m³) by the Potential Gas Agency (1981). The volume of gas estimated to be present as gas hydrates is about one-third the amount of recoverable conventional natural gas (estimated at approximately 8.0 x 10¹¹ m³ [29 tcf]) in the Prudhoe Bay field, which is the single largest gas deposit in North America as estimated by the Alaska Oil and Gas Conservation Commission (1984).

Our resource estimate of 2.4 x 10¹¹ to 2.9 x 10¹¹ m³ must be considered to be relatively conservative because most of the North Slope is sparsely drilled. Outside of the Prudhoe Bay and Kuparuk River development units, drilling density is less than one well for every 500 km². Our

Table VI-3. Volume of gas (m^3) attributed to the gas hydrates of Units A, B, C, D, E, and F in the Prudhoe Bay--Kuparuk River area, North Slope, Alaska.

Hydrate Bearing Unit	Total m^3 of Porosity ($\times 10^6$) table VI-2	Average Gas Hydrate Saturation (%) table VI-2	Volume of Gas if $n=7.475$ ($\times 10^9 m^3$)	Volume of Gas if $n=6.325$ ($\times 10^9 m^3$)
A	499.2	85	59.0	69.6
B	76.0	86	9.1	10.7
C	729.6	84	85.2	100.5
D	608.4	85	71.9	84.8
E	132.0	85	15.6	18.4
F	10.7	85	1.3	1.5
Total ≈ 2055.9		Average ≈ 85	Total 242.1	Total 285.5

[Conversion Factor $1m^3 = 35.3 ft^3$]

resource evaluation considers the well-log delineated gas-hydrate occurrences which cover an area of only approximately 200 km². Regional geologic information and seismic data suggest that large areas of the North Slope are underlain by relatively good reservoir rocks within the zone of gas-hydrate stability. Because of the low well density of this region, our resource estimate should be considered a minimum value.

CHAPTER VII. RECOMMENDED CORE-SITES

One of the primary objectives of this project was to identify a site at which drilling and coring would have a high probability of recovering a gas-hydrate sample. To increase the likelihood of encountering gas hydrates, we established and evaluated five criteria in the site selection process. These criteria are: (1) Proximity to known gas hydrate occurrences along the eastern boundary of the Kuparuk River Oil Field; (2) availability and quality of geologic data indicating the presence of gas hydrates; (3) number and thickness of gas-hydrate occurrences that may be encountered; (4) existence of special geologic problems; (5) location of the site relative to roads, production facilities (pads), and existing wells. Coring operations could be undertaken in one of two ways: (1) In a "piggyback" operation in an industry oil-field production well, or (2) in a dedicated well drilled specifically to study gas hydrates. Each option has its advantages and disadvantages which will be discussed at the end of this chapter.

VII.A. COOPERATIVE INDUSTRY-GOVERNMENT CORE-HOLE

Industry production drilling is planned for the area of the most probable gas-hydrate occurrences in both the Prudhoe Bay and Kuparuk River oil fields. Most wells on the North Slope are directionally drilled, and economic concerns make it necessary to drill a number of wells from each raised-gravel production pad. Shown on the map in figure VII-1 are the production pads, present and proposed, in the Kuparuk River Oil Field and the distribution of the inferred gas hydrate occurrences. Production-drilling is planned for eight of the pads within the area of presumed gas hydrate occurrences. With industry cooperation it would be possible to conduct coring operations within the suspected gas-hydrate bearing units at these eight locations. Because numerous wells are drilled from the same pad, the cored well could be "previewed" with well-log data obtained from one of the earliest drilled wells on the same pad.

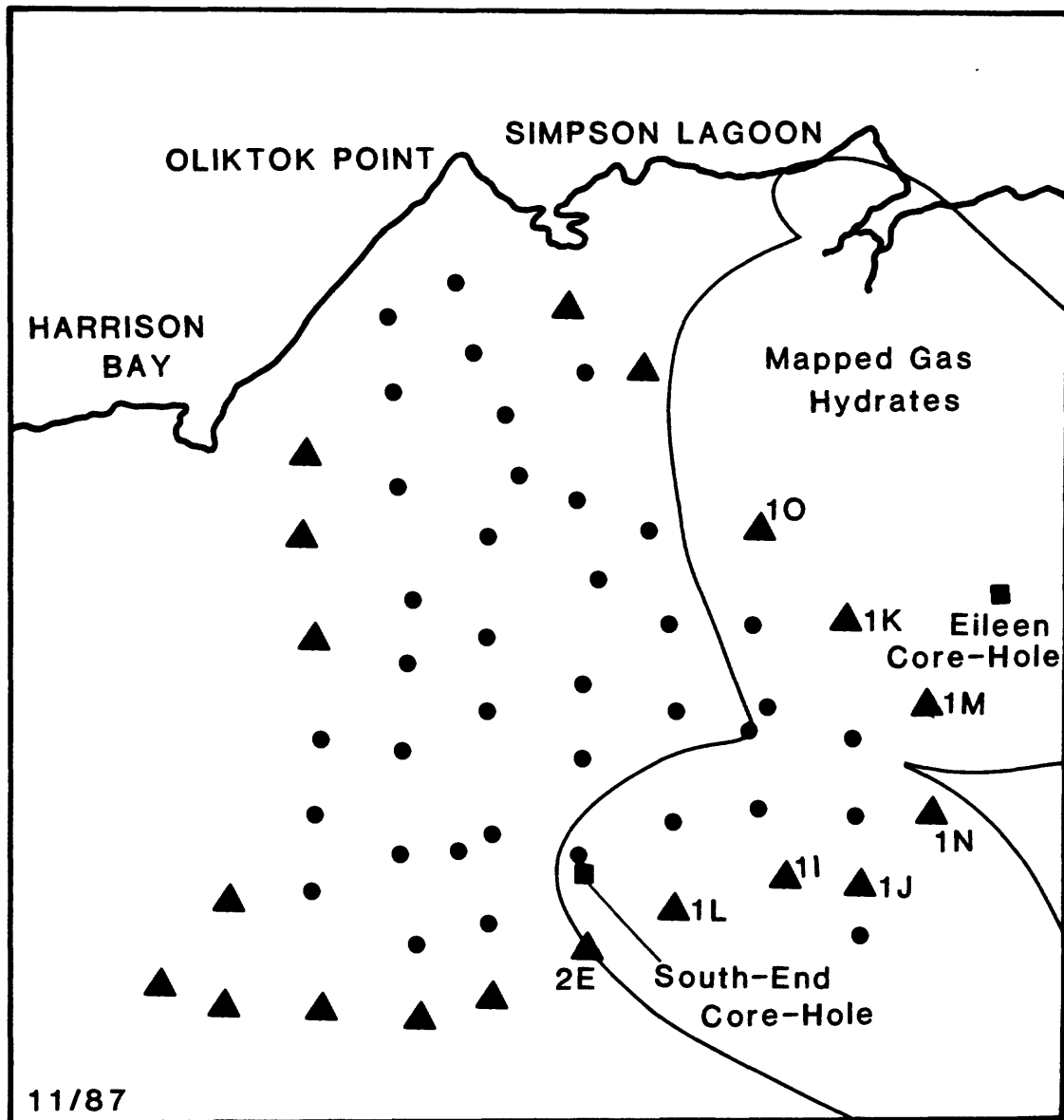
A review of regional geologic data and an appreciation of the proposed locations of the Kuparuk production wells suggests that the most likely place to recover a gas hydrate in a cooperative core-site would be at the Kuparuk 1K production pad (fig. VII-1). At this site a minimum of four gas-hydrate bearing stratigraphic units may be encountered (fig. IV-7; Units A, C, D and E). To examine the relation between gas hydrate and the origin of its contained gas, coring operations at the Kuparuk 1M production pad, near the Eileen fault zone, could produce a wealth of relevant geologic and geochemical data. At present little is known about the possible distribution of the gas hydrates at the site of the Kuparuk 1M pad (Chapter IV).

VII.B. DEDICATED CORE-HOLE

EILEEN CORE-HOLE

We have identified two "dedicated" core-hole sites, the Eileen and the South-End core-holes, each with different targeted gas-hydrate-bearing units. In table VII-1 we list the depth information from nearby wells that is relevant to exploring for gas hydrates in the two proposed core-holes. Listed data include depth to the top and bottom of the methane-hydrate stability field, depth to the base of ice-bearing permafrost, and the depth interval of the targeted gas-hydrate occurrences. Non-standard units (English) are used in this chapter, because most well logs and drillers reports are recorded in non-metric units. The depths of the inferred gas-hydrate occurrences (table VII-1, core targets) are taken directly from the well logs and are measured from the kelly bushing on the drilling rig.

The Northwest Eileen State-2 and SOCAL 33-29E wells, located about 4,000 ft apart, have been used to describe the Eileen core-hole (table VII-1, figures VII-2 and VII-3). On the map (figure VII-2) the location of these wells plus Northwest Eileen State-1 have been plotted along with the location of the proposed Eileen Core-Hole. This site was selected primarily because of the wealth of information available from the nearby Northwest Eileen State-2 well, the site of the only confirmed natural gas hydrate on the North Slope. Our site is selected to be as close as practical to this now abandoned well. Well-log data suggest that at least three stratigraphic units may contain gas hydrate at this site. The main production facilities in the Kuparuk Oil Field are about 13 miles from the site



- ▲ Site of future production pads
- Location of existing production pads
- Site of proposed core-holes

Figure VII-1. Map of existing and proposed production pads and inferred gas-hydrate occurrences in the Kuparuk River oil field (written communication, ARCO Alaska Inc., Anchorage, Alaska).

Eileen Core-Hole

		SOCAL 33-29E	Northwest Eileen State-2	Eileen Core-Hole
(1)	Elev. K.B. (ft)	65	63.43	-64
(2)	Depth to HT (ft)	754	755	756
(3)	Depth BIBPF (ft)	1788	1785	1781
(4)	Depth to HB (ft)	3198	3195	3191
(5)	Depth Unit E (ft)	1740-1805	1873-1930	1869-1926
(6)	Depth Unit D (ft)	1862-1897	2005-2027	2001-2023
(7)	Depth Unit C (ft)	2020-2140	2162-2257	2158-2253

South-End Core-Hole

		West Sak-3	KRU 2D-15	South-End Core-Hole
(1)	Elev. K.B. (ft)	118	126.6	-127
(2)	Depth to HT (ft)	829	824	824
(3)	Depth BIBPF (ft)	1522	1525	1525
(4)	Depth to HB (ft)	2437	2440	2440
(5)	Depth Unit A	1162-1252	1224-1310	1218-1304

- (1) Elevation of kelly bushing above mean-sea-level (ft).
- (2) Depth to the top of the methane-hydrate stability field (ft).
- (3) Depth to the base of ice-bearing permafrost (ft).
- (4) Depth to the base of the methane-hydrate stability field (ft).
- (5,6,7) Depth of gas-hydrate-bearing units (fig IV-7) (ft).

Table VII-1. List of depth information from wells located near the proposed Eileen and South-End core-holes.

EILEEN CORE-HOLE

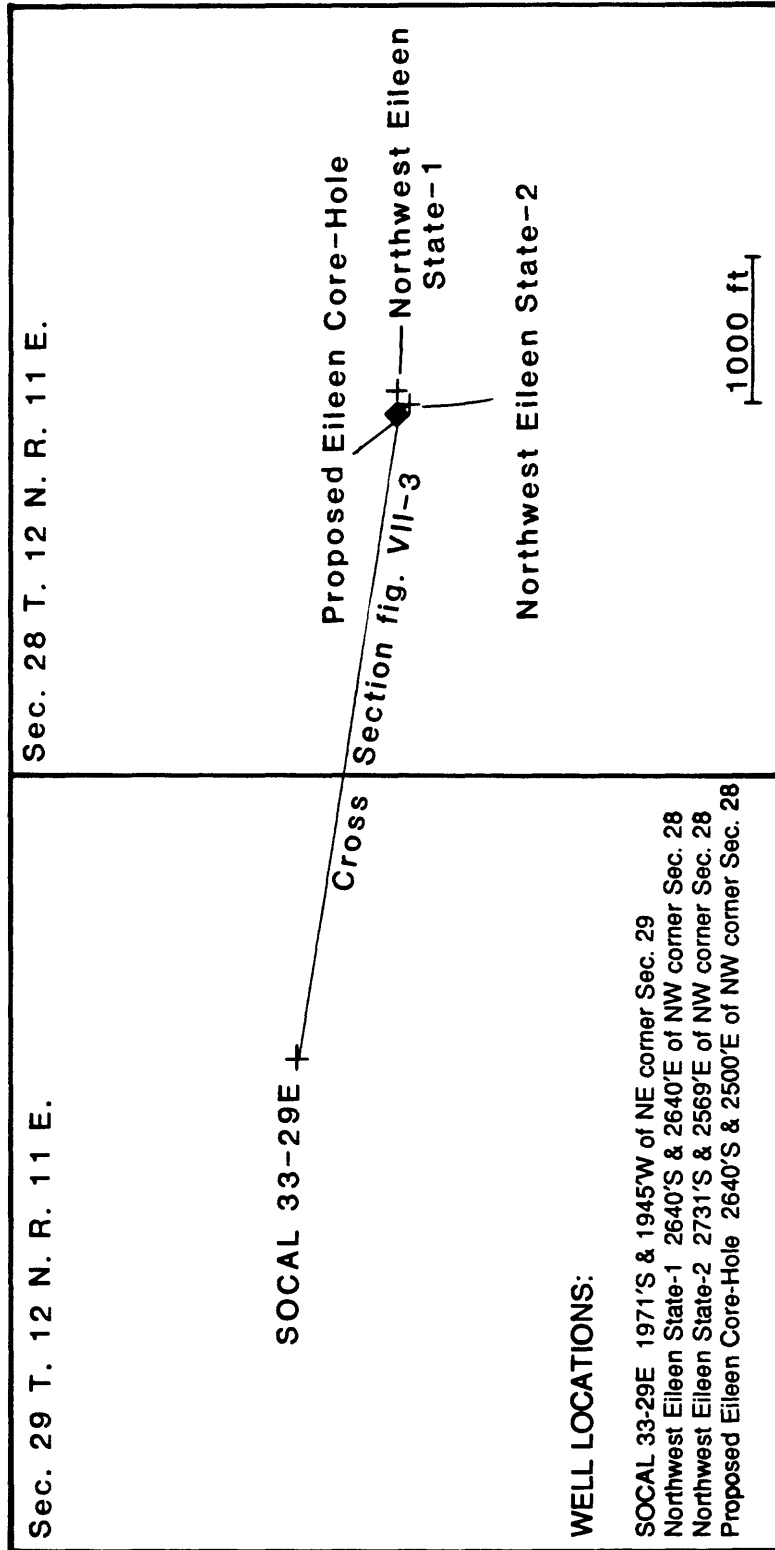


Figure VII-2. Map showing the location of the proposed site of the Eileen core-hole relative to the locations of the Northwest Eileen State-1, Northwest Eileen State-2, and SOCAL 33-29E wells.

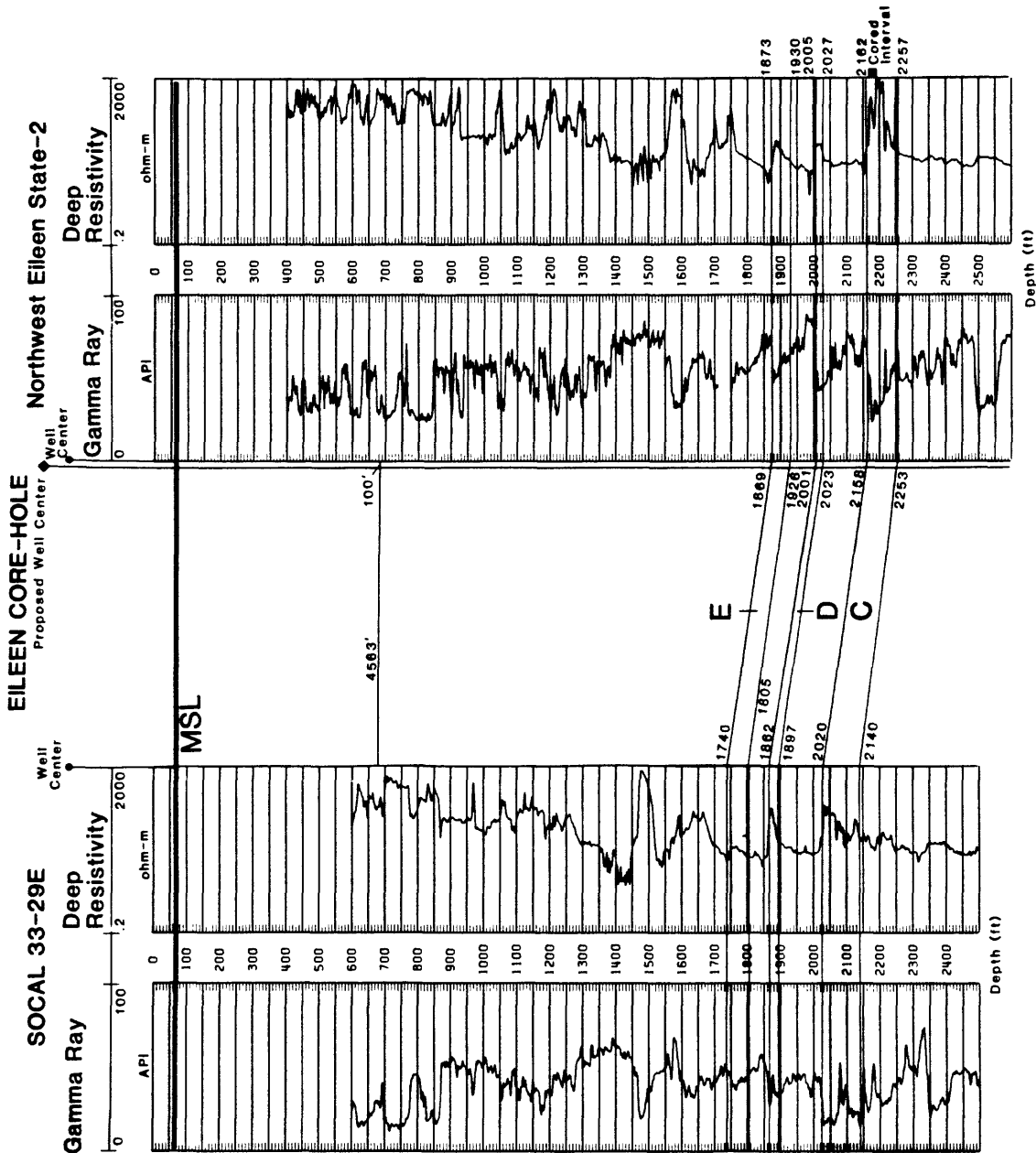


Figure VII-3. Well log cross section through the proposed Eileen Core-Hole, showing the depth and lateral relation of the inferred gas-hydrate occurrences in Units C, D, and E (core-targets).

of the proposed well, and the nearest road access is 2 miles.

It is known that drilling can affect the thermal stability of gas hydrates some distance into the rock formation from the well-bore. The depth of this thermal disturbance cannot be precisely determined. There is no evidence that the gas hydrates recovered in the Northwest Eileen State-2 well were affected by the previous drilling of the Northwest Eileen State-1 well, located approximately 100 ft to the northeast (fig. VII-3). Therefore, we have selected the minimum well spacing for a gas hydrate core-hole to be 100 ft. The thermal effect of pre-existing wells should be further modeled in the final core-hole site selection process.

In the proposed Eileen Core-Hole (table VII-1, figures VII-2 and VII-3) a minimum of three gas-hydrate occurrences should be encountered (fig. IV-7; Units C, D, and E). From the elevation of the assumed kelly bushing (64 ft), the top of the first gas-hydrate occurrence (Unit E) will be at a depth of 1,869 ft and should be approximately 57 ft thick. The second gas hydrate deposit (Unit D) will be at a depth from 2,001 to 2,023 ft, and the deepest occurrence (Unit C) should be from 2,158 to 2,253 ft.

SOUTH-END CORE-HOLE

West Sak-3 and Kuparuk River Unit 2D-15 wells, located about 4,000 ft apart, have been used to describe the South-End Core-Hole (table VII-1, figures VII-4 and VII-5). On the map (figure VII-4) the location of two existing wells have been plotted along with the location of the proposed South-End Core-Hole. This site was selected to study the interrelation between the gas hydrate and oil in Unit A (Chapter IV). The proposed South-End Core-Hole is on the Kuparuk River 2D production pad, about 220 ft from the existing 2D-15 well (figures VII-4 and VII-5); which is approximately 6 miles from the main production facilities in the Kuparuk River oil field; the site is accessible by road.

In the proposed South-End Core-Hole (table VII-1, figures VII-4 and VII-5) only one occurrence of gas hydrate is likely to be encountered (Unit A). From the elevation of the assumed kelly bushing (127 ft), the top of the targeted unit (Unit A) should be at 1,162 ft and extend to a depth of 1,224 ft (62 ft thick).

In summary, the most likely place on the North Slope to successfully recover a gas hydrate is at the site of the proposed Eileen Core-Hole. To examine the relation between gas hydrate and oil the proposed South-End Core-Hole should yield a wealth of relevant information. To increase the likelihood of recovering a gas-hydrate sample, new regional and local geologic data could be obtained to examine more thoroughly the proposed core-holes. For example, borehole gravity and temperature surveys could be used to study the lateral continuity and the thermal stability of the natural gas hydrates. To further study the location of the proposed core-holes, a borehole seismic survey, run in a nearby well, would give additional insight into the lateral continuity of the gas hydrates.

Both the cooperative and the dedicated core-hole options have positive and negative features. One major disadvantage of working with industry is the possible time restriction: gas hydrate coring operations and subsequent formation testing may require more time than the company is willing to spend in delaying their own production drilling. A dedicated gas-hydrate research well, with proper funding, would not have these time restrictions, and it may be possible to conduct continuous coring throughout the entire zone of gas-hydrate stability. However, a cooperative effort could significantly reduce the costs in comparison with the expense of a dedicated research well.

SOUTH-END CORE-HOLE

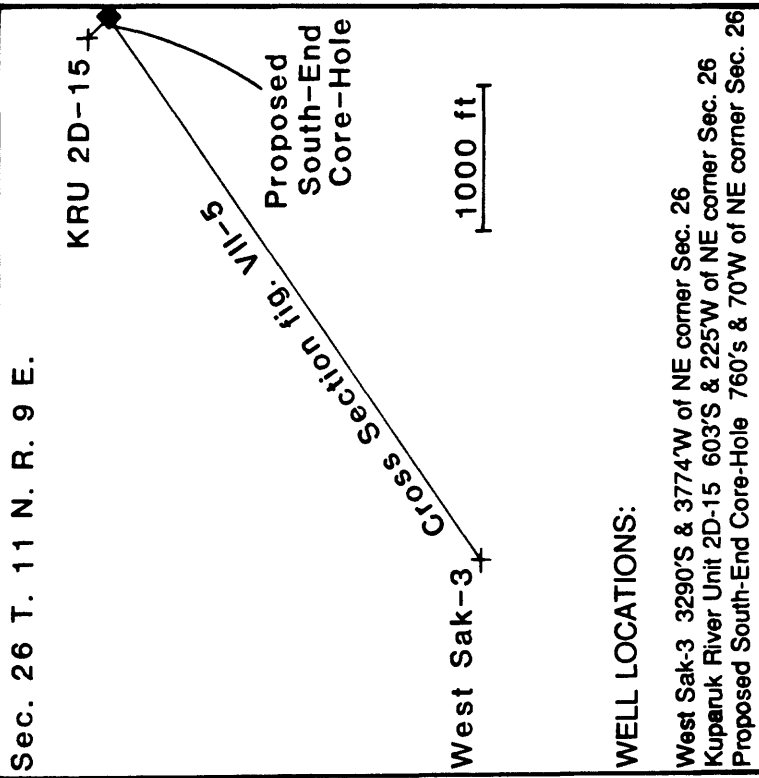


Figure VII-4. Map showing the location of the proposed site of the South-End core-hole relative to the locations of the Kupaaruk River Unit 2D-15 and West Sak-3 wells.

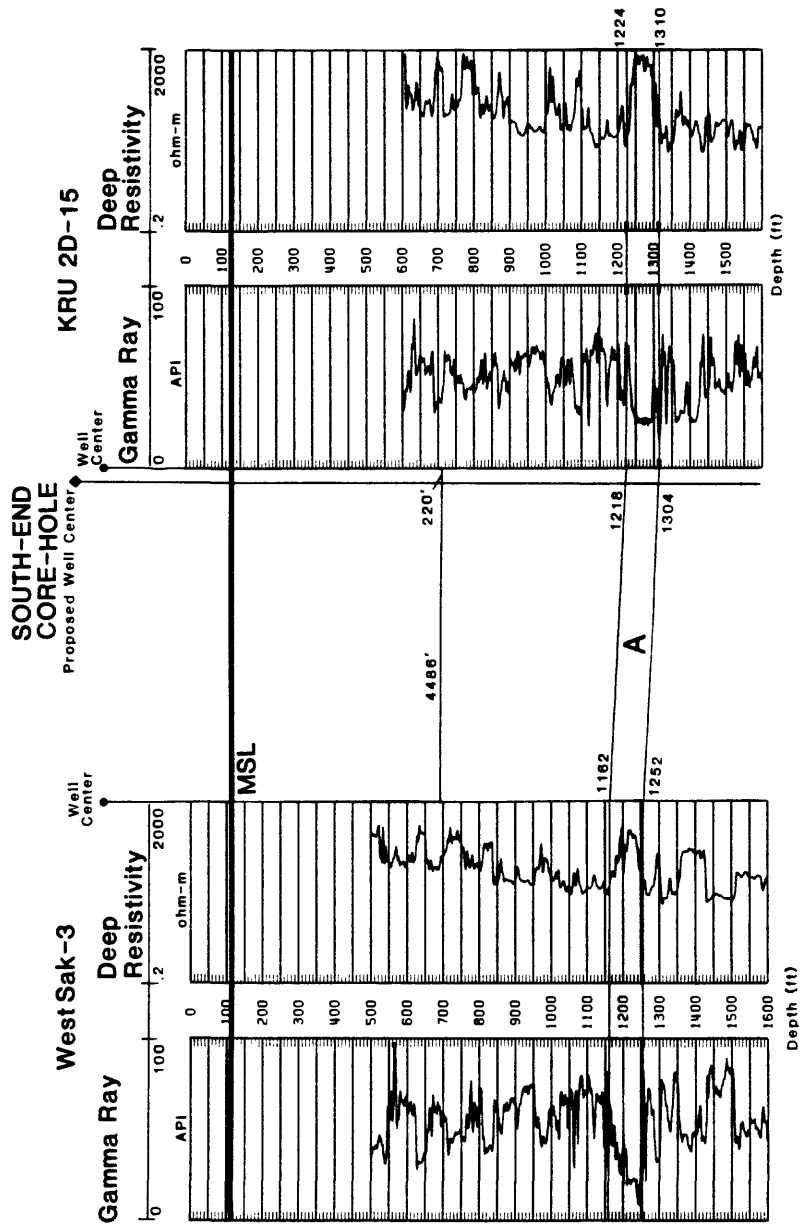


Figure VII-5. Well log cross section through the proposed South-End Core-Hole, showing the depth and lateral relation of the inferred gas-hydrates in Unit A (core-target).

REFERENCES CITED

- Ahlbrandt, T.S., 1979, Preliminary geologic, petrologic, and paleontologic results of the study of Nanushuk Group rocks, North Slope, Alaska: U.S. Geological Survey Circular 794.
- Alaska Geological Society, 1972, Northwest to southeast stratigraphic correlation section, Prudhoe Bay to Ignek Valley, Arctic North Slope Alaska: Alaska Geological Society, Anchorage, Alaska, 1 plate.
- _____, 1977, North Slope stratigraphic correlation section, Beaufort Sea-Prudhoe Bay-Nora No. 1, Arctic Slope, Alaska: Alaska Geological Society, Anchorage, Alaska, 1 plate.
- _____, 1979, West to east stratigraphic correlation section, Point Barrow to Ignek Valley, Arctic North Slope, Alaska: Alaska Geological Society, Anchorage, Alaska, 1 plate.
- Alaska Oil and Gas Conservation Commission, 1984, Statistical Report: Anchorage, Alaska, 185p.
- Anderson, D.M., Tice, A.R., and McKim, H.L., 1973, The unfrozen water and the specific heat capacity of frozen soils, in *Proceedings of the Second International Conference on Permafrost*, Yakutsk, U.S.S.R.: National Academy of Sciences, Washington, D.C., p. 257-288.
- Armstrong, A.K., and Mamet, B.L., 1975, Carboniferous biostratigraphy, northeastern Brooks Range, Arctic Alaska: U.S. Geological Survey Professional Paper 884.
- Bily, C., and Dick, J.W.L., 1974, Naturally occurring gas hydrates in the Mackenzie Delta, N.W.T.: *Bulletin of Canadian Petroleum Geology*, v. 22, no. 3, p. 340-352.
- Bird, K.J., 1978, New information on Lisburne Group (Carboniferous and Permian) in Naval Petroleum Reserve, Alaska: *American Association of Petroleum Geologists Bulletin*, v. 62, p. 880.
- Bird, K.J., 1986, The framework geology of the North Slope of Alaska as related to oil-source rock correlations, in Magoon, L.B., and Claypool, G.E., eds., *Alaska North Slope oil/rock correlation study*: American Association of Petroleum Geologists Studies in Geology no. 20, p. 3-29.
- Bird, K.J., Connor, C.L., Tailleur, I.L., Silberman, M.L., and Christie, J.L., 1978, Granite on the Barrow arch, northeast NPRA, in Johnson, K.M., ed., *the United States Geological Survey in Alaska--accomplishments during 1977*: U.S. Geological Survey Circular 772-B, p. B24-B25.
- Bird, K.J., and Jordon, C.F., 1977, Lisburne Group (Mississippian and Pennsylvanian)—potential major hydrocarbon objective of Arctic Alaska: *American Association of Petroleum Geologists Bulletin*, v. 61, no. 9, p. 1493-1512.
- Bird, K.J., and Magoon, L.B., 1987, Petroleum geology of the northern part of the Arctic National Wildlife Refuge, Northeastern Alaska: U.S. Geological Survey Bulletin 1778, 324p.
- Brewer, M.C., 1958, Some results of geothermal investigations of permafrost in northern Alaska: *Transactions of the American Geophysical Union*, v. 39, no. 1, p. 19-26.
- Brosge, W.P., and Tailleur, I.L., 1971, Northern Alaska petroleum province; future petroleum provinces of the United States—their geology and potential: *American Association of Petroleum Geologists Memoir 15*, p. 68-99.
- Brown, R.J.E., and Kupsch, W.O., 1974, Permafrost terminology: Canada, National Research Council, Associate Committee on Geotechnical Research, Technical Memorandum 111, 62p.
- Butler, B.D., Pilger, R.H., Jr., and Nunn, J.A., 1985, Tectonic model of the central Brooks Range, Alaska: *Geological Society of America Abstracts with Program*, v. 17, no. 7, p. 536.
- Carman, G.J., and Hardwick, P., 1983, Geology and regional setting of Kuparuk Oil Field, Alaska: *American Association of Petroleum Geologists Bulletin*, v. 67, no. 6, p. 1014-1031.
- Carter, R.D., Mull, C.G., Bird, K.J., and Powers, R.B., 1977, The petroleum geology and hydrocarbon potential of Naval Petroleum Reserve No. 4, North Slope, Alaska: U.S. Geological Survey Open-File Report 77-475, 61p.
- Carter, R.D., and Laufeld, S., 1975, Ordovician and Silurian fossils in well cores from North Slope of Alaska: *American Association of Petroleum Geologists Bulletin*, v. 59, no. 3, p. 457-462.
- Collett, T.S., 1983a, Detection and evaluation of natural gas hydrates from well logs, Prudhoe Bay, Alaska: Masters Thesis, University of Alaska, Fairbanks, Alaska, 77p.
- _____, 1983b, Detection and evaluation of natural gas hydrates from well logs, Prudhoe Bay, Alaska; in *Proceedings of the Fourth International Conference on Permafrost*, Fairbanks, Alaska: National Academy of Sciences, Washington D.C., p. 169-174.
- Collett, T.S., Bird, K.J., Kvenvolden, K.A., and Magoon, L.B., [in press-a], Map of the depth to the base of the deepest ice-bearing permafrost as determined from well logs, North Slope, Alaska:

REFERENCES CITED

- U.S. Geological Survey Oil and Gas Investigations Map, 1 plate.
- Collett, T.S., Bird, K.J., Kvenvolden, K.A., and Magoon, L.B., [in press-b], Subsurface temperatures and geothermal gradients on the North Slope of Alaska; *Journal of Petroleum Technology*, 28 p., 12 fig.
- Collett, T.S., Godbole, S.P., and Economides, C.E., 1984, Quantification of in-situ gas hydrates with well logs: Proceedings of the 35th Annual Technical Meeting of the Petroleum Society of CIM, Calgary, Canada, June 10-13, p. 571-582.
- Collett, T.S., and Kvenvolden, K.A., 1987, Evidence of naturally occurring gas hydrates on the North Slope of Alaska: U.S. Geological Survey Open-File Report 87-255, 8p.
- Desai, K.P., and Moore, E.J., 1968, Well log interpretation in permafrost: *The Log Analyst*, v. 10, no. 1, p. 13-25.
- Detterman, R., Reiser, H.N., Brosge, W.P., and Dutro, J.T., Jr., 1975, Post-Carboniferous stratigraphy, northeastern Alaska: U.S. Geological Survey Professional Paper 886, 46p.
- Downey, M.W., 1984, Evaluating seals for hydrocarbon accumulations: *American Association of Petroleum Geologists Bulletin*, v. 68, no. 11, p. 1752-1763.
- Edwardson, M.J., Girner, H.M., Parkison, H.R., Williams, C.D., and Matthews, C.S., 1962, Calculation of formation temperature disturbances caused by mud circulation: *Journal of Petroleum Technology*, April, p. 416-426.
- Ellersieck, Inyo, Mayfield, C.F., Tailleux, I.L., and Curtis, S.M., 1979, Thrust sequence in the Misheguk Mountain Quadrangle, Brooks Range, Alaska, in Johnson, K.M., and Williams, J.R., eds., *The United States Geological Survey in Alaska--accomplishments during 1978: U.S. Geological Survey Circular 804-B*, p. B8-B9.
- Evrenos, A.I., Heathman, J., and Ralstin, J., 1971, Impermeation of porous media by forming hydrates in-situ; *Journal of Petroleum Technology*, v. 23, p. 1059-1066.
- Ferrians, O.J., Jr., 1965, Permafrost map of Alaska: U.S. Geological Survey Miscellaneous Geologic Investigations Map I-445, scale 1:2,500,000.
- Ferrians, O.J., Jr., Kachadoorian, Reuben, and Greene, G.W., 1969, Permafrost and related engineering problems in Alaska: U.S. Geological Survey Professional Paper 678, 37 p.
- Galate, J.W., and Goodman, M.A., 1982, Review and evaluation of evidence of in-situ gas hydrates in the National Petroleum Reserve in Alaska: U.S. Geological Survey unpublished report, Contract No. 14-08-000119148, 102p.
- Gold, L.W., and Lachenbruch, A.H., 1973, Thermal conditions in permafrost—a review of North American Literature, in Proceedings of the Second International Conference on Permafrost, Yakutsk, U.S.S.R.: National Academy of Sciences, Washington, D.C., p. 169-175.
- Gondouin, M., Tixier, M.P., and Simard, G.L., 1957, An experimental study on the influence of the chemical composition of electrolytes on the SP curve: *Petroleum Transactions, American Institute of Mineralogists, Metallurgists, and Engineers*, v. 210, p. 58-72.
- Grantz, Arthur, Eittreim, S., and Dinter, D.A., 1979, Geology and tectonic development of the continental margin north of Alaska: *Tectonophysics*, v. 59, p. 263-291.
- Grantz, Arthur, Holmes, M.L., and Kososki, B.A., 1975, Geologic framework of the Alaskan continental terrace in the Chukchi and Beaufort Seas in Canada's continental margins and offshore petroleum exploration, eds., Yorath, Parker, and Glass: *Canadian Society of Petroleum Geologists Memoir 4*, p. 669-700.
- Grantz, Arthur, Mann, D.M., and May, S.D., 1982, Tracklines of multichannel seismic-reflection data collected by the U.S. Geological Survey in the Beaufort Sea in 1977 for which profiles and stack tapes are available: U.S. Geological Survey Open-File Report 82-735, 1 map sheet with text.
- Grantz, Arthur, and May, S.D., 1983, Rifting history and structural development of the continental margin north of Alaska, in Watkins, J.S., and Drake, C., eds., *Studies in continental margin geology: American Association of Petroleum Geologists Memoir 34*, p. 77-100.
- Grantz, Arthur, and Mull, C.G., 1978, Preliminary analysis of the petroleum potential of the Arctic National Wildlife Range, Alaska: U.S. Geological Survey Open-File Report 78-489, 21p.
- Hammerschmidt, E.D., 1934, Formation of gas hydrates in natural gas transmission lines: *Industrial and Engineering Chemistry*, v. 26, p. 851-855.
- Hilchie, D.W., 1982, Applied openhole log interpretation: D.W. Hilchie Inc., Golden Colorado, 205p.
- Hnatiuk, J., and Randall, A.G., 1977, Determination of permafrost thickness in wells in northern

- Canada: *Canadian Journal of Earth Science*, v. 14, p. 375-383.
- Holder, G.D., Malone, R.D., and Lawson, W.F., 1985, The effects of gas composition and geothermal properties on the thickness and depth of natural gas hydrate zones, *in* Proceedings of the 55th annual California regional meeting of the Society of Petroleum Engineers: Bakersfield, California, March 27-29, p. 51-58.
- Howitt, Frank, 1971, Permafrost geology at Prudhoe Bay, Alaska: *World Petroleum*, v. 42, no. 8, p. 28-38.
- Hoyer, W.A., Simmons, S.O., Span, M.M. and Watson, A.T., 1975, Evaluation of permafrost with logs, *in* Proceedings of the 16th Annual Society of Petroleum Well Log Analyst Logging Symposium, June 4-7, Dallas, Texas: Transactions Society of Petroleum Well Log Analyst, p. 13-25.
- Hunt, J.M., 1979, *Petroleum geology and geochemistry*: W.H. Freeman and Company, San Francisco, California, 617p.
- Jamison, H.C., Brockett, L.D., and McIntosh, R.A., 1980, Prudhoe Bay—a 10 year perspective, *in* Halbouty, M.T., ed., *Giant Oil and Gas Fields of the Decade 1968-1978*: American Association of Petroleum Geologists Memoir 30, p. 289-314.
- Jones, H.P., and Speers, R.G., 1976, Permo-Triassic reservoirs of Prudhoe Bay Field, North Slope, Alaska, *in* Braunstein, J., ed., *North American Oil and Gas Fields*: American Association of Petroleum Geologists Memoir 24, p. 23-50.
- Katz, D.L., 1971, Depths to which frozen gas fields (gas hydrates) may be expected: *Journal of Petroleum Technology*, v. 23, p. 419-423.
- Kososki, B.A., Reiser, H.N., Cavit, C.D., and Detterman, R.I., 1978, A gravity study of the northern part of the Arctic National Wildlife Range, Alaska: *U.S. Geological Survey Bulletin* 1440, 21p.
- Kvenvolden, K.A., and McMenamin, M.A., 1980, Hydrates of natural gas—a review of their geologic occurrence: *U.S. Geological Survey Circular* 825, 11p.
- Lachenbruch, A.H., 1957, Thermal effects of ocean on permafrost: *Geological Society of America Bulletin*, v. 68, no. 11, p. 1515-1529.
- Lachenbruch, A.H., and Brewer, M.C., 1959, Dissipation of the temperature effect of drilling a well in Arctic Alaska: *U.S. Geological Survey Bulletin* 1083-C, p. 71-109.
- Lachenbruch, A.H., Greene, G.W., and Marshall, B.V., 1966, Permafrost and the geothermal regimes, environment of the Cape Thompson region, Alaska: USAEC, Division of Technical Information, Washington, D.C., Chapter 10, p. 149-165.
- Lachenbruch, A.H., and Marshall, B.V., 1969, Heat flow in the Arctic: *Arctic*, v. 22, p. 300-311.
- Lachenbruch, A.H., Sass, J.H., Lawver, L.A., Brewer, M.C., Marshall, B.V., Munroe, R.J., Kennelly, J.P., Jr., Galanis, S.P., Jr., and Moses, T.H., Jr., 1987, Temperature and depth of permafrost on the Alaskan Arctic Slope, *in* Tailleir, I.L., and Weimer, Paul, eds., *Alaskan North Slope geology*: Bakersfield, California, Pacific Section, Society of Economic Paleontologists and Mineralogists and the Alaska Geological Society, Book 50, v. 2, p. 545-558.
- Lachenbruch, A.H., Sass, J.H., Marshall, B.V., and Moses, T.H., 1982, Permafrost heat flow, and the geothermal regime at Prudhoe Bay, Alaska: *Journal of Geophysical Research*, v. 87, no. B11, p. 9301-9316.
- Lerand, M., 1973, Beaufort Sea, *in* McCrossan, R.G., ed., *The Future Petroleum Provinces of Canada—Their Geology and Potential*: Canadian Society of Petroleum Geologists Memoir 1, p. 315-386.
- Lewin and Associates, Inc., 1983, *Handbook of gas hydrates properties and occurrence*: Report for U.S. Department of Energy, Office of Fossil Energy, Morgantown Energy Technology Center, Morgantown, West Virginia, Contract No. DE-AC21-82MC19239, 234p.
- MacCarthy, G.R., 1952, Geothermal investigations on the Arctic Slope of Alaska: *Transactions of the American Geophysical Union*, v. 33, no. 4, p. 589-593.
- Magoon, L.B., and Claypool, G.E., 1979, Two oil types on the North Slope of Alaska—implications for future exploration: *U.S. Geological Survey Open-File Report* 79-1649.
- Makogon, Y.F., 1981, *Hydrates of natural gas*: Penn Well Publishing Company, Tulsa, Oklahoma, 237p.
- Martin, A.J., 1970, Structure and tectonic history of the western Brooks Range, De Long Mountains and Lisburne Hills, northern Alaska: *Geological Society of America Bulletin*, v. 81, p. 3605-3622.
- Mayfield, C.F., Tailleir, I.L., and Ellersieck, Inyo, 1983, Stratigraphy, structure, and palinspastic synthesis of the western Brooks Range, northwestern Alaska: *U.S. Geological Survey Open-File*

Report 83-779, 58p.

- Melvin, John, and Knight, Angela, 1984, Lithofacies, diagenesis, and porosity of the Ivishak Formation, Prudhoe Bay area, Alaska, *in* McDonald, D.A., and Surdam, R.C., eds., *Clastic diagenesis: American Association of Petroleum Geologists Memoir 37*, p. 347-365.
- Molenaar, C.M., Bird, K.J., and Collett, T.S., 1986, Regional correlation sections across the North Slope of Alaska: U.S. Geological Survey Miscellaneous Field Studies Map MF-1907, 1 plate.
- Molenaar, C.M., Bird, K.J., and Kirk, A.R., 1987, Cretaceous and Tertiary stratigraphy of northeastern Alaska, *in* Tailleux, I.L., and Weimer, Paul, eds., *Alaskan North Slope geology: Bakersfield, California, Pacific Section, Society of Economic Paleontologists and Mineralogists and the Alaska Geological Society*, v. 50, 45p.
- Morgridge, D.L., and Smith, W.B., 1972, Geology and discovery of Prudhoe Bay Field, eastern Arctic Slope, Alaska, *in* King, R.E., ed., *Stratigraphic Oil and Gas Fields—Classification, Exploration Methods, and Case Histories: American Association Petroleum Geologists Memoir 16*, p. 489-501.
- O'Donnell, J.P., 1976, Refrigeration is key to Arctic gas-pipeline system: *Oil and Gas Journal*, January 5, p. 88-96.
- Osterkamp, T.E., 1975, Structure and properties of ice lenses in frozen ground: Report No. UAG-R233, Geophysical Institute, University of Alaska, Fairbanks, Alaska, 36p.
- Osterkamp, T.E., and Payne, M.W., 1981, Estimates of permafrost thickness from well logs in northern Alaska: *Cold Regions Science and Technology*, v. 5, p. 13-27.
- Osterkamp, T.E., Petersen, J.K., and Collett, T.S., 1985, Permafrost thickness in the Oliktok Point, Prudhoe Bay and Mikkelsen Bay areas of Alaska: *Cold Regions Science and Technology*, v. 11, p. 99-105.
- Palmer, I.F., Bolm, J.R., Maxey, L.R., and Lyle, W.M., 1979, Petroleum source rock and reservoir quality data from outcrop samples, onshore North Slope of Alaska east of Prudhoe Bay: U.S. Geological Survey Open-File Report 79-1634, 52p.
- Pandit, B.I., and King, M.S., 1979, A study of the effects of pore-water salinity on some physical properties of sedimentary rocks at permafrost temperature: *Canadian Journal of Earth Sciences*, v. 16, p. 1566-1580.
- Parent, J.D., 1984, A survey of United States and total world production, proved reserves, and remaining recoverable resources of fossil fuels and uranium as of December 31, 1982: Institute of Gas Technology, Chicago, Illinois.
- Potential Gas Agency, 1981, Gas hydrates; *in* Potential supply of natural gas in the United States (as of December 31, 1980): Colorado School of Mines, Golden, Colorado, p. 76-89.
- Pratt, R.M., 1979, Gas hydrate evaluation and recommendations, National Petroleum Reserve, Alaska: U.S. Geological Survey Special Report TC-7916, 27p.
- Pusch, R., 1979, Unfrozen water as a function of clay microstructure: *Engineering Geology*, v. 13, p. 157-162.
- Reiser, H.N., Brosge, W.P., Dutro, J.T., Jr., and Detterman, R.L., 1971, Preliminary geologic map, Mt. Michelson Quadrangle, Alaska: U.S. Geological Survey Open-File Report 71-237, scale 1:200,000.
- Reiser, H.N., Brosge, W.P., Dutro, J.T., Jr., and Detterman, R.L., 1978, Geologic map of the Demarcation Point Quadrangle, Alaska: U.S. Geological Survey Open-File Report 78-526.
- Reiser, H.N., Brosge, W.P., Dutro, J.T., Jr., and Detterman, R.L., 1979, Upper Paleozoic volcanic rocks in the eastern and central Brooks Range, *in* Johnson, K.M., and Williams, J.R., eds., *The United States Geological Survey in Alaska—accomplishments during 1978: U.S. Geological Survey Circular 804-B, B25-B27*.
- Rickwood, F.K., 1970, The Prudhoe Bay field, *in* Adkison, W.L., and Brosge, M.M., eds., *Proceedings of the Geologic Seminar on the North Slope of Alaska: Pacific Section, American Association of Petroleum Geologists, Los Angeles, California*, p. L1-L11.
- Sable, E.G., 1977, Geology of the western Romanzof Mountains, Brooks Range, northeastern Alaska: U.S. Geological Survey Professional Paper 897, 84p.
- Schlumberger, C., Schlumberger, M., and Leonard, E.G., 1934, Electrical coring; a method of determining bottom-hole data by electrical measurements: *Geophysical Prospecting, American Institute of Mineralogists, Metallurgists, and Engineers*, v. 110, p. 237-272.
- Snelson, S., and Tailleux, I.L., 1968, Large-scale thrusting and migrating Cretaceous foredeeps in western Brooks Range and adjacent regions of northeastern Alaska: *American Association of*

- Petroleum Geologists Bulletin, v. 52, no. 3, p. 567.
- Stoneley, Robert, 1970, Discussion, *in* Adkison, W.L., and Brosge, M.M., eds., Proceedings of the Geological Seminar on the North Slope of Alaska: Pacific Section, American Association of Petroleum Geologists, Los Angeles, California, p. J2-J4.
- Tailleur, I.L., 1964, Rich oil shale from northern Alaska, *in* Short Papers in Geology and Hydrology: U.S. Geological Survey Professional Paper 475-D, p. D131-D133.
- Tailleur, I.L., 1969, Rifting speculation on the geology of Alaska's North Slope: Oil and Gas Journal, v. 67, p. 128-130.
- Tailleur, I.L., Pessel, G.H., and Engwicht, S.E., 1978, Subcrop map at Lower Cretaceous unconformity, and maps of Jurassic and Lower Cretaceous seismic horizons, eastern North Slope petroleum province, Alaska: U.S. Geological Survey Miscellaneous Field Studies Map MF-928I, scale 1:500,000, 1 sheet.
- Tailleur, I.L., and Weimer, Paul, 1987, Alaskan North Slope geology: Bakersfield, California, Pacific Section, Society of Economic Paleontologists and Mineralogists and the Alaska Geological Society, Book 50, v. 1, 874p.
- U.S. Geological Survey, 1978, Folio, eastern North Slope petroleum province, Alaska: U.S. Geological Survey Miscellaneous Field Studies Maps MF-928-A through MF-928-V.
- Walker, J.H.D., and Stuart, A.J., 1976, Permafrost investigations by crystal cable surveys, Mackenzie Delta, N.W.T., *in* Proceedings of the 17th Annual Society of Petroleum Well Log Analyst Logging Symposium, June 3-6, Houston, Texas: Transactions Society of Petroleum Well Log Analyst, p. 16-28.
- Werner, M.R., 1987, Tertiary and Upper Cretaceous heavy oil sands, Kuparuk River area, Alaskan North Slope, *in* Tailleu, I.L., and Weimer, Paul, eds., Alaskan North Slope geology: Bakersfield, California, Pacific Section, Society of Economic Paleontologists and Mineralogists and the Alaska Geological Society, Book 50, v. 1, p. 109-118.
- Whiffen, B.L., Kiefte, H., and Clouter, M.J., 1982, Determination of acoustic velocities in xenon and methane hydrates by brillouin spectroscopy: Geophysical Research Letters, v. 9, no. 6, p. 645-648.
- Whittaker, A., 1985, Theory and evaluation of formation pressures—a pressure detection reference handbook: International Human Resources Development Corporation, Boston, Massachusetts, p. 73-134.
- Woodward, P.V., 1987, Regional evaluation of formation fluid salinity by spontaneous potential log, Ivishak Sandstone (Triassic), North Slope, Alaska: Master of Science Thesis, San Jose State University, San Jose, California, 71p.
- Wyllie, M.R., 1949, A quantitative analysis of the electrochemical component of the S.P. curve: Petroleum Transactions, American Institute of Mineralogists, Metallurgists, and Engineers, v. 86, p. 17-26.
- Zoller, W.A., 1984, Determine pore pressure from MWD gamma ray logs: World Oil, March, p. 97-102.